

Synthesis of cyclometalated gold (III) complexes  
functionalized by alkynyl derivatives. Study of the  
interaction with DNA secondary structures.

---

Ángel Bajo Sánchez

A thesis submitted in part fulfilment of the requirements for the degree  
of Master of Philosophy



School of Chemistry

University of East Anglia, Norwich

April 2016

Supervised by Prof Manfred Bochmann and Prof Simon J. Lancaster

This copy of the thesis has been supplied on condition that anyone who consults it is understood to recognise that its copyright rests with the author and that use of any information-derived there-from must be in accordance with current UK Copyright Law. In addition, any quotation or extract must include full attribution.



## **STATEMENT OF ORIGINAL WORK**

The research described in this thesis has been conducted by the author, Mr Ángel Bajo Sánchez, and is, to the best of his knowledge, original. Where other people's work has been referred to, this has been cited by corresponding references.

Ángel Bajo Sánchez



## AKNOWLEDGEMENTS

I would like to express my gratitude to my supervisor, Prof. Manfred Bochmann, because without his guidance and support this work would have not been possible. Thank you for your help, for your advices, for teaching how to think about chemistry, for your orientation when I was stuck with the project. Thanks a lot, Manfred.

I would like to thank Prof. Simon Lancaster, for his generous advices, support and guidance, as well as for his teachings in the project and throughout these years at the UEA. Thank you very much, Simon.

Many thanks to Dr. Zoe Waller, for giving me the opportunity to carry out this collaboration. Thank you very much for your advices and teachings, as well for your support on this part of the project.

I would like to thank to Dr. Julio Fernandez, not only for his advices throughout the project, but also for his moral support, his encouragement and his friendship. I still can remember when he arrived to the lab, his enthusiasm and his good ideas gave a breath of fresh air and an impulse to the project. Thank you, Julio.

I would also like to thank Dr. Mark Schormann and Dr. David Hughes for their time spent with the refinement and solving of the X-Ray structures presented on this thesis.

I would like to express my gratitude to all members of Bochmann, Lancaster and Wildgoose groups for making the lab a comfortable place to work. Thanks to Dr. Dragos Rosca, not only for his advices about gold(III) chemistry but also for all the funny times we spent, to Dr. Elizabeth Jacobs for her help when I arrived to Norwich, to Dr. Chrisa Pateraki, for her friendship and support throughout my time in Norwich, and also to Dr. Julio Fernandez, Dr. James Morris, Dr. Alexander Romanov, Dr. Anna Pintus, Dr. Benoit Bertrand, Lucy Carry and Morwen Williams for all your help and the fabulous coffee sessions in the morning that we spent.

I can not forget one person, James Woods. Thanks James for all the funny times we have spent over these years, for the trips to the pub, for the visit to the stadium to watch that football match (I still can remember that funny afternoon we spent), and also for all the advices you have given me during these years. Thank you very much for your friendship, James.

I would like to mention to my friends from my hometown, Alejandro, Julio, Alvaro and Alfonso. Thank you very much for your support during this stage of my life, for your friendship and, in spite of the distance, for being always willing to help me at any time. Thanks a lot guys.

I would like to express my gratitude to my parents, Angel and Mari Carmen, and my sister, Cristina. It is now a long time since I left Spain to start a new life in the UK. Although it was a difficult time because it was the first time that my family and I would be separated from each other, they gave me their unconditional support at all time in this new adventure in Norwich. Thank you very much for your support in both the happy times and bad times, for your wise advices in all aspects of my life, for your guidance, for your moral support at any time. I will never be able to find the right words to express the enormous gratitude that I feel.

Finally, I would like to mention one special person, my partner, my friend, my confidant, Leyre. Thank you very much for being my main support, for being there in the difficult times, for knowing what is the right word to say at any time to make me feel better and push me to go ahead. Thank you very much for all, Lilly.

## ABSTRACT

This thesis explores the synthesis of cyclometalated gold(III) complexes functionalized by alkynyl ligands, as well as the study of the interaction of the studied complexes with DNA secondary structures. In this work, bidentate and tridentate ligands, in particular derived from both phenylpyridine and diphenylpyridine, respectively, have been employed as framework structure in order to stabilize the studied gold complexes.

Chapter 1 studies the synthesis of cyclometalated gold(III) complexes functionalized by alkynyl derivatives. The main feature of the employed alkynyl derivatives was its functionalization by amino ester terminal groups, suitable to be converted to amino acids, which are overexpressed in cells and may promote the interaction of the studied complexes with DNA.

Chapter 2 explores a study of the interaction of the synthesized gold(III) complexes with DNA secondary structures. Making use of a variety of analytical techniques, such as circular dichroism (CD), FRET melting experiments, FRET titration and UV difference spectrum, we have observed that a selection of the studied gold complexes may exert interaction with certain DNA secondary structure in physiological media.

Chapter 3 reports the attempts to conduct the synthesis of a family of cyclometalated (C<sup>N</sup>) gold(III) complexes capable of bearing two functionalisable substituents. In recent years, our research group has proven the excellent reactivity of certain tridentate (C<sup>N</sup><sup>C</sup>) gold (III) complexes as mild base, allowing C–H or N–H activation to synthesize gold aryls, alkynyls and heteroaryl derivatives. However, the rigidity of the tridentate framework has limited the reactivity of this system. Accordingly, the aim of this chapter is the synthesis of bidentate gold (III) derivatives, which may provide a wide range of reactivity possibilities because of the presence of two functionalisable positions.

## LIST OF ABBREVIATIONS

et al.	et alia
cisplatin	cisdiamminedichloroplatinum
<i>p</i> -	para
<i>o</i> -	meta
%	Percentage
OAc	acetate
NMR	Nuclear Magnetic Resonance
PPh <sub>3</sub>	Triphenylphosphine
Me	methyl
TrxR	seleno-enzyme thioredoxin reductase
OAc <sup>F</sup>	trifluoroacetate
Δ	delta
ppm	parts-per-million
d	doublet
t	triplet
q	quartet
s	singlet
m	multiplet
bs	broad signal
IR	Infrared
DMSO	dimethylsulfoxide
td	triplet of doublets
Ar	Aromatic

J	coupling constant
°C	Degrees Celsius
Hz	Hertz
MHz	Megahertz
mmol	millimol
Anal. Calcd	Analysis calculated
gDNA	genomic DNA
TrxR1	Thioredoxin reduced cytosolic
TrxR2	Thioredoxin reduced mitochondrial
Hif-1- $\alpha$	hypoxia-inducible factor 1 $\alpha$
DNA	Deoxyribonucleic acid
RNA	ribonucleic acid
mg	milligrams
dl	decilitre
Py	pyridyl
dsDNA	double stranded DNA
CD	circular dichroism
G	guanidine
T	Thymine
A	Adenine
C	Cytosine
HTelo	Human telomeric
FID	Fluorescent intercalator displacement
mM	millimolar

$\mu\text{M}$	micromolar
FRET	Förster Resonance Energy Transfer
UV	ultraviolet
$E_{\text{FRET}}$	FRET efficiency
$\tau_{\text{DA}}$	Fluorescence lifetime of the donor molecule in absence of acceptor
$\tau_{\text{D}}$	Fluorescence lifetime of the donor molecule in presence and absence of acceptor
$R_0$	Förster distance
$r_0$	energy acceptor
$I_{\text{DA}}$	Fluorescence intensity of the energy donor molecule in presence
$I_{\text{D}}$	Fluorescence intensity of the energy donor molecule in absence of acceptor
$T_{\text{m}}$	Melting temperature
TDS	thermal difference spectrum
HPLC	High Performance Liquid Chromatography
min	minutes
<sup>t</sup> Bu	<i>tert</i> -butyl
BINAP	2,2'-bis(diphenylphosphino)-1,1'-binaphthyl
dba	Bis(dibenzylideneacetone)
Et	ethyl
<sup>n</sup> Bu	<i>n</i> -butyl
Å	Amstromg

◦	degree
THF	Tetrahydrofuran
iPr	isopropyl
DABCO	1,4-diazabicyclo[2,2,2]octane

## TABLE OF CONTENTS

<b>Statement of original work</b>	<b>ii</b>
<b>Acknowledgements</b>	<b>iv</b>
<b>Abstract</b>	<b>vi</b>
<b>List of Abbreviations</b>	<b>vii</b>

### INTRODUCTION

1. Gold(III) complexes as alternative to cis-platin.....	2
2. The importance of the ligand choice.....	2
3. The role of amino acids and peptides as good carriers. ....	3

### CHAPTER 1

#### **Synthesis of bi- and tri- dentate gold(III) complexes functionalized by alkynyl derivatives**

1.1. INTRODUCTION .....	6
1.2. RESULTS AND DISCUSSION .....	14
1.2.1. Synthesis of tri-dentate gold(III) complexes functionalized with alkynyl derivatives .....	14
1.2.1.1. Synthesis of precursors .....	14
1.2.1.2. Synthesis of complexes .....	28
1.2.1.2.1. Synthesis of (C <sup>N</sup> C)Au-C≡C-C <sub>6</sub> H <sub>4</sub> -4-CHO ( <b>4</b> ) .....	31
1.2.1.2.2. Synthesis of (C <sup>N</sup> C)Au-C≡C-C <sub>6</sub> H <sub>4</sub> -4-[CH <sub>2</sub> -NH-CH(CH <sub>3</sub> )-COOCH <sub>3</sub> ] ( <b>5</b> ) .....	36

1.2.1.2.3.	Synthesis of $(C^{\wedge}N^{\wedge}C)Au-C\equiv C-C_6H_4-4-[CH_2-NH-CH(CH_2OH)-COOCH_3]$ ( <b>6</b> ) .....	43
1.2.1.2.4.	Synthesis of $(C^{\wedge}N^{\wedge}C)Au-C\equiv C-C_6H_4-4-(CH_2-NH-CH_2-COOCH_2CH_3)$ ( <b>7</b> ) .....	48
1.2.1.2.5.	Synthesis of $(C^{\wedge}N^{\wedge}C)Au-C\equiv C-C_6H_4-4-CH_2OH$ ( <b>8</b> ) .....	53
1.2.2.	Synthesis of mono- and di-substituted bi-dentate gold(III) complexes functionalized with alkynyl derivatives .....	60
1.2.2.1.	Synthesis of $(C^{\wedge}N)Au(Cl)C\equiv C-C_6H_4-4-CHO$ ( <b>11</b> ) .....	64
1.2.2.2.	Synthesis of $(C^{\wedge}N)Au(Cl)C\equiv C-C_6H_4-4-[CH_2-NH-CH(CH_3)-COOCH_3]$ ( <b>12</b> ) .....	68
1.2.2.3.	Synthesis of $(C^{\wedge}N)Au(Cl)C\equiv C-C_6H_4-4-[CH_2NH-CH-(CH_2OH)-COOCH_3]$ ( <b>13</b> ) .....	74
1.2.2.4.	Synthesis of $(C^{\wedge}N)Au-(Cl)C\equiv C-C_6H_4-4-[CH_2-NH-CH(CH_2OH)-COOCH_3]$ ( <b>14</b> ).....	81
1.2.3.	Synthesis of di-substituted bi-dentate gold(III) complexes functionalized with alkynyl derivatives .....	87
1.2.3.1.	Synthesis of $(C^{\wedge}N)Au(-C\equiv C-C_6H_4-CHO)_2$ ( <b>15</b> ) .....	89
1.2.3.2.	Synthesis of $(C^{\wedge}N)Au[-C\equiv C-C_6H_4-4-CH_2-NH-CH(CH_3)-COOCH_3]_2$ ( <b>16</b> ) .....	93
1.3.	SUMMARY .....	98
1.4.	CONCLUDING REMARKS AND PERSPECTIVES .....	99
1.5.	EXPERIMENTAL.....	100

## CHAPTER 2

### Interaction of bi- and tri-dentate cyclometalated gold(III) complexes with DNA secondary structures.

2.1.	INTRODUCTION	
2.1.1.	Metal complexes in cancer therapy	121
2.1.2.	Anti-cancer gold organometallic complexes	123
2.1.2.1.	Gold(I) organometallic complexes with anti-tumor activity	124
2.1.2.2.	Gold(I) alkynyl complexes	126
2.1.2.3.	Gold(I) complexes bearing amino acid moieties	126
2.1.2.4.	Gold (III) complexes with anti-tumour activity	128
2.1.3.	Stabilization of secondary DNA structures by gold – based complexes	129
2.1.3.1.	Double stranded DNA structures stabilized by gold complexes	129
2.1.3.2.	G-quadruplex DNA structures. Interaction with Gold(III) complexes	132
2.1.3.3.	i-motif DNA structures. Interaction with Gold(III) complexes	136
2.2.	RESULTS AND DISCUSSION	139
2.2.1.	Förster Resonance Energy Transfer (FRET) melting	140
2.2.1.1.	FRET melting experiments employing 50, 10 and 1 $\mu$ M solutions of complexes <b>4 – 7</b> and <b>11 – 14</b>	141
2.2.2.	Circular dichroism (CD) experiments	148
2.2.3.	FRET titration experiment	151
2.2.4.	UV difference spectrum	153
2.3.	CONCLUDING REMARKS AND PERSPECTIVES	156
2.4.	EXPERIMENTAL	158

## CHAPTER 3

### Miscellaneous results

3.1. INTRODUCTION .....	167
3.2. RESULTS AND DISCUSSION .....	166
3.2.1. Synthesis of pro-ligand <b>L</b> <sup>5</sup> .....	166
3.2.2. Metalation attempts of pro-ligand <b>L</b> <sup>5</sup> .....	170
3.2.3. Synthesis of pro – ligand <b>L</b> <sup>6</sup> .....	176
3.2.4. Metalation attempts of pro-ligand <b>L</b> <sup>6</sup> .....	178
3.2.5. Phenylpyridine derivative ligands: Pro – ligands <b>L</b> <sup>7</sup> and <b>L</b> <sup>8</sup> .....	179
3.2.6. Synthesis of five membered ring cycloaurated complexes <b>10</b> and <b>18</b> .....	180
3.3. EXPERIMENTAL .....	185
<b>REFERENCES</b> .....	193

## INTRODUCTION

Nowadays, cancer is widely prevalent in today's society, being one of the leading causes of death among population. Cancer is characterized by uncontrolled division of cells and the ability of these cells to invade other tissues leading to the formation of tumour mass, vascularization, and metastasis<sup>1</sup>.

Chemotherapy is one of the major approaches to treat cancer by delivering a cytotoxic agent to the cancer cells. During the last decades, investigations in order to find therapeutic applications of metal-based compounds have been widely studied. In 1965 Rosenberg et al.<sup>2</sup> discovered the antiproliferative activity of a platinum complex called cisdiamminedichloroplatinum (**cisplatin**) (Figure 1), which was successfully employed in testicular cancer therapy.

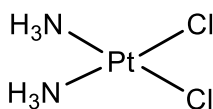


**Figure 1.** *Chemical structure of cisplatin.*

Cis-diamminedichloroplatinum (**cisplatin**) and some of its analogues have been widely administered as drugs against prostate, ovarian, head and neck tumours, small-lung carcinoma and bladder cancer cells.

However, DNA interaction is considered to be the primary target for metal-based complexes, and the cytotoxic effects of them may be a consequence of a direct interaction with nuclear DNA.

Despite the remarkable effectiveness of **cisplatin** against certain cancer cells, some tumours have started to show an intrinsic resistance to this drug. This fact and the

significant side effects, such as loss of fertility and appetite, have inspired the search of alternative metal – based complexes capable to exhibit anti-tumour effect.

### **1. Gold (III) complexes as alternative to cisplatin.**

In recent years, gold compounds have drawn special attention as a new generation of anticancer agents, showing anti-tumour properties both *in vitro* and *in vivo*.<sup>3</sup> From a chemical point of view, the similarities between gold(III) and platinum(II) atoms, both isoelectronic, featuring a square-planar coordination geometry (corresponding to the  $5d^8$  outer shell electronic configuration), have encouraged a variety of investigations in the last years in order to study gold(III) compounds as alternative to **cisplatin** in both DNA interaction and cancer treatment.

### **2. The ligand influence in biological applications of metal-based complexes.**

In the course of investigations, the limited stability of gold(III) complexes has been the main obstacle in biological studies. Gold(III) complexes have exhibited a low stability in physiological media, reductive elimination to gold(0) being the preferred route. Stability in physiological media is considered the most important and necessary feature that complexes must meet in order to be suitable to exert anti-tumour activity. Accordingly, the proper choice of ligands has become the most important aspect in the synthesis of metal-based complexes with biological applications, allowing the establishment of an equilibrium of the hydrophilic and lipophilic properties of the complex.<sup>4</sup> The use of bi, tri or poly-dentate ligand frameworks coordinated to the gold metallic centre plays a key role in order to reach this stabilization. Bi-dentate ligands of the type (C<sup>^</sup>N) and tri-dentate ligand types (C<sup>^</sup>N<sup>^</sup>C), (N<sup>^</sup>N<sup>^</sup>N) and (N<sup>^</sup>N<sup>^</sup>C), surrounding the gold metallic centre, are examples of ligands that can provide a

considerable redox and thermodynamic stability to gold complexes. The coordination of these ligands to the gold atom can modify the steric and electronic properties of the complex, which can be reflected in an increase of the lipophilic character. In addition, the coordination of these nitrogen donor ligands prevents ligand exchange in solution state, a commonly observed phenomenon which leads to the reduction of Au(III) in biological solutions.<sup>4</sup>

### **3. The role of amino acids and peptides as good carriers.**

One of the main issues for cancer chemotherapeutics and, in particular for gold(III) complexes, is to cross the cell membrane, a key factor of anti-tumour action and DNA binding. Accordingly, the presence of appropriated substituents, such as amino acids and peptides, is a key factor in order to reach this goal.

In spite of the wide number of gold complexes that have shown activity in biological systems, the number of gold complexes with amino acids and peptides is very scarce. There are only a few reports of gold(III) complexes with amino acids, such as cysteine.<sup>5</sup> The introduction of amino acids and peptides as substituents can play an important role in the biological activity of the complexes. The presence of amino acids and peptides in the complex can cause a considerable reduction of the side effects associated to the biological activity of the complex. In addition, as these groups are over-expressed receptors in some type of tumours, they can act as good carriers, allowing the transport of the gold atom to the biological target.

In this thesis we report the synthesis of bi- and tri-dentate cyclometallated gold(III) complexes functionalized by amino ester derivatives, as well as study of the interaction and binding of them with secondary DNA structures

## **CHAPTER 1**

**BI- AND TRI-DENTATE CYCLOMETALATED GOLD (III)  
COMPLEXES FUNCTIONALIZED BY ALKYNYL LIGANDS.**



## 1.1. INTRODUCTION

Chelating ligands around gold(III) centre are commonly used in order to avoid reductive elimination reactions. Recent work has proven the efficiency of the use of some examples of (N<sup>^</sup>N) and (C<sup>^</sup>N) type bidentate ligands such as 2,2'-bipyridyl or 2-phenylpyridine respectively, to stabilize species including gold chloride complexes, terminal anilides, acetylides and cis-diarylgold(III) species<sup>6</sup> (Figure 2).

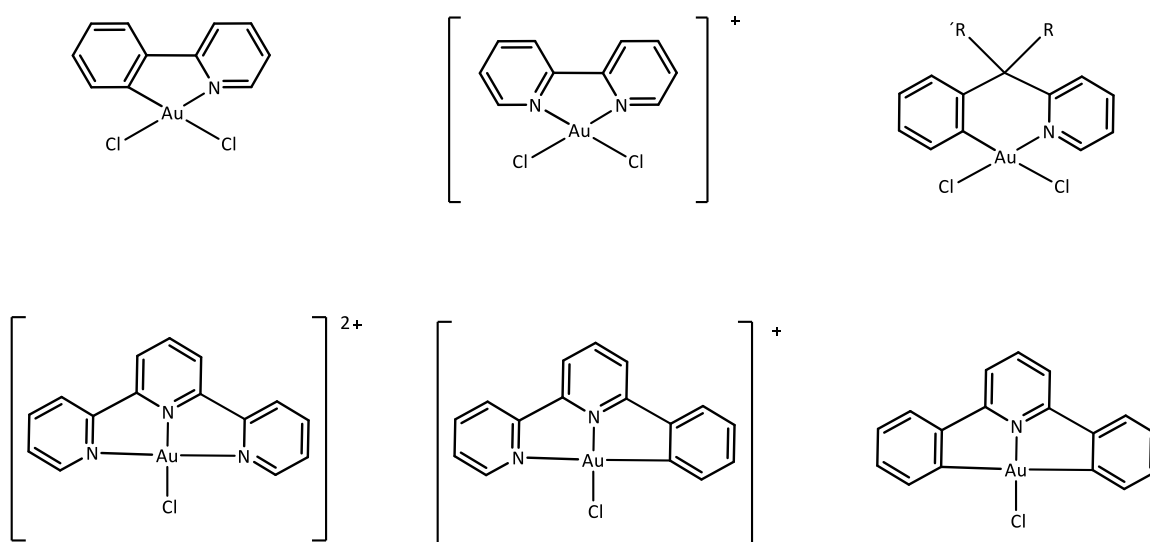


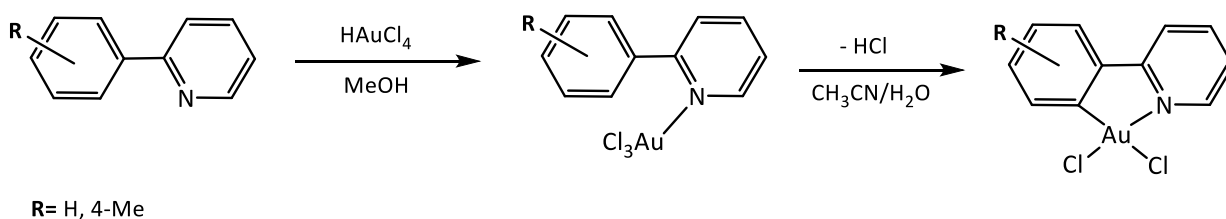
**Figure 2.** Examples of gold(III) centers stabilized by chelating ligands.

In this chapter we focus on the synthesis of cyclometalated gold(III) complexes functionalized by alkyne derivatives, employing (C<sup>^</sup>N<sup>^</sup>C) and (C<sup>^</sup>N) ligands to stabilize the gold (III) complexes.

For the synthesis of these complexes and incorporation of the alkynyl ligand into the cyclometalated gold(III) moiety, chlorogold(III) precursors have been used as starting materials. In recent years, both direct auration and transmetallation from organomercury derivatives have been the frequently used route to synthesize chlorogold(III) precursors (C<sup>^</sup>N)AuCl<sub>2</sub> and (C<sup>^</sup>N<sup>^</sup>C)AuCl.

a. Direct auration.

Chlorogold(III) precursors type  $(C^{\wedge}N)AuCl_2$  can be synthesized by direct auration between the ligand and  $[AuCl_4]^-$ . The direct auration of aromatic ligands was firstly achieved in 1931 by Kharasch<sup>7</sup> but it was not for a further 50 years that other concrete examples were obtained. Constable and co-workers reported the *ortho*-metalation of 2-phenyl-pyridine,<sup>8a</sup> giving stable five-membered  $C^{\wedge}N$ -chelates. Other substituted pyridines were shown to undergo similar reactions,<sup>9,10</sup> as well as more recent examples,<sup>8b,11,12</sup> forming five- or six-membered chelates (Scheme 1).



**Scheme 1.** Examples of synthesis of chlorogold(III) precursors type  $(C^{\wedge}N)AuCl_2$  by direct auration.

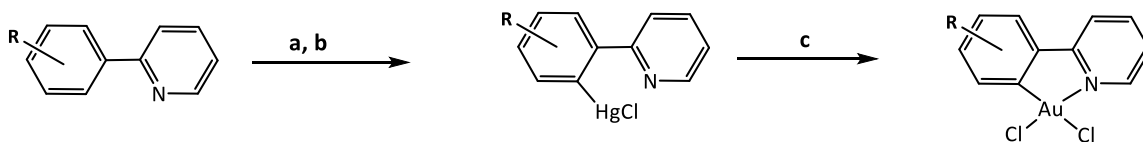
As it shown on Scheme 1, direct auration of chlorogold(III) precursors type  $(C^{\wedge}N)AuCl_2$  is a two step reaction. The first step implies the synthesis of the intermediate  $(HC^{\wedge}N)AuCl_3$ . This intermediate can be synthesized making use of both  $H[AuCl_4]$  and  $[AuCl_4]^-$  salt as reagents. The synthesis of the intermediate  $(HC^{\wedge}N)AuCl_3$  using  $H[AuCl_4]$  as reagent has been carried out in both ethanol<sup>8a</sup> and methanol<sup>8b</sup> at room temperature. The formation of a yellow precipitate was observed after 30 minutes, which was filtered off and dried under vacuum. Yields of over 90% have been reported by this method. In addition, this intermediate can be also prepared using  $[AuCl_4]^-$  derivatives such as  $Na[AuCl_4]$  and  $K[AuCl_4]$ , in acetonitrile/water at room temperature.<sup>8a,11</sup> The second stage involves the formation of chlorogold product

$(C^{\wedge}N)AuCl_2$ . The preparation of this complex has been carried out from the  $(HC^{\wedge}N)AuCl_3$  intermediate in refluxed acetonitrile, in order to activate the Au–C bond. Yields over 35% have been reported.

In spite of the advantage that mercury salts are not used in the synthesis, which is beneficial from an ecological point of view, the main disadvantages are both the lower yield obtained by this method (over 35 %) and the longer reaction times compared to the transmetalation pathway.

*b. Transmetalation from organomercury compounds.*

Transmetalation from organomercury compounds is the most commonly employed strategy for the synthesis of  $(C^{\wedge}N)AuCl_2$  and  $(C^{\wedge}N^{\wedge}C)AuCl$  derivatives. Over the last decades, this has been the preferred route to synthesize several of these complexes<sup>6,7</sup> and is still commonly employed<sup>14,15</sup> (Scheme 2 and 3).



R= H; 3-Me; 3,5-Me<sub>2</sub>; 4-<sup>t</sup>Bu

Hg(OAc)<sub>2</sub>, ethanol reflux.    b. LiCl, methanol.    c. K[AuCl<sub>4</sub>],

acetonitrile/dichloromethane.

**Scheme 2.** Literature example for the synthesis of chlorogold(III) complexes

$(C^{\wedge}N)AuCl_2$  by transmetalation from the  $(C^{\wedge}N)HgCl$  organomercury compounds.



R, R', R''=H

R, R'=<sup>t</sup>Bu ; R''=H

R, R'=H ; R''=C<sub>6</sub>H<sub>4</sub>-CH<sub>3</sub>-*p*

- a. Hg(OAc)<sub>2</sub>, ethanol reflux. b. LiCl, methanol. c. K[AuCl<sub>4</sub>], acetonitrile/dichloromethane.

**Scheme 3.** *Synthetic route of (C<sup>N</sup>C)AuCl by transmetalation from an organomercury precursor.*

The first step shown in Schemes 2 and 3 involves the mercuriation using Hg(OAc)<sub>2</sub> as reagent in refluxed ethanol, and the consequent metathesis employing LiCl, to afford (C<sup>N</sup>)HgCl and (C<sup>N</sup>C)HgCl derivatives, respectively. The second stage involves the transmetalation step making use of K[AuCl<sub>4</sub>] or Na[AuCl<sub>4</sub>], in acetonitrile/dichloromethane as solvents, at room temperature.

In general terms, transmetalation route has been proven to be more efficient, giving cleaner products by quicker reactions. In addition, slightly better yields than the direct auration<sup>8</sup> can be obtained.

Our efforts focused on the functionalization of the synthesized chlorogold(III) precursors (C<sup>N</sup>)AuCl<sub>2</sub> and (C<sup>N</sup>C)AuCl with different alkynyl derivatives. In recent years, several examples of gold(III) alkynyl complexes have been reported. In 1977, Johnson et al.<sup>17,18</sup> reported the synthesis of mononuclear gold(III) complexes type [Au(C≡CCF<sub>3</sub>)Me<sub>2</sub>(L)] and [Au(C≡CR)Me<sub>2</sub>(PPh<sub>3</sub>)], containing one alkynyl ligand. Yam et al.<sup>16,19,20</sup> synthesized (C<sup>N</sup>C)gold(III) mono-alkynyl complexes type [Au(C<sup>N</sup>C)(C≡CR)], carrying out studies of luminescence behaviour. Mononuclear

gold(III) complexes substituted by two, three and four alkynyl ligands type [(phenylpyridine)Au(C≡CR)<sub>2</sub>],<sup>21</sup> [Au(C≡CR)<sub>3</sub>(L)] and four alkynyl ligands [ER<sub>4</sub>]<sup>+</sup>[Au(C≡CR)<sub>4</sub>]<sup>-</sup><sup>22, 23</sup> respectively, have been also reported (Figure 3).

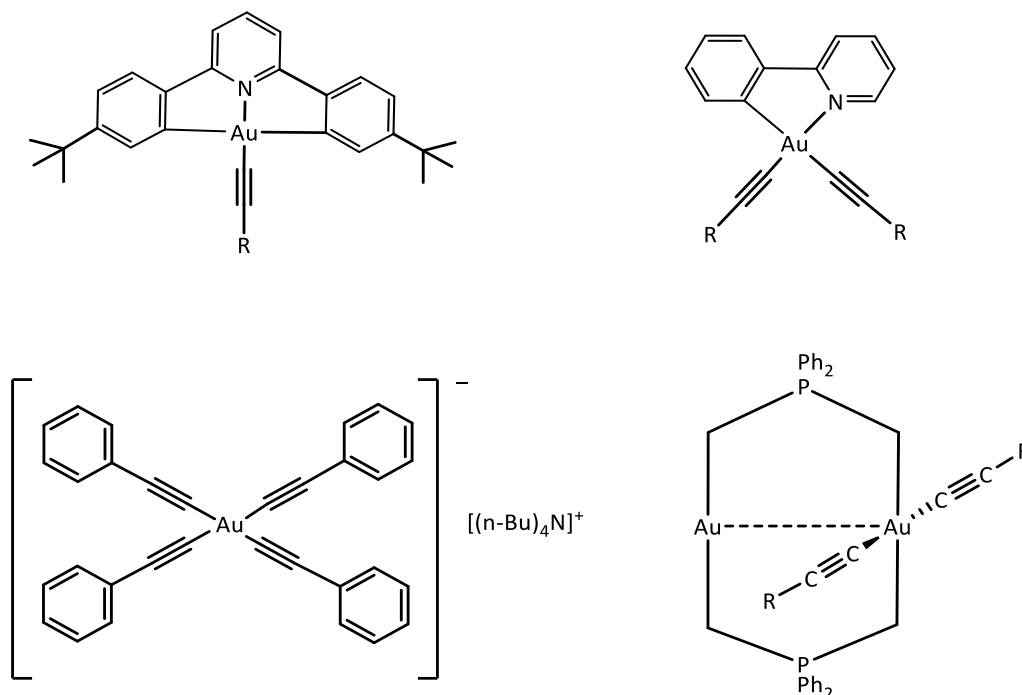


**Figure 3.** Examples of gold(III) mono-, di-, and tetra-alkynyl complexes.

The study of the luminescence behaviour has been the main application of alkynyl gold complexes. In contrast to the gold(I) systems, bi- and tri- dentate gold(III) complexes have been rarely observed to be photo-emissive, and even if they do emit, they usually do at low temperature in the solid state, with very few examples that would emit at room temperature in solution.<sup>24</sup> Nevertheless, the rigid structure from the alkynyl group, as well as its ability to interact with the metal centre and its  $\delta$ -electron delocalization can strengthen the metal-carbon bonds, favouring the design of luminescent organometallic materials.

The applications of Au(I) and Au(III) complexes as anticancer agents have also gained a considerable importance over the last years.<sup>26,27</sup> Recent studies have shown that

mononuclear alkynyl gold complexes type alkynyl(triphenylphosphine)gold(I) (Figure 4) exhibit a promising potential as future anti-tumour agents.<sup>28, 29</sup>

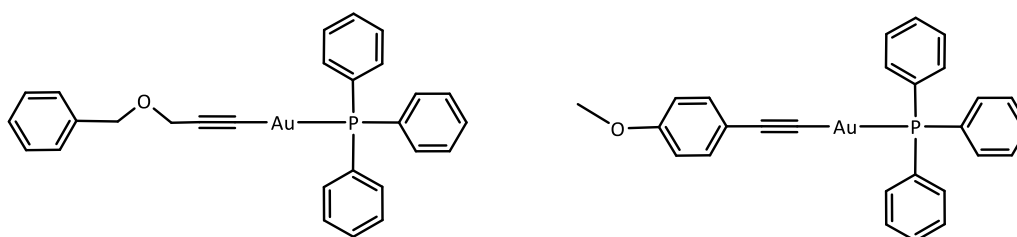


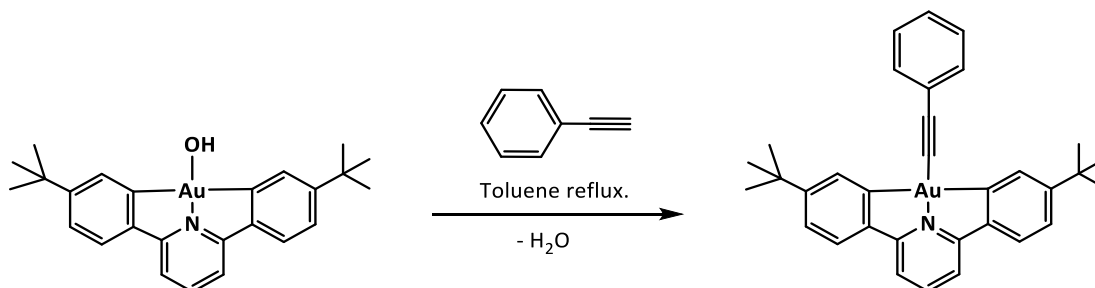
**Figure 4.** Examples of cytotoxic gold(I) alkynyl complexes.

These promising results with gold(I) alkyne complexes encouraged us to extend our research to the study of gold(III) alkynyl complexes. Accordingly, in this chapter we report the synthesis of (C<sup>^</sup>N<sup>^</sup>) and (C<sup>^</sup>N<sup>^</sup>C)Au(III) complexes functionalized by different alkynyl derivatives, such as 4-ethynylbenzaldehyde and 1-ethynyl-4-benzyl-L-amino esters.

In recent years three pathways have been developed in order to attach alkynyl derivatives to the gold(III) atom:

- Method a

In 2012, Bochmann et al.<sup>30</sup> reported the synthesis of (C<sup>^</sup>N<sup>^</sup>C)AuOH. This complex showed an excellent reactivity as a mild metal base, being able to activate C–H and N–H bonds. The reaction of (C<sup>^</sup>N<sup>^</sup>C)AuOH with alkyne derivatives was studied (Scheme 4), giving cleanly (C<sup>^</sup>N<sup>^</sup>C)Au(III) alkynyl complexes.



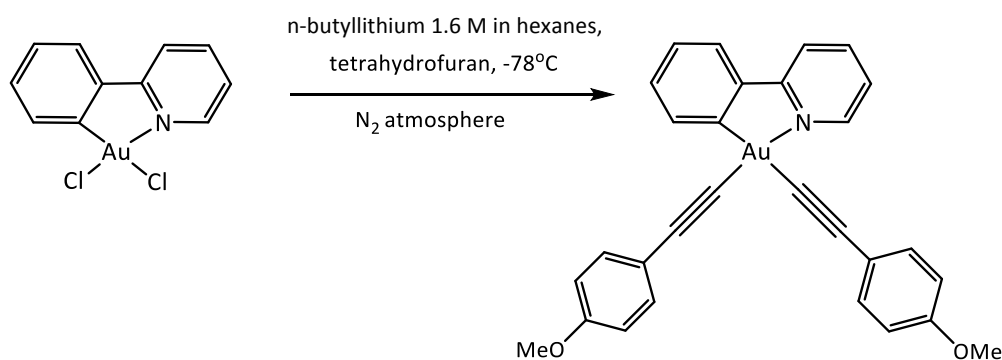
**Scheme 4.** Synthesis of (C<sup>^</sup>N<sup>^</sup>C)Au(III)phenylacetylide from (C<sup>^</sup>N<sup>^</sup>C)Au(III)OH.

As it is shown in Scheme 4, the reported synthesis (C<sup>^</sup>N<sup>^</sup>C)Au(III)phenylacetylide involves an acid–base reaction, which requires high temperatures in order to activate the Au–OH bond.

This result encouraged us to investigate the synthesis of (C<sup>^</sup>N)Au(OH)<sub>2</sub>, as well as its reactivity as a base. In addition, the synthesis of (C<sup>^</sup>N)Au(OH)<sub>2</sub> would be a significant advance in order to establish a successful novel method to synthesize dialkynyl (C<sup>^</sup>N)Au(III) complexes. The preparation of this complex was explored by different pathways (detailed in Chapter 3), such as the previously detailed method reported by Bochmann et al.,<sup>30</sup> using (C<sup>^</sup>N)AuCl<sub>2</sub> precursor as starting material and cesium hydroxide as reagent, in a mixture of toluene/tetrahydrofuran/water (1:1:1) at room temperature. Nevertheless, our efforts to synthesize (C<sup>^</sup>N)Au(OH)<sub>2</sub> were unsuccessful, generating mixtures of different products, which could not be converted into (C<sup>^</sup>N)Au(III) dialkynyl complexes.

- *Method b*

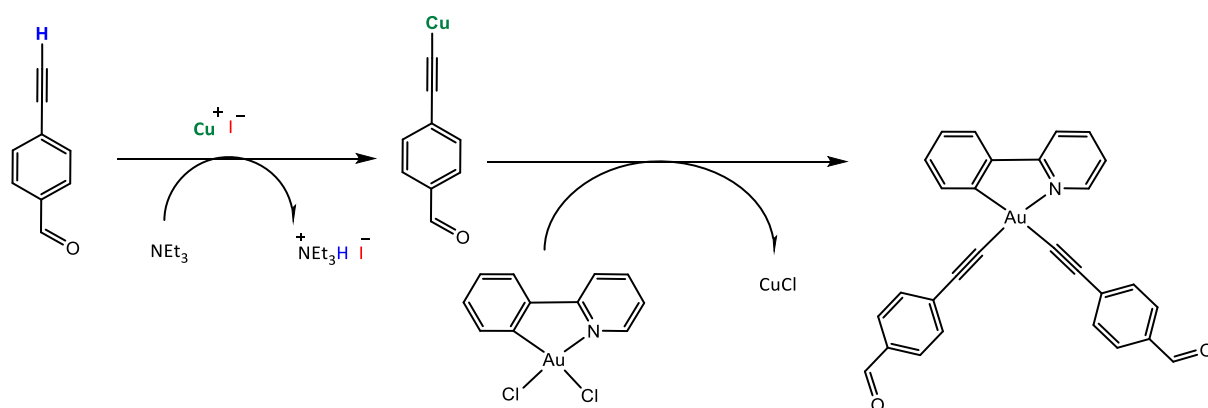
Yam et al.<sup>19</sup> reported the synthesis of (C<sup>^</sup>N)Au(III)dialkynyl complexes by the reaction of the corresponding dichlorogold(III) precursor with different alkynyllithium reagents (Scheme 5).



**Scheme 5.** Synthesis of (phenylpyridyl)Au(-C≡C-C<sub>6</sub>H<sub>4</sub>-4-OCH<sub>3</sub>)<sub>2</sub> from (C<sup>^</sup>N)AuCl<sub>2</sub> precursor.

- Method c

Venkatesan et al.<sup>21</sup> introduced a modification regarding the previously reported methods of synthesis of (C<sup>^</sup>N)Au(III)dialkynyl complexes. Utilizing the dichlorogold(III) precursor and the corresponding alkynyl ligand as starting materials, this method introduces the use of NEt<sub>3</sub>, which serves as a mild enough base for an *in situ* deprotonation of the acidic acetylenic proton, and the substitution is supported by the addition of a catalytic amount of CuI (Scheme 6).



**Scheme 6.** Reaction mechanism of synthesis of (C<sup>^</sup>N)Au(III)dialkynyl complexes.

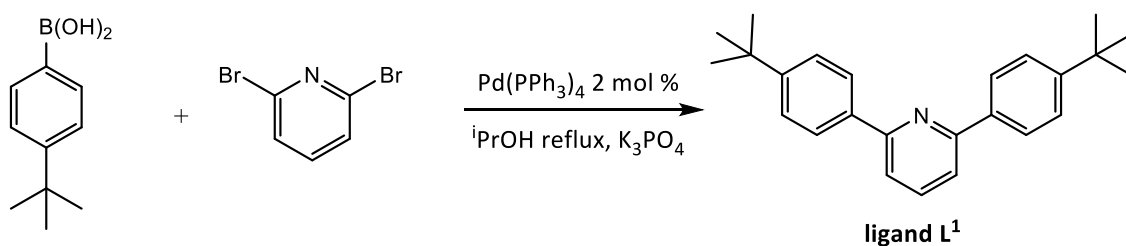
In this chapter we report the synthesis of bi- and tri-dentate gold(III) complexes functionalized by alkynyl derivatives. The synthesis of (C<sup>^</sup>N)Au(III) mono-alkynyl and (C<sup>^</sup>N)Au(III) di-alkynyl complexes has been only explored by methods *a* and *c*

## 1.2. RESULTS AND DISCUSSION

### 1.2.1. Synthesis of tri-dentate gold(III) complexes functionalized with alkynyl derivatives.

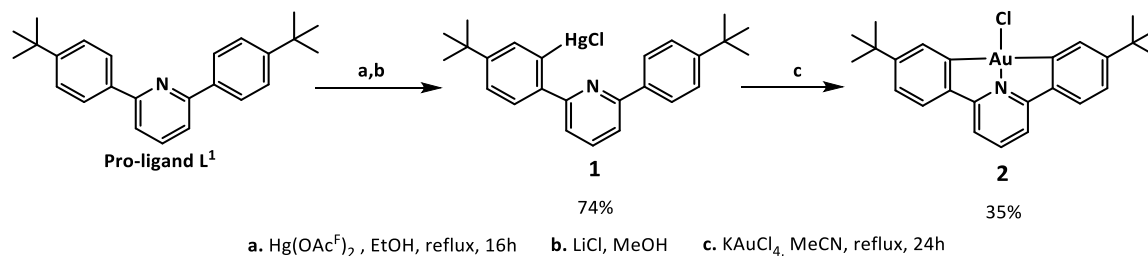
#### 1.2.1.1. Synthesis of precursors.

The synthesis of ligand **L**<sup>1</sup> has been carried out via a single step Suzuki cross-coupling of the commercially available 4-tert-butylphenyl boronic acid and 2,6-dibromopyridine, employing Pd(PPh<sub>3</sub>)<sub>4</sub> as catalyst (Scheme 7).



**Scheme 7.** Synthesis for the ligand **L**<sup>1</sup>.

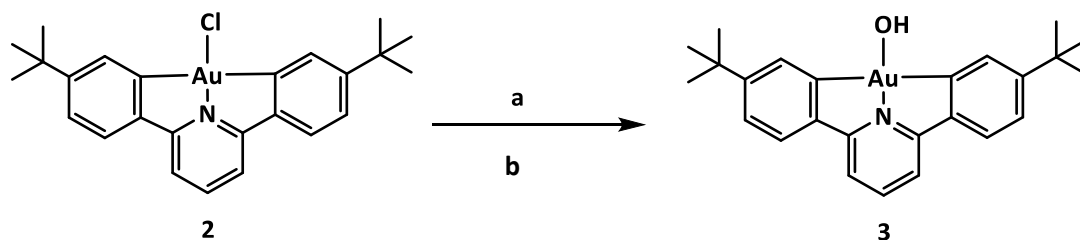
Ligand **L**<sup>1</sup> has been subjected to *ortho*-mercuration employing Hg(OAc<sup>F</sup>)<sub>2</sub>, followed by salt metathesis with LiCl to yield the organomercury(II) species (HC<sup>N</sup>C)HgCl (**1**). Next step involves transmetalation and C–H activation with K[AuCl<sub>4</sub>] in refluxing acetonitrile, following the procedure reported in the literature,<sup>31</sup> to give the corresponding cyclometallated gold(III) chloride (C<sup>N</sup>C)AuCl (**2**) in moderate yield (35%) (Scheme 8).



**Scheme 8.** Synthesis of (C<sup>N</sup>C)AuCl (**2**)

The synthesis of complex **3** was carried out following the experimental procedure reported in the literature.<sup>30</sup> 10 equiv. of CsOH were added to a suspension of complex **2**

in THF/Toluene/Water (1:1:1). The mixture was allowed to stir for 16 hours at 60°C. The mixture was filtered off, to yield a yellow solid. A mixture of dichloromethane/water (1:1) was added. The mixture was allowed to stir overnight at room temperature. The observed precipitate was filtered off and it was washed with petrol ether 40/60, to yield a palid yellow precipitate (Scheme 9).



a. CsOH, THF/toluene/water, 60°C, 16h. b. CH<sub>2</sub>Cl<sub>2</sub>/water, r.t.

**Scheme 9.** Synthesis of (C<sup>N</sup>C)AuOH (3).

The synthesis of the ligands **L**<sup>2</sup>, **L**<sup>3</sup> and **L**<sup>4</sup> has been achieved by reaction of (*L*)-alanine methyl ester hydrochloride, (*L*)-serine methyl ester hydrochloride and glycine ethyl ester hydrochloride, respectively, with 4-ethynylbenzaldehyde and the consequent reduction step employing sodium borohydride,<sup>32</sup> to afford ligands **L**<sup>2</sup>, **L**<sup>3</sup> and **L**<sup>4</sup> (Figure 5).

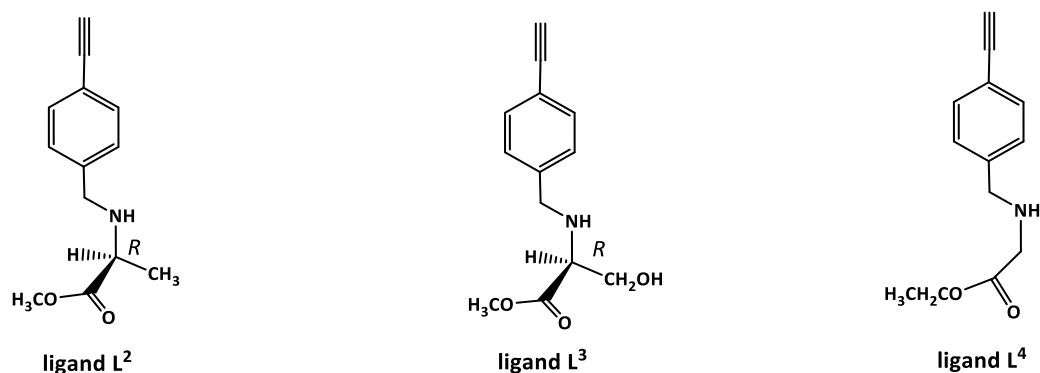
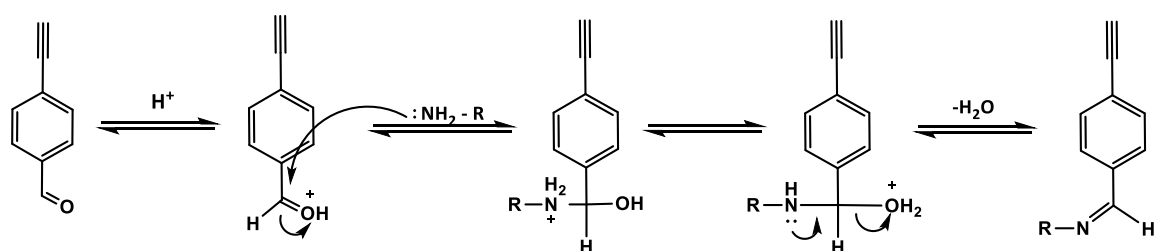


**Figure 5.** Chemical structure of ligands **L**<sup>2</sup> — **L**<sup>4</sup>.

The experiment was carried out in dry dichloromethane, in presence of triethylamine, employing a stoichiometric amount of the amino ester derivatives and anhydrous

MgSO<sub>4</sub> as dehydrating agent. The reaction mixture was allowed to stir for 16 hours at room temperature.



R<sub>1</sub>= -L-Ala-Methyl ester  
 R<sub>2</sub>= -L-Ser-Methyl ester  
 R<sub>3</sub>= -L-Gly-Ethyl ester

**Scheme 10.** Mechanism of imine (Schiff Base) formation.

The formation of the imine derivative (Scheme 10) is an equilibrium reaction. Therefore, the use of dehydrating agent becomes necessary in order to move the equilibrium and promote the formation of the aryl imines.

After 16 hours, an aliquot from the crude of reaction was taken in order to check by <sup>1</sup>H-NMR spectroscopy the reaction progress. Although the <sup>1</sup>H-NMR spectrum showed the aryl imine derivative as the main product, a small percentage of 4-ethynylbenzaldehyde was observed. Identical result was observed after 24 hours. Despite the fact that the reaction had not proceeded quantitatively, the second stage of the reaction was carried out. As it is known, imine derivatives are susceptible to be hydrolysed in presence of water or under acidic conditions. In order to avoid this step and simplify the reaction conditions for the consequent experiments of synthesis of gold(III) complexes, reduction of the -C=N bond to -C-NH was planned. Accordingly, the reaction mixture was filtered off and dichloromethane was removed under vacuum. The residue was dissolved in dry methanol and sodium borohydride was slowly added at 0 °C. After 12 hours, the <sup>1</sup>H-NMR spectrum from the crude reaction showed a mixture of the expected aryl amine derivative and another product, identified as (4-ethynylphenyl)methanol (Figure 6) by comparison with the reported <sup>1</sup>H-NMR spectroscopic data for this

compound.<sup>33</sup> The formation of this product can be explained due to the reduction of the aldehyde function from 4-ethynylbenzaldehyde in presence of sodium borohydride.

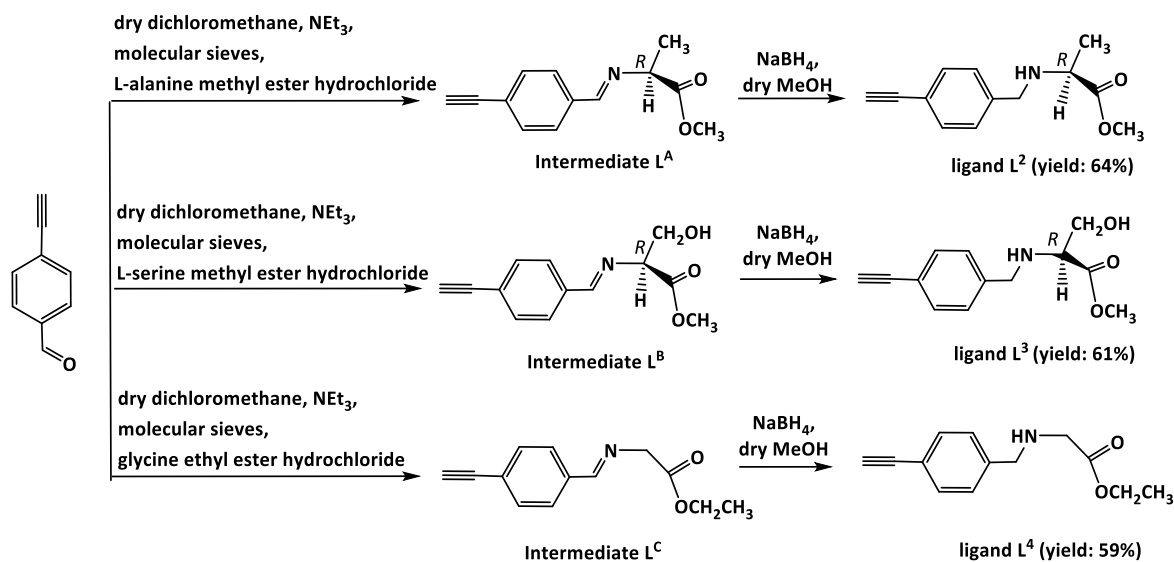


$R_1$ = -L-Ala-Methyl ester  
 $R_2$ = -L-Ser-Methyl ester  
 $R_3$ = -L-Gly-Ethyl ester

**(4-ethynylphenyl) methanol**

**Figure 6.** Products obtained after reduction employing sodium borohydride.

A modification of the synthetic procedure was introduced, in order to drive the reaction to completion. Excess of the starting amino ester derivatives was employed and anhydrous  $MgSO_4$  was replaced by activated molecular sieves, which is known to be a more effective water scavenger. These reaction conditions allowed us to obtain imine intermediates  $L^A$ ,  $L^B$  and  $L^C$  in situ as pure products and the corresponding ligands  $L^2$ ,  $L^3$  and  $L^4$  by reduction employing sodium borohydride as reagent. These ligands were isolated as pale yellow oils in yields over 60% (Scheme 11).



**Scheme 11.** Synthesis of ligands  $\text{L}^2$ — $\text{L}^4$ .

Ligands  $\text{L}^2$ ,  $\text{L}^3$  and  $\text{L}^4$  have demonstrated to be soluble in non-polar solvents, such as chloroform and dichloromethane. In addition these ligands have also exhibited a considerable solubility in protic media, being soluble in ethanol and partially soluble in water.

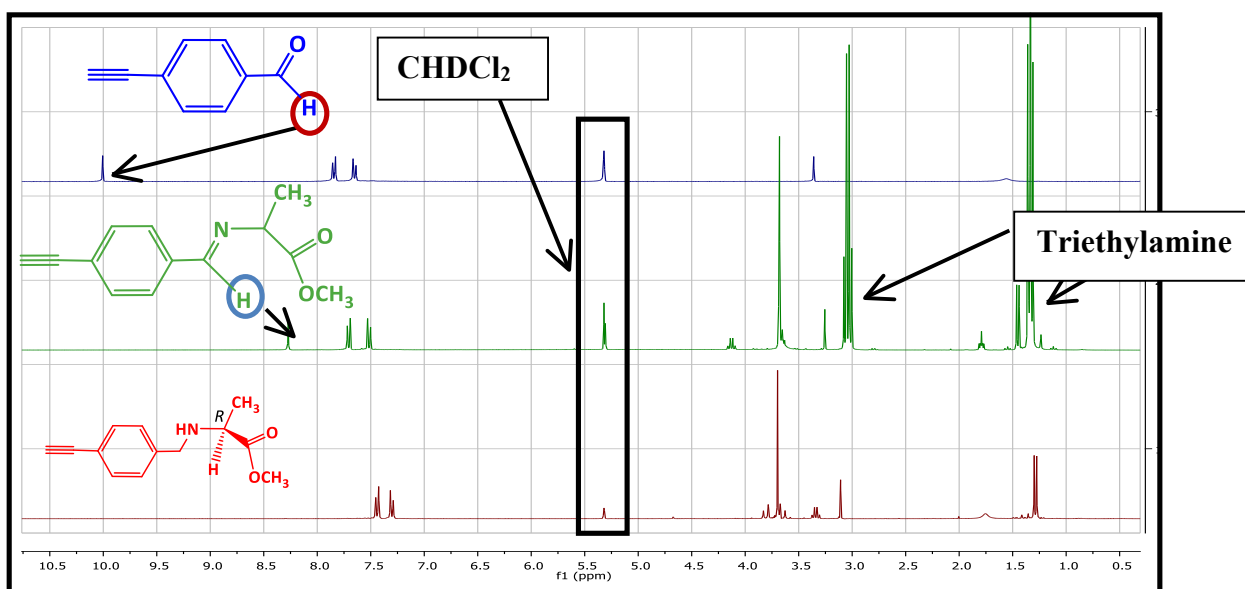
Ligands  $\text{L}^2$  –  $\text{L}^4$  have been characterized by  $^1\text{H}$ -NMR,  $^{13}\text{C}\{^1\text{H}\}$ -NMR and IR spectroscopy.

Ligand  $\text{L}^2$  shows a weak band at  $2105\text{ cm}^{-1}$  in the stretch of  $\text{C}\equiv\text{C}$  and a strong band at  $1732\text{ cm}^{-1}$  corresponding to the vibration mode of  $\text{C}=\text{O}$  from the ester function. Ligands  $\text{L}^3$  and  $\text{L}^4$  show IR absorption bands of similar intensity and located in the same region than the observed ones for ligand  $\text{L}^2$ .

The chemical shifts corresponding to  $^1\text{H}$ -NMR spectrum for ligand  $\text{L}^2$  in  $\text{CDCl}_3$  at room temperature are recorded in Table 1.

**Table 1.**  $^1\text{H-NMR}$  data of ligand  $\text{L}^2$  in  $\text{CD}_2\text{Cl}_2$ ,  $\delta(\text{ppm})$  and multiplicity.

LIGAND $\text{L}^2$	ASSIGNMENT	$^1\text{H}$ (ppm)
	a	1.37 (d, $J = 7.0$ Hz, 3H)
	b	2.76 (s, 1H)
	c	3.17 (q, $J = 7.0$ Hz, 1H)
	d, e	3.65 (d, $J = 13.5$ , 1H), 3.81 (d, $J = 13.5$ , 1H)
	f	3.31 (s, 3H)
	g, h	7.32 (d, $J = 8.3$ Hz, 2H), 7.43 (d, $J = 8.3$ Hz, 2H)

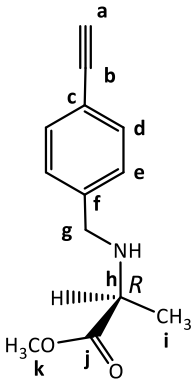


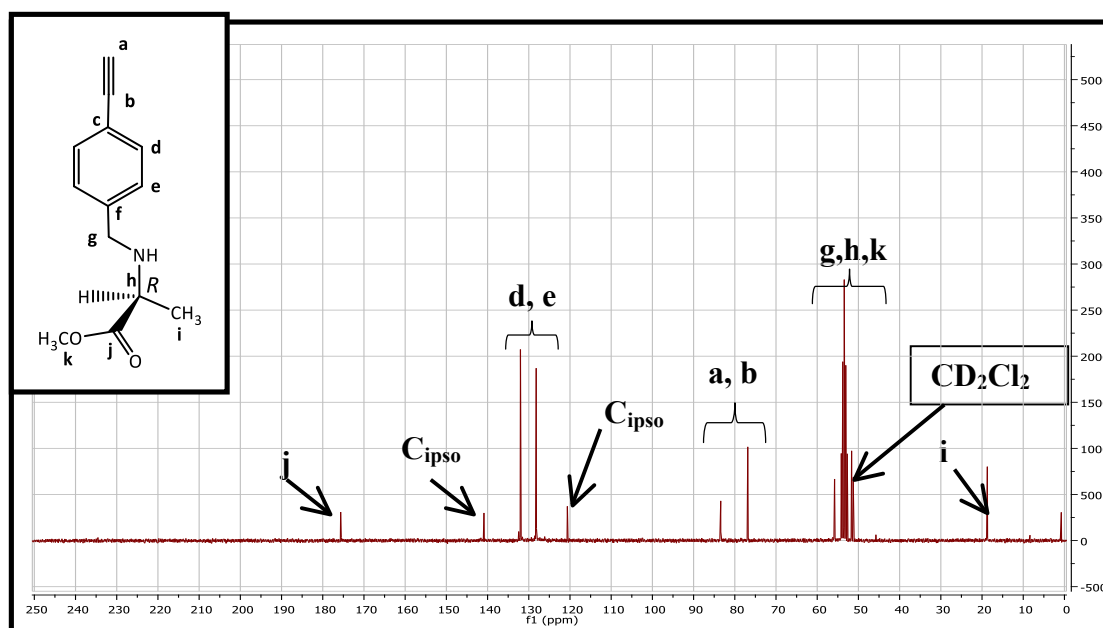
**Figure 7:** Comparison between  $^1\text{H-NMR}$  spectrum of ligand  $\text{L}^2$  (red spectrum), 4-ethynylbenzaldehyde (blue spectrum) and Intermediate  $\text{L}^A$  (green spectrum) in  $\text{CD}_2\text{Cl}_2$ . Figure 7 shows the reaction progress through a comparison between  $^1\text{H-NMR}$  spectrum of 4-ethynylbenzaldehyde (blue spectrum), intermediate  $\text{L}^A$  (green spectrum) and ligand  $\text{L}^2$  (red spectrum). Both the absence of the singlet signal corresponding to the aldehyde function (red circle) and the presence of a new singlet signal at  $\delta$  8.29 (blue

circle) indicate the formation of the imine group of intermediate  $L^A$ . The addition of sodium borohydride led the reduction of C=N bond to –C–NH and formation of pro-ligand  $L^2$ .

The chemical shifts corresponding to  $^{13}C\{^1H\}$ -NMR spectrum of pro-ligand  $L^2$  in  $CD_2Cl_2$  at room temperature have been recorded in Table 2.

**Table 2:**  $^{13}C\{^1H\}$ -NMR data of ligand  $L^2$  in  $CD_2Cl_2$  ( $\delta$ (ppm)).

LIGAND $L^2$	ASSIGNMENT	$^1H$ (ppm)
	i	18.7
	g, h, k	51.3, 51.7, 55.8
	a, b	73.9, 83.4
	Aromatic region	120.6 ( $C_{ipso}$ , c or f), 128.2 (d or e), 132.0 (d or e), 132.4 ( $C_{ipso}$ , c or f)
	j	175.6

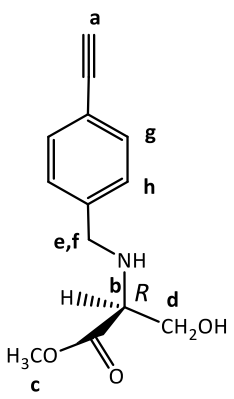


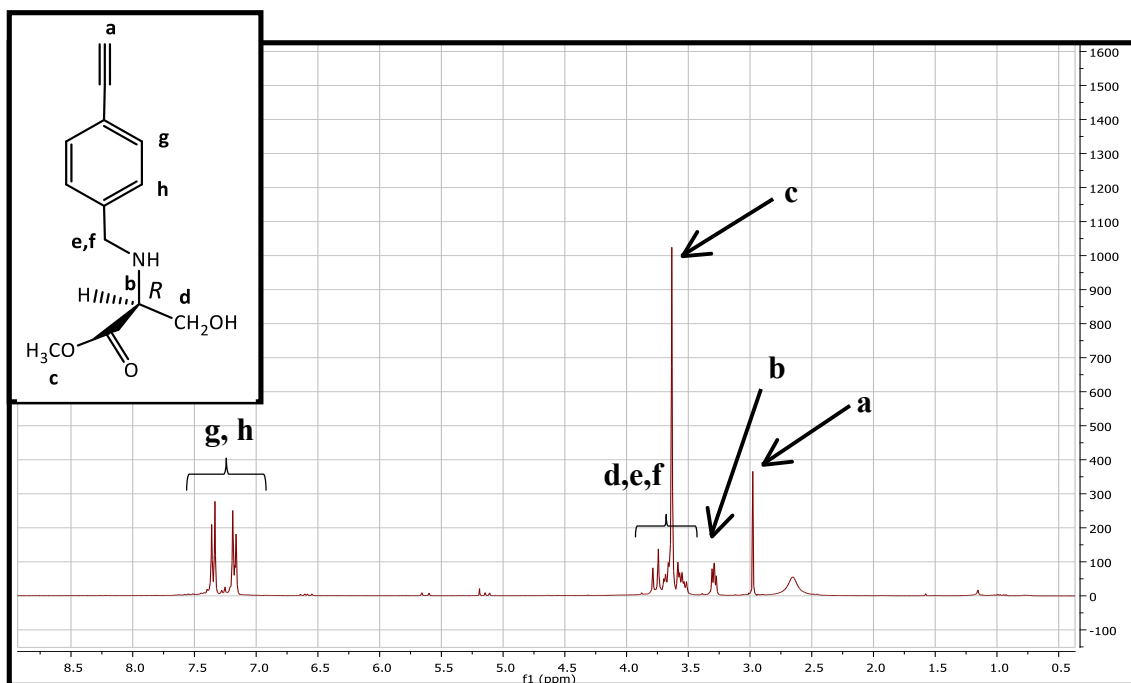
**Figure 8:**  $^{13}C$  NMR spectrum of ligand  $L^2$  in  $CD_2Cl_2$ .

As it is shown in Figure 8, the  $^{13}\text{C}$  NMR spectrum of ligand  $\text{L}^2$  in  $\text{CD}_2\text{Cl}_2$  exhibits a signal at  $\delta$  175.6 corresponding to the carbon atom of  $\text{C}=\text{O}$  group from the ester function (f). The signal corresponding to an aldehyde group, which would be shown in the region between  $\delta$  190 – 200, is not observed, indicating that the aryl amine derivative has been formed. In addition, two chemical shifts at  $\delta$  73.9 and 83.4 (a and b), corresponding to the alkyne function, were observed on the spectrum.

The chemical shifts corresponding to the  $^1\text{H}$ -NMR spectrum for ligand  $\text{L}^3$  in  $\text{CDCl}_3$  at room temperature are presented in Table 3.

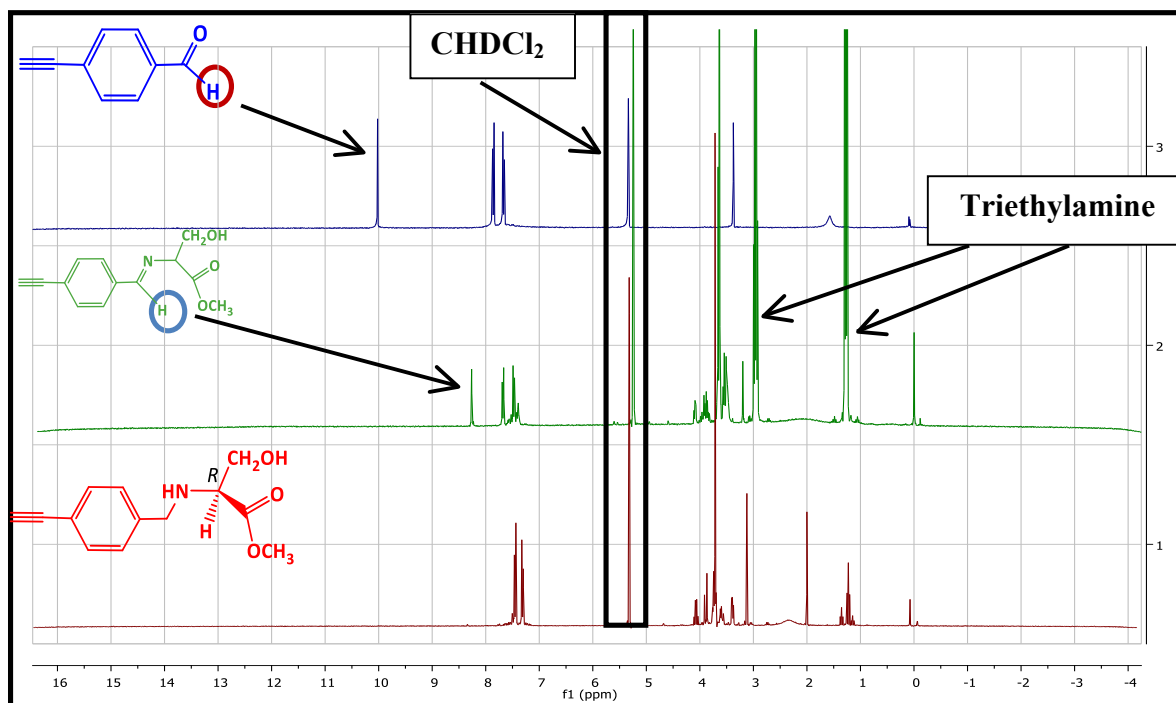
**Table 3.**  $^1\text{H}$ -NMR data of ligand  $\text{L}^3$  in  $\text{CDCl}_3$ ,  $\delta(\text{ppm})$  and multiplicity.

LIGAND $\text{L}^3$	ASSIGNMENT	$^1\text{H}$ (ppm)
	a	3.12 (s, 1H)
	-NH/-OH	2.36(br, s, 2H)
	b	3.29 (q, J = 4.5 Hz, 1H)
	d	3.56-3.62 (m, 2H)
	e, f	3.72 (d, J = 8.1 Hz, 1H), 3.89 (d, J = 8.1 Hz, 1H)
	c	3.63 (s, 3H)
	g, h	7.18 (d, J = 8.1 Hz, 2H), 7.35 (d, J = 8.1 Hz, 2H)



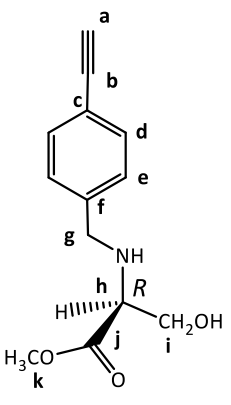
**Figure 9.**  $^1\text{H-NMR}$  spectrum of ligand  $\text{L}^3$  in  $\text{CDCl}_3$ .

As it is shown in Figure 9,  $^1\text{H-NMR}$  spectrum of ligand  $\text{L}^3$  in  $\text{CDCl}_3$  exhibits a singlet signal at  $\delta$  2.98 integrating for one proton corresponding to proton  $\text{H}^a$ . The expected AB system corresponding to  $\text{H}^e$  and  $\text{H}^f$  is overlapped with protons  $\text{H}^d$ , showing as multiplet signal at  $\delta$  3.45 – 3.86. Both the chemical shifts corresponding to  $\text{H}^e$  and  $\text{H}^f$  and the absence of the chemical shift of the aldehyde proton (it would be shown over  $\delta$  10.00) indicate that the amine product has been formed. Regarding the chemical shifts corresponding to the  $-\text{NH}$  and the  $-\text{OH}$  functions, the only signal observed that may correspond with one of them is a broad signal at  $\delta$  2.65 integrating by two protons. As we will check later in the thesis for complex **13** ( $\text{C}^{\wedge}\text{N}$  derivative with ligand  $\text{L}^3$  coordinated to the metallic centre) the addition of a drop of  $\text{D}_2\text{O}$  will suppose the absence of this broad signal for this complex, which prove that it corresponds to the  $-\text{NH}$  or the  $-\text{OH}$  functions.



**Figure 10:** Comparison between  $^1\text{H}$ -NMR spectra of ligand  $\mathbf{L}^3$  (red spectrum), 4-ethynylbenzaldehyde (blue spectrum) and Intermediate  $\mathbf{L}^B$  (green spectrum) in  $\text{CD}_2\text{Cl}_2$ . As it is shown in Figure 10, the  $^1\text{H}$ -NMR spectrum of intermediate  $\mathbf{L}^B$  (green spectrum) does not show any starting material, represented by the absence of the singlet signal corresponding to proton  $-\text{CHO}$  from the aldehyde function (red circle). In addition, a new singlet signal at  $\delta$  8.25, corresponding to the proton from the imine group of intermediate  $\mathbf{L}^B$  was observed (blue circle). The subsequent addition of  $\text{NaBH}_4$  allowed the reduction of  $\text{C}=\text{N}$  bond to  $\text{C}-\text{NH}$  and formation of pro-ligand  $\mathbf{L}^3$ , represented in  $^1\text{H}$ -NMR spectrum of ligand  $\mathbf{L}^3$  (red spectrum) by the absence of the singlet signal at  $\delta$  8.25, previously shown in the  $^1\text{H}$ -NMR spectrum of intermediate  $\mathbf{L}^B$  (green spectrum). The chemical shifts corresponding to the  $^{13}\text{C}\{^1\text{H}\}$ -NMR spectrum of ligand  $\mathbf{L}^3$  in  $\text{CDCl}_3$  at room temperature have been recorded in Table 4.

**Table 4:**  $^{13}\text{C}\{^1\text{H}\}$ -NMR data of ligand  $\text{L}^3$  in  $\text{CDCl}_3$  ( $\delta(\text{ppm})$ ).

LIGAND $\text{L}^3$	ASSIGNMENT	$^1\text{H}$ (ppm)
	k, h	51.7, 52.2
	g, i	61.9, 62.6
	a, b	77.3, 83.5
	Aromatic region	120.1 ( $\text{C}_{\text{ipso}}$ , c or f), 128.2 (d or e), 132.3 (d or e), 139.7 ( $\text{C}_{\text{ipso}}$ , c or f)
	j	173.5

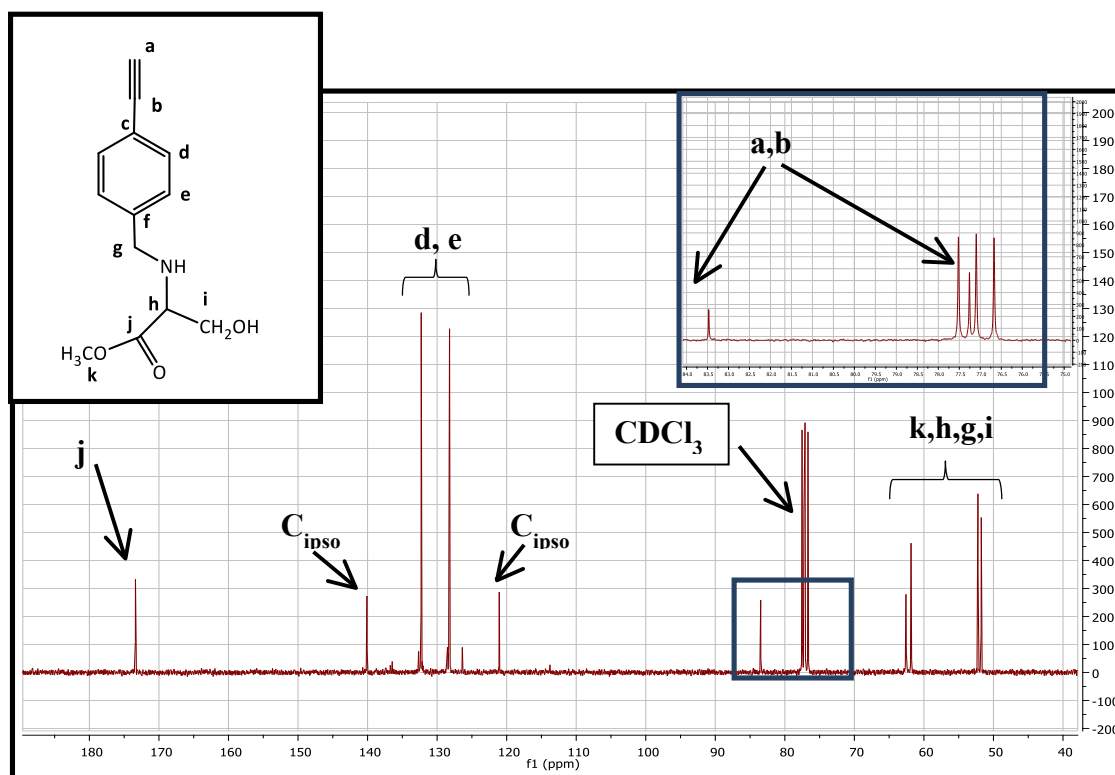


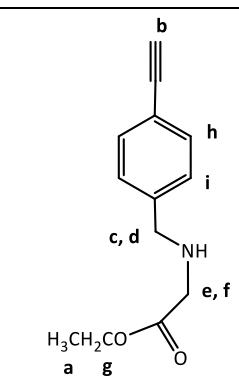
**Figure 11:**  $^{13}\text{C}\{^1\text{H}\}$ -NMR spectrum of ligand  $\text{L}^3$  in  $\text{CDCl}_3$ .

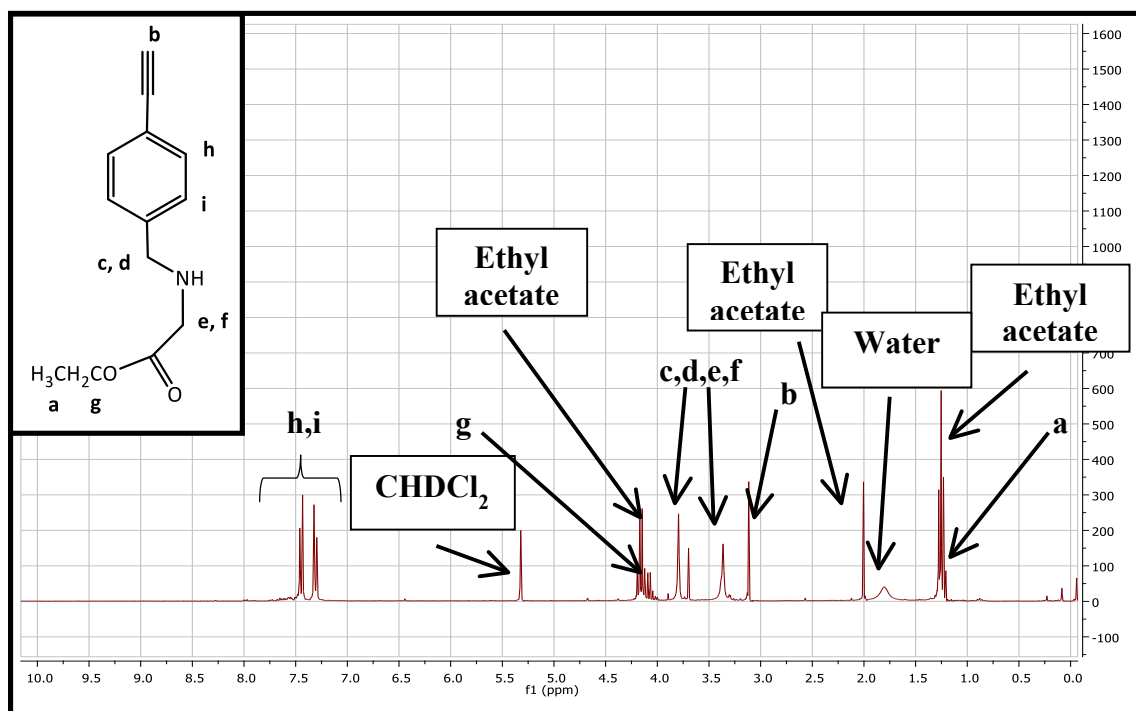
According to Figure 11, the  $^{13}\text{C}\{^1\text{H}\}$ -NMR spectrum of ligand  $\text{L}^3$  in  $\text{CDCl}_3$  shows a signal at  $\delta$  173.5 corresponding to the  $-\text{C}=\text{O}$  function from the ester group. No signal corresponding to the carbon  $-\text{CHO}$  from the aldehyde function was observed, indicating that the condensation product has been formed. In addition, two chemical shifts

corresponding to the carbons from the alkyne group were observed at  $\delta$  73.9 and 83.4, one of these overlapped with the signal corresponding to  $\text{CDCl}_3$ .

The chemical shifts corresponding to the  $^1\text{H}$ -NMR spectrum for ligand  $\text{L}^4$  in  $\text{CD}_2\text{Cl}_2$  at room temperature are recorded in Table 5.

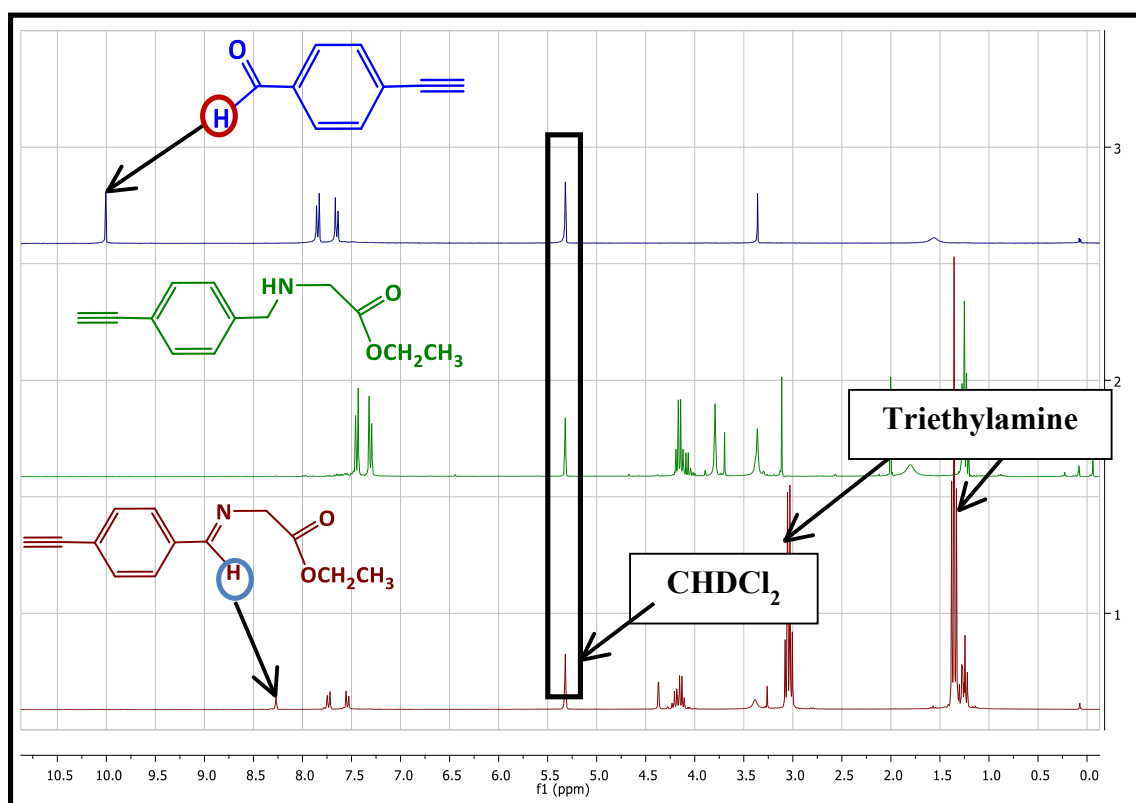
**Table 5.**  $^1\text{H}$ -NMR data of ligand  $\text{L}^4$  in  $\text{C}_2\text{DCl}_2$ ,  $\delta(\text{ppm})$  and multiplicity.

LIGAND $\text{L}^4$	ASSIGNMENT	$^1\text{H}$ (ppm)
	a	1.25 (t, $J = 7.0$ Hz, 3H)
	b	3.11 (s, 1H)
	c,d and e,f	3.36 (bs, 2H), 3.79 (bs, 2H)
	g	3.31 (q, $J = 7.0$ Hz, 2H)
	h,i	7.31 ( $J = 8.1$ Hz, 2H), 7.44 ( $J = 8.1$ Hz, 2H).



**Figure 12:**  $^1\text{H}$ -NMR spectrum of ligand  $\text{L}^4$  in  $\text{CD}_2\text{Cl}_2$ .

Figure 12 shows the  $^1\text{H-NMR}$  spectrum of ligand  $\mathbf{L}^4$  in  $\text{CD}_2\text{Cl}_2$ . The spectrum exhibits a triplet signal at  $\delta$  1.25 and a quartet signal at  $\delta$  4.16 corresponding to protons  $\text{H}^a$  from methyl group and  $\text{H}^g$  from methylene group, respectively. Although the expected integrations of these signals should be three and two protons respectively, it is slightly higher because of the presence of the triethylamine in the sample. The chemical shift corresponding to the proton  $\text{H}^b$  is observed as a singlet signal at  $\delta$  3.11. Protons  $\text{H}^c$ ,  $\text{H}^d$ ,  $\text{H}^e$  and  $\text{H}^f$  are represented as two broad singlet signals at  $\delta$  3.36 and 3.79 integrating for two protons each. Although these protons and the one corresponding to the  $\text{HC}\equiv\text{C}$ -group did not undergo remarkable variations compared to the starting material (Figure 13), the absence of the proton  $-\text{CHO}$  from the aldehyde function is the main indication that the condensation product was achieved. Protons  $\text{H}^h$  and  $\text{H}^i$  from the aromatic ring are represented as an AB system at  $\delta$  7.31 and 7.44.

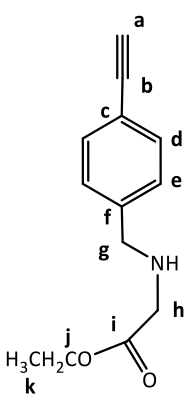


**Figure 13:** Comparison between  $^1\text{H-NMR}$  spectra of ligand  $\mathbf{L}^4$  (green spectrum), 4-ethynylbenzaldehyde (blue spectrum) and Intermediate  $\mathbf{L}^C$  (red spectrum) in  $\text{CD}_2\text{Cl}_2$ .

According to the Figure 13, the comparison between  $^1\text{H}$ -NMR spectra of 4-ethynylbenzaldehyde and intermediate  $\text{L}^{\text{C}}$  shows a new singlet signal at  $\delta$  8.26 integrating for one proton corresponding to the proton of the imine group from intermediate  $\text{L}^{\text{C}}$  (blue circle). Both this chemical shift and the absence of the singlet signal corresponding to the proton  $-\text{CHO}$  from the aldehyde function (red circle) of 4-ethynylbenzaldehyde are indicative that intermediate  $\text{L}^{\text{C}}$  was prepared. The reduction of the  $\text{C}=\text{N}$  bond of intermediate  $\text{L}^{\text{C}}$  to  $\text{C}-\text{NH}$  bond is achieved by addition of sodium borohydride, to afford the formation of ligand  $\text{L}^4$  (green spectrum).

The chemical shifts corresponding to  $^{13}\text{C}\{^1\text{H}\}$ -NMR spectrum of ligand  $\text{L}^4$  in  $\text{CD}_2\text{Cl}_2$  at room temperature have been recorded in Table 6.

**Table 6:**  $^{13}\text{C}\{^1\text{H}\}$ -NMR data of ligand  $\text{L}^4$  in  $\text{CD}_2\text{Cl}_2$  ( $\delta(\text{ppm})$ ).

LIGAND $\text{L}^4$	ASSIGNMENT	$^1\text{H}$ (ppm)
	k	14.3
	g, h	50.4, 52.0
	j	61.0
	a, b	77.2, 83.8
	Aromatic region	121.0 ( $\text{C}_{\text{ipso}}$ , c or f), 128.5 (d or e), 132.2 (d or e), 141.5 ( $\text{C}_{\text{ipso}}$ , c or f)
	i	172.6

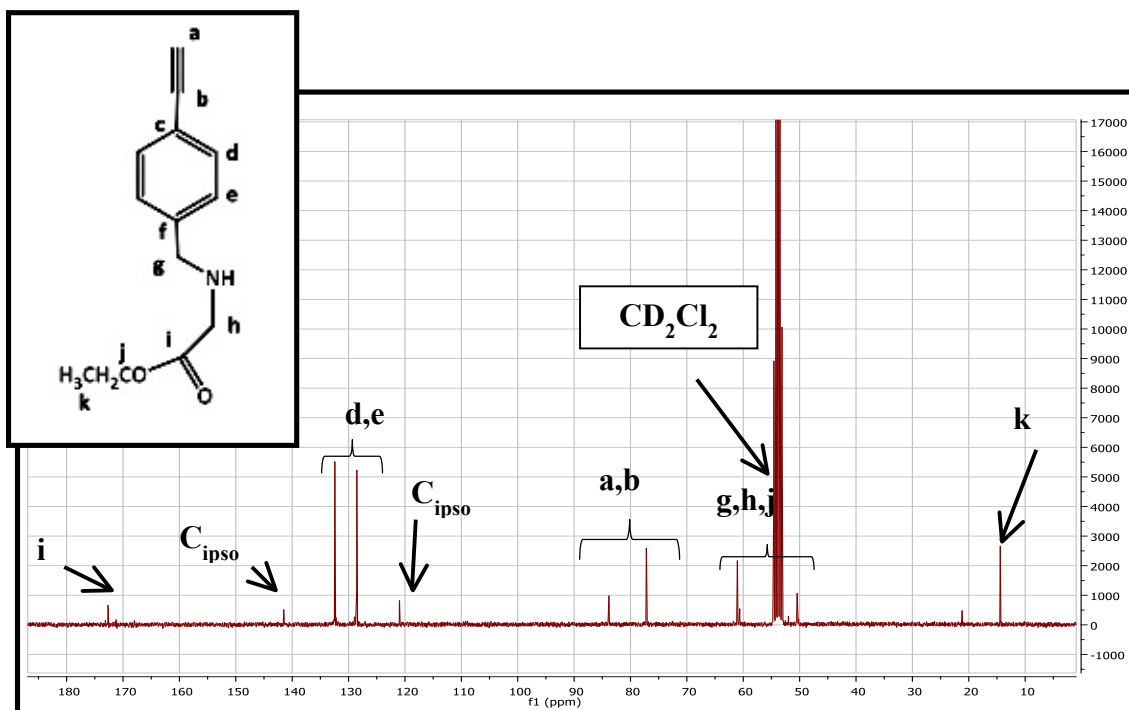


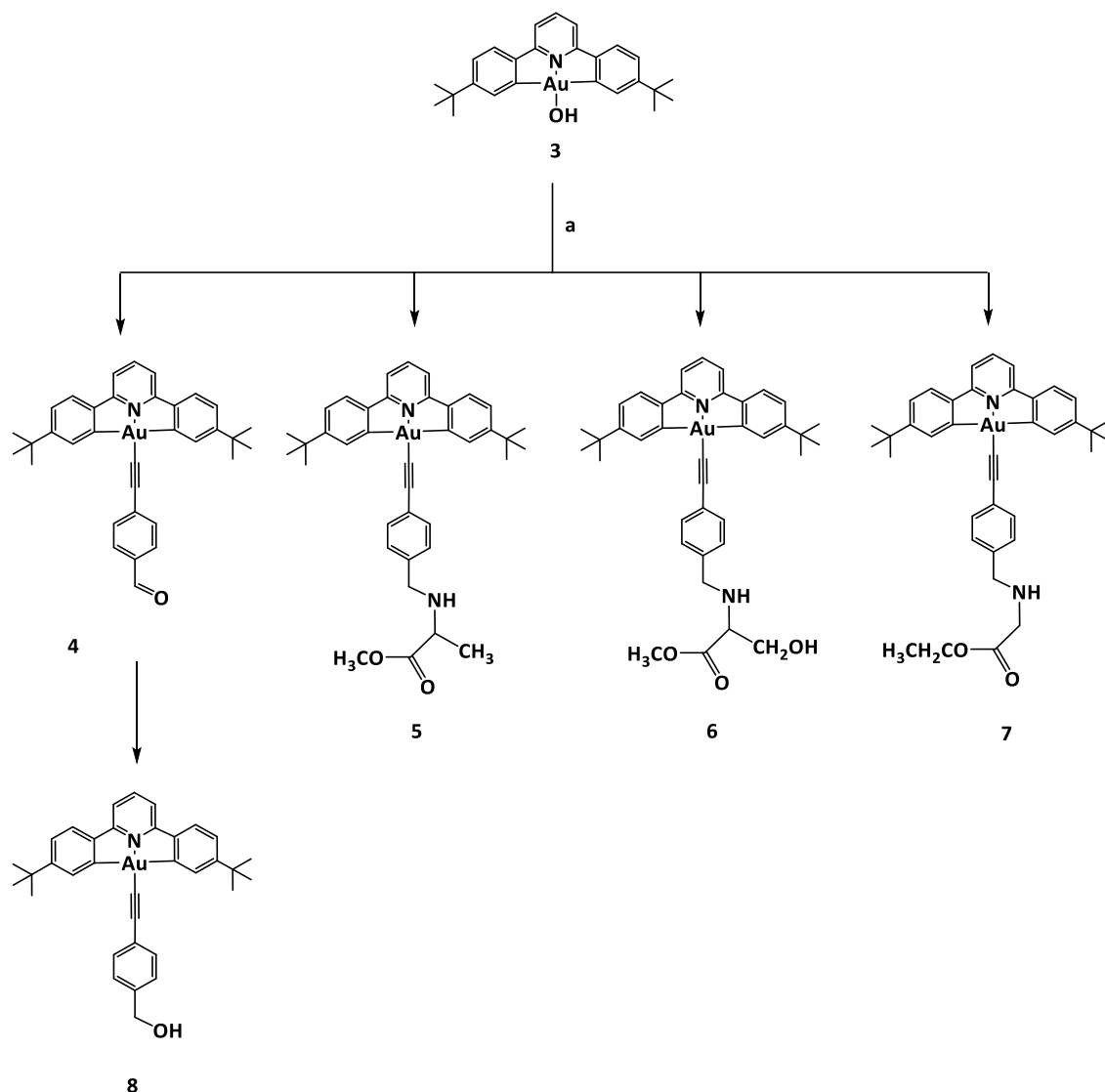
Figure 14:  $^{13}\text{C}\{^1\text{H}\}$ -NMR spectrum of ligand **4** in  $\text{CD}_2\text{Cl}_2$ .

The  $^{13}\text{C}\{^1\text{H}\}$ -NMR spectrum of ligand **L**<sup>4</sup> in  $\text{CD}_2\text{Cl}_2$  shows a weak signal  $\delta$  172.6 corresponding to the  $-\text{C}=\text{O}$  group from the ester function. The absence of the signal corresponding to the carbon  $-\text{CHO}$  from the aldehyde function indicates that pro-ligand **L**<sup>4</sup> has been formed.

#### 1.2.1.2. Synthesis of complexes.

We focused on the synthesis of bi- and tri-dentate gold(III) complexes functionalized by alkynyl derivatives. The incorporation of alkynyl ligands into the cyclometalated gold(III) moiety has been achieved by two methodologies. In *method a*, the reaction of  $(\text{C}^{\wedge}\text{N}^{\wedge}\text{C})\text{AuOH}$  (**3**) with the alkynyl derivative allowed the formation of the  $[(\text{C}^{\wedge}\text{N}^{\wedge}\text{C})\text{AuC}\equiv\text{CR}]$  derivatives. In *method c*, a reaction mixture of the chlorogold(III) precursor  $(\text{C}^{\wedge}\text{N}^{\wedge}\text{C})\text{AuCl}$  (**2**), the alkynyl ligand, triethylamine, and a catalytic amount of copper(I) iodide led to the formation of the  $[(\text{C}^{\wedge}\text{N}^{\wedge}\text{C})\text{AuC}\equiv\text{CR}]$  derivatives.<sup>16</sup>

According to *method a*, the reaction of the (C<sup>^</sup>N<sup>^</sup>C)AuOH (**3**) with 4-ethynylbenzaldehyde and the previously synthesized *N*-1-ethynylbenzyl methyl ester of (L)-alanine (ligand **L**<sup>2</sup>), *N*-1-ethynylbenzyl methyl ester of (L)-serine (ligand **L**<sup>3</sup>) and *N*-1-ethynylbenzyl ethyl ester of glycine (ligand **L**<sup>4</sup>) was studied. The corresponding alkynyl derivative was added to a solution of (C<sup>^</sup>N<sup>^</sup>C)AuOH in toluene. The mixture was allowed to stir for 24 hours under reflux, to afford the complexes **5**, **6**, **7** and **8**, respectively, as yellow solids in moderated yields, over 50 % (Scheme 12). In this method, the use of high temperatures became necessary in order to activate the Au–OH bond. In addition, although a water molecule was also obtained in these reactions, no reversible steps were observed, and the addition of any dehydrating agent was not needed.



24—48 hours, toluene, reflux. **a**: 4-ethynylbenzaldehyde (yield : 75 %) (**4**), *N*-1-ethynylbenzyl methyl ester of (L)-alanine (yield : 32 %) (**5**), (L)-serine (yield : 45 %) (**6**), glycine (yield : 40 %) (**7**). 4-ethynylbenzaldehyde, sodium borohydride, 2 hours, methanol, 0°C (**8**) (yield : 63.5 %).

**Scheme 12.** *Synthesis of tri-dentate gold(III) complexes functionalized with alkynyl derivatives.*

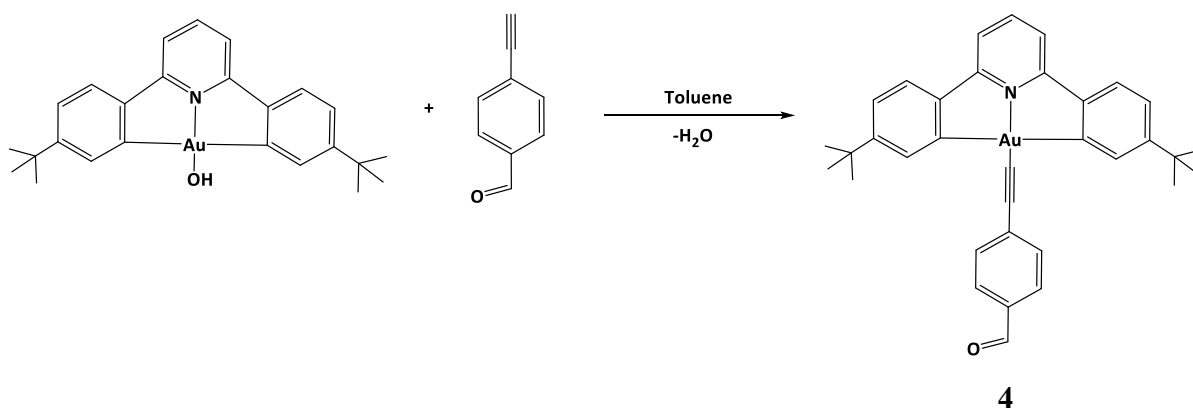
Complexes **4—8** were soluble in non-polar solvents, such as toluene, dichloromethane and chloroform. As we will explain during this thesis, the synthesis of these complexes was also checked by the copper method (*method c*), using the chlorogold precursor (C<sup>^</sup>N<sup>^</sup>C)AuCl (**2**) as starting material. In this experiment, it was possible to observe the

remarkable change in solubility in protic media when the alkynyl ligand was introduced, compared to the starting material. In contrast to (C<sup>^N^C</sup>)AuCl (**2**), complexes **4** – **8** exhibited high solubility in protic solvents. This feature was a useful tool in order to isolate these complexes as pure products by extraction with ethanol, when the reaction was unfinished and (C<sup>^N^C</sup>)AuCl (**2**) was still in the reaction medium.

In addition, these complexes are air and moisture stable, showing partial reductive elimination to gold(0) in solution after one week.

#### 1.2.1.2.1. Synthesis of (C<sup>^N^C</sup>)Au–C≡C–C<sub>6</sub>H<sub>4</sub>–4–CHO (**4**).

The reaction of 1-ethynylbenzaldehyde and (C<sup>^N^C</sup>)AuOH (**3**) (2:1 ratio) in refluxed toluene for 24 hours gives the formation of complex **4** (75%). Complex **4** is a yellow solid, air stable, soluble in toluene and dichloromethane and not soluble in petrol ether 40/60 (Scheme 13).



**Scheme 13.** *Synthesis of complex 4.*

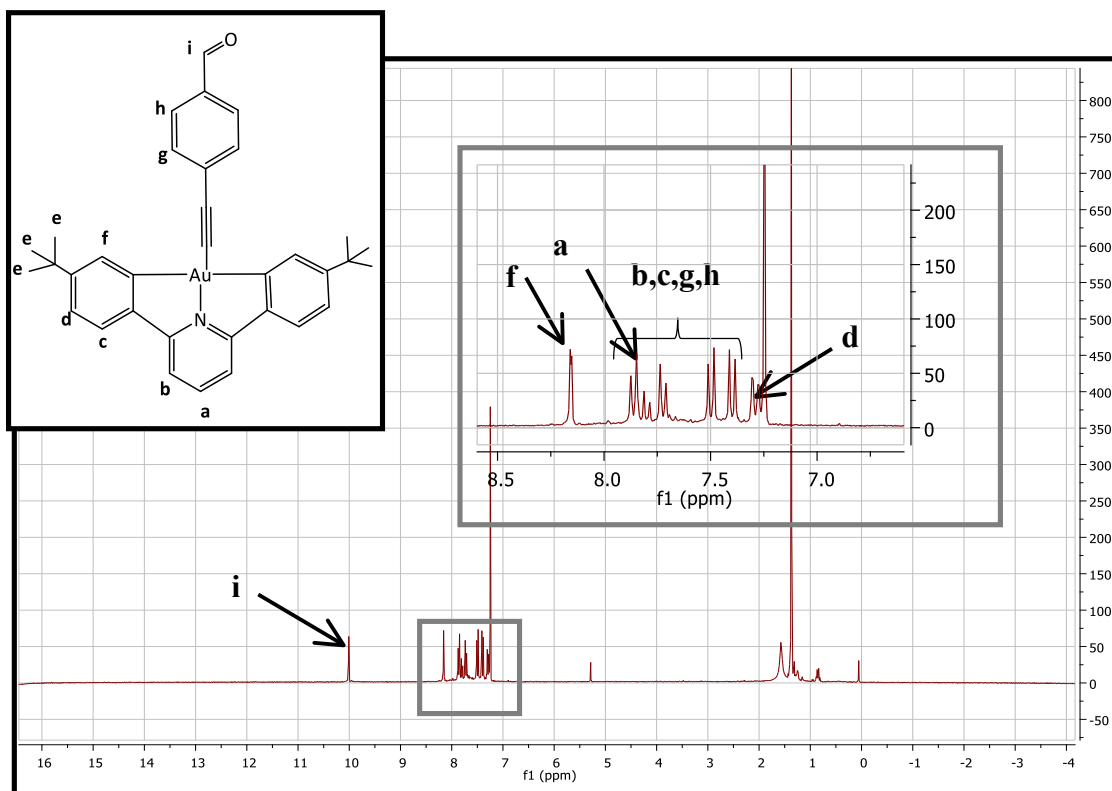
Complex **4** was characterized by <sup>1</sup>H–NMR, <sup>13</sup>C{<sup>1</sup>H}–NMR, IR spectroscopy and elemental analysis.

The IR spectrum for complex **4** shows a strong absorption peak at 1595 cm<sup>-1</sup> corresponding to the aldehyde C=O stretch, and a weak absorption band at 2149 cm<sup>-1</sup>, corresponding to the stretch of the C≡C bond of the di-substituted alkyne group.<sup>11,16</sup>

The chemical shifts corresponding to  $^1\text{H}$ -NMR spectrum for complex **4** in  $\text{CDCl}_3$  at room temperature are recorded in Table 7.

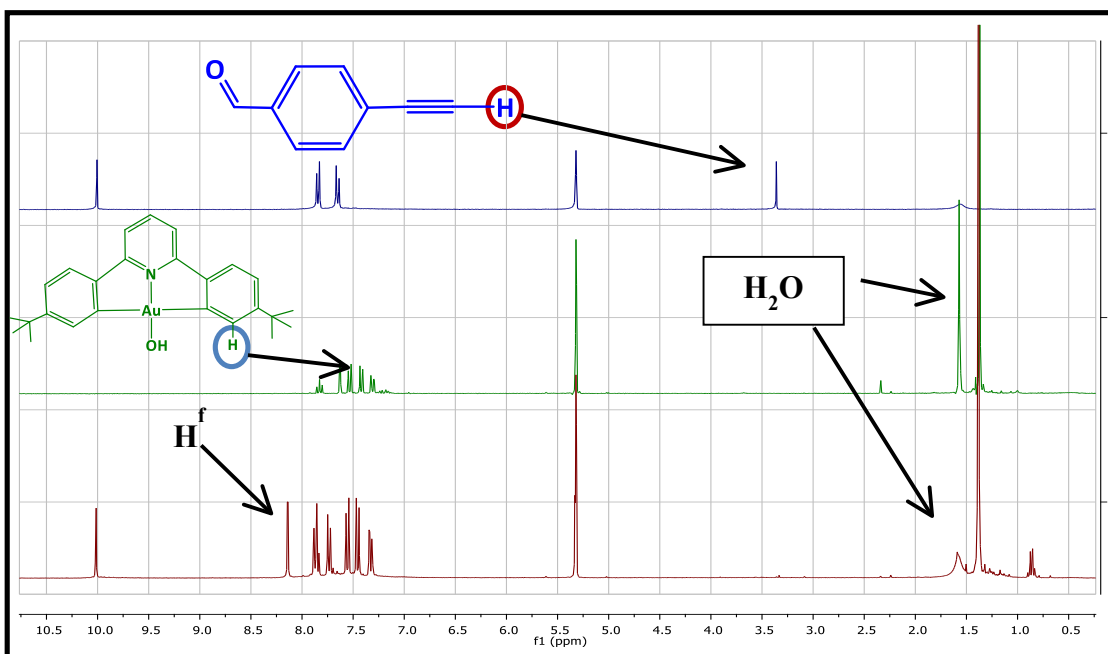
**Table 7:**  $^1\text{H}$ -NMR data of complex **4** in  $\text{CDCl}_3$ ,  $\delta(\text{ppm})$  and multiplicity.

COMPLEX 4	ASSIGNMENT	$^1\text{H}$ (ppm)
	e	1.37 (s, 18H)
	$\text{H}_2\text{O}$	1.56 (br, s)
	d	7.32 – 7.26 (m, 2H)
	b,c	7.40 (d, $J = 8.0$ Hz, 2H), 7.50 (d, $J = 8.0$ Hz, 2H)
	g,h	7.86 (d, $J = 8.1$ Hz, 2H), 7.72 (d, $J = 8.1$ Hz, 2H)
	a	7.80 (t, $J = 7.9$ Hz, 1H)
	f	8.16 (d, $J = 1.8$ Hz, 2H)
	i	10.01 (s, 1H)



**Figure 15:**  $^1\text{H-NMR}$  spectrum of complex **4** in  $\text{CDCl}_3$ .

As is shown in Figure 15, the  $^1\text{H-NMR}$  spectrum exhibits a singlet signal at  $\delta$  1.37 corresponding to protons  $\text{H}^e$  from the *tert*-butyl groups. Regarding the aromatic region, proton  $\text{H}^f$  is shown as a doublet signal at  $\delta$  8.16, as is coupled to  $\text{H}^d$ . This fact has been also observed in complexes **5** – **8**. In addition, this signal provided the most considerable proof that complex **4** was synthesized. The remarkable shift exhibited by this signal compared to the precursor  $(\text{C}^{\wedge}\text{N}^{\wedge}\text{C})\text{AuOH}$  (**3**) represented the main indication that complex **4** had been formed (Figure 16). The chemical shifts corresponding to the aromatic ring from the 4-ethynylbenzaldehyde bonded to the gold metallic centre are observed as an AB system at  $\delta$  7.72 and 7.86 integrating for four protons ( $\text{H}^g$  and  $\text{H}^h$ ). The proton  $\text{H}^i$  from the aldehyde function of the 4-ethynylbenzaldehyde bonded to the metallic centre is shown as a singlet signal at  $\delta$  10.01. These chemical shifts did not undergo remarkable variations compared to the ones showed by the free ligand 4-ethynylbenzaldehyde (Figure 16).

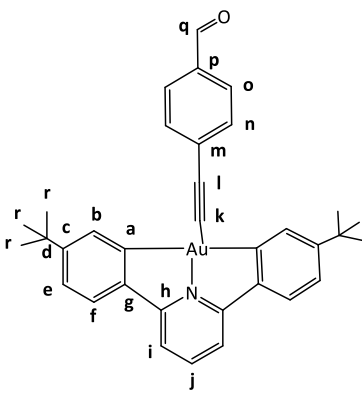


**Figure 16:** Comparison between  $^1\text{H}$ -NMR spectrum of complex **4** (red spectrum),  $(\text{C}^{\wedge}\text{N}^{\wedge}\text{C})\text{AuOH}$  (green spectrum) and 4-ethynylbenzaldehyde (blue spectrum) in  $\text{CD}_2\text{Cl}_2$ .

According to Figure 16, proton  $\text{H}^{\text{f}}$  (doublet signal at  $\delta$  8.16) is shifted with respect to the corresponding proton from the  $(\text{C}^{\wedge}\text{N}^{\wedge}\text{C})\text{AuOH}$ , that is shown as a doublet signal at  $\delta$  7.65 (**blue circle**). This shift and the absence of the singlet signal corresponding to the proton from the alkynyl functional group of 4-ethynylbenzaldehyde (**red circle**), indicate that complex **4** (red spectrum) has been synthesized, through the coordination of one 4-ethynylbenzaldehyde molecule to the metal centre.

The chemical shifts corresponding to  $^{13}\text{C}\{^1\text{H}\}$ -NMR spectrum of complex **4** in  $\text{CDCl}_3$  at room temperature have been recorded in Table 8.

**Table 8:**  $^{13}\text{C}\{^1\text{H}\}$ -NMR data of complex **4** in  $\text{CDCl}_3$  ( $\delta(\text{ppm})$ ).

COMPLEX 4	ASSIGNMENT	$^{13}\text{C}$ (ppm)
	r	31.2
	d	35.0
	k, l	100.9 (weak signals. One of the carbon atoms from this group is not shown)
	Aromatic region	116.1 (i), 123.9 (e), 125.0 (f), 129.7 (n or o), 132.2 (a), 133.5 (n or o), 134.4 ( $\text{C}_{\text{ipso}}$ , m or p) 142.2 (g), 146.3 (j), 155.5 (c), 165.0 (h), 166.9 (a)
	q	191.8

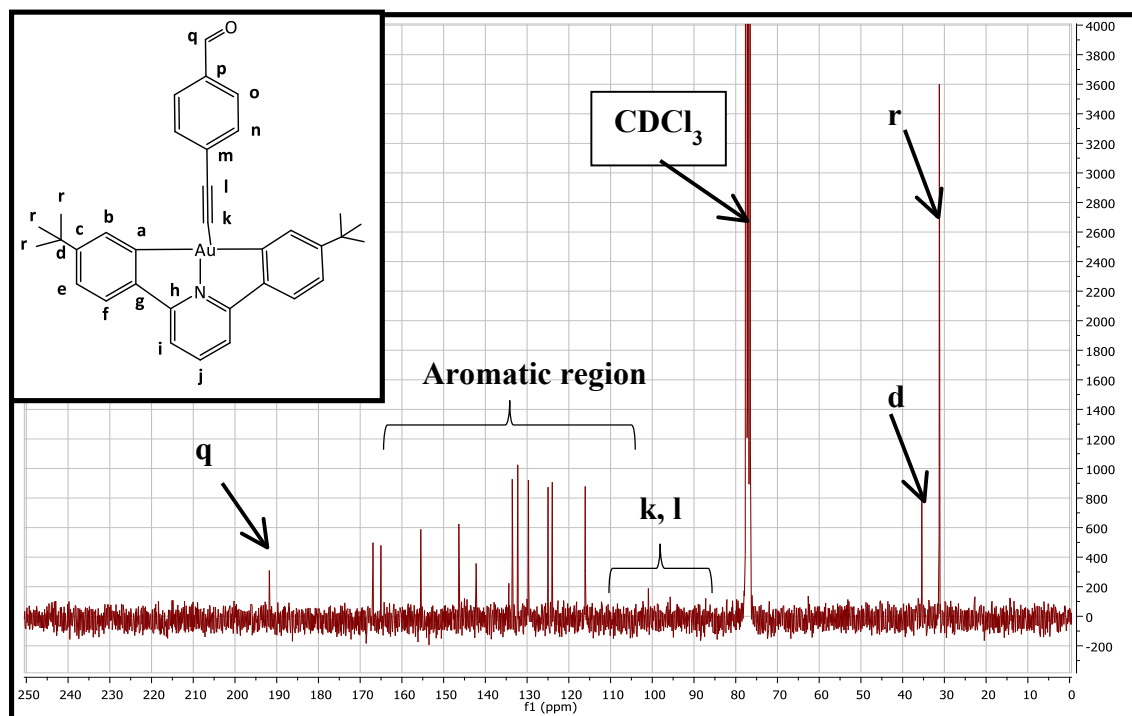


**Figure 17:**  $^{13}\text{C}\{^1\text{H}\}$ -NMR spectrum of complex **4** in  $\text{CDCl}_3$ .

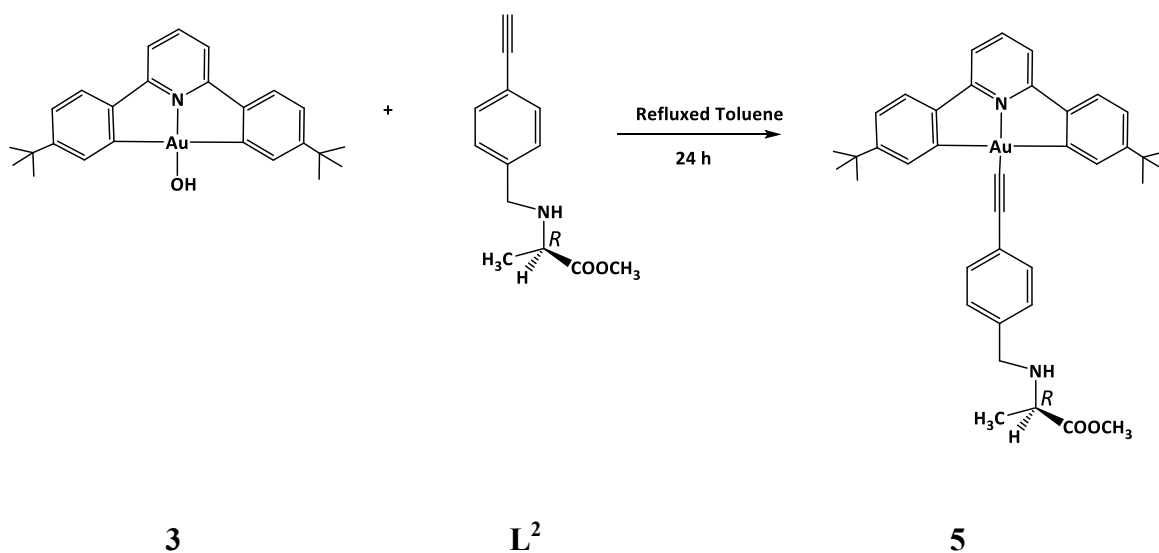
The  $^{13}\text{C}\{^1\text{H}\}$ -NMR spectrum of complex **4** shows a chemical shift at  $\delta$  191.8 corresponding to the carbon atom of  $-\text{C}=\text{O}$  group from the aldehyde function of the 4-

ethynylbenzaldehyde molecule coordinated to the metal centre. The signals corresponding to the carbons of the alkyne group are observed as weak signals at  $\delta$  100.9. One of the carbon atoms from this group is not shown in the spectrum. These signals are shifted compared to the ones reported in the literature for the carbon atoms of the alkyne group of 4-ethynylbenzaldehyde ( $\delta$  81.02, 82.09).<sup>34</sup>

#### 1.2.1.2.2. Synthesis of $(C^{\wedge}N^{\wedge}C)Au-C\equiv C-C_6H_4-4-[CH_2-NH-CH(CH_3)-COOCH_3]$

(5)

The reaction of 1-ethynyl-4-benzyl-L-alanine methyl ester ( $L^2$ ) and  $(C^{\wedge}N^{\wedge}C)AuOH$  (**3**) (2:1 ratio) in refluxed toluene for 24 hours gives complex **5** as a yellow solid (32%). Complex **5** is air stable, soluble in toluene, dichloromethane and ethanol, and insoluble in petrol ether (40/60) (Scheme 14).



**Scheme 14.** Synthesis of complex **5**.

Complex **5** has been characterized by  $^1H$ -NMR,  $^{13}C\{^1H\}$ -NMR, IR spectroscopy, elemental analysis and X-Ray diffraction.

The IR spectrum shows a weak absorption band at  $2151\text{ cm}^{-1}$ , corresponding to the  $C\equiv C$  stretch of the di-substituted alkyne.<sup>11,16</sup>

The  $^1\text{H-NMR}$  chemical shifts of **5** are recorded on Table 9.

**Table 9:**  $^1\text{H-NMR}$  data of complex **5** ( $\text{CD}_2\text{Cl}_2$ , RT)  $\delta(\text{ppm})$  and multiplicity.

COMPLEX 5	ASSIGNMENT	$^1\text{H}$ (ppm)
	k	1.32 (d, J = 7.0 Hz, 3H)
	e	1.39 (s, 18H)
	j	3.40 (q, J = 7.0 Hz, 1H)
	i	3.68 (d, J = 13.2 Hz, 1H), 3.81 (d, J = 13.2 Hz, 1H).
	l	3.72 (s, 3H)
	d	7.32 (d, J = 7.0 Hz, 2H)
	b,c,g,h (overlapped)	7.32 (d, J = 8.1 Hz, 2H), 7.46 (d, J = 8.1 Hz, 2H), 7.55 (d, J = 8.0 Hz, 4H)
	a	7.85 (t, J = 8.0 Hz, 1H)
f	8.18 (d, J = 2.0 Hz, 2H)	

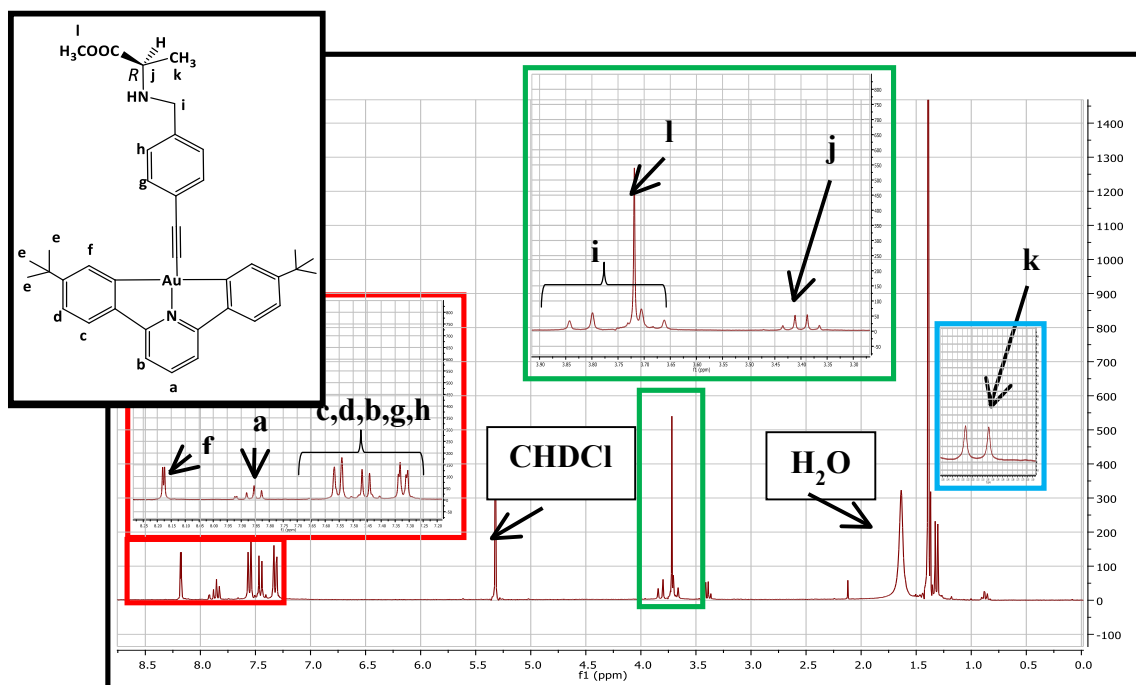


**Figure 18:**  $^1\text{H-NMR}$  spectrum of complex **5** in  $\text{CD}_2\text{Cl}_2$ .

Figure 18 shows a doublet signal at  $\delta$  1.32 associated to the protons  $\text{H}^k$  corresponding to the methyl group bonded to the carbon  $\alpha$  of the 1-ethynyl-4-benzyl-L-alanine methyl ester molecule bonded to the metallic centre. Proton  $\text{H}^l$ , corresponding to the methyl group from the ester function of the 1-ethynyl-4-benzyl-L-alanine methyl ester molecule bonded to the metallic centre, is shown as a singlet signal at  $\delta$  3.72. This signal is shown in the same region as the AB system associated to the protons  $\text{H}^i$  ( $\delta$  3.68–3.81). Regarding the aromatic region, proton  $\text{H}^f$  (doublet signal at  $\delta$  8.18) represents the main indicator that complex **5** has been synthesized, due to the considerable variation exhibited compared to the same proton from the precursor  $(\text{C}^{\wedge}\text{N}^{\wedge}\text{C})\text{AuOH}$  (Figure 18).  $\text{H}^f$  is shown as a doublet signal due to its coupling to  $\text{H}^d$ . The chemical shifts corresponding to the aromatic ring of 1-ethynyl-4-benzyl-L-alanine methyl ester molecule bonded to the metal centre are observed as an AB system at  $\delta$  7.45 and 7.55 integrating by four protons ( $\text{H}^g$  and  $\text{H}^h$ ). These signals exhibited a slight variation compared to the free ligand 1-ethynyl-4-benzyl-L-alanine methyl ester ( $\delta$  7.32 and 7.43, Table 1).

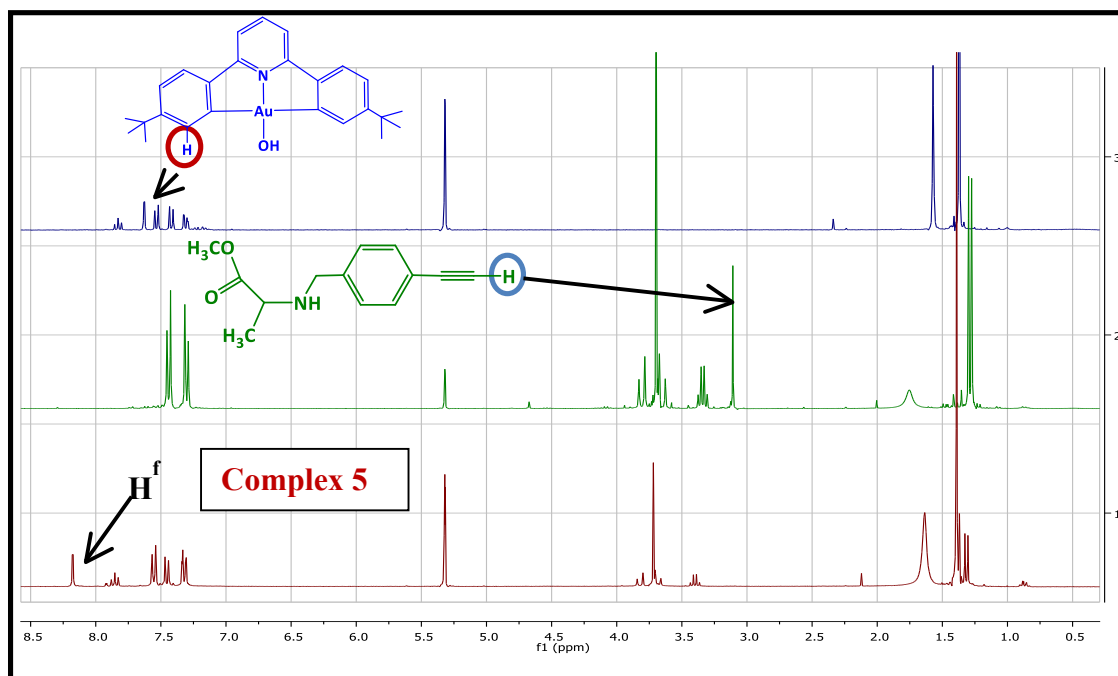


**Figure 19:** Comparison between  $^1\text{H}$ -NMR spectra of complex **6** (red),  $(\text{C}^{\wedge}\text{N}^{\wedge}\text{C})\text{AuOH}$  (blue) and 1-ethynyl-4-benzyl-L-alanine methyl ester in  $\text{CD}_2\text{Cl}_2$ .

As is shown in Figure 19, the  $^1\text{H}$ -NMR spectrum of complex **5** does not show the singlet signal corresponding to the proton from the alkynyl functional group of the 1-ethynyl-4-benzyl-L-alanine methyl ester molecule (green spectrum, **blue circle**), which indicates the coordination of this molecule to the gold atom. In addition, the shift showed by  $\text{H}^f$  ( $\delta$  8.18) regarding the same proton from  $(\text{C}^{\wedge}\text{N}^{\wedge}\text{C})\text{AuOH}$  ( $\delta$  7.65, **red circle**) indicates that Au-C bond has been formed, to afford the complex **5** (red spectrum).

The chemical shifts corresponding to  $^{13}\text{C}\{^1\text{H}\}$ -NMR spectrum of complex **5** in  $\text{CD}_2\text{Cl}_2$  at room temperature have been recorded on Table 10.

**Table 10:**  $^{13}\text{C}\{^1\text{H}\}$ -NMR data of complex **5** in  $\text{CD}_2\text{Cl}_2$  ( $\delta(\text{ppm})$ ).

COMPLEX 5	ASSIGNMENT	$^{13}\text{C}$ (ppm)
	s	18.9
	v	30.9
	d	35.2
	u, q	51.5, 51.6
	r	56.2
	k, l	91.9, 100.9 (weak signals)
	Aromatic region	116.2 (i), 123.8 (e), 124.9 (f), 125.3 ( $\text{C}_{\text{ipso}}$ , m or p), 128.0 (n or o), 131.7 (b), 133.3 (n or o), 139.1 ( $\text{C}_{\text{ipso}}$ , m or p), 142.2 (g), 146.6 (j), 155.2 (c), 164.8 (h), 166.9 (a)
	t	175.9 (weak signal)

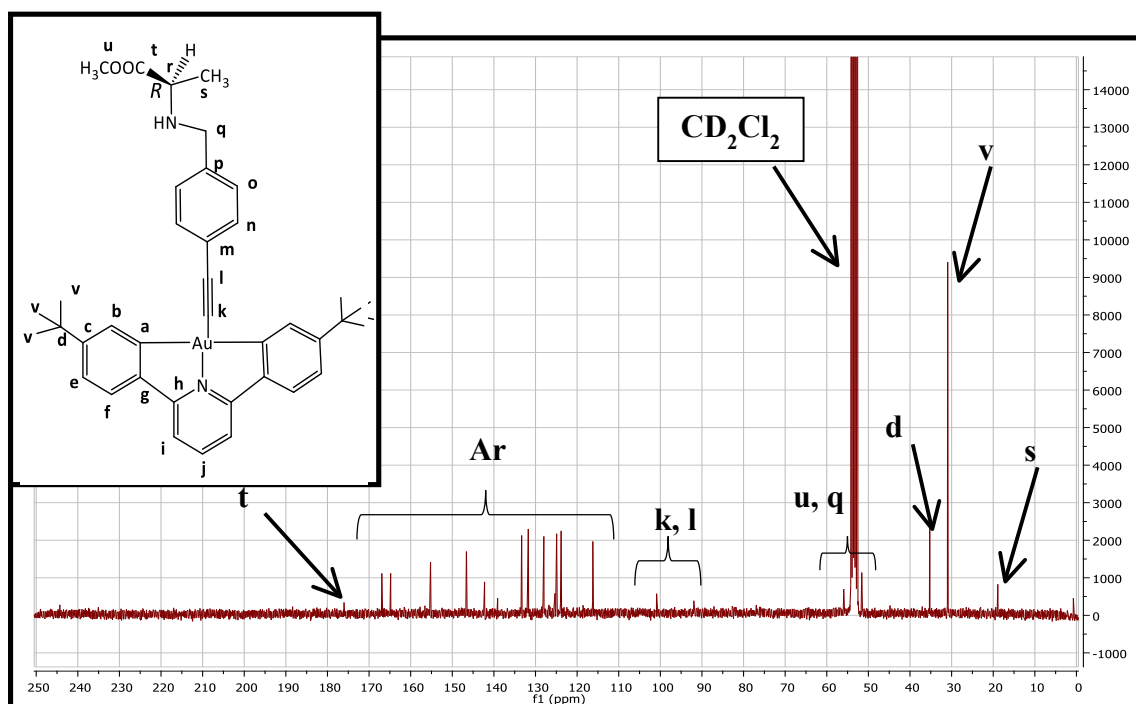


**Figure 20:**  $^{13}\text{C}\{^1\text{H}\}$ -NMR spectrum of complex **5** in  $\text{CD}_2\text{Cl}_2$ .

The  $^{13}\text{C}\{^1\text{H}\}$ -NMR spectrum of complex **5** in  $\text{CD}_2\text{Cl}_2$  shows a weak signal at  $\delta$  175.9 corresponding to the carbon of the  $-\text{CO}$  group from the ester function of the 1-ethynyl-4-benzyl-L-alanine methyl ester coordinated to the metallic centre (**t**). In addition, the chemical shifts corresponding to the carbon atoms of the alkyne group are observed as weak signals at 91.9 and 100.9 (**l** and **k**). These signals underwent a slight shift compared to the signals corresponding to the carbon atoms of the alkyne group of the ligand 1-ethynyl-4-benzyl-L-alanine methyl ester ( $\delta$  73.9 and 83.4, Table 2), which indicates the coordination of this molecule to the gold metallic centre.

Complex **5** was isolated from dichloromethane/petroleum ether 40/60 at room temperature as colourless crystals. The structural characterization of complex **5** has been solved by X-Ray diffraction.

A crystal of complex **5** showed two independent molecules. In both, the  $\text{Au}(\text{C}^{\wedge}\text{N}^{\wedge}\text{C})$  group was well resolved, showing the gold atom bonded to two carbon atoms, the nitrogen atom from the pyridine group, and the carbon atom corresponding to the alkyne functional group, which is located in *trans* position to the nitrogen atom from the pyridine moiety. However, the ethynyl ligand was less resolved, the atoms of the alanine methyl ester group in one molecule were barely resolved and in the second molecule only a cluster of electron density was found in this region. Only the gold atoms were refined anisotropically; the carbon, nitrogen and oxygen atoms were refined with isotropic thermal parameters. Hydrogen atoms were included (in all but the alanine residue of the second molecule) in idealised positions and their  $U_{\text{iso}}$  values were set to ride on the  $U_{\text{eq}}$  values of the parent carbon and nitrogen atoms.

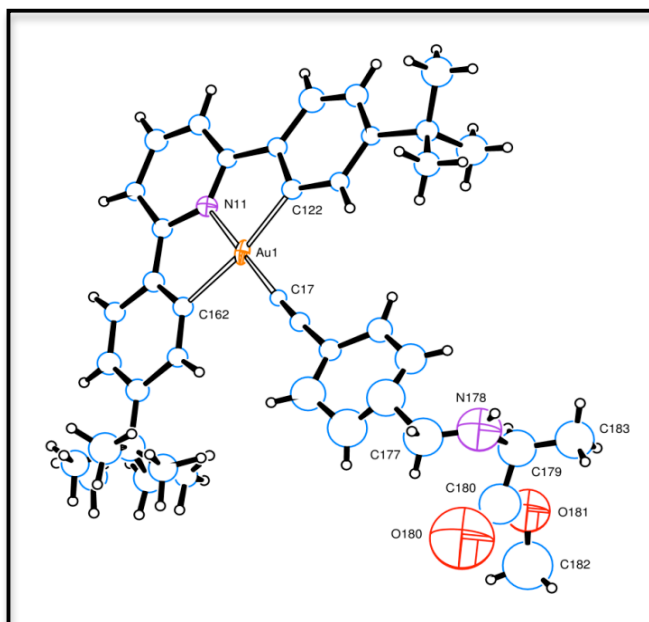


**Figure 21.** ORTEP diagram of complex **5**. (X-Ray structure refined and solved by Dr. David Hughes)

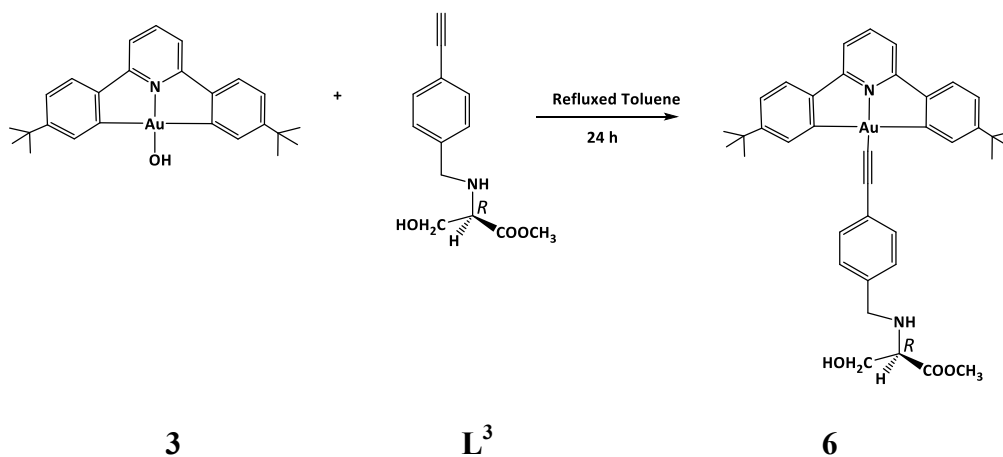
Complex **5** gives a distorted square-planar geometry, characteristic of  $d^8$  metal complexes, producing a N(11)-Au(1)-C(122) angle of  $81.9(11)^\circ$  and N(11)-Au(1)-C(162) angle of  $80.9(10)^\circ$  about the gold(III) metal center (table 11), found to deviate from the ideal  $90^\circ$  angle. Au(1)-N(11), Au(1)-C(122) and Au(1)-C(162) bond lengths of 1.98(2), 2.00(3) and 2.15(3) Å, respectively, are found in the observed range for another similar compounds.

**Table 11.** Most representative angles (°) and bond distances (Å) of complex 5.

BOND LENGTHS (Å)		ANGLES(°)	
Au(1)-N(11)	1.98(2)	C(17)-Au(1)-N(11)	179.4(11)
Au(1)-C(122)	2.00(3)	C(17)-Au(1)-C(122)	97.7(11)
Au(1)-C(162)	2.15(3)	N(11)-Au(1)-C(122)	81.9(11)
Au(1)-C(17)	1.97(3)	C(17)-Au(1)-C(162)	99.4(11)
		N(11)-Au(1)-C(162)	80.9(10)
		C(122)-Au(1)-C(162)	162.4(11)

**1.2.1.2.3. Synthesis of  $(C^{\wedge}N^{\wedge}C)Au-C\equiv C-C_6H_4-4-[CH_2-NH-CH(CH_2OH)-COOCH_3]$  (6).**

The reaction of 1-ethynyl-4-benzyl-L-serine methyl ester ( $L^3$ ) and  $(C^{\wedge}N^{\wedge}C)AuOH$  (3) (2:1 ratio) in refluxing toluene for 24h generated complex 6 as a yellow solid, which is air stable, soluble in toluene, dichloromethane and ethanol, and insoluble in petrol ether 40/60 (Scheme 15).



**Scheme 15.** Synthesis of complex 6.

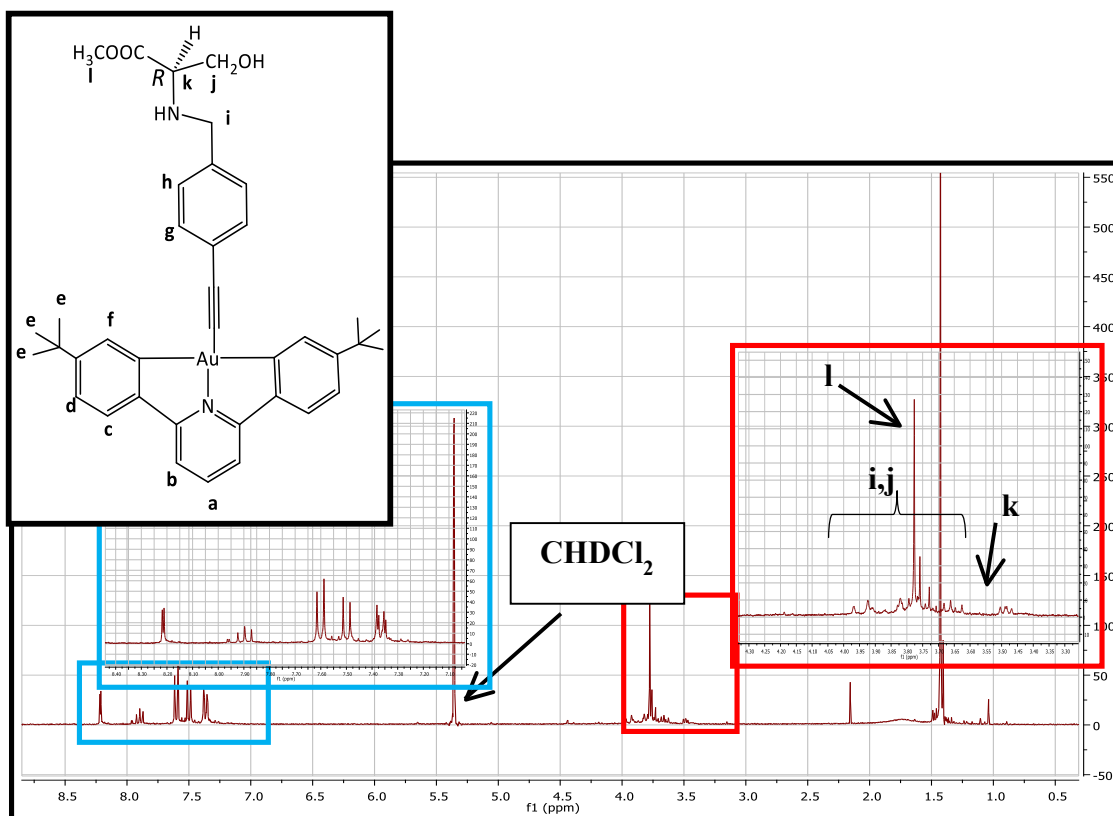
Complex **6** has been characterized by  $^1\text{H-NMR}$ ,  $^{13}\text{C}\{^1\text{H}\}\text{-NMR}$ , infrared spectroscopy and elemental analysis.

The IR spectrum shows a strong absorption peak at  $1738\text{ cm}^{-1}$  and a weak absorption peak at  $2153\text{ cm}^{-1}$ , for the stretch of  $\text{C=O}$  and  $\text{C}\equiv\text{C}$ , respectively.

The chemical shifts corresponding to the  $^1\text{H-NMR}$  spectrum for complex **6** in  $\text{CD}_2\text{Cl}_2$  at room temperature are recorded in Table 12.

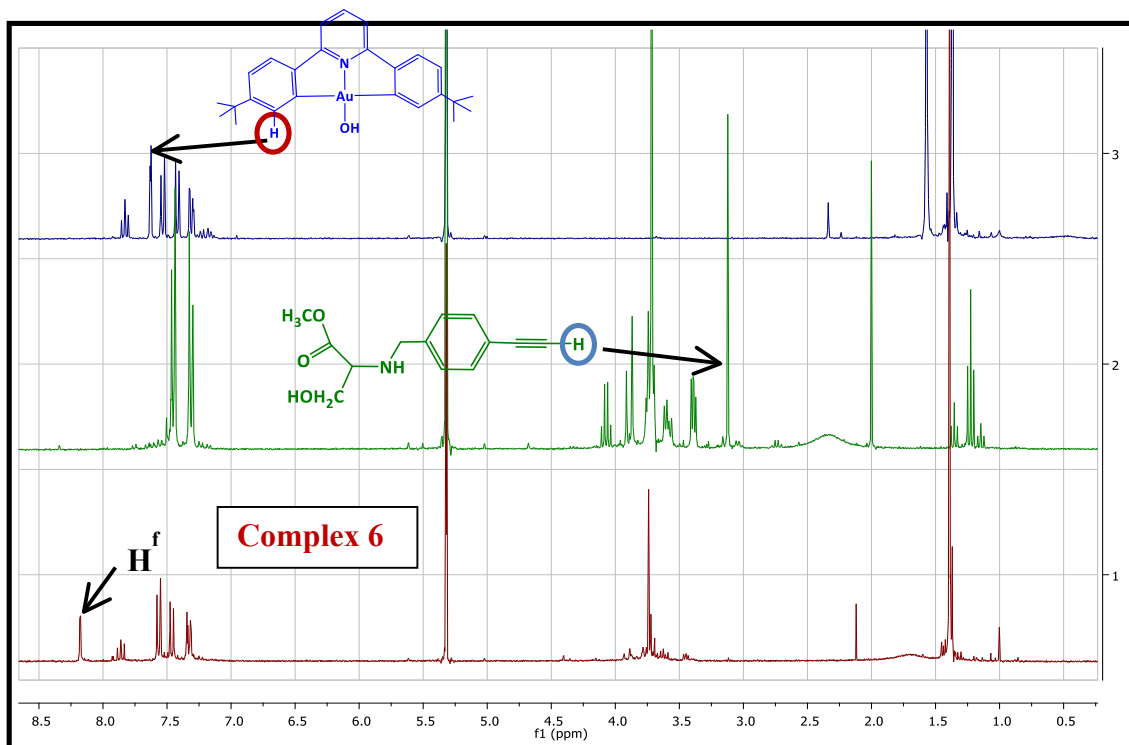
**Table 12:**  $^1\text{H-NMR}$  data of complex **6** in  $\text{CD}_2\text{Cl}_2$ ,  $\delta(\text{ppm})$  and multiplicity.

COMPLEX <b>6</b>	ASSIGNMENT	$^1\text{H}$ (ppm)
	e	1.43 (s, 18H)
	k	3.47 (q, $J = 4.6\text{ Hz}$ , 1H)
	l	3.81 (s, 3H)
	i,j (overlapped)	3.89-3.72 (m, 4H)
	d	7.36 (d, $J = 8.1\text{ Hz}$ , 2H)
	g, h	7.60 (d, $J = 8.1\text{ Hz}$ , 2H), 7.50 (d, $J = 8.1\text{ Hz}$ , 2H)
	c, b	7.60 (d, $J = 8.1\text{ Hz}$ , 2H), 7.37 (d, $J = 8.1\text{ Hz}$ , 2H)
	a	7.89 (t, $J = 9.4\text{ Hz}$ , 1H)
f	8.21 (d, $J = 2.0\text{ Hz}$ , 2H)	



**Figure 22:**  $^1\text{H-NMR}$  spectrum of complex **6** in  $\text{CD}_2\text{Cl}_2$ .

Proton  $\text{H}^i$  and  $\text{H}^j$  corresponding to the protons of methylene and  $-\text{CH}_2\text{OH}$  groups are overlapped in the spectrum, observed as a multiplet integrating for four protons. Protons  $\text{H}^l$  of the methyl group from the ester function of the 1-ethynyl-4-benzyl-L-serine methyl ester molecule bonded to the metallic centre are shown as a singlet signal at  $\delta$  3.81. The chemical shifts corresponding to the aromatic ring of this molecule are observed as AB system at  $\delta$  7.45 and 7.55 integrating by four protons ( $\text{H}^g$  and  $\text{H}^h$ ). These signals are shifted compared to the free ligand 1-ethynyl-4-benzyl-L-serine methyl ester ( $\delta$  7.18 and 7.35, Table 3).

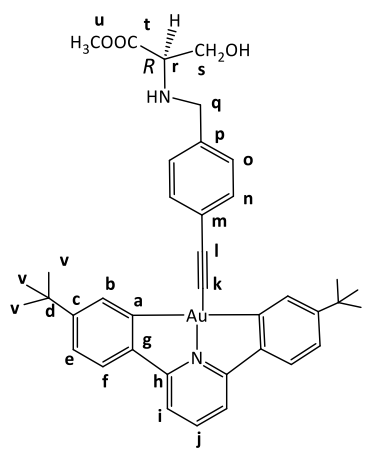


**Figure 23:** Comparison between  $^1\text{H}$ -NMR spectrum of complex **6** (red spectrum),  $(\text{C}^{\wedge}\text{N}^{\wedge}\text{C})\text{AuOH}$  (blue spectrum) and 1-ethynyl-4-benzyl-L-serine methyl ester (green spectrum) in  $\text{CD}_2\text{Cl}_2$ .

According to Figure 23, the singlet signal corresponding to the proton from the alkynyl functional group of the 1-ethynyl-4-benzyl-L-serine methyl ester molecule (green spectrum, **blue circle**) is not shown in the  $^1\text{H}$ -NMR spectrum of complex **6** (red spectrum). Either this feature and the significant shift showed by  $\text{H}^f$  of complex **6** ( $\delta$  8.21) with respect to the same proton of  $(\text{C}^{\wedge}\text{N}^{\wedge}\text{C})\text{AuOH}$  ( $\delta$  7.65, **red circle**) are indicative that 1-ethynyl-4-benzyl-L-serine methyl ester molecule is coordinated to the metallic centre.

The chemical shifts corresponding to  $^{13}\text{C}\{^1\text{H}\}$ -NMR spectrum of complex **6** in  $\text{CD}_2\text{Cl}_2$  at room temperature have been recorded on Table 13.

**Table 13:**  $^{13}\text{C}\{^1\text{H}\}$ -NMR data of complex **6** in  $\text{CD}_2\text{Cl}_2$  ( $\delta(\text{ppm})$ ).

COMPLEX 6	ASSIGNMENT	$^{13}\text{C}$ (ppm)
	v	30.9
	d	35.2
	q, r, s, u	51.8, 52.0, 61.3, 62.4
	k, l	92.3, 100.8
	Aromatic region	116.4 (i), 123.8 (e), 124.3 ( $\text{C}_{\text{ipso}}$ , m or p), 124.9 (f), 128.1 (n or o), 131.8 (n or o), 133.3 (b), 138.5 ( $\text{C}_{\text{ipso}}$ , m or p), 142.3 (j), 146.6 (g), 155.2 (c), 164.8 (h), 166.9 (a).
t	This chemical shift is not clearly distinguished.	

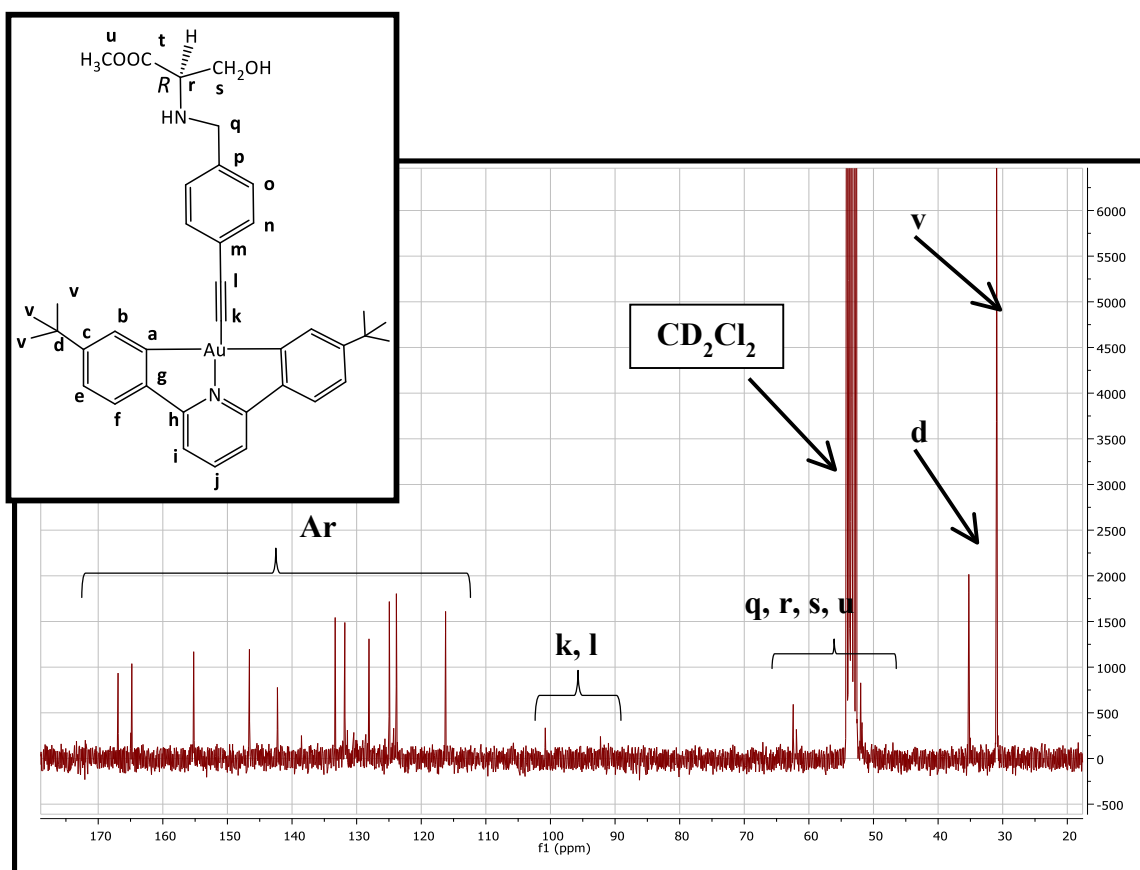
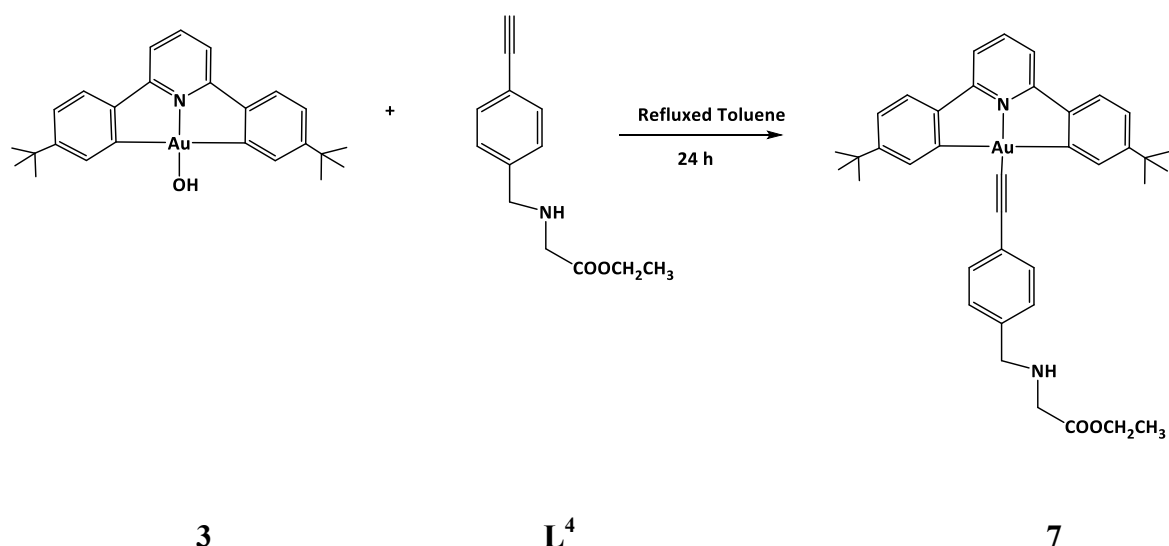


**Figure 24:**  $^{13}\text{C}\{^1\text{H}\}$ -NMR data of complex **6**.

As is shown in Figure 24, the chemical shifts corresponding to the carbons from the alkyne group are observed at  $\delta$  92.3 and 100.8 (**k** and **l**) as weak signals. These signals exhibited a considerable change compared to the ones from the free ligand 1-ethynyl-4-benzyl-L-serine methyl ester ( $\delta$  77.3 and 83.5, Table 4). The chemical shift corresponding to the carbon atom of the -CO group from the ester function of the 1-ethynyl-4-benzyl-L-serine methyl ester molecule bonded to the metallic centre is not properly distinguished in the spectrum.

**1.2.1.2.4. Synthesis of  $(C^{\wedge}N^{\wedge}C)Au-C\equiv C-C_6H_4-4-(CH_2-NH-CH_2-COOCH_2CH_3)$  (7).**

The reaction of 1-ethynyl-4-benzyl-L-glycine ethyl ester (**L<sup>4</sup>**) and  $(C^{\wedge}N^{\wedge}C)AuOH$  (**3**) (2:1 ratio) in refluxed toluene for 24 hours affords complex **7**. Complex **7** is a yellow solid, air and water stable, soluble in toluene, dichloromethane and ethanol, and not soluble in petrol ether 40/60 (Scheme 16).



**Scheme 16.** *Synthesis of complex 7.*

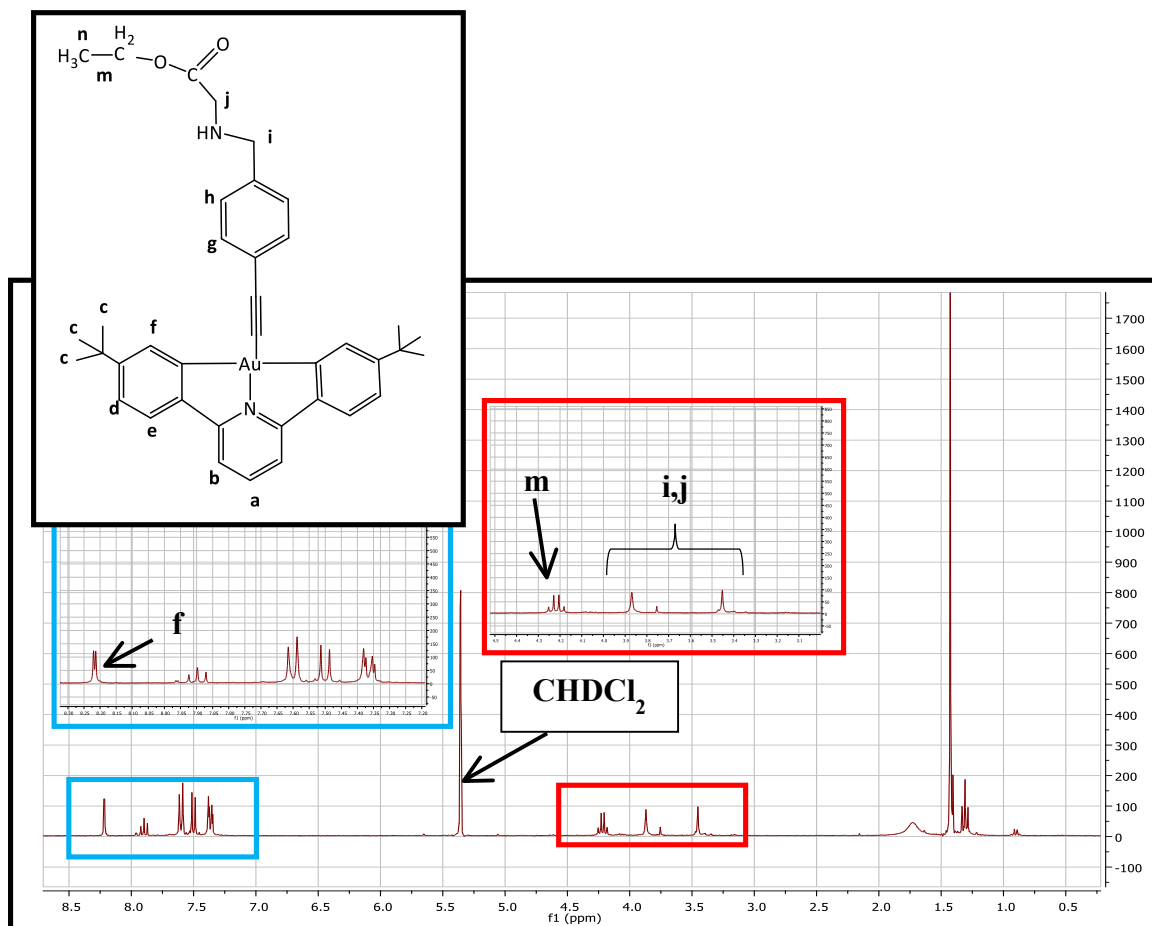
Complex **7** has been characterized by  $^1H$ -NMR,  $^{13}C\{^1H\}$ -NMR, IR spectroscopy and elemental analysis.

The IR spectrum shows a weak absorption peak at  $2149\text{ cm}^{-1}$ , corresponding to the vibration mode of the  $\text{C}\equiv\text{C}$  bond of the di-substituted alkyne group. This peak is shown on the same range than the ones reported on the literature for similar examples.<sup>16,25</sup> In addition, the spectrum exhibits a strong absorption peak at  $1737\text{ cm}^{-1}$  corresponding to the  $\text{C}=\text{O}$  stretch.

The chemical shifts corresponding to the  $^1\text{H}$ -NMR spectrum for complex **7** in  $\text{CD}_2\text{Cl}_2$  at room temperature are recorded in Table 14.

**Table 14:**  $^1\text{H}$ -NMR data of complex **7** in  $\text{CD}_2\text{Cl}_2$ ,  $\delta(\text{ppm})$  and multiplicity.

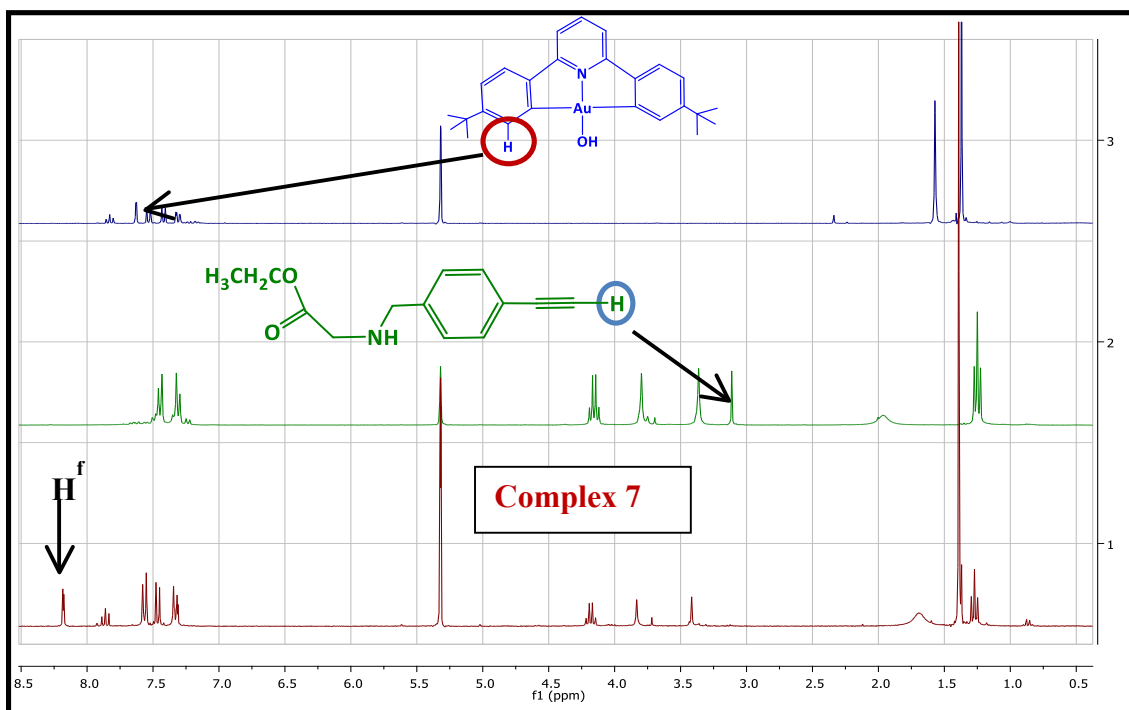
COMPLEX 7	ASSIGNMENT	$^1\text{H}$ (ppm)
	n	1.31 (t, $J = 7.2\text{ Hz}$ , 3H)
	c	1.43 (s, 18H)
	i,j	3.45 (s, br, 2H)
		3.87 (s, br, 2H)
	m	4.21 (q, $J = 7.2\text{ Hz}$ , 2H)
	d	7.32 (d, $J = 7.0\text{ Hz}$ , 2H)
	b, e, g, h (overlapped)	7.37 (d, $J = 8.1\text{ Hz}$ , 2H), 7.50 (d, $J = 8.1\text{ Hz}$ , 2H), 7.60 (d, $J = 8.2\text{ Hz}$ , 4H)
	a	7.90 (t, $J = 8.0\text{ Hz}$ , 1H)
	f	8.22 (d, $J = 2.0\text{ Hz}$ , 2H)



**Figure 25:**  $^1\text{H-NMR}$  spectrum of complex 7 in  $\text{CD}_2\text{Cl}_2$ .

Figure 25 exhibits a triplet signal at 1.31 ppm corresponding to the protons  $\text{H}^n$  from the methyl group of the glycine ester. Protons  $\text{H}^i$  and  $\text{H}^j$  represent the methylene groups of the 1-ethynyl-4-benzyl-L-glycine ethyl ester molecule. They are observed as two broad singlet signals at  $\delta$  3.45 and 3.87 integrating for two protons each. Protons  $\text{H}^m$  from the methylene group of the ethyl ester function are observed as a quartet signal integrating for two protons.

The chemical shifts corresponding to the aromatic ring of the 1-ethynyl-4-benzyl-L-serine methyl ester molecule bonded to the metallic centre are observed as AB system at  $\delta$  7.50 and 7.60 integrating by four protons ( $\text{H}^g$  and  $\text{H}^h$ ). These signals are slightly shifted compared to the free ligand 1-ethynyl-4-benzyl-L-serine methyl ester ( $\delta$  7.31 and 7.44, Table 5).

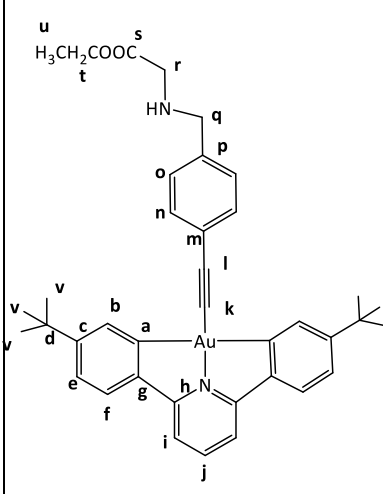


**Figure 26:** Comparison between  $^1\text{H}$ -NMR spectrum of complex **7** (red spectrum),  $(\text{C}^{\wedge}\text{N}^{\wedge}\text{C})\text{AuOH}$  (blue spectrum) and 1-ethynyl-4-benzyl-L-glycine ethyl ester (green spectrum) in  $\text{CD}_2\text{Cl}_2$ .

As is shown in  $^1\text{H}$ -NMR spectrum of complex **7** (red spectrum, Figure 26), the two broad singlet signals ( $\delta$  3.45 and 3.87) corresponding to the protons  $\text{H}^i$  and  $\text{H}^j$ , as well as the chemical shift associated to the ethyl ester function (protons  $\text{H}^m$  and  $\text{H}^n$ ) do not show remarkable variations regarding the same signals of the 1-ethynyl-4-benzyl-L-glycine ethyl ester molecule (green spectrum). However,  $\text{H}^f$  of complex **7** ( $\delta$  8.21) shows a significant shift regarding the same proton of  $(\text{C}^{\wedge}\text{N}^{\wedge}\text{C})\text{AuOH}$  ( $\delta$  7.65, **red circle**). This feature and the absence of the singlet signal corresponding to the proton from the alkynyl functional group of the 1-ethynyl-4-benzyl-L-glycine ethyl ester molecule (**blue circle**) indicate that this molecule is coordinated to the metallic centre, to afford the complex **7** through formation of an Au-C bond.

The chemical shifts corresponding to  $^{13}\text{C}\{^1\text{H}\}$ -NMR spectrum of complex **7** in  $\text{CD}_2\text{Cl}_2$  at room temperature have been recorded on Table 15.

**Table 15:**  $^{13}\text{C}\{^1\text{H}\}$ -NMR data of complex 7 in  $\text{CD}_2\text{Cl}_2$  ( $\delta(\text{ppm})$ ).

COMPLEX 7	ASSIGNMENT	$^{13}\text{C}$ (ppm)
	u	14.0
	v	31.0
	d	35.2
	q or r	60.7 (only one signal is observed)
	k, l	100.9, 92.0
	Aromatic region	116.3 (i), 123.8 (e), 124.9 (f), 125.5 ( $\text{C}_{\text{ipso}}$ , m or p. One of these carbons is not shown in the spectrum), 128.2 (n or o), 131.8 (b), 133.3 (n or o), 142.3 (g), 146.6 (j), 155.2 (c), 164.8 (h), 166.9 (a).
s	Not shown in the spectrum.	

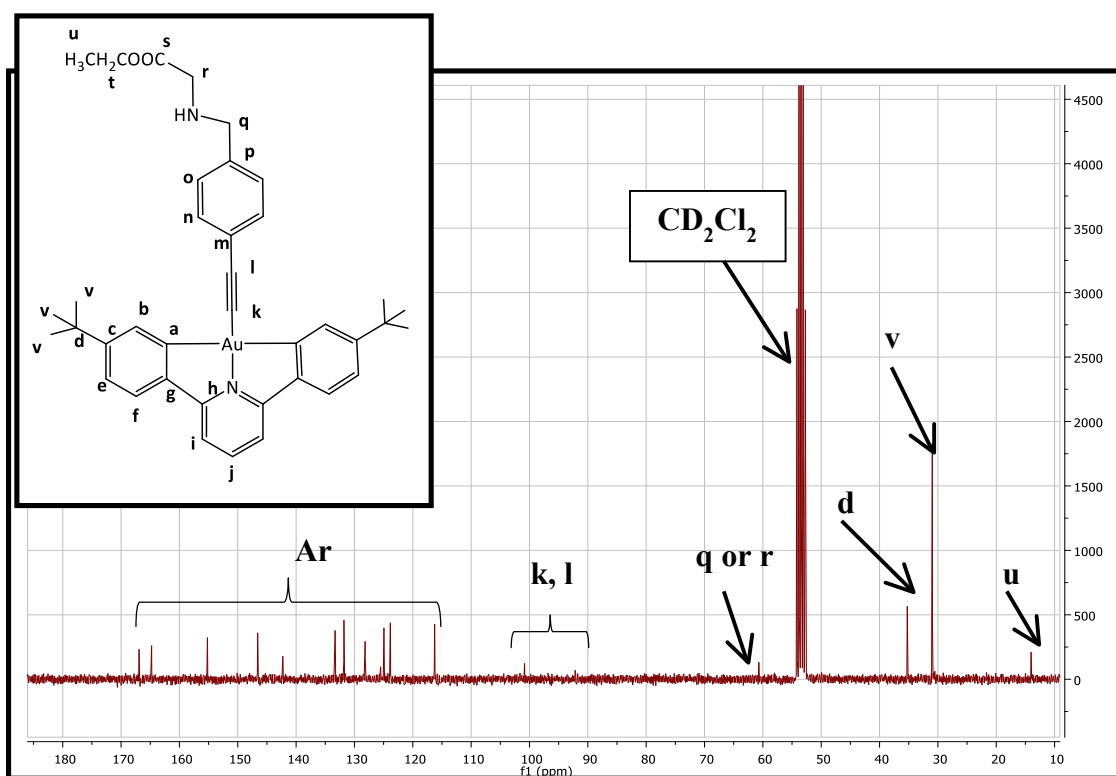


**Figure 27:**  $^{13}\text{C}\{^1\text{H}\}$ -NMR spectrum of complex 7 in  $\text{CD}_2\text{Cl}_2$ .

As is shown in the  $^{13}\text{C}\{^1\text{H}\}$ -NMR spectrum of complex **7** in  $\text{CD}_2\text{Cl}_2$  (Figure 27), the signal corresponding to the carbon atom of the  $-\text{CO}$  group from the ester function of the 1-ethynyl-4-benzyl-L-glycine ethyl ester molecule bonded to the gold metallic centre (**s**) is not shown in the spectrum. The chemical shifts corresponding to the alkyne group (weak signals at  $\delta$  92.0 and 100.9) have provided us the most significant datum to justify the coordination of the 1-ethynyl-4-benzyl-L-glycine ethyl ester molecule to the metallic centre, due to the significant shift compared to the free ligand ( $\delta$  77.2 and 83.8, Table 6). One of the methylene groups from the 1-ethynyl-4-benzyl-L-glycine ethyl ester molecule coordinated to the metallic centre (**q** or **r**) is not shown in the spectrum.

#### 1.2.1.2.5. Synthesis of $(\text{C}^{\wedge}\text{N}^{\wedge}\text{C})\text{Au}-\text{C}\equiv\text{C}-\text{C}_6\text{H}_4-4-\text{CH}_2\text{OH}$ (**8**)

In order to expand and develop our studies, we investigated the synthesis of gold(III) complexes functionalized by alkynyl-amino acid derivatives. This has been a preliminary experiment, carried out in the final stage of our research. The observed results have not been conclusive, being required to attempt this approach in depth in future investigations.

In contrast to the previously synthesized gold(III) complexes functionalized by alkynyl-amino ester derivatives (complexes **4**, **5**, **6** and **7**), the  $-\text{COOH}$  terminal position of the targeted complexes may allow a consequent condensation reaction with other amino acids and peptides, expanding our investigations on this field.

The previously synthesized complex **4** has been employed as precursor on these experiments. The  $-\text{CHO}$  functional group of complex **4** can condense with the  $-\text{NH}_2$  function from amino acids, to lead to an imine derivative. This reaction was investigated employing D-alanine as amino acid. Amino acids are soluble in polar solvents, such as

water and methanol; this solubility behaviour was one of the main disadvantages we found in our experiments. The imine formation is an equilibrium that, in presence of water in the medium, can be moved to the starting materials (complex 4 and alanine). The use of dried methanol as solvent became needed in order to drive the reaction to the imine formation. The experiment was conducted under nitrogen atmosphere, employing D-Alanine in excess (1:5 ratio) and 4Å molecular sieves as dehydrating agent, in order to remove the formed water as second product. The reaction mixture was allowed to stir 16 hours under reflux. After this time, a  $^1\text{H-NMR}$  test sample in MeOD confirmed the absence of the  $-\text{CHO}$  signal at  $\delta$  10.00. In addition, a new singlet was observed at  $\delta$  8.50, corresponding to the  $\text{HC}=\text{N}$  imine group (Figure 28).

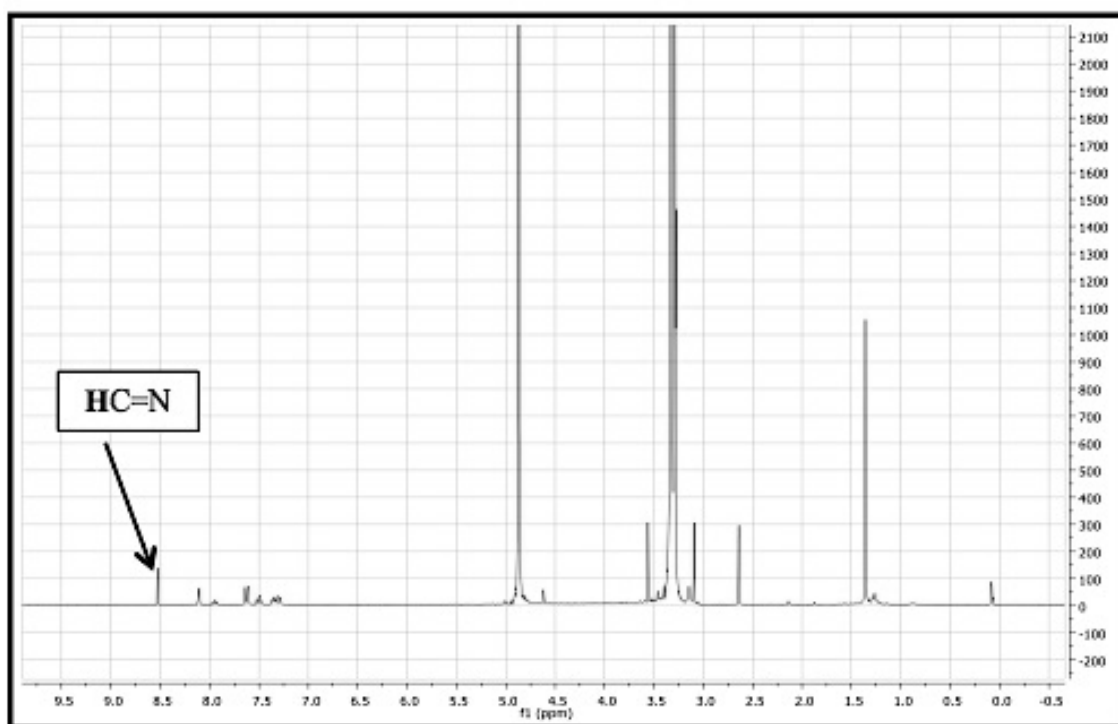


**Figure 28.**  $^1\text{H-NMR}$  spectrum of crude of reaction from complex 4 in MeOD, before addition of sodium borohydride.

The solvent was removed and the residue was washed under nitrogen atmosphere and dried with light petroleum. The yellow residue was then washed quickly with cold

water, in order to remove any excess of D-alanine. The product was dried under vacuum.

As it was mentioned previously, the  $-C=N$  group is susceptible to hydrolysis in presence of water or under acidic conditions, to regenerate the starting carbonyl and amine derivatives. In order to avoid this step and simplify the consequent ways to work with this complex, reduction of the imine function to  $-C-NH$  was planned. As it was studied for the synthesis of ligands  $L^2$ ,  $L^3$  and  $L^4$ , the residue was dissolved in dried methanol, and sodium borohydride was slowly added at  $0^\circ\text{C}$ . The reaction mixture was warmed to room temperature and stirred overnight. After 12 hours the solvent was removed and dichloromethane was added. Although the complex was not expected to be soluble in dichloromethane because of its expected polar character, we observed that most of residue was soluble. The product (complex **8**) was analysed by  $^1\text{H-NMR}$  spectroscopy in  $\text{CD}_2\text{Cl}_2$  (Figure 29).

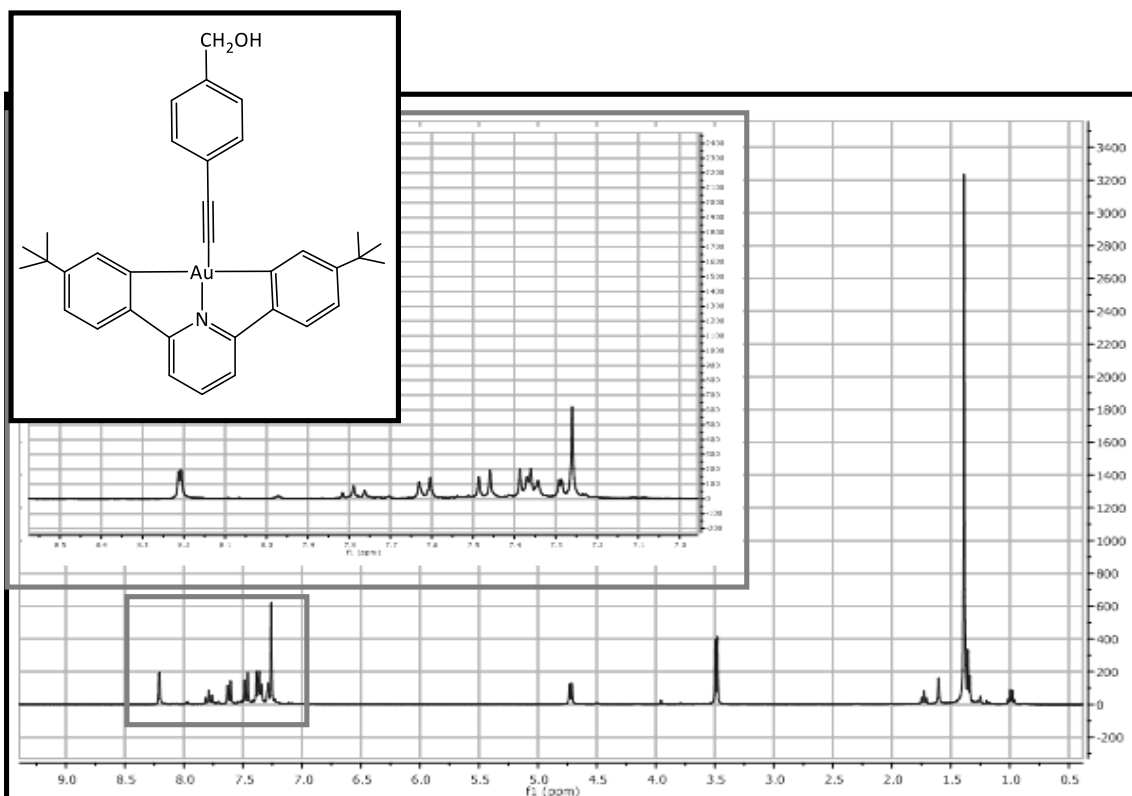


**Figure 29:**  $^1\text{H-NMR}$  spectrum of complex **8** in  $\text{CD}_2\text{Cl}_2$ .

The  $^1\text{H}$ -NMR spectrum from the residue did not show any chemical shift on the aldehyde region. In addition, a doublet signal at  $\delta$  4.72 was observed. The analysis of this complex was completed through  $^{13}\text{C}\{^1\text{H}\}$ -NMR spectroscopy (Figure 30). The  $^{13}\text{C}\{^1\text{H}\}$ -NMR spectrum showed two signals at  $\delta$  92.3 and 100.9 corresponding to the carbons of alkyne group. The chemical shift at  $\delta$  191.8 corresponding to the carbon atom of the  $-\text{CO}$  group from the aldehyde function of complex **4** was not observed. In addition, the signal corresponding to methanol and hexane were observed at  $\delta$  51.04 and 31.4, respectively. Nevertheless, the most interesting signal was observed as a new chemical shift at  $\delta$  65.3 corresponding to the  $-\text{CH}_2\text{OH}$  group.

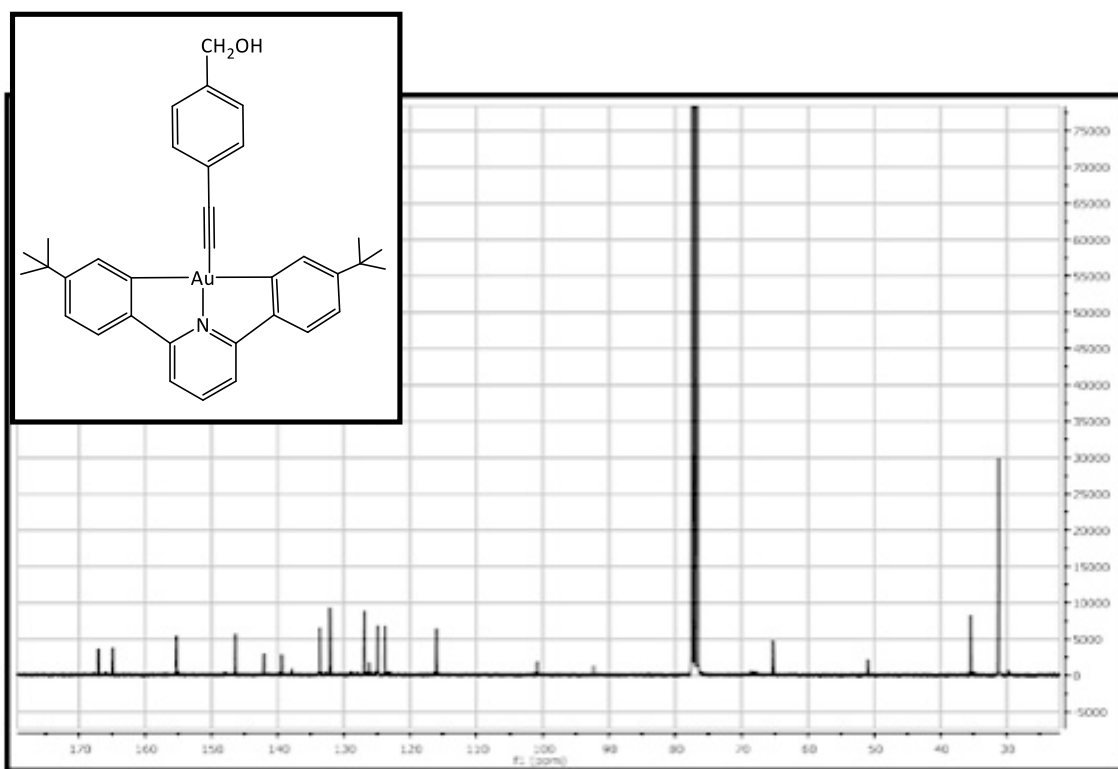
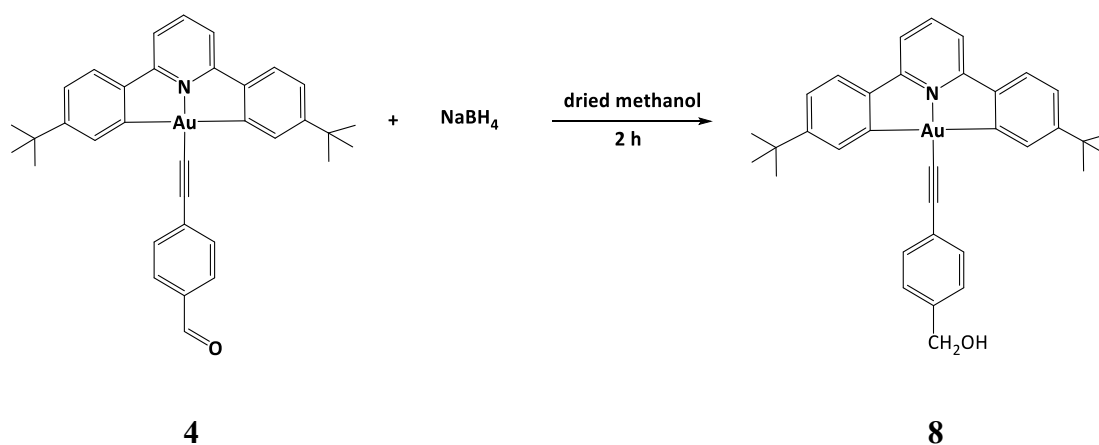


**Figure 30:**  $^{13}\text{C}\{^1\text{H}\}$ -NMR spectrum of complex **8** in  $\text{CDCl}_3$ .

As it was mentioned in the synthesis of ligands  $\text{L}^2$ ,  $\text{L}^3$  and  $\text{L}^4$ , we found that sodium borohydride promoted the reduction of the aldehyde group  $-\text{CHO}$  to  $-\text{CH}_2\text{OH}$ <sup>34</sup> instead of the imine (Figure 6). The obtained results by  $^1\text{H}$ -NMR and  $^{13}\text{C}\{^1\text{H}\}$ -NMR

spectroscopy showed that the reduction of the aldehyde group of complex **4** had taken place, producing a  $-\text{CH}_2\text{OH}$  functional group.

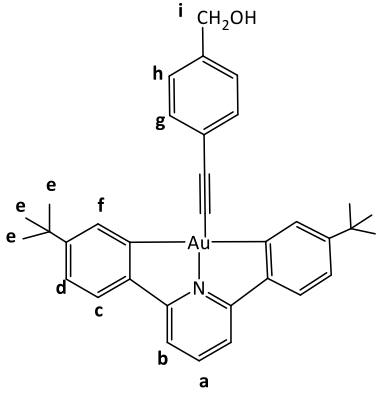
This complex was independently confirmed by its direct synthesis from complex **4**. The reaction of sodium borohydride and  $(\text{C}^{\wedge}\text{N}^{\wedge}\text{C})\text{Au}-\text{C}\equiv\text{C}-\text{C}_6\text{H}_4-\text{CHO}$  (**4**) (10:1 ratio) in dried methanol was allowed to stir for 2 hours at room temperature. Both  $^1\text{H}$ -NMR and  $^{13}\text{C}\{^1\text{H}\}$ -NMR spectroscopy confirmed the same complex than the one previously synthesized accidentally. Complex **8** is a yellow solid, air stable, soluble in dichloromethane and ethanol, and not soluble in petrol ether 60/40 (Scheme 17).



**Scheme 17.** *Synthesis of complex 8.*

The chemical shifts corresponding to  $^1\text{H}$ -NMR spectrum for complex **8** in  $\text{CDCl}_3$  at room temperature are recorded on Table 16.

**Table 16:**  $^1\text{H}$ -NMR data of complex **8** in  $\text{CDCl}_3$ ,  $\delta(\text{ppm})$  and multiplicity.

COMPLEX <b>8</b>	ASSIGNMENT	$^1\text{H}$ (ppm)
	e	1.39 (s, 18H)
	i, j	4.72 (d, $J = 6.0$ Hz, 2H)
	b (overlapped with $\text{CDCl}_3$ residual signal)	7.32 (m, 2H)
	g, h	7.38 (d, $J = 8.1$ , 2H), 7.37 (d, $J = 8.1$ , 2H)
	d, c	7.36 (d, $J = 8.0$ , 2H), 7.62 (d, $J = 8.0$ , 2H)
	a	7.79 (t, $J = 8.0$ Hz, 1H)
	f	8.21 (d, $J = 2.0$ Hz, 2H)

As it is shown in  $^1\text{H}$ -NMR spectrum of complex **8** (Figure 28, Table 15), the protons  $\text{H}^{\text{i,j}}$ , corresponding to the  $-\text{CH}_2\text{OH}$  function, are observed as a doublet signal at  $\delta$  4.72. Despite the fact that protons  $\text{H}^{\text{i,j}}$  were expected to be shown as a singlet signal, because of the presumably equivalence of these protons, they are shown as a doublet. This can be explained because of, when one molecule presents restricted rotation; atoms bonded to the same carbon atom may not be equivalent. If this occurs, non-equivalent  $^1\text{H}$  nuclei on the same carbon atom will couple to each other and cause splitting. This fact is also observed for proton  $\text{H}^{\text{f}}$ , shown as a doublet signal at  $\delta$  8.21.

The chemical shifts corresponding to  $^{13}\text{C}\{^1\text{H}\}$ -NMR spectrum of complex **8** in  $\text{CDCl}_3$  at room temperature have been recorded on Table 17.

**Table 17:**  $^{13}\text{C}\{^1\text{H}\}$ -NMR data for complex **8** in  $\text{CDCl}_3$ .

COMPLEX <b>8</b>	ASSIGNMENT	$^{13}\text{C}$ (ppm)
	r	31.2
	d	35.4
	q	65.3
	k, l	92.3, 100.9
	Aromatic region	116.0 (i), 123.8 (e), 124.9 (f), 126.2 ( $\text{C}_{\text{ipso}}$ , m or p), 126.9 (n or o), 132.1 (b), 133.6 ( $\text{C}_{\text{ipso}}$ , m or p), 142.1 (j), 146.4 (g), 155.2 (c), 164.9 (h), 167.1 (a).

These results allow us to confirm that the  $(\text{C}^{\wedge}\text{N}^{\wedge}\text{C})\text{Au}(\text{III})$  alkynyl derivatives functionalized by aldehyde groups can be reduced to primary alcohols in presence of sodium borohydride. Despite the fact that it is very difficult to figure out any conclusion after these results, one explanation may be that the equilibrium has not been completely moved to the formation of the imine group and complex **4** and D-alanine are partially presented in the medium. For this reaction, dried methanol was used as solvent, in order to move the equilibrium to the imine derivative formation. Although the hydrolysis is not a fast step, methanol is highly hygroscopic, being able to absorb water after long reaction times. If this happens, the equilibrium would not be completely moved to the imine formation, and complex **4** and D-alanine would be presented in the medium. In this point, the use of IR spectroscopy would be an useful technique in order to check if the  $\text{C}=\text{N}$  bond has been formed (an absorption band between  $1640\text{--}1690\text{ cm}^{-1}$  would be expected). After the addition of sodium borohydride, methanol was removed and the residue was extracted with dichloromethane. As it was mentioned before, most of the

product was soluble in dichloromethane. When dichloromethane was removed, complex **8** was observed. Because of the polarity of the D-alanine functional group, it would be expected (C<sup>^</sup>N<sup>^</sup>C)Au(III) amino acid complexes to be considerably polar, being not soluble in dichloromethane. This result may justify that the equilibrium was not completely moved in the first stage. Although the residue that was not soluble in dichloromethane was checked by <sup>1</sup>H-NMR spectroscopy in MeOD, the small amount present of this product did not allow to observe signals clearly differentiated, being not possible to make any conclusion.

Despite the fact that conclusive results have not been obtained, some modifications are suggested in order to attempt this section of the project in future investigations. Dried methanol would be the most convenient solvent to conduct this experiment, under inert atmosphere. As it was mentioned before, excess of amino acid would help to move the equilibrium to the imine formation, employing IR spectroscopy in order to check the C=N formation. At this point, instead of adding in situ sodium borohydride to reduce the imine bond, the isolation and characterization of this complex would be our aim, washing off first and quickly with cold water (to remove the excess of D-alanine) and dichloromethane (to remove starting material in case that the reaction is unfinished), and dry it under vacuum. The final step would be the reduction of C=N bond, in dried methanol, using excess of sodium borohydride as reducing agent.

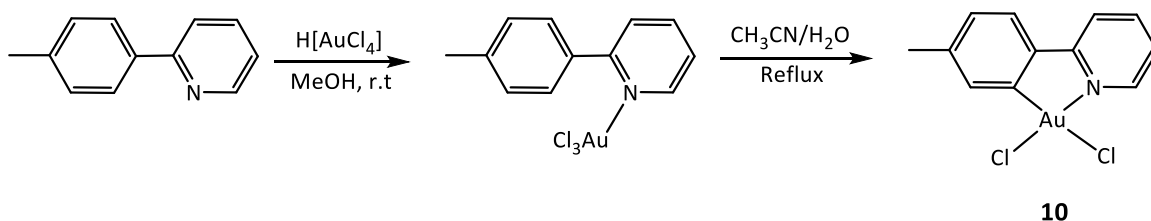
### **1.2.2. Synthesis of mono- and di-substituted bi-dentate gold(III) complexes functionalized with alkynyl derivatives.**

We focused on the synthesis of bidentate gold(III) complexes functionalized by alkynyl derivatives. In the first instance, the target of the project was to use complexes **2** and **15** (these complexes will be discussed later in the thesis) as precursors, and trying to attach amino acid and amino ester derivatives from them. However, this approach failed,

because the condensation product between aldehyde and amine functional groups was not achieved. This result encouraged us to propose an alternative approach, which was based on synthesizing the alkynyl derivative first, and attach it to the metallic centre.

In order to synthesize and characterize these complexes, (2-*para*-tolylpyridyl)AuCl<sub>2</sub> (**10**) was employed as precursor, because of the commercial availability of the ligand (2-*para*-tolylpyridine). The synthesis of (2-*para*-tolylpyridyl)AuCl<sub>2</sub> (**10**) was explored by two different pathways:

- a. In the first route we carried out the direct auration of 2-*para*-tolylpyridine via two steps reaction. The first step involves the reaction of (2-*para*-tolylpyridine) and H[AuCl<sub>4</sub>] in MeOH<sup>35</sup> to give the intermediate (HC<sup>^</sup>N)AuCl<sub>3</sub>, which reacts further to give the cyclometallated complex **10** in moderate yield (35—37%)<sup>12</sup> when it is refluxed in a mixture of acetonitrile/water (1:1) (Scheme 18).

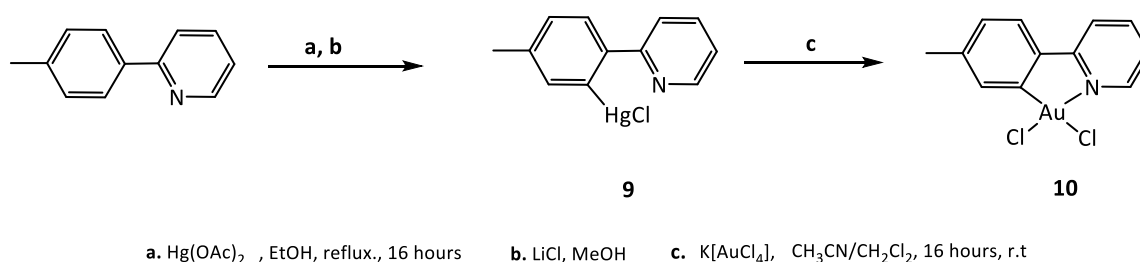


**Scheme 18.** Synthesis of (2-*para*-tolylpyridyl)AuCl<sub>2</sub> **10** by direct auration.

- b. The second route involves the initial mercuration reaction of 2-*para*-Tolylpyridine, using Hg(OAc)<sub>2</sub> as metallating agent, and the consequent transmetallation step employing K[AuCl<sub>4</sub>].

The synthesis of the organomercury substrate has been carried out according to the experimental procedure reported on the literature<sup>3</sup>. 2-*para*-Tolylpyridine has been subjected to mercuration with Hg(OAc)<sub>2</sub> followed by salt metathesis with LiCl to give the complex (N<sup>^</sup>C)HgCl (**9**). The mercury salt then undergoes transmetallation and C–H activation with K[AuCl<sub>4</sub>] to yield complex **10** in moderate yield (38 %)

(Scheme 19). Partial reductive elimination to gold(0) was observed in the transmetallation step.



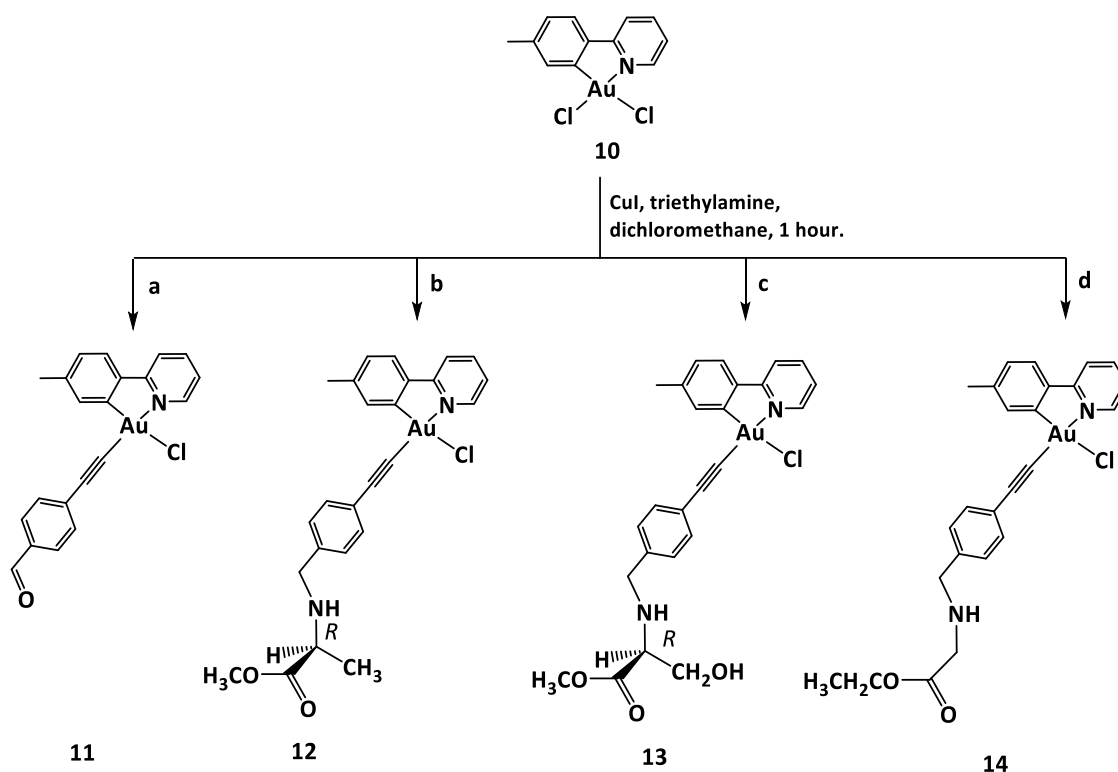
**Scheme 19.** *Synthesis of (2-para-tolylpyridyl)gold(III)Cl<sub>2</sub> **10** by transmetallation reaction.*

The prepared (2-para-tolylpyridyl)AuCl<sub>2</sub> derivative by these two pathways was analysed by <sup>1</sup>H-NMR spectroscopy in DMSO-*d*<sup>6</sup>. The observed chemical shifts were consistent with the ones reported in the literature for this complex.<sup>12</sup>

The use of these two different methods showed us that mercuration of 2-para-tolylpyridine and consequent transmetallation did not show remarkable improvements in terms of yield and reaction times compared to the direct auration. In addition, transmetallation step produced partial reductive elimination to gold(0), which was not observed during the direct auration. This may be explained because of the reaction conditions employed during the mercuration and transmetallation stages. These reaction steps have been carried out in refluxed methanol. Methanol can act as reducing agent that, at high temperatures, may cause the partial reductive elimination to gold(0). However, direct auration is conducted under smoother conditions, avoiding the reductive elimination step.

The incorporation of the alkynyl ligand into the cyclometalated gold(III) moiety has been achieved following the experimental procedure reported by Venkatesan et al.,<sup>21</sup> which involves the reaction of (2-para-tolylpyridyl)AuCl<sub>2</sub>, alkynyl derivative,

triethylamine, and a catalytic amount of copper(I) iodide in dichloromethane, to lead to the formation of the mono- and di-substituted gold(III) alkynyl derivatives **11**, **12**, **13** and **14** as yellow solids in moderated yields, over 50 % (Scheme 20).



Reaction conditions: CuI, NEt<sub>3</sub>, dichloromethane, ligand (L<sup>x</sup>).

L<sup>x</sup>:

**x = 0** : 4-ethynylbenzaldehyde (**a**).

**x = 2** : 1-ethynyl-4-benzyl-L-alanine methyl ester (**b**).

**x = 3** : 1-ethynyl-4-benzyl-L-serine methyl ester (**c**).

**x = 4** : 1-ethynyl-4-benzyl-L-glycine ethyl ester (**d**).

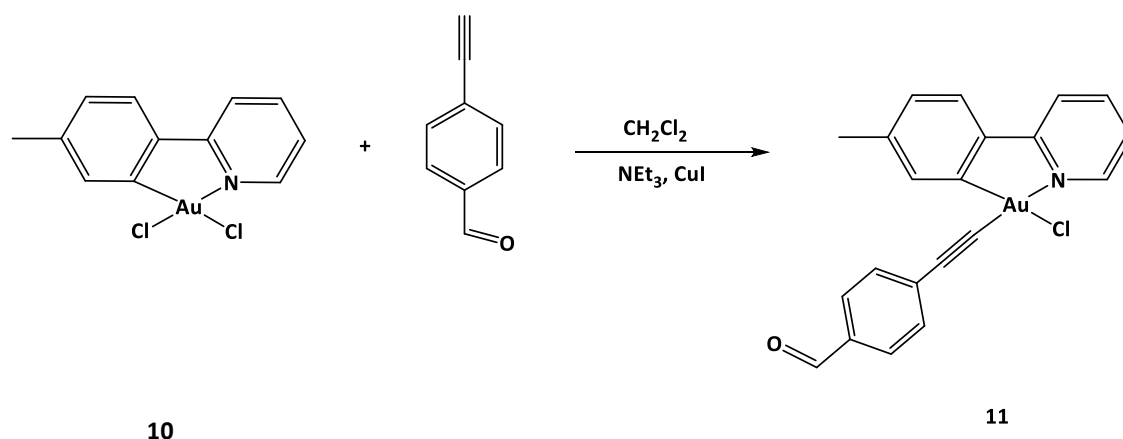
**Scheme 20.** *Synthesis of bi-dentate gold(III) complexes functionalized with alkynyl derivatives.*

Complexes **11**—**14** showed high solubility in non-polar solvents, such as dichloromethane. This feature played an important role as indicator of absence of

starting material. In contrast to complexes **11** – **14**, the chlorogold precursor (2-*para*-tolylpyridyl)AuCl<sub>2</sub> (**10**) exhibited poor solubility in non-polar solvents. Accordingly, when the initial suspension observed in the experiments turned into solution, it was indicative that complexes **11**–**14** have been synthesized. This change of solubility when the alkynyl ligand is coordinated to the metallic centre was also observed in protic media. In contrast to the precursor (2-*para*-tolylpyridyl)AuCl<sub>2</sub> (**10**), complexes **11**–**14** exhibited high solubility in protic solvents, such as alcohols, but not in water. This feature was a useful tool to isolate these complexes as pure products.

#### 1.2.2.1. Synthesis of (C<sup>^</sup>N)Au(Cl)C≡C–C<sub>6</sub>H<sub>4</sub>–4–CHO (**11**).

The reaction of 4-ethynylbenzaldehyde and (2-*para*-tolylpyridyl)AuCl<sub>2</sub> (**10**) (1:1 ratio) in dichloromethane, in presence of excess of triethylamine and a catalytic amount of CuI for 2 hours allowed the synthesis of complex **11** (13 mg, 33 %). Complex **11** is a yellow solid, air stable, soluble in dichloromethane and ethanol, and not soluble in petrol ether 40/60 (Scheme 21).



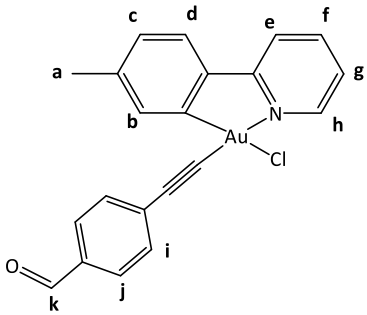
**Scheme 21.** Synthesis of complex **11**.

Complex **11** has been characterized by <sup>1</sup>H–NMR, <sup>13</sup>C {<sup>1</sup>H}–NMR, infrared spectroscopy and elemental analysis.

The IR spectrum shows a weak absorption peak at 1691 and 2164  $\text{cm}^{-1}$ , corresponding to the stretch of the C=O bond of the aldehyde function and the C $\equiv$ C bond of the di-substituted alkyne group,<sup>21,25</sup> respectively.

The chemical shifts corresponding to  $^1\text{H}$ -NMR spectrum for complex **11** in  $\text{CD}_2\text{Cl}_2$  at room temperature are recorded on Table 18.

**Table 18:**  $^1\text{H}$ -NMR data of complex **11** in  $\text{CD}_2\text{Cl}_2$ ,  $\delta(\text{ppm})$  and multiplicity.

COMPLEX 11	ASSIGNMENT	$^1\text{H}$ (ppm)
	a	2.42 (s, 3H)
	c	7.24 (d, J = 7.8 Hz, 1H)
	g	7.46-7.54 (m, 1H)
	d	7.59 (d, J = 7.9 Hz, 1H)
	i,j	7.70 (d, J = 8.2 Hz, 2H), 7.86 (d, J = 8.2 Hz, 2H)
	e	7.90 (d, J = 7.5 Hz, 1H)
	b	7.98 (s, 1H)
	f	8.10 (td, J = 8.0, 1.5 Hz, 1H)
	h	9.50 (d, J = 5.8 Hz, 1H)
	k	10.01 (s, 1H)

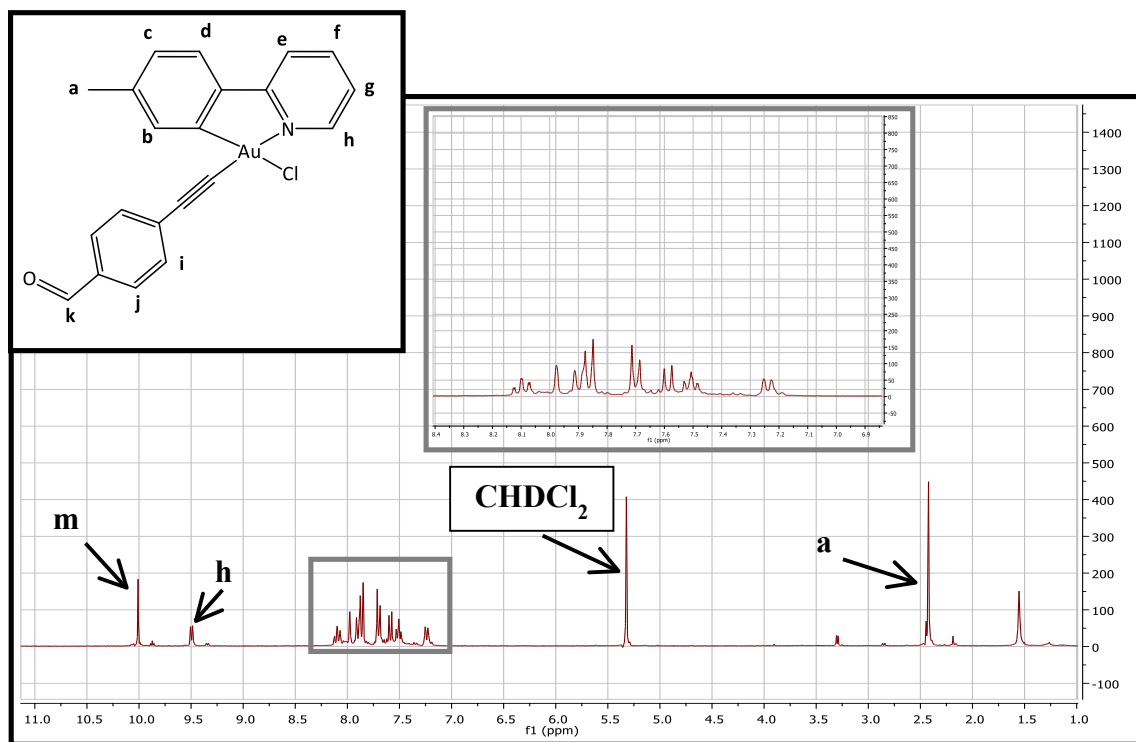


**Figure 31:**  $^{13}\text{H}$ -NMR spectrum of complex **11** in  $\text{CD}_2\text{Cl}_2$ .

As it is observed in Figure 32,  $\text{H}^{\text{h}}$  of complex **11** ( $\delta$  9.50) is shifted regarding the same proton from the (2-*para*-tolylpyridyl)AuCl<sub>2</sub> ( $\delta$  9.75, **red circle**). Both this feature and the absence of the proton of the alkynyl function of 4-ethynylbenzaldehyde (**blue circle**) indicate that one molecule of 4-ethynylbenzaldehyde is coordinated to the metallic centre through Au-C bond formation.

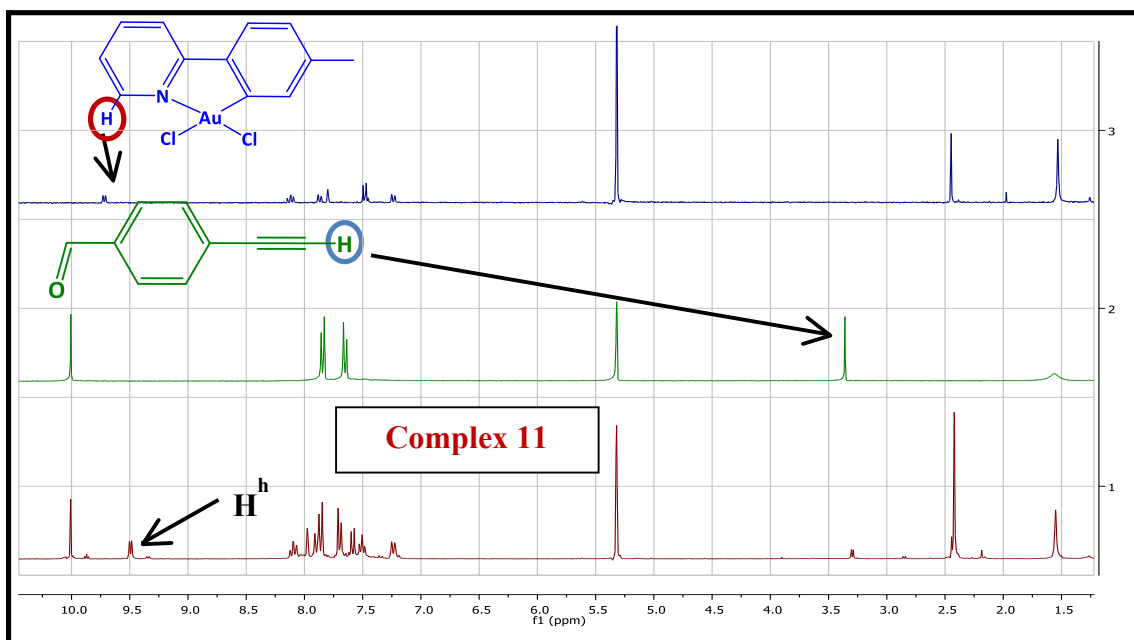


**Figure 32:** Comparison between  $^1\text{H}$ -NMR spectra of complex **11** (red spectrum), (2-*para*-tolylpyridyl) $\text{AuCl}_2$  (blue spectrum) and 4-ethynylbenzaldehyde (green spectrum) in  $\text{CD}_2\text{Cl}_2$ .

The chemical shifts corresponding to  $^{13}\text{C}\{^1\text{H}\}$ -NMR spectrum of complex **11** in  $\text{CD}_2\text{Cl}_2$  at room temperature have been recorded in Table 19.

**Table 19.**  $^{13}\text{C}\{^1\text{H}\}$ -NMR data of complex **11** in  $\text{CD}_2\text{Cl}_2$  ( $\delta(\text{ppm})$ ).

COMPLEX 11	ASSIGNMENT	$^{13}\text{C}$ (ppm)
	s	21.8
	l, m	96.9, 90.2
	Aromatic region	120.15 (d), 123.8 (b or g), 125.4 ( $\text{C}_{\text{ipso}}$ , n or q), 129.3 (b or g), 129.4 (o or p), 131.5 (h), 132.3 (o or p), 135.1 (j), 135.3 ( $\text{C}_{\text{ipso}}$ , n or q), 139.6 (c or f), 142.3 (c or f), 143.4 ( $\text{C}_{\text{ipso}}$ , a, i or k), 147.0 ( $\text{C}_{\text{ipso}}$ , a, l or k), 147.6 ( $\text{C}_{\text{ipso}}$ , a, i or k), 164.1 ( $\text{C}_{\text{ipso}}$ , e).
	r	191.5

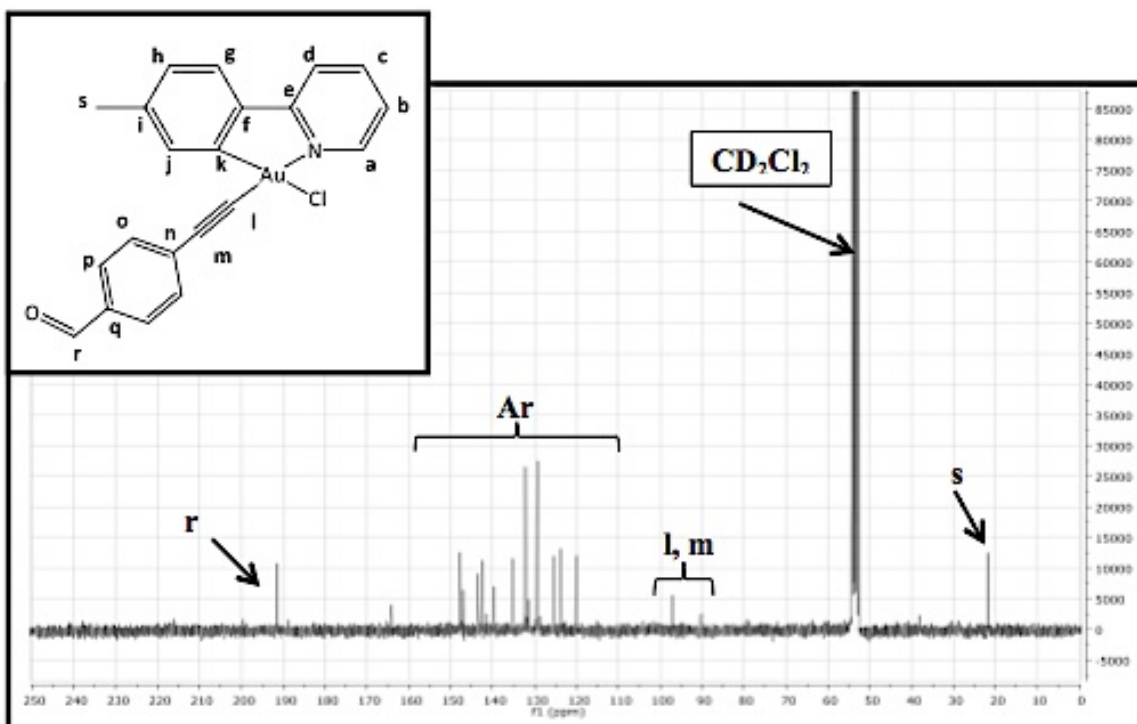


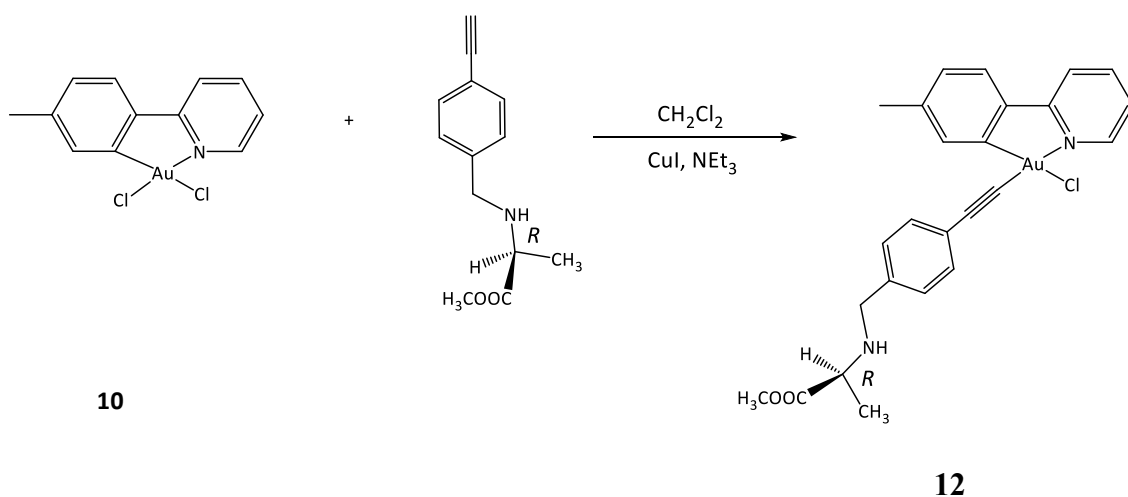
**Figure 33.**  $^{13}\text{C}\{^1\text{H}\}$ -NMR spectrum of complex **11** in  $\text{CD}_2\text{Cl}_2$ .

The  $^{13}\text{C}\{^1\text{H}\}$ -NMR spectrum of complex **11** in  $\text{CD}_2\text{Cl}_2$  shows one signal at  $\delta$  191.5 corresponding to the carbon atom of the  $-\text{CO}$  group from the aldehyde function of the 4-ethynylbenzaldehyde molecule coordinated to the metallic centre (**r**). The signals corresponding to the alkyne group are observed as weak signals at  $\delta$  90.2, 96.9 (**l** and **m**). They are a slightly shifted compared to the chemical shifts reported on the literature for the carbon atoms of the alkyne group of 4-ethynylbenzaldehyde ( $\delta$  81.02, 82.09).<sup>34</sup>

#### 1.2.2.2. Synthesis of $(\text{C}^{\wedge}\text{N})\text{Au}(\text{Cl})\text{C}\equiv\text{C}-\text{C}_6\text{H}_4-4-[\text{CH}_2-\text{NH}-\text{CH}(\text{CH}_3)-\text{COOCH}_3]$ (**12**).

The reaction of 1-ethynyl-4-benzyl-L-alanine methyl ester and (2-p-tolylpyridyl) $\text{AuCl}_2$ (**10**) (1:1 ratio) in dichloromethane, in presence of excess of triethylamine and a catalytic amount of  $\text{CuI}$  for 2 hours led the synthesis of complex **12**

(94.5 mg, 41 %). Complex **12** is a yellow solid, air stable, soluble in dichloromethane and ethanol, and not soluble in petrol ether 40/60 (Scheme 22).



**Scheme 22.** *Synthesis of complex 12.*

Complex **12** has been characterized by  $^1\text{H-NMR}$ ,  $^{13}\text{C}\{^1\text{H}\}\text{-NMR}$ , infrared spectroscopy and elemental analysis.

The IR spectrum shows a weak absorption band at 1733 and 2164  $\text{cm}^{-1}$ , corresponding to the stretch of the C=O bond of the ester group and the C $\equiv$ C bond of the di-substituted alkyne group,<sup>21,25</sup> respectively.

The chemical shifts corresponding to  $^1\text{H-NMR}$  spectrum for complex **12** in  $\text{CD}_2\text{Cl}_2$  at room temperature are recorded in Table 20.

**Table 20:**  $^1\text{H-NMR}$  data of complex **12** in  $\text{CD}_2\text{Cl}_2$ ,  $\delta(\text{ppm})$  and multiplicity.

COMPLEX 12	ASSIGNMENT	$^1\text{H}$ (ppm)
	n	1.30 (d, $J = 7.0$ Hz, 3H)
	a	2.42 (s, 3H)
	m	3.38 (q, $J = 7.0$ Hz, 1H)
	k	3.67 (d, $J = 13.4$ Hz, 1H), 3.82 (d, $J = 13.4$ Hz, 1H)
	l	3.71 (s, 3H)
	c	7.22 (dd, $J = 7.9, 0.8$ Hz, 1H)
	i, j	7.32 (d, $J = 8.0$ Hz, 1H), 7.50 (d, $J = 8.0$ Hz, 1H)
	g	7.31 – 7.40 (m, 1H)
	d	7.58 (d, $J = 7.9$ Hz, 1H)
	e	7.89 (d, $J = 8.1$ Hz, 1H)
	b	8.02 (d, $J = 0.8$ Hz, 1H)
	f	8.05-8.08 (m, 1H)
h	9.48 (dd, $J = 5.8, 1$ Hz, 1H)	

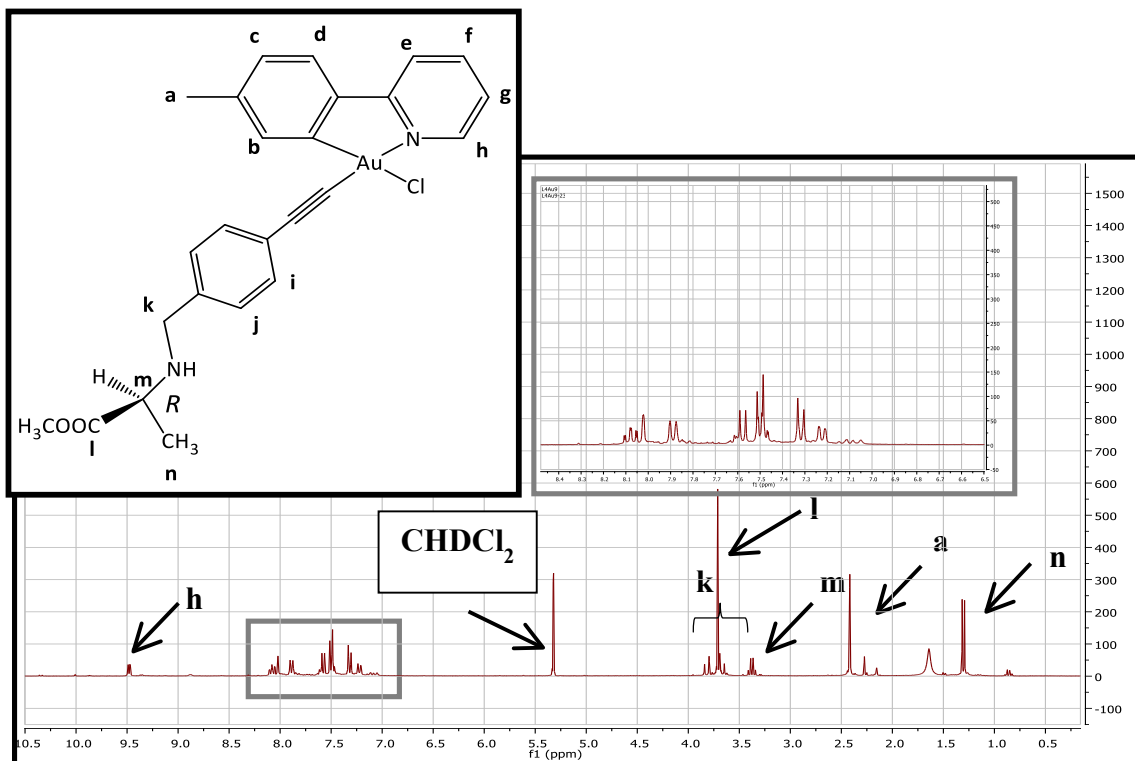


**Figure 34:**  $^1\text{H}$ -NMR spectrum of complex **12** in  $\text{CD}_2\text{Cl}_2$ .

As it is shown in Figure 34, the doublet signal at  $\delta$  1.30, associated to protons  $\text{H}^n$  from the methyl group of the carbon  $\alpha$  from the 1-ethynyl-4-benzyl-L-alanine methyl ester molecule bonded to the gold atom, did not undergo a remarkable shift compared to the free ligand (Figure 35, blue spectrum). This was also observed in the case of protons  $\text{H}^i$ ,  $\text{H}^j$ ,  $\text{H}^k$  and  $\text{H}^l$  ( $\delta$  3.67—3.82). Regarding the aromatic area, proton  $\text{H}^b$  is observed as a doublet signal at  $\delta$  8.02 because of its coupling to  $\text{H}^c$ .

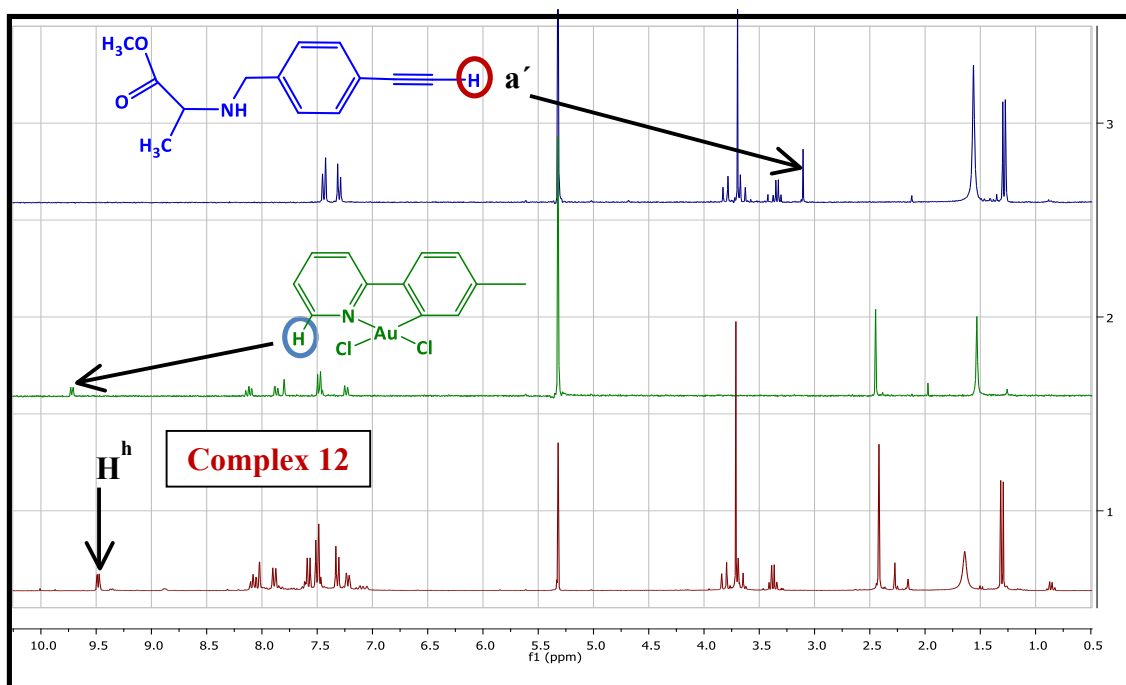


**Figure 35:** Comparison between  $^1\text{H}$ -NMR spectrum of complex **12** (red spectrum), (2-*para*-tolylpyridyl) $\text{AuCl}_2$  (green spectrum) and 1-ethynyl-4-benzyl-L-alanine methyl ester (blue spectrum) in  $\text{CD}_2\text{Cl}_2$ .

As it is shown in Figure 35, one of the most remarkable features of  $^1\text{H}$ -NMR spectrum of complex **12** is the absence of the chemical shift corresponding to the proton of the alkyne functional group of 1-ethynyl-4-benzyl-L-alanine methyl ester (**red circle**). This feature and the significant shift shown by the proton  $\text{H}^{\text{h}}$  of complex **12** ( $\delta$  9.48) compare to the same proton from (2-*para*-tolylpyridyl) $\text{AuCl}_2$  precursor ( $\delta$  9.75, **blue circle**) indicate that one 1-ethynyl-4-benzyl-L-alanine methyl ester molecule is coordinated to the gold metallic centre, forming an Au-C bond.

The chemical shifts corresponding to  $^{13}\text{C}\{^1\text{H}\}$ -NMR spectrum of complex **12** in  $\text{CD}_2\text{Cl}_2$  at room temperature have been recorded in Table 21.

**Table 21.**  $^{13}\text{C}\{^1\text{H}\}$ -NMR data of complex **12** in  $\text{CD}_2\text{Cl}_2$  ( $\delta(\text{ppm})$ ).

COMPLEX 12	ASSIGNMENT	$^{13}\text{C}$ (ppm)
	t or w	18.9
	s	21.2
	t or w	21.8
	r, v	51.6, 54.2
	l, m	97.0, 84.3
	Aromatic region	120.1 (d), 123.7 (b or g), 123.8 (b or g), 125.3 ( $\text{C}_{\text{ipso}}$ , n or q), 128.0 (o or p), 129.1 (h), 131.7 (o or p), 135.4 ( $\text{C}_{\text{ipso}}$ , n or q), 139.6 (j), 139.9 (c or f), 142.1 (c or f), 143.2 ( $\text{C}_{\text{ipso}}$ , a, i or k), 146.9 ( $\text{C}_{\text{ipso}}$ , a, i or k), 147.6 ( $\text{C}_{\text{ipso}}$ , a, i or k), 164.1 ( $\text{C}_{\text{ipso}}$ , e).
	u	176.0

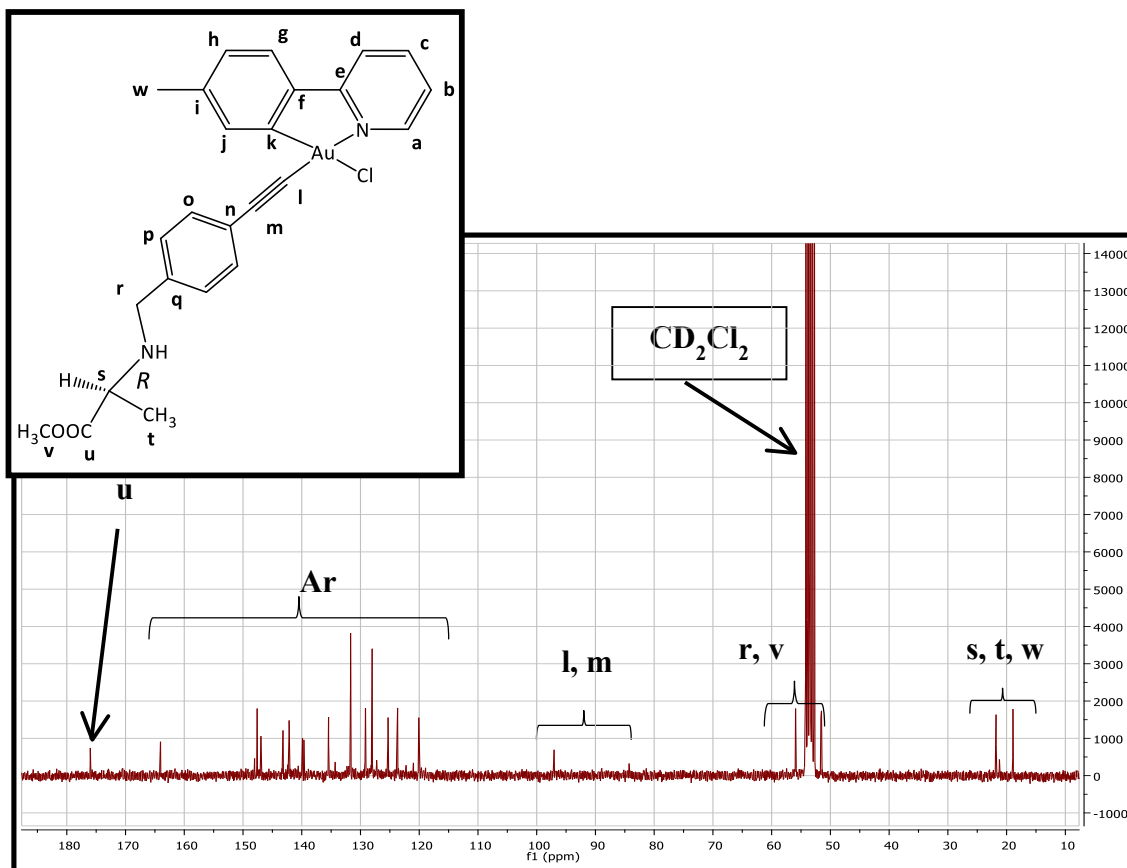


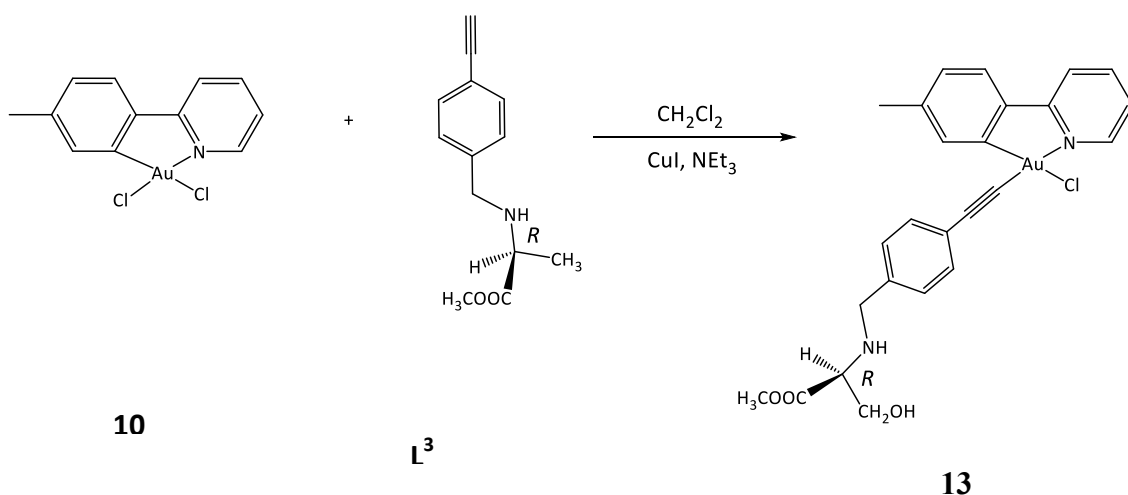
**Figure 36.**  $^{13}\text{C}\{^1\text{H}\}$ -NMR spectrum of complex **12** in  $\text{CD}_2\text{Cl}_2$ .

The  $^{13}\text{C}\{^1\text{H}\}$ -NMR spectrum of complex **12** in  $\text{CD}_2\text{Cl}_2$  exhibits one signal at  $\delta$  176.0 corresponding to the carbon atom of the  $-\text{CO}$  group from the ester function of the 1-ethynyl-4-benzyl-L-alanine methyl ester molecule bonded to Au atom (**g**). The signals corresponding to the carbons of the alkyne group are observed as weak signals at  $\delta$  84.3, 97.0 (**l** and **m**), slightly shifted compared to the ones observed for the ligand 1-ethynyl-4-benzyl-L-alanine methyl ester ( $\delta$  73.9, 83.4, Table 3).

### 1.2.2.3. Synthesis of $(\text{C}^{\wedge}\text{N})\text{Au}(\text{Cl})\text{C}\equiv\text{C}-\text{C}_6\text{H}_4-4-[\text{CH}_2\text{NH}-\text{CH}-(\text{CH}_2\text{OH})-\text{COOCH}_3]$ (**13**).

The reaction of 1-ethynyl-4-benzyl-L-serine methyl ester and (2-*para*-tolylpyridyl) $\text{AuCl}_2$  (**10**) (1:1 ratio) in dichloromethane, in presence of excess of triethylamine and a catalytic amount of  $\text{CuI}$  for 2 hours led the synthesis of complex **13**

(68.0 mg, 38 %). Complex **13** is a yellow solid, air stable, soluble in dichloromethane and ethanol, and not soluble in petrol ether 40/60 (Scheme 23).



**Scheme 23.** *Synthesis of complex 13.*

Complex **13** has been characterized by  $^1\text{H-NMR}$ ,  $^{13}\text{C}\{^1\text{H}\}\text{-NMR}$ , infrared spectroscopy and elemental analysis.

The IR spectrum shows a weak absorption peak at  $1731$  and  $2154\text{ cm}^{-1}$ , corresponding to the stretch of the  $\text{C=O}$  bond of the ester function and the  $\text{C}\equiv\text{C}$  bond of the di-substituted alkyne group,<sup>21,25</sup> respectively.

The chemical shifts corresponding to  $^1\text{H-NMR}$  spectrum for complex **13** in  $\text{CD}_2\text{Cl}_2$  at room temperature are recorded in Table 22.

**Table 22:**  $^1\text{H-NMR}$  data of complex **13** in  $\text{CD}_2\text{Cl}_2$ ,  $\delta(\text{ppm})$  and multiplicity.

COMPLEX 13	ASSIGNMENT	$^1\text{H}$ (ppm)
	a	2.40 (s, 3H)
	n	3.43 (dd, $J = 5.8, 4.7$ Hz, 1H)
	l	3.74 (s, 3H)
	m, k (overlapped)	3.57 – 3.94 (m, 4H)
	c	7.24 (d, $J = 7.1$ Hz, 1H)
	i, j	7.33 (d, $J = 8.0$ Hz, 2H), 7.52 (d, $J = 8.0$ Hz, 2H)
	g	7.47 – 7.53 (m, 1H)
	d	7.59 (d, $J = 7.9$ Hz, 1H)
	e	7.90 (d, $J = 7.9$ Hz, 1H)
	b	8.05 (d, $J = 0.7$ Hz, 1H)
	f	8.06 – 8.13 (td, $J = 8.0, 1.5$ Hz, 1H)
	h	9.51 (d, $J = 5.0$ Hz, 1H)

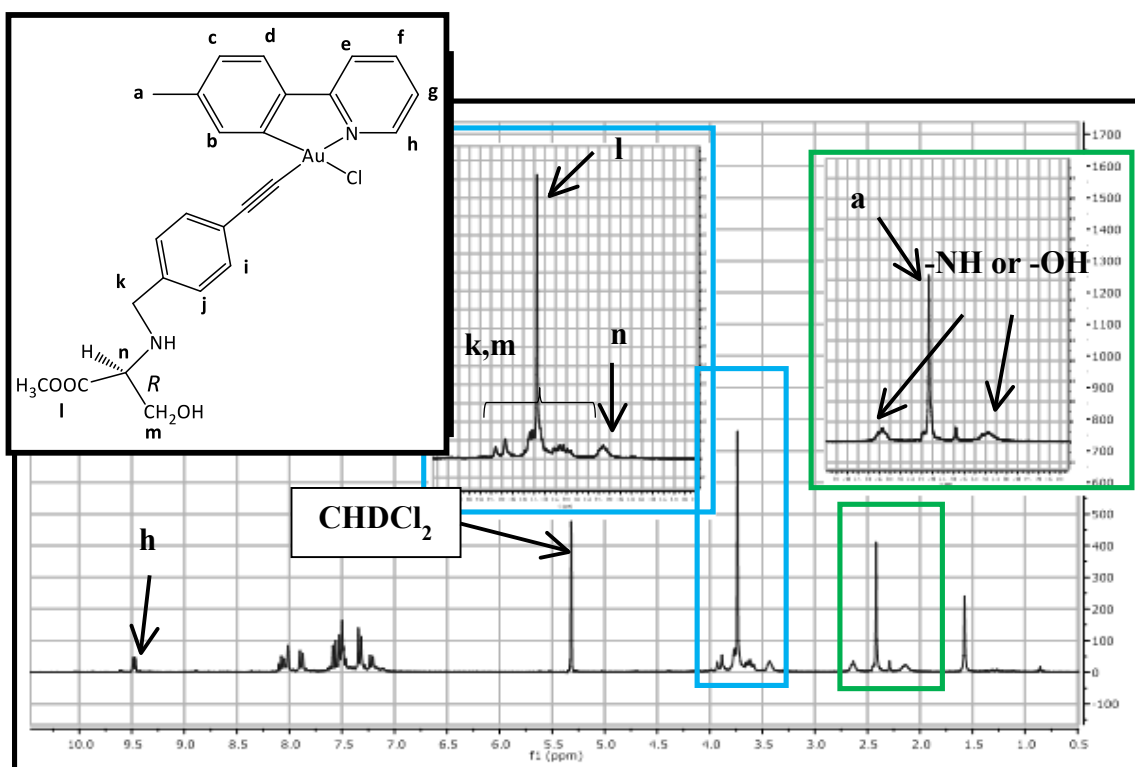


**Figure 37:**  $^1\text{H-NMR}$  spectrum of complex **13** in  $\text{CD}_2\text{Cl}_2$ .

As it is shown in Figure 37, the  $^1\text{H-NMR}$  spectrum of complex **13** shows two broad signals integrating by one proton between  $\delta$  2—3. These two signals may correspond to the chemical shifts from the  $-\text{NH}$  and the  $-\text{OH}$  functions, which are expected to be observed in that region of the  $^1\text{H-NMR}$  spectrum. In order to check if these chemical shifts correspond to the mentioned functional groups, a drop of  $\text{D}_2\text{O}$  was added to the NMR tube in  $\text{CD}_2\text{Cl}_2$ . Because of the enhanced acidity of the hydrogen atom of the  $-\text{OH}$  and  $-\text{NH}$  groups, the addition of a drop of  $\text{D}_2\text{O}$  promotes and isotopic exchange, which implies a replacing of a hydrogen atom by a deuterium atom. If the observed broad signals correspond to the  $-\text{NH}$  and  $-\text{OH}$  functions, they should not be observed in the  $^1\text{H-NMR}$  spectrum after addition of  $\text{D}_2\text{O}$ .

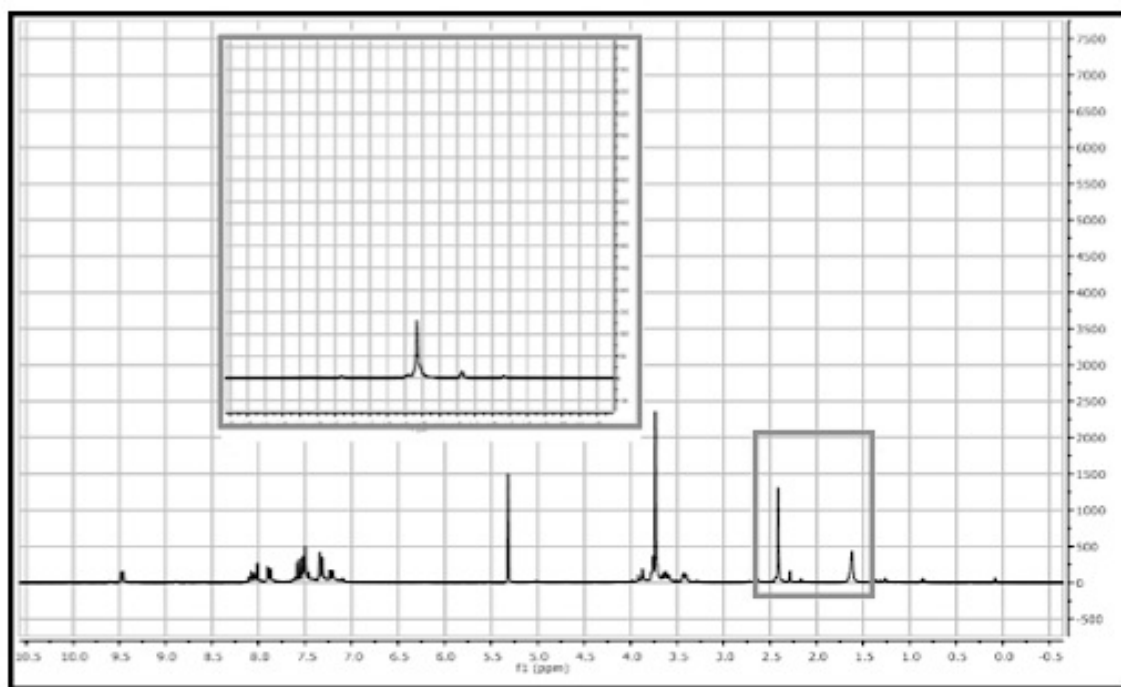


**Figure 38:**  $^1\text{H}$ -NMR spectrum of complex **13** in  $\text{CD}_2\text{Cl}_2$ , after addition of  $\text{D}_2\text{O}$ .

Figure 38 shows the  $^1\text{H}$ -NMR spectrum of complex **13** in  $\text{CD}_2\text{Cl}_2$ , after addition of one drop of  $\text{D}_2\text{O}$ . As is shown on the spectrum, the two broad singlet signals are not presented after adding one drop of  $\text{D}_2\text{O}$ . This result confirms that these broad signals correspond to the  $-\text{OH}$  and  $-\text{NH}$  functional groups, and the addition of  $\text{D}_2\text{O}$  has prompted the isotopic exchange of the hydrogen atom by deuterium atom.

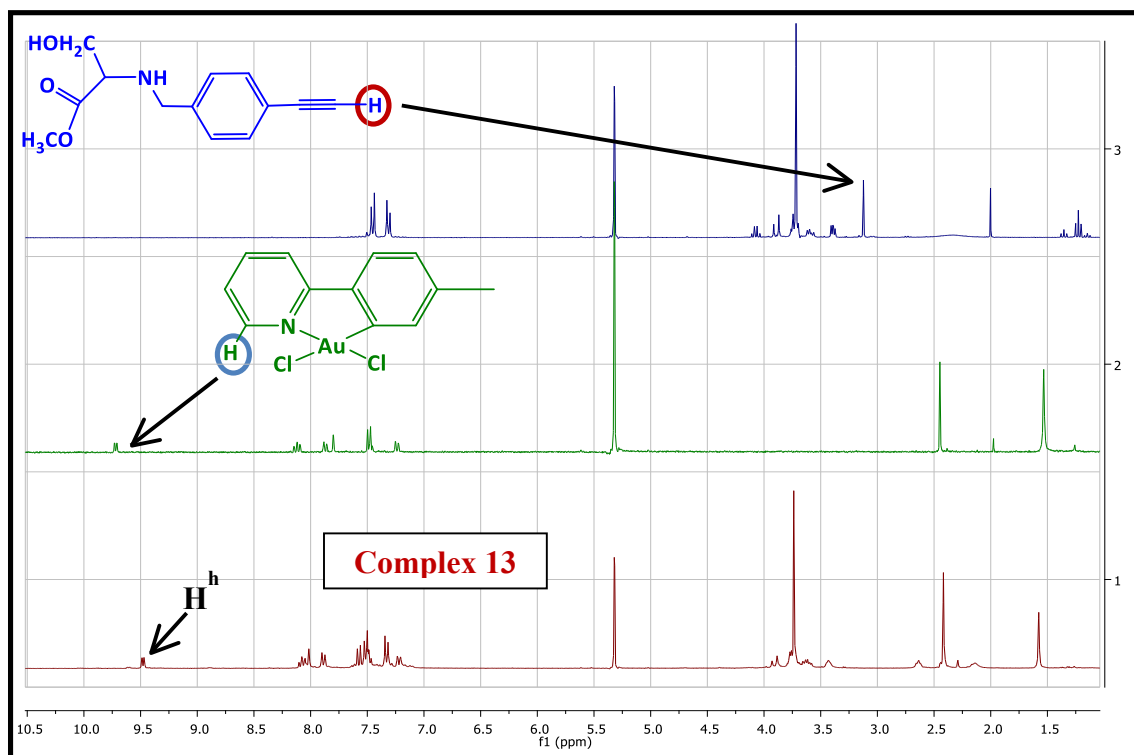


**Figure 39:** Comparison between  $^1\text{H}$ -NMR spectra of complex **13** (red spectrum), (2-*para*-tolylpyridyl) $\text{AuCl}_2$  (green spectrum) and 1-ethynyl-4-benzyl-*L*-serine ethyl ester (blue spectrum) in  $\text{CD}_2\text{Cl}_2$ .

As it is shown in Figure 39, proton  $\text{H}^{\text{h}}$  of complex **13** ( $\delta$  9.51, red spectrum) is shifted compared to the same proton from (2-*para*-tolylpyridyl) $\text{AuCl}_2$  precursor ( $\delta$  9.75, **blue circle**). Although  $^1\text{H}$ -NMR spectrum of complex **13** does not show remarkable variations in the chemical shifts compared to the  $^1\text{H}$ -NMR spectrum of the ligand 1-ethynyl-4-benzyl-*L*-serine ethyl ester (blue spectrum), the absence of the proton of the alkyne functional group (**red circle**) in the  $^1\text{H}$ -NMR spectrum of complex **13** indicates that 1-ethynyl-4-benzyl-*L*-serine methyl ester molecule is coordinated to the metallic centre.

The  $^{13}\text{C}\{^1\text{H}\}$ -NMR spectrum for the complex **13** has been carried out in  $\text{CD}_2\text{Cl}_2$  at room temperature. The chemical shifts are recorded in Table 23.

**Table 23.**  $^{13}\text{C}\{^1\text{H}\}$ -NMR data of complex **13** in  $\text{CD}_2\text{Cl}_2$  ( $\delta(\text{ppm})$ ).

COMPLEX 13	ASSIGNMENT	$^{13}\text{C}(\text{ppm})$
	w	21.8
	v	51.3
	r, t	61.0, 62.4
	l, m	84.0, 96.9
	Aromatic region	120.0 (d), 123.7 (b or g), 123.8 (b or g), 125.3 ( $\text{C}_{\text{ipso}}$ , n or q), 128.1 (o or p), 129.1 (h), 131.8 (o or p), 135.5 ( $\text{C}_{\text{ipso}}$ , n or q), 139.3 (j), 139.7 (c or f), 142.2 (c or f), 143.2 ( $\text{C}_{\text{ipso}}$ , a, i or k), 146.9 ( $\text{C}_{\text{ipso}}$ , a, i or k), 147.6 ( $\text{C}_{\text{ipso}}$ , a, i or k), 164.1 ( $\text{C}_{\text{ipso}}$ , e).
	u	173.2

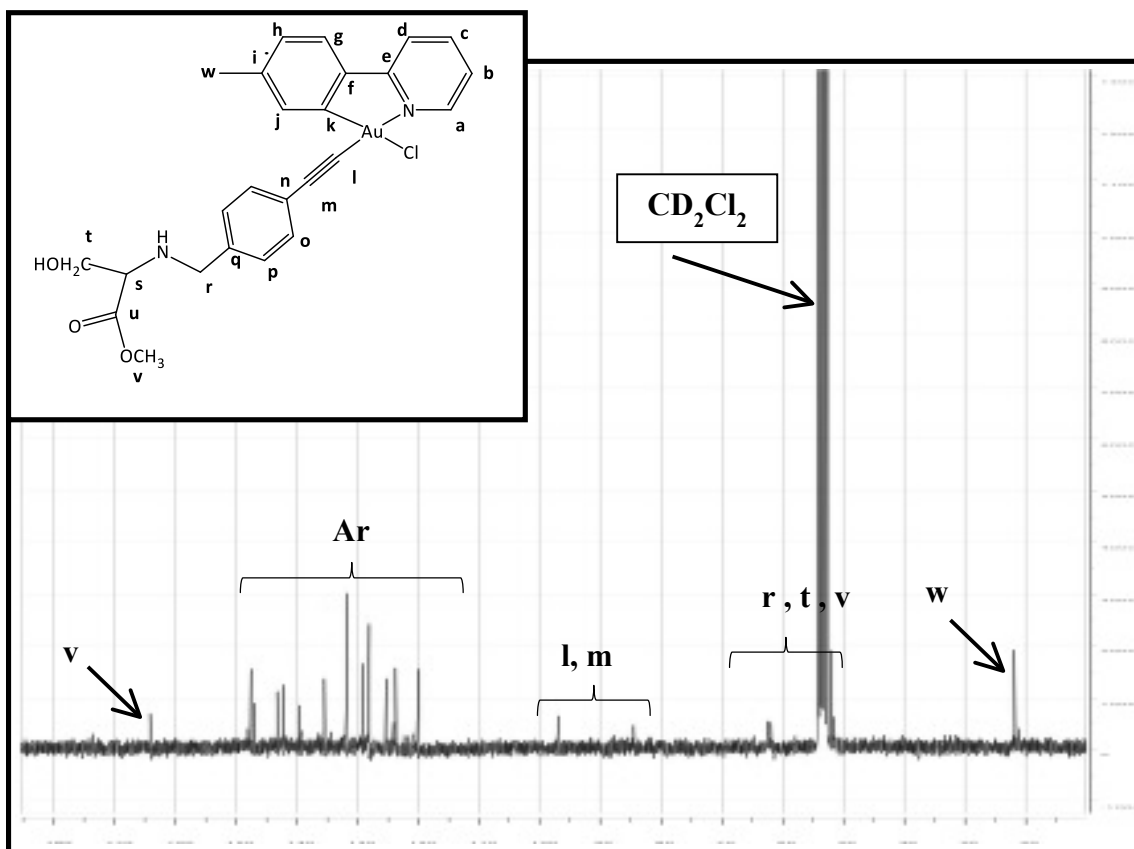


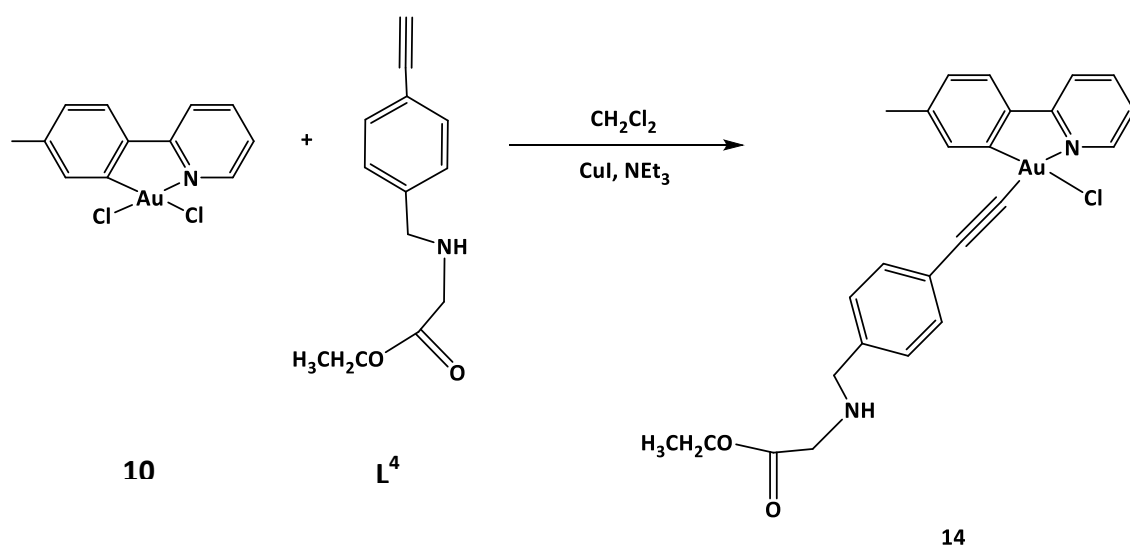
**Figure 40:**  $^{13}\text{C}\{^1\text{H}\}$ -NMR spectrum of complex **13** in  $\text{CD}_2\text{Cl}_2$ .

The  $^{13}\text{C}\{^1\text{H}\}$ -NMR spectrum of complex **13** in  $\text{CD}_2\text{Cl}_2$  shows one signal at  $\delta$  173.2 corresponding to the carbon atom of  $-\text{CO}$  group from the ester function of the 1-ethynyl-4-benzyl-L-serine methyl ester molecule coordinated to the metallic centre (**h**). The signals corresponding to the carbon atoms from alkyne group are observed as weak signals at  $\delta$  84.0 and 96.9 (**l** and **m**), slightly shifted regarding the ones observed for the ligand 1-ethynyl-4-benzyl-L-serine methyl ester ( $\delta$  77.3, 83.5, Table 5).

#### 1.2.2.4. Synthesis of $(\text{C}^{\wedge}\text{N})\text{Au}-(\text{Cl})\text{C}\equiv\text{C}-\text{C}_6\text{H}_4-4-[\text{CH}_2-\text{NH}-\text{CH}(\text{CH}_2\text{OH})-\text{COOCH}_3]$ (**14**).

The reaction of 1-ethynyl-4-benzyl-L-glycine methyl ester and (2-*para*-tolylpyridyl) $\text{AuCl}_2$  (**10**) (1:1 ratio) in dichloromethane, in presence of excess of triethylamine and a catalytic amount of  $\text{CuI}$  for 2 hours gave complex **14** (94.5 mg, 41

%). Complex **14** is a yellow solid, air stable, soluble in dichloromethane and ethanol, and not soluble in petrol ether 40/60 (Scheme 24).



**Scheme 24.** *Synthesis of complex 14.*

Complex **14** has been characterized by  $^1\text{H}$ -NMR,  $^{13}\text{C}\{^1\text{H}\}$ -NMR, infrared spectroscopy and elemental analysis.

The IR spectrum shows a weak absorption band at  $1736$  and  $2161\text{ cm}^{-1}$ , corresponding to the stretch of the  $\text{C}=\text{O}$  bond of the ester function and the  $\text{C}\equiv\text{C}$  bond of the di-substituted alkyne group,<sup>21,25</sup> respectively.

The chemical shifts corresponding to  $^1\text{H}$ -NMR spectrum for complex **14** in  $\text{CD}_2\text{Cl}_2$  at room temperature are recorded in Table 24.

**Table 24:**  $^1\text{H-NMR}$  data of complex **14** in  $\text{CD}_2\text{Cl}_2$ ,  $\delta(\text{ppm})$  and multiplicity.

COMPLEX 14	ASSIGNMENT	$^1\text{H}$ (ppm)
	m	1.26 (t, $J = 7.1$ Hz, 2H)
	a	2.42 (s, 3H)
	k, l	3.39 (s, b, 2H), 3.81 (s, b, 2H)
	n	4.17 (q, $J = 7.1$ Hz, 3H)
	c	7.23 (d, $J = 7.8$ Hz, 1H)
	i, j	7.32 (d, $J = 8.0$ Hz, 2H), 7.51 (d, $J = 8.0$ Hz, 2H)
	g	7.48 – 7.51 (m, 1H)
	d	7.59 (d, $J = 7.9$ Hz, 1H)
	e	7.90 (d, $J = 7.9$ Hz, 1H)
	b	8.05 (d, $J = 0.8$ Hz, 1H)
	f	8.05 – 8.13 (td, $J = 8.0, 1.5$ Hz, 1H)
	h	9.50 (d, $J = 4.8$ Hz, 1H)

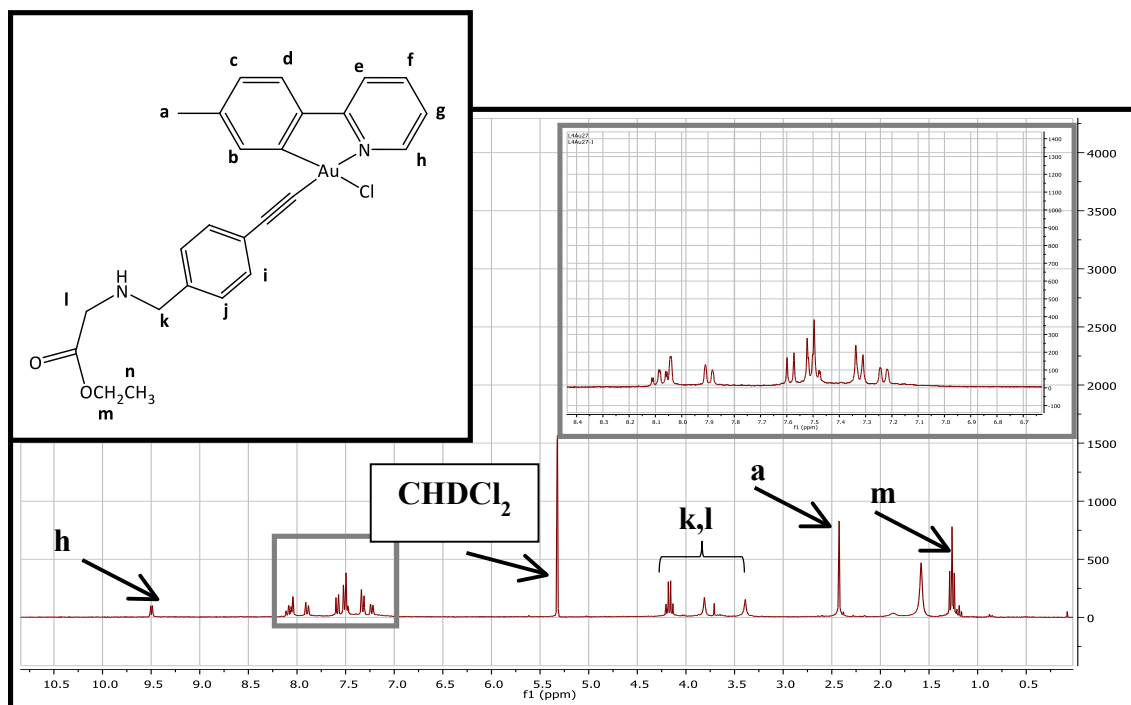


**Figure 41:**  $^1\text{H-NMR}$  spectrum of complex **14** in  $\text{CD}_2\text{Cl}_2$ .

The comparison between  $^1\text{H-NMR}$  spectra of complex **14** (red spectrum), (2-*para*-tolylpyridyl) $\text{AuCl}_2$  (blue spectrum) and 1-ethynyl-4-benzyl-L-glycine ethyl ester (green spectrum) in  $\text{CD}_2\text{Cl}_2$  shows that both the chemical shifts corresponding to the methylene and methyl groups ( $\text{CH}_3\text{CH}_2\text{-O-}$ ) of the 1-ethynyl-4-benzyl-L-glycine ethyl ester function of complex **14** did not undergo significant variations compared to the chemical shifts shown by ligand 1-ethynyl-4-benzyl-L-glycine ethyl ester (Figure 42). However,  $\text{H}^{\text{h}}$  of complex **14** ( $\delta$  9.50) exhibits a notable shift compared to the same proton from (2-*para*-tolylpyridyl) $\text{AuCl}_2$  precursor ( $\delta$  9.75, **red circle**). This feature and the absence of the proton of the alkynyl function from 1-ethynyl-4-benzyl-L-glycine ethyl ester molecule (**blue circle**) indicate that coordination of the 1-ethynyl-4-benzyl-L-serine has taken place successfully.

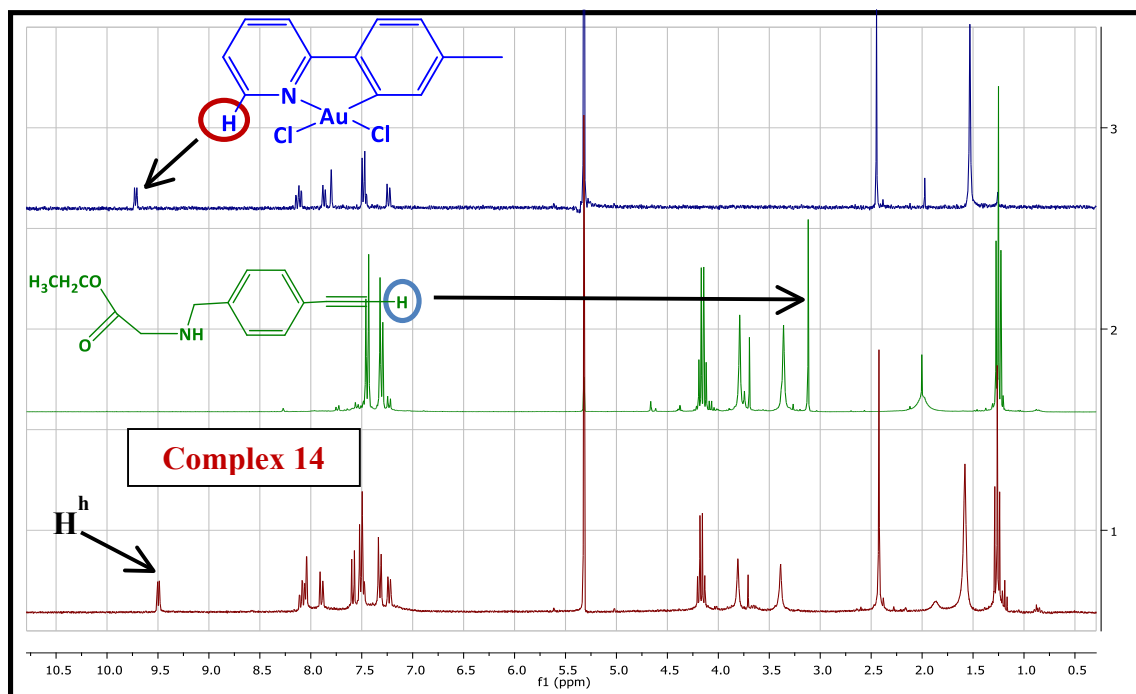


**Figure 42:** Comparison between  $^1\text{H}$ -NMR spectra of complex **14** (red spectrum), (2-*para*-tolylpyridyl) $\text{AuCl}_2$  (blue spectrum) and 1-ethynyl-4-benzyl-*L*-serine ethyl ester (green spectrum) in  $\text{CD}_2\text{Cl}_2$ .

The  $^{13}\text{C}\{^1\text{H}\}$ -NMR spectrum for the complex **14** has been carried out in  $\text{CD}_2\text{Cl}_2$  at room temperature. The chemical shifts are recorded in Table 25.

**Table 25.**  $^{13}\text{C}\{^1\text{H}\}$ -NMR data of complex **14** in  $\text{CD}_2\text{Cl}_2$  ( $\delta(\text{ppm})$ ).

COMPLEX 14	ASSIGNMENT	$^{13}\text{C}$ (ppm)
	v	14.0
	w	21.8
	u	29.0
	s, r	50.1, 60.6
	l, m	97.1, 84.3
	Aromatic region	120.0 (d), 123.7 (b or g), 123.9 (b or g), 125.3 ( $\text{C}_{\text{ipso}}$ , n or q), 128.1 (o or p), 129.1 (h), 131.7 (o or p), 135.5 ( $\text{C}_{\text{ipso}}$ , n or q), 139.6 (j), 142.1 (c or f), 143.2 ( $\text{C}_{\text{ipso}}$ , a, i or k), 146.9 ( $\text{C}_{\text{ipso}}$ , a, i or k), 147.6 ( $\text{C}_{\text{ipso}}$ , a, i or k), 164.1 ( $\text{C}_{\text{ipso}}$ , e).
	t	This signal is not shown in the spectrum.

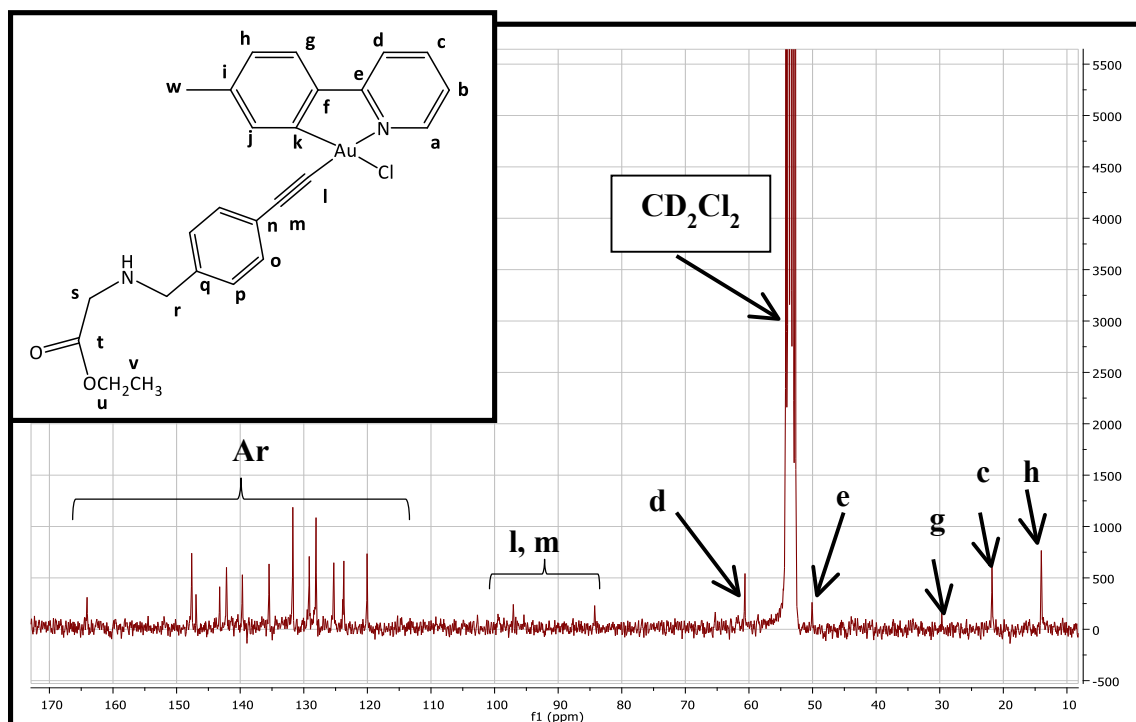


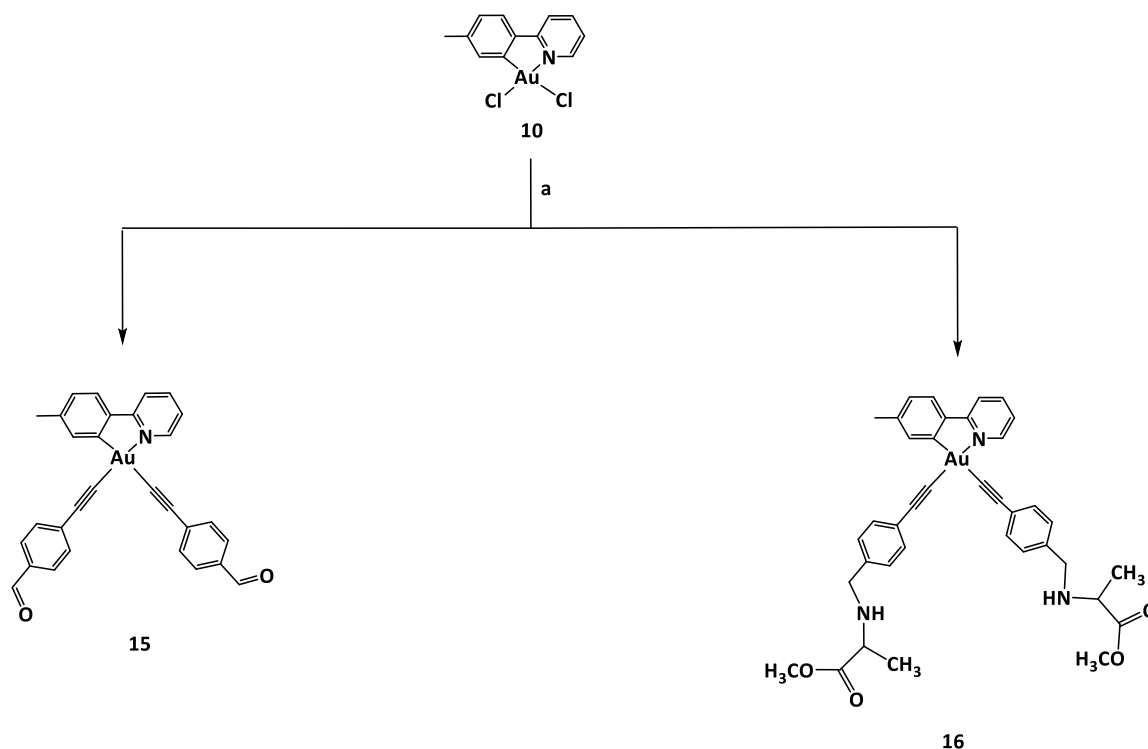
**Figure 43:**  $^{13}\text{C}\{^1\text{H}\}$ -NMR spectrum of complex **14** in  $\text{CD}_2\text{Cl}_2$ .

As is shown in Figure 43, the signal corresponding to the  $-\text{CO}$  group from the ester function of the 1-ethynyl-4-benzyl-L-glycine ethyl ester molecule coordinated to the Au atom is not shown in the  $^{13}\text{C}\{^1\text{H}\}$ -NMR spectrum. The chemical shifts corresponding to the alkyne group were shown as two weak signals at  $\delta$  84.3 and 97.1, slightly shifted compared to those chemical shifts on the free ligand ligand 1-ethynyl-4-benzyl-L-glycine ethyl ester ( $\delta$  77.2 and 83.8, Table 7).

### 1.2.3. Synthesis of di-substituted bi-dentate gold(III) complexes functionalized with alkyne derivatives.

The incorporation of two alkyne ligands into the cyclometalated gold (III) moiety has been achieved following the experimental procedure previously reported on the synthesis of mono-substituted derivatives, employing (2-*para*-tolylpyridyl) $\text{AuCl}_2$  as precursor, alkyne ligand, triethylamine, and a catalytic amount of copper(I) iodide in

dichloromethane. The  $[(C^{\wedge}N)Au(C\equiv CR)_2]$  derivatives **15** and **16** have been isolated as yellow solids in moderated yields, over 40% (Scheme 25).



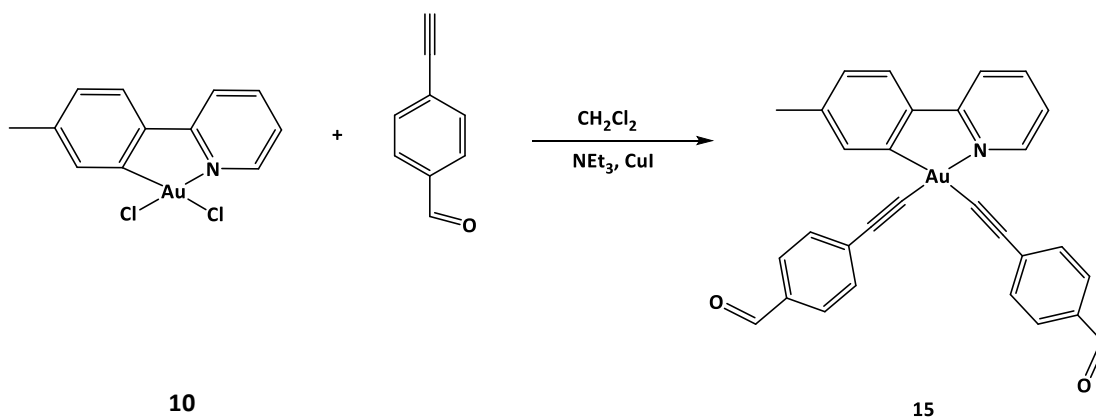
a. 4-ethynylbenzaldehyde (**15**), *N*-1-ethynylbenzyl methyl ester of (L)-alanine (**16**), CuI, NEt<sub>3</sub>, dichloromethane.

**Scheme 25.** *Synthesis of di-substituted bi-dentate gold(III) complexes functionalized with alkynyl derivatives.*

As was shown for mono-substituted complexes, **15** and **16** exhibited high solubility in non-polar solvents, such as dichloromethane, and protic solvents, such as alcohols. In contrast, the chlorogold precursor  $(2\text{-}p\text{-tolylpyridyl})AuCl_2$  (**10**) exhibited a poor solubility in these media, which provided as an useful tool to isolate pure products and also to identify when the reaction had been completed (this was shown once the initial suspension turned into solution).

### 1.2.3.1. Synthesis of $(C^{\wedge}N)Au(-C\equiv C-C_6H_4-CHO)_2$ (**15**).

The reaction of 4-ethynylbenzaldehyde and (2-*para*-tolylpyridyl)AuCl<sub>2</sub> (**10**) (2:1 ratio) in dichloromethane, in presence of excess of triethylamine and a catalytic amount of CuI, was stirred for 2 hours at room temperature, to allow the synthesis of complex **15** (61.3 mg, 62 %). Complex **15** was isolated as yellow solid, air stable, soluble in dichloromethane and ethanol, and not soluble in petrol ether 40/60 (Scheme 26).



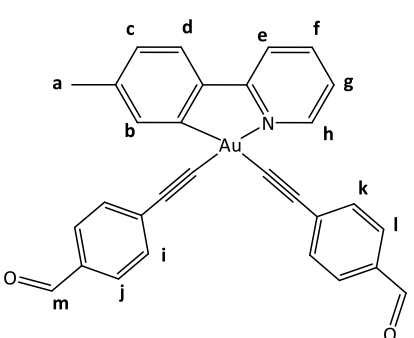
**Scheme 26.** Synthesis of complex **15**.

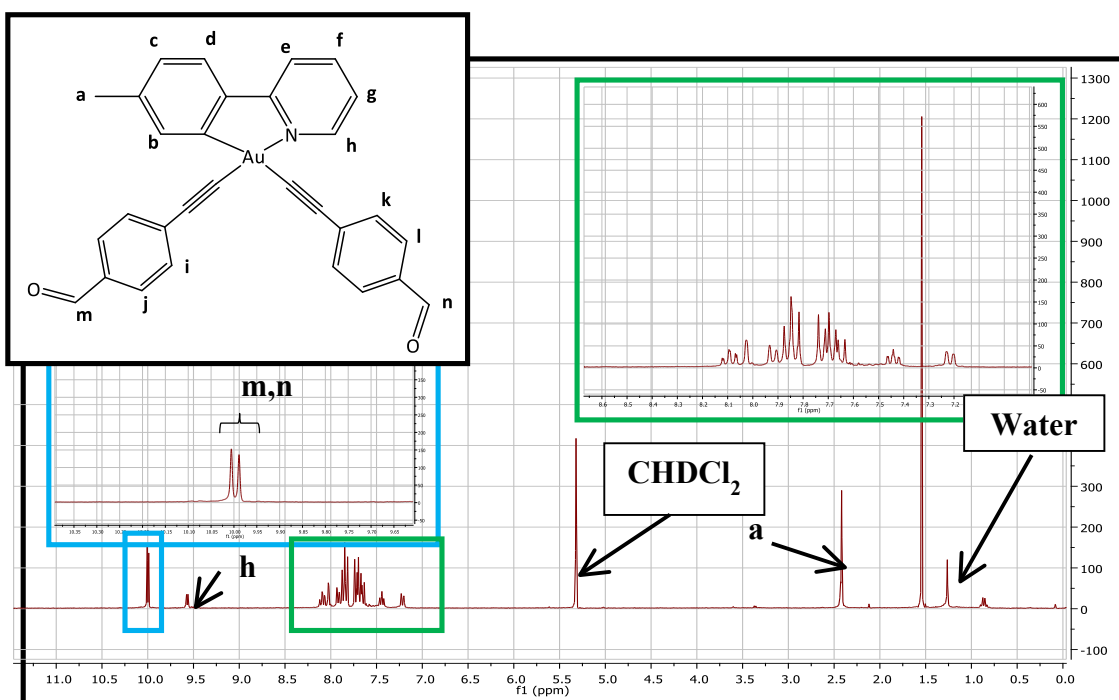
Complex **15** has been characterized by <sup>1</sup>H-NMR, <sup>13</sup>C{<sup>1</sup>H}-NMR, infrared spectroscopy and elemental analysis.

The IR spectrum shows a weak absorption band at 2131 and 2162 cm<sup>-1</sup>, corresponding to the stretch of the C≡C of the di-substituted alkyne group. This chemical shift is on the same range than the ones reported on the literature for another similar examples.<sup>16,21</sup>

The chemical shifts corresponding to <sup>1</sup>H-NMR spectrum for complex **15** in CD<sub>2</sub>Cl<sub>2</sub> at room temperature are recorded in Table 26.

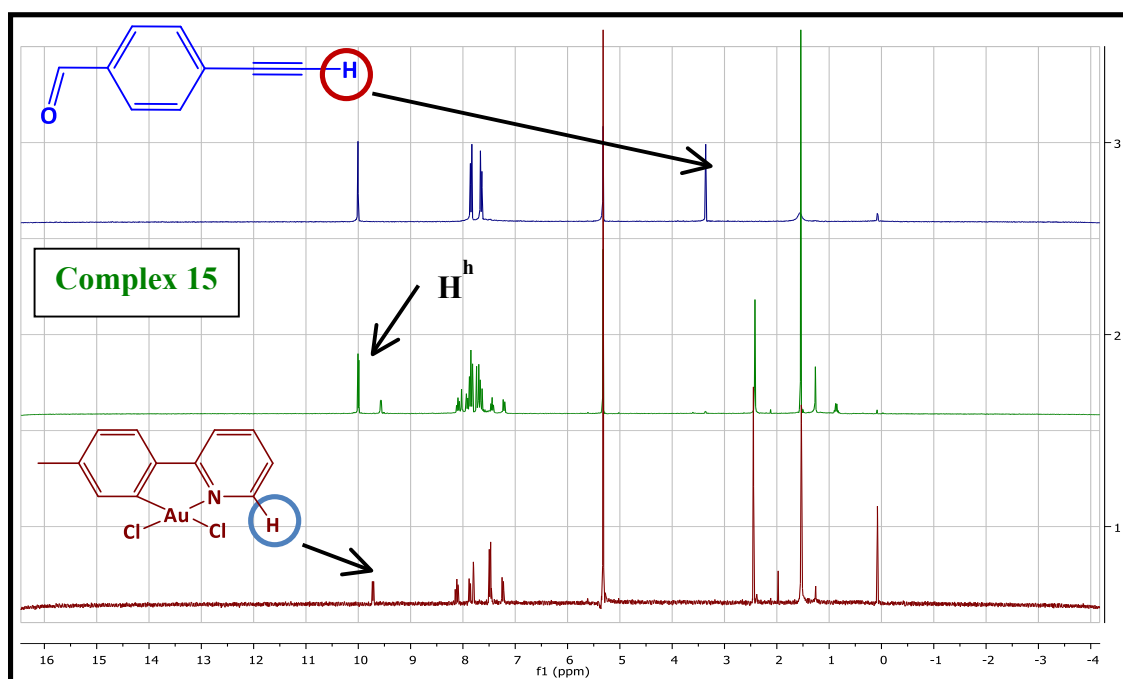
**Table 26:**  $^1\text{H}$ -NMR data of complex **15** in  $\text{CD}_2\text{Cl}_2$ ,  $\delta(\text{ppm})$  and multiplicity.

COMPLEX 15	ASSIGNMENT	$^1\text{H}$ (ppm)
	a	2.42 (s, 3H)
	c	7.23 (d, $J = 7.6$ Hz, 1H)
	g	7.44 (m, 1H)
	d	7.64 (d, $J = 8.1$ Hz, 1H)
	i – j, k – l (overlapped)	7.61 – 7.89 (m, 8H)
	e	7.92 (d, $J = 8.0$ Hz, 1H)
	b	8.02 (s, 1H)
	f	8.09 (d, $J = 8.2, 1.3$ Hz, 1H)
	h	9.57 (d, $J = 5.1$ Hz, 1H)
	m, n	9.99 (s, 1H), 10.01 (s, 1H)



**Figure 44:**  $^1\text{H}$ -NMR spectrum of complex **15** in  $\text{CD}_2\text{Cl}_2$ .

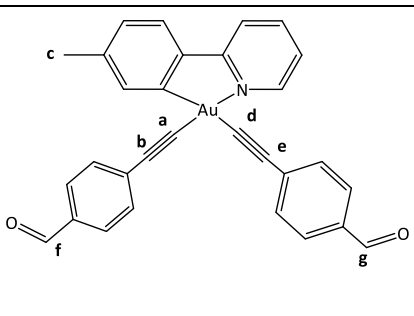
As it shown in Figure 44,  $^1\text{H}$ -NMR spectrum of complex **15** exhibits two singlet signals at  $\delta$  9.99 and 10.01 corresponding to the 4-ethynylbenzaldehyde molecules coordinated to the metallic centre. In addition, a comparison between the  $^1\text{H}$ -NMR spectrum of complex **15** (green spectrum), 4-ethynylbenzaldehyde (blue spectrum) and (2-*para*-tolylpyridyl)AuCl<sub>2</sub> precursor (red spectrum) (Figure 45) shows a remarkable shift of the signal corresponding to H<sup>h</sup> of complex **15** ( $\delta$  9.57), compared to the same proton from (2-*para*-tolylpyridyl)AuCl<sub>2</sub> precursor ( $\delta$  9.75, **blue circle**). This feature and the absence of the proton from the alkynyl function of 4-ethynylbenzaldehyde (**red circle**) indicate the formation of Au-C bond, and coordination of two 4-ethynylbenzaldehyde molecules to the gold metallic centre.



**Figure 45:** Comparison between  $^1\text{H}$ -NMR spectra of complex **15** (green spectrum), (2-*para*-tolylpyridyl)AuCl<sub>2</sub> (red spectrum) and 4-ethynylbenzaldehyde (blue spectrum) in  $\text{CD}_2\text{Cl}_2$ .

The  $^{13}\text{C}\{^1\text{H}\}$ -NMR spectrum for the complex **15** has been carried out in  $\text{CD}_2\text{Cl}_2$  at room temperature. The chemical shifts are recorded in Table 27.

**Table 27:**  $^{13}\text{C}\{^1\text{H}\}$ -NMR data of complex **15** in  $\text{CD}_2\text{Cl}_2$  ( $\delta(\text{ppm})$ ).

COMPLEX 15	ASSIGNMENT	$^{13}\text{C}$ (ppm)
	c	21.8
	a, b, d, e	86.1, 90.7, 103.6 (one signal not observed)
	Aromatic region	120.3, 123.7, 123.8, 124.9, 128.5, 129.4, 132.0, 132.2, 134.7, 135.0, 136.3, 141.8, 142.6, 142.7, 150.7, 155.2, 167.0.
	f, g	191.4 (one signal not observed)

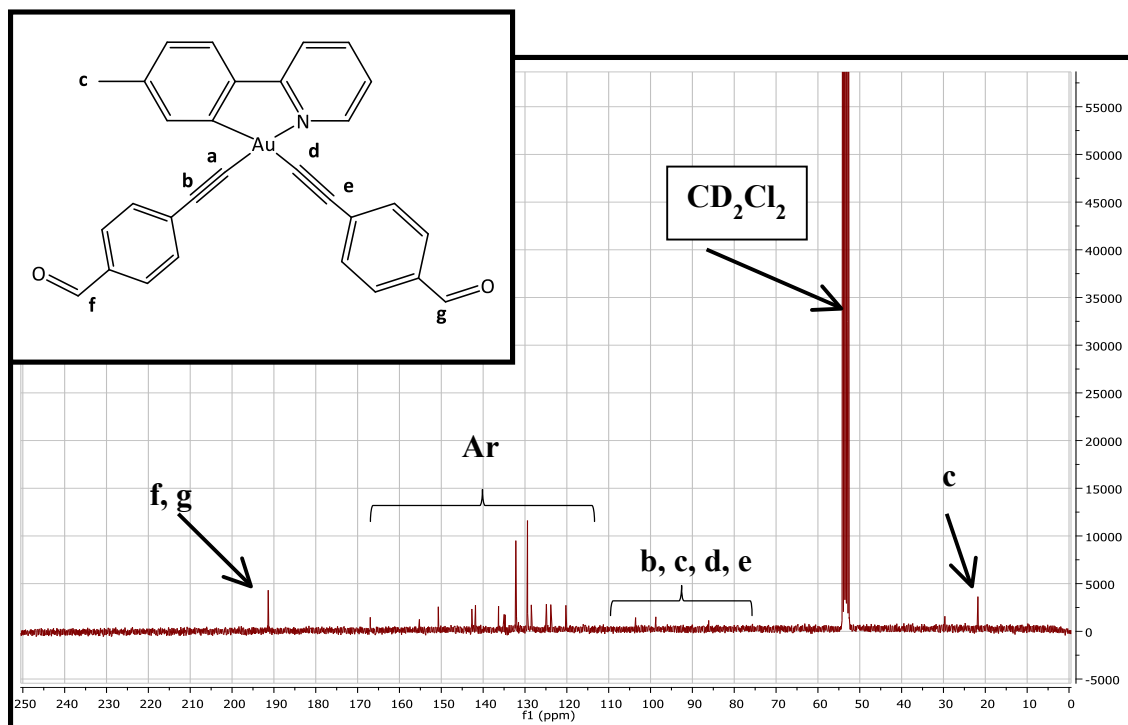


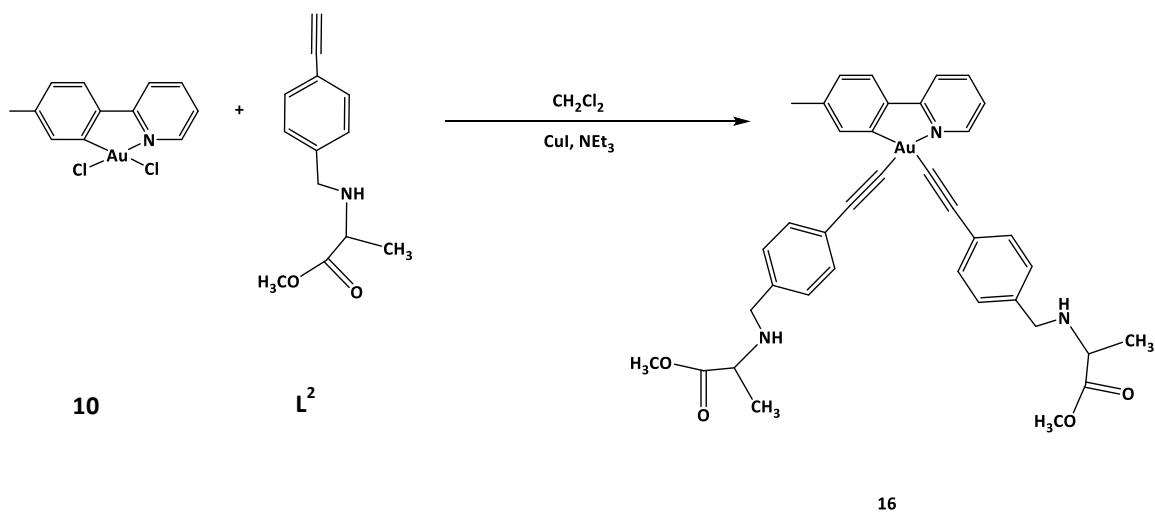
**Figure 46:**  $^{13}\text{C}\{^1\text{H}\}$ -NMR spectrum of complex **15** in  $\text{CD}_2\text{Cl}_2$ .

The  $^{13}\text{C}\{^1\text{H}\}$ -NMR spectrum of complex **15** in  $\text{CD}_2\text{Cl}_2$  shows only one signal at  $\delta$  191.5 corresponding to the carbon of  $-\text{CO}$  group from the aldehyde function of the 4-ethynylbenzaldehyde molecule coordinated to the metallic centre. The signals

corresponding to the carbon atoms from alkyne group are observed as weak signals at  $\delta$  86.1, 90.7 and 103.6. One of the carbon atoms from these bonds is not shown in the spectrum.

### 1.2.3.2. Synthesis of $(C^{\wedge}N)Au[-C\equiv C-C_6H_4-4-CH_2-NH-CH(CH_3)-COOCH_3]_2$ (**16**).

The reaction of 1-ethynyl-4-benzyl-L-alanine methyl ester and (2-*para*-tolylpyridyl)AuCl<sub>2</sub> (**10**) (4:1 ratio) in dichloromethane, in presence of excess of triethylamine and a catalytic amount of CuI for 48 hours allowed the synthesis of complex **16** (43.0 mg, 32 %). Complex **16** is a yellow solid, air stable, soluble in dichloromethane and ethanol, and not soluble in petrol ether 40/60 (Scheme 27).



**Scheme 27:** Synthesis of complex **16**.

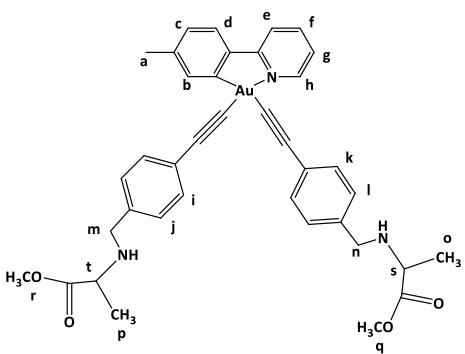
Complex **16** has been only characterized by <sup>1</sup>H-NMR, <sup>13</sup>C{<sup>1</sup>H}-NMR and infrared spectroscopy.

The IR spectrum shows only one weak broad absorption peak at 2153 cm<sup>-1</sup> corresponding to the stretch of the C≡C bonds of the di-substituted alkyne groups. Although it was expected to observe two peaks on this region, corresponding to the two

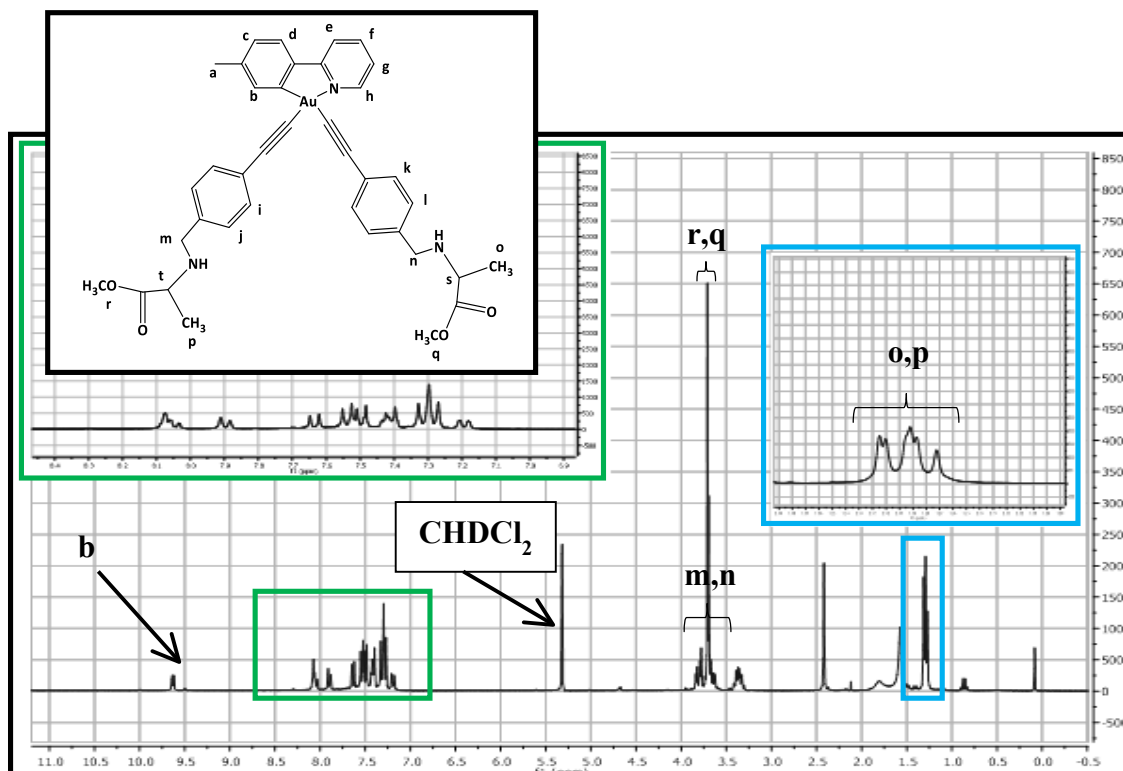
C≡C bonds of each alkyne group, the presence of a broad signal may be because of overlapping of them.

The chemical shifts corresponding to  $^1\text{H-NMR}$  spectrum for complex **16** in  $\text{CD}_2\text{Cl}_2$  at room temperature are recorded in Table 28.

**Table 28:**  $^1\text{H-NMR}$  data of complex **16** in  $\text{CD}_2\text{Cl}_2$ ,  $\delta(\text{ppm})$  and multiplicity.

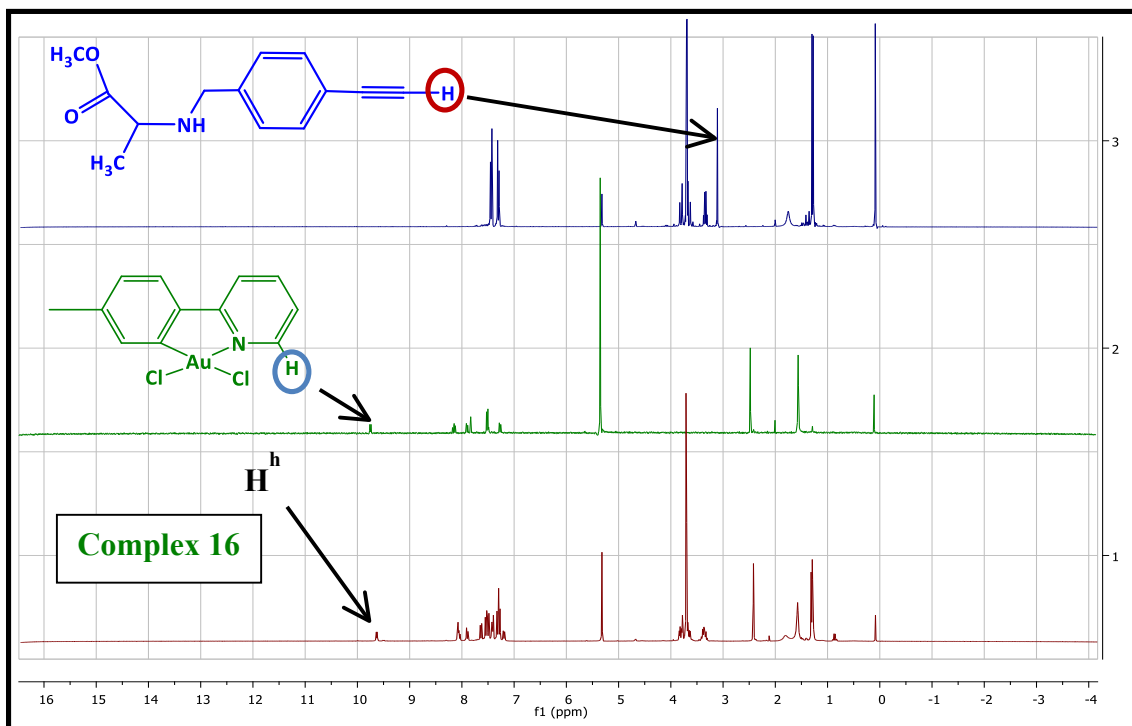
COMPLEX 16	ASSIGNMENT	$^1\text{H}$ (ppm)
	o, p	1.30 (d, $J = 6.8$ Hz, 3H), 1.31 (d, $J = 6.9$ Hz, 1H)
	a	2.42 (s, 3H)
	s, t	3.33 – 3.42 (m, 2H)
	m, n (overlapped)	3.62 – 3.84 (m, 4H)
	r, q	3.64 (s, 3H), 3.66 (s, 3H)
	c	7.20 (d, $J = 8.0$ Hz, 1H)
	g	7.42 (m, 1H)
	d	7.63 (d, $J = 8.0$ Hz, 1H)
	e	7.90 (d, $J = 8.1$ Hz, 1H)
	f, b (overlapped)*	8.03 – 8.09 (m, 2H)
	h	9.63 (d, $J = 5.1$ Hz, 1H)

\*Despite the fact that protons  $H^f$  and  $H^b$  of complex **16** are shown as overlapped signals and they could not be assigned individually (Figure 47),  $H^f$  is expected to be a singlet signal and  $H^b$  a triplet of doublets.



**Figure 47:**  $^1\text{H-NMR}$  spectrum of complex **16** in  $\text{CD}_2\text{Cl}_2$ .

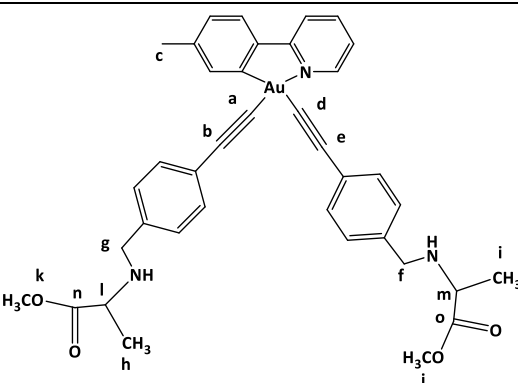
$^1\text{H-NMR}$  spectrum of complex **16** in  $\text{CD}_2\text{Cl}_2$  shows two doublet signals at  $\delta$  1.29 and 1.31 integrating for six protons, corresponding to protons  $\text{H}^a$  and  $\text{H}^b$  from the methyl groups of the  $\alpha$ -carbons of the 1-ethynyl-4-benzyl-L-alanine methyl ester coordinated to the metallic centre (Figure 47). These signals are overlapped with the chemical shifts of light petroleum. As it is shown in Figure 48, proton  $\text{H}^h$  of complex **16** ( $\delta$  9.63, red spectrum) is shifted regarding the same proton from (2-*para*-tolylpyridyl) $\text{AuCl}_2$  ( $\delta$  9.75, blue circle). In addition, the absence of the proton from the alkynyl function of 1-ethynyl-4-benzyl-L-alanine methyl ester (red circle) in the  $^1\text{H-NMR}$  spectrum of complex **16** and the presence of two different doublet signals at  $\delta$  1.30 and 1.31 integrating for three protons each, corresponding the methyl group bonded to the carbon  $\alpha$ , indicate that two molecules of 1-ethynyl-4-benzyl-L-alanine methyl ester are coordinated to the gold atom.



**Figure 48:** Comparison between  $^1\text{H}$ -NMR spectra of complex **16** (green spectrum), (2-*para*-tolylpyridyl) $\text{AuCl}_2$  (red spectrum) and 4-ethynylbenzaldehyde (blue spectrum) in  $\text{CD}_2\text{Cl}_2$ .

The  $^{13}\text{C}\{^1\text{H}\}$ -NMR spectrum for the complex **16** has been carried out in  $\text{CD}_2\text{Cl}_2$  at room temperature. The chemical shifts are recorded in Table 29.

**Table 29:**  $^{13}\text{C}\{^1\text{H}\}$ -NMR data of complex **16** in  $\text{CD}_2\text{Cl}_2$  ( $\delta(\text{ppm})$ ).

COMPLEX 16	ASSIGNMENT	$^{13}\text{C}$ (ppm)
	h, i	18.9
	c	21.8
	k, j, g, f	51.5, 51.6, 55.4, 55.9
	a, b, c, d	78.1, 80.2, 98.8, 103.7
	Aromatic region	117.7, 120.1, 123.7, 124.3, 124.5, 124.7, 128.0, 128.2, 131.6, 131.7, 136.3, 139.6, 141.6, 142.5, 142.7, 150.7, 155.8, 166.9.
n, o	176.0	

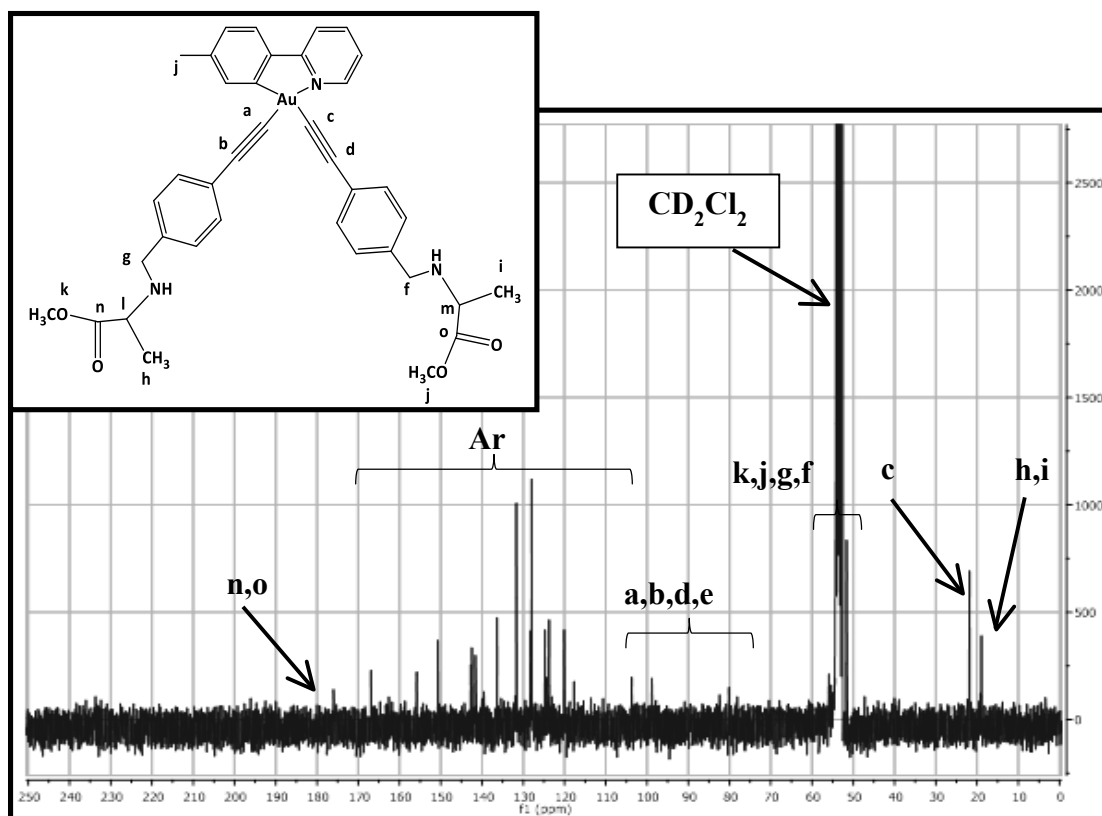


**Figure 49:**  $^{13}\text{C}\{^1\text{H}\}$ -NMR spectrum of complex **16** in  $\text{CD}_2\text{Cl}_2$ .

The  $^{13}\text{C}\{^1\text{H}\}$ -NMR spectrum of complex **16** in  $\text{CD}_2\text{Cl}_2$  showed only one signal at  $\delta$  176.0 corresponding to the carbon of the  $-\text{CO}$  group from the ester function of the two 1-ethynyl-4-benzyl-L-alanine methyl ester molecules coordinated to the metallic centre. Despite the fact that two signals should be observed, the large number of bonds between the substituent and gold metallic centre may explain the presence of the two ester functions on the same chemical shift. This fact may also explain the presence of only one chemical shift corresponding to the methyl group bonded to the carbon  $\alpha$ . The signals corresponding to the carbon atoms from alkyne group are observed as weak signals at  $\delta$  78.1, 80.2, 98.8 and 103.7.

### 1.3. SUMMARY.

- The research work has focused on the synthesis of bi- and tri-dentate gold(III) complexes functionalized by alkynyl ligands, such as 4-ethynylbenzaldehyde and alkynyl benzyl amino ester derivatives.
- $(\text{C}^{\wedge}\text{N}^{\wedge}\text{C})\text{AuCl}$  (**2**) and  $(\text{C}^{\wedge}\text{N}^{\wedge}\text{C})\text{AuOH}$  (**3**) have been employed as precursors to tri-dentate gold(III) complexes functionalized by alkynyl ligands. They have been prepared according to the experimental procedure reported in the literature.<sup>30,31</sup> The incorporation of alkynyl ligands into the cyclometalated gold(III) moiety to synthesize the tri-dentate gold(III) complexes **4**, **5**, **6** and **7**, has been achieved by reaction of  $(\text{C}^{\wedge}\text{N}^{\wedge}\text{C})\text{AuOH}$  (**3**) with the corresponding alkynyl derivative. Complexes **4**, **5**, **6** and **7** have been obtained in moderate yield, over 50%. In addition, the synthesis of complexes **4** and **5** have been also successfully tested by reaction of  $(\text{C}^{\wedge}\text{N}^{\wedge}\text{C})\text{AuCl}$  (**2**), alkynyl derivative, triethylamine, and a catalytic amount of copper(I) iodide.<sup>16</sup> This method has not introduced significant improvements in terms of yield compared to the method employing  $(\text{C}^{\wedge}\text{N}^{\wedge}\text{C})\text{AuOH}$  (**3**) as precursor.

- The synthesis of complex **8** has been achieved by reduction of the aldehyde terminal function of complex **4**, employing sodium borohydride as reducing agent. The formation of complex **8** was observed in the experiment to incorporate amino acids to the cyclometalated gold(III) moiety. This experiment was planned as reaction of complex **4** with the amino acid (D-alanine), in order to achieve the condensation between the aldehyde functional group of complex **4** with the amine group from the amino acid.
- (2-*para*-tolylpyridyl)AuCl<sub>2</sub> (**10**) has been used as precursor on the synthesis of bidentate gold(III) complexes functionalized by alkynyl ligands. This precursor has been prepared by direct auration<sup>12,8b</sup> and transmetalation<sup>8</sup> from the organomercury derivative (C<sup>^</sup>N)HgCl. The incorporation of alkynyl ligands into the cyclometalated gold(III) moiety has been achieved by reaction of (C<sup>^</sup>N)AuCl<sub>2</sub> (**10**), alkynyl derivative, triethylamine, and a catalytic amount of copper(I) iodide.<sup>21</sup> This method has been employed to synthesize both mono- and di-substituted bidentate derivatives. Accordingly, the synthesis of complexes **11**, **12**, **13**, **14**, **15** and **16** has been achieved in moderate yields through this route.

#### 1.4. CONCLUDING REMARKS AND PERSPECTIVES.

We have shown that cyclometallated (C<sup>^</sup>N<sup>^</sup>C)Au(III) alkynyl complexes could be readily obtained through acid – base reactions, employing (C<sup>^</sup>N<sup>^</sup>C)AuOH (**3**) as starting material. In these reactions, the excellent reactivity as a mild metal base showed by complex **3** led us the synthesis of complexes **5** – **8** through an acid – base reaction, allowing the Au – C bond activation at high temperatures. We also investigated the synthesis of these complexes using (C<sup>^</sup>N<sup>^</sup>C)AuCl (**2**) as starting material. By testing for complexes **4** and **5**, we observed that the addition of a mild base, such as triethylamine, may allow the deprotonation of the acidic proton from the alkynyl functional group, in

presence of a catalytic amount of CuI, affording the synthesis of these complexes in comparable yields.

Because we were unable to synthesize  $(C\wedge N)Au(OH)_2$  derivative,  $(C\wedge N)Au(III)$  alkynyl complexes could be only synthesized by the second method previously presented. The use of triethylamine, in presence of a catalytic amount of CuI, allowed the deprotonation of the acidic proton from the alkynyl functional group, to yield the formation of Cu(I) alkynyl compound, which reacts with (2-*para*-tolylpyridyl)AuCl<sub>2</sub> to afford the mono- and bi- dentate complexes **11** – **16** and CuCl as reaction products.

In recent years, some examples of cyclometallated gold(III) complexes have shown a remarkable enhancement in terms of stability for biological studies, exhibiting anti-tumor activity against different cell lines. This fact and the demonstrated ability of amino acids derivatives to deliver the gold atom to the biological target<sup>35</sup> (because of they are overexpressed in tumor cells), have encouraged us to explore the biological activity of the synthesized complexes, in particular, the interaction of the studied gold(III) complexes with secondary DNA structures.

## **1.5. EXPERIMENTAL SECTION**

### **1.5.1. GENERAL CONSIDERATIONS**

Unless otherwise stated, all experiments were performed in air using bench solvents. In such exceptions, manipulations were performed using standard Schlenk techniques under dry nitrogen or a Saffron Scientific glovebox. Nitrogen was purified by passing through columns of supported P<sub>2</sub>O<sub>5</sub>, with moisture indicator, and activated 4 Å molecular sieves. Anhydrous solvents were freshly distilled from appropriate drying agents.  $(HC\wedge N\wedge C)HgCl$  (**1**),  $(C\wedge N\wedge C)AuCl$  (**2**),  $(C\wedge N\wedge C)AuOH$ <sup>30</sup> (**3**),  $(C\wedge N)HgCl$ <sup>13</sup> (**9**)

and (C<sup>^</sup>N)AuCl<sub>2</sub> (**10**) (synthesis of complex **10** explored by transmetalation<sup>8</sup> and direct auration<sup>8b,12</sup>) were prepared using literature methods (Figure 50). 2-*para*-tolylpyridine (Aldrich), CsOH·H<sub>2</sub>O (Aldrich), phenylacetylene (Aldrich), 4-ethynylbenzaldehyde, (Fluorochem), glycine ethyl ester hydrochloride (Aldrich), L-serine methyl ester hydrochloride (Aldrich), L-alanine methyl ester hydrochloride (Aldrich), copper iodide (Aldrich), triethylamine (Aldrich) were commercially available and used as received. <sup>1</sup>H and <sup>13</sup>C{<sup>1</sup>H} spectrum were recorded using a Bruker DPX300 spectrometer. <sup>1</sup>H-NMR spectrum (300.13 MHz) were referenced to the residual protons of the deuterated solvent used. <sup>13</sup>C{<sup>1</sup>H}-NMR spectrum (75.47 MHz) were referenced internally to the proton-decoupled <sup>13</sup>C resonances of the NMR solvent. Elemental analyses were performed by London Metropolitan University.

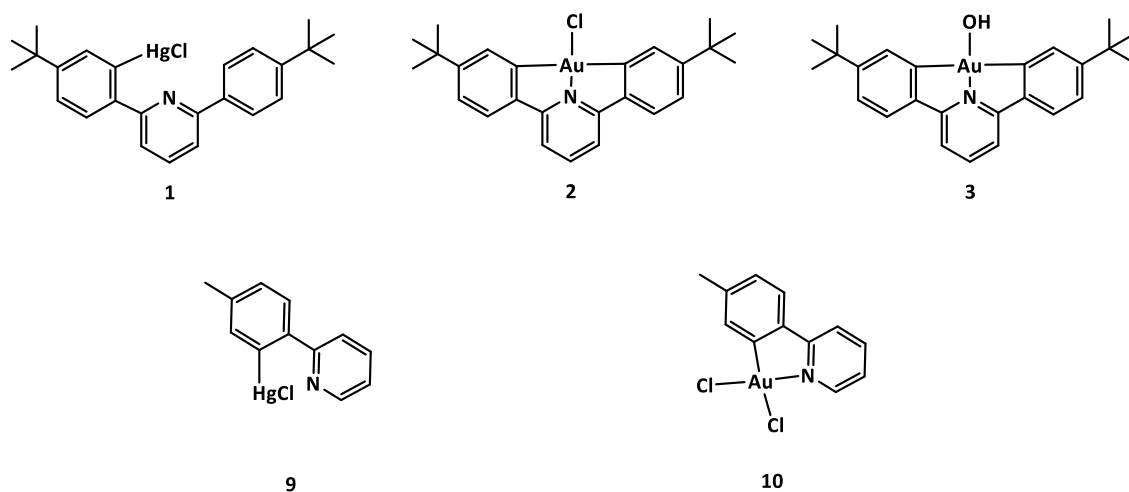
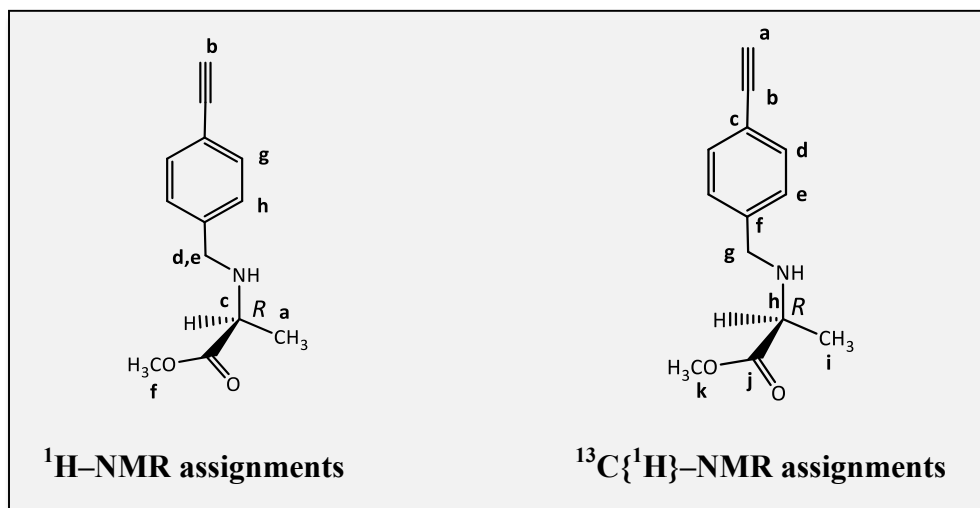


**Figure 50.** Complexes **1**, **2**, **3**, **9** and **10**, employed as precursors.

## 1.5.2. SYNTHESIS OF LIGANDS AND COMPLEXES.

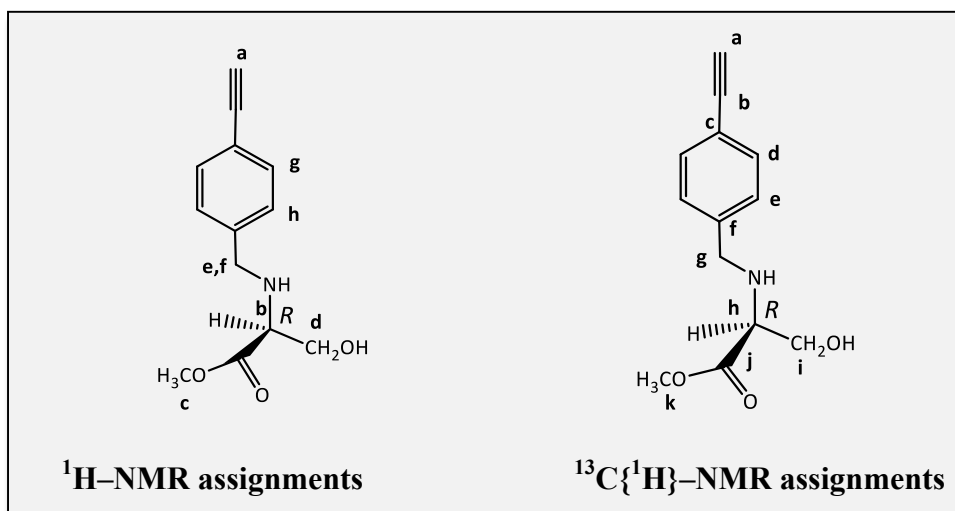
### 1.5.2.1. $\text{HC}\equiv\text{C}-\text{C}_6\text{H}_4-\text{CH}_2-\text{NH}-\text{CH}(\text{CH}_3)-\text{COOCH}_3$ (ligand $\text{L}^2$ ).



4-Ethynylbenzaldehyde (120.0 mg, 0.92 mmol) was added to a solution of L-alanine methyl ester hydrochloride (520.0 mg, 3.70 mmol), triethylamine, (0.52 ml, 3.70 mmol), in dry dichloromethane (20 ml), over 4A molecular sieves. The mixture was allowed to stir for 24 hours at room temperature. The solvent was removed under vacuum and the residue was dissolved in dry metanol (20 ml).  $\text{NaBH}_4$  (170.0 mg, 4.60 mmol) was added slowly at 0 °C. The mixture was warmed to room temperature and it was allowed to stir for 16 hours. The reaction mixture was quenched with water and it was extracted three times with ethyl acetate (3x10 ml). The organic layer was dried over  $\text{MgSO}_4$ . The organic layer was filtered off and the solvent was removed under vacuum, to yield a yellow oil. (126 mg, 0.59 mmol, 64%).  $^1\text{H}$ -NMR (300 MHz,  $\text{CDCl}_3$ )  $\delta$  7.43 ( $\text{H}^g$  or  $\text{H}^h$ , d,  $J = 8.3$  Hz, 2H), 7.32 ( $\text{H}^g$  or  $\text{H}^h$ , d,  $J = 8.3$  Hz, 2H), 3.81 ( $\text{H}^d$  or  $\text{H}^e$ , d,  $J = 13.5$ , 1H), 3.65 ( $\text{H}^d$  or  $\text{H}^e$ , d,  $J = 13.5$ , 1H), 3.31 ( $\text{H}^f$ , s, 3H), 3.17 ( $\text{H}^c$ , q,  $J = 7$  Hz, 1H), 2.76 ( $\text{H}^b$ , s, 1H), 1.37 ( $\text{H}^a$ , d,  $J = 7$  Hz, 3H).  $^{13}\text{C}\{^1\text{H}\}$ -NMR (75 MHz,  $\text{CDCl}_3$ )  $\delta$  18.7 ( $\text{C}^i$ ), 51.3 ( $\text{C}^g$ ,  $\text{C}^h$  or  $\text{C}^k$ ), 51.7 ( $\text{C}^g$ ,  $\text{C}^h$  or  $\text{C}^k$ ), 55.8 ( $\text{C}^g$ ,  $\text{C}^h$  or  $\text{C}^k$ ), 73.9 ( $\text{C}^a$  or  $\text{C}^b$ ), 83.4

(C<sup>a</sup> or C<sup>b</sup>), 120.6 (C<sub>ipso</sub>, H<sup>c</sup> or C<sup>f</sup>), 128.2 (C<sup>d</sup> or C<sup>e</sup>), 132.0 (C<sup>d</sup> or C<sup>e</sup>), 132.4 (C<sub>ipso</sub>, C<sup>c</sup> or C<sup>f</sup>), 175.6 (C<sup>f</sup>). (C≡C): 2105(w) cm<sup>-1</sup>, ν(C=O): 1732 cm<sup>-1</sup>.

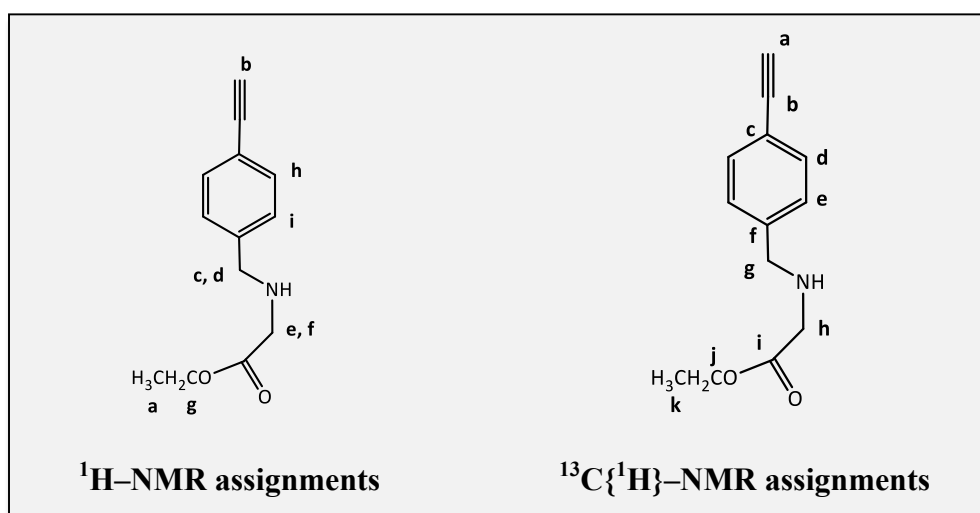
**1.5.2.2. HC≡C-C<sub>6</sub>H<sub>4</sub>-CH<sub>2</sub>-NH-CH(CH<sub>2</sub>OH)-COOCH<sub>3</sub> (ligand L<sup>3</sup>).**



4-Ethynylbenzaldehyde (100 mg, 0.77 mmol) was added to a solution of L-serine methyl ester hydrochloride (480.0 mg, 3.1 mmol), triethylamine, (0.43 ml, 3.1 mmol), in dry dichloromethane (20 ml), over 4A molecular sieves. The mixture was allowed to stir for 24 hours at room temperature. The solvent was removed under vacuum and the residue was dissolved in dry methanol (20 ml). NaBH<sub>4</sub> (150.0 mg, 3.85 mmol) was added slowly at 0 °C. The mixture was warmed to room temperature and it was allowed to stir for 16 hours. The reaction mixture was quenched with water and it was extracted three times with ethyl acetate (3x10 ml). The organic layer was dried over MgSO<sub>4</sub>. The organic layer was filtered off and the solvent was removed under vacuum, to yield yellow oil. (121.8 mg, 0.53 mmol, 68.8%). <sup>1</sup>H-NMR (300 MHz, CDCl<sub>3</sub>) δ 7.18 (H<sup>g</sup> or H<sup>h</sup>, d, J = 8.1 Hz, 2H), 7.35 (H<sup>g</sup> or H<sup>h</sup>, d, J = 8.1 Hz, 2H), 3.63 (H<sup>c</sup>, s, 3H), 3.72 (H<sup>e</sup> or H<sup>f</sup>, d, J = 8.1 Hz, 1H), 3.89 (H<sup>e</sup> or H<sup>f</sup>, d, J = 8.1 Hz, 1H), 3.56-3.62 (H<sup>d</sup>, m, 2H), 3.29

(H<sup>b</sup>, q, J = 4.5, 4.5 Hz, 1H), 2.36 (-HN/-OH, br, s, 2H), 3.12 (H<sup>a</sup>, s, 1H). <sup>13</sup>C{<sup>1</sup>H}-NMR (75 MHz, CDCl<sub>3</sub>) δ 51.7 (C<sup>k</sup> or C<sup>h</sup>), 52.2 (C<sup>k</sup> or C<sup>h</sup>), 61.9 (C<sup>g</sup> or C<sup>i</sup>), 62.6 (C<sup>g</sup> or C<sup>i</sup>), 77.3 (C<sup>a</sup> or C<sup>b</sup>), 83.5 (C<sup>a</sup> or C<sup>b</sup>), 120.1 (C<sub>ipso</sub>, C<sup>c</sup> or C<sup>f</sup>), 128.2 (C<sup>d</sup> or C<sup>e</sup>), 132.3 (C<sup>d</sup> or C<sup>e</sup>), 139.7 (C<sub>ipso</sub>, C<sup>c</sup> or C<sup>f</sup>), 173.5. IR spectroscopy to be made.

### 1.5.3. HC≡C-C<sub>6</sub>H<sub>4</sub>-CH<sub>2</sub>-NH-CH<sub>2</sub>-COOCH<sub>2</sub>CH<sub>3</sub> (ligand L<sup>4</sup>).

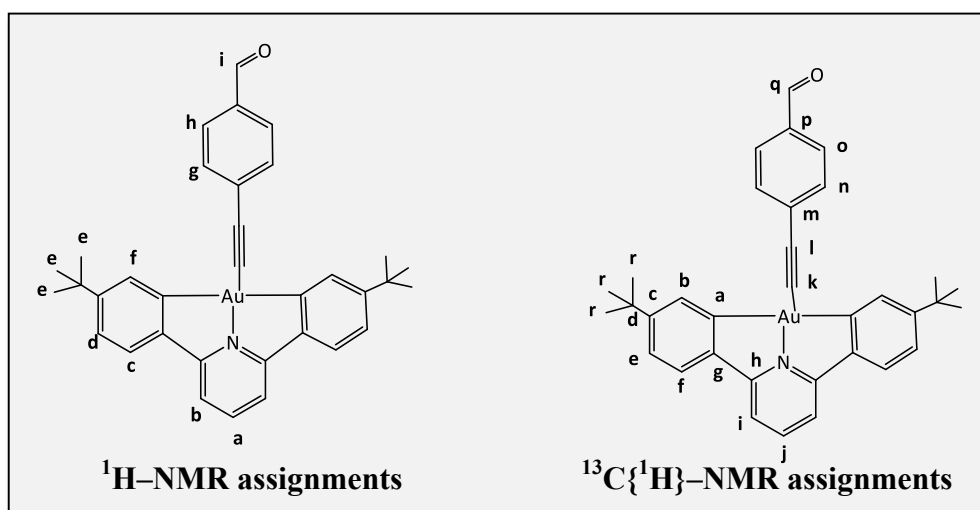


4-Ethynylbenzaldehyde (200.0 mg, 1.54 mmol) was added to a solution of L-glycine ethyl ester hydrochloride (860.0 mg, 6.16 mmol), triethylamine, (0.86 ml, 6.16 mmol), in dry dichloromethane (20 ml), over 4A molecular sieves. The mixture was allowed to stir for 24 hours at room temperature. The solvent was removed under vacuum and the residue was dissolved in dry methanol (20 ml). NaBH<sub>4</sub> (291.2 mg, 7.70 mmol) was added slowly at 0 °C. The mixture was warmed to room temperature and it was allowed to stir for 16 hours. The reaction mixture was quenched with water and it was extracted three times with ethyl acetate (3x10 ml). The organic layer was dried over MgSO<sub>4</sub>. The organic layer was filtered off and the solvent was removed under vacuum, to a yield yellow oil. (196 mg, 0.91 mmol, 59%). <sup>1</sup>H-NMR (300 MHz, CDCl<sub>3</sub>) δ 7.31 (H<sup>h</sup> or H<sup>i</sup>, J = 8.1 Hz, 2H), 7.44 (H<sup>h</sup> or H<sup>i</sup>, J = 8.1 Hz, 2H), 3.31 (H<sup>g</sup>, q, J = 7.0 Hz, 2H), 3.36 (H<sup>c</sup> and H<sup>d</sup> or H<sup>e</sup> and H<sup>f</sup>, bs, 2H), 3.79 (H<sup>c</sup> and H<sup>d</sup> or H<sup>e</sup> and H<sup>f</sup>, bs, 2H), 3.11 (H<sup>b</sup>, s, 1H), 1.25

(H<sup>a</sup>, t, J =7.0 Hz, 3H). <sup>13</sup>C{<sup>1</sup>H}-NMR (75 MHz, CDCl<sub>3</sub>) δ 14.3 (C<sup>k</sup>), 50.4 (C<sup>g</sup> or C<sup>h</sup>), 52.0 (C<sup>g</sup> or C<sup>h</sup>), 61.0 (C<sup>j</sup>), 77.2 (C<sup>a</sup> or C<sup>b</sup>), 83.8 (C<sup>a</sup> or C<sup>b</sup>), 121.0 (C<sub>ipso</sub>, C<sup>c</sup> or C<sup>f</sup>), 128.5 (C<sup>d</sup> or C<sup>e</sup>), 132.2 (C<sup>d</sup> or C<sup>e</sup>), 141.5 (C<sub>ipso</sub>, C<sup>c</sup> or C<sup>f</sup>), 172.6 (C<sup>i</sup>). (C≡C): 2107(w) cm<sup>-1</sup>, ν(C=O): 1735 cm<sup>-1</sup>.

\* Note: High resolution mass spectroscopy should be carried out for the reported ligands L<sup>2</sup> – L<sup>4</sup>.

#### 1.5.4. (C<sup>^</sup>N<sup>^</sup>C)Au–C≡C–C<sub>6</sub>H<sub>4</sub>–CHO (complex 4).



#### Method 1:

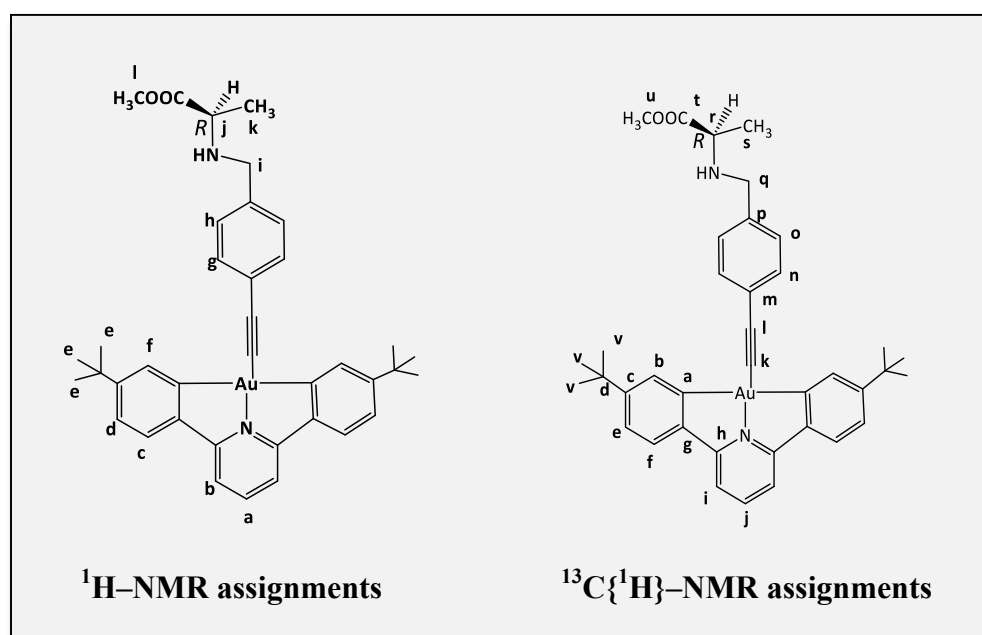
1-ethynylbenzaldehyde (76.0 mg, 0.60 mmol) was added to a solution of (C<sup>^</sup>N<sup>^</sup>C)AuOH (167.5 mg, 0.30 mmol) in toluene (20 ml). The mixture was refluxed for 24 hours. The crude product, which was obtained upon removal the solvent under vacuum, was washed off with petrol ether 40/60 (10 ml) and vacuum dried, to yield an off yellow solid (150 mg, 0.45 mmol, 75%). <sup>1</sup>H-NMR (300 MHz, CDCl<sub>3</sub>) δ 10.01 (H<sup>i</sup>, s, 1H), 8.16 (H<sup>f</sup>, d, J=1.8 Hz, 2H), 7.86 (H<sup>g</sup> or H<sup>h</sup>, d, J=8.1 Hz, 2H), 7.72 (H<sup>g</sup> or H<sup>h</sup>, d, J=8.1 Hz, 2H), 7.80 (H<sup>a</sup>, t, J= 7.9 Hz, 1H), 7.50 (H<sup>b</sup> or H<sup>c</sup>, d, J= 8.0 Hz, 2H), 7.40 (H<sup>b</sup> or H<sup>c</sup>, d, J= 8.0 Hz, 2H), 7.32 – 7.26 (H<sup>d</sup>, m, 2H), 1.37 (H<sup>e</sup>, s, 18H). <sup>13</sup>C{<sup>1</sup>H}-NMR (75 MHz, CDCl<sub>3</sub>) δ 31.2 (C<sup>f</sup>), 35.0 (C<sup>d</sup>), 100.9 (C<sup>k</sup> or C<sup>l</sup>), 116.1 (C<sup>i</sup>), 123.9 (C<sup>e</sup>), 125.0 (C<sup>f</sup>),

129.7 (C<sup>n</sup> or C<sup>o</sup>), 132.2 (C<sup>a</sup>), 133.5 (C<sup>n</sup> or C<sup>o</sup>), 142.2 (C<sup>g</sup>), 146.3 (C<sup>j</sup>), 155.5 (C<sup>c</sup>), 165.0 (C<sup>h</sup>), 166.9 (C<sup>a</sup>), 191.8 (C<sup>q</sup>). Anal. Calcd. C<sub>34</sub>H<sub>32</sub>AuNO (found): C, 61.17 (61.03); H, 4.83 (4.84); N, 2.10 (2.22).  $\nu(\text{C}\equiv\text{C})$ : 2149 cm<sup>-1</sup>,  $\nu(\text{C}=\text{O})$ : 1595 cm<sup>-1</sup>.

*Method 2:*

1-ethynylbenzaldehyde (40.0 mg, 0.29 mmol), triethylamine (40.3  $\mu\text{L}$ , 0.29 mmol) and CuI (0.88 mg, 4.62 mmol) were added to a solution of (C<sup>^N^C</sup>)AuCl (110.4 mg, 0.19 mmol) in dichloromethane (10 ml). The mixture was allowed to stir for 1 hour at room temperature. The solution was washed with water, and the organic layer was isolated. The solvent was removed under vacuum and the residue was washed off with petrol ether 40/60 (10 ml) and vacuum dried, to yield a yellow solid (71.0 mg, 0.16 mmol, 56 %).

**1.5.5. (C<sup>^N^C</sup>)Au-C $\equiv$ C-C<sub>6</sub>H<sub>4</sub>-CH<sub>2</sub>-NH-CH(CH<sub>3</sub>)-COOCH<sub>3</sub> (complex 5).**



*Method 1:*

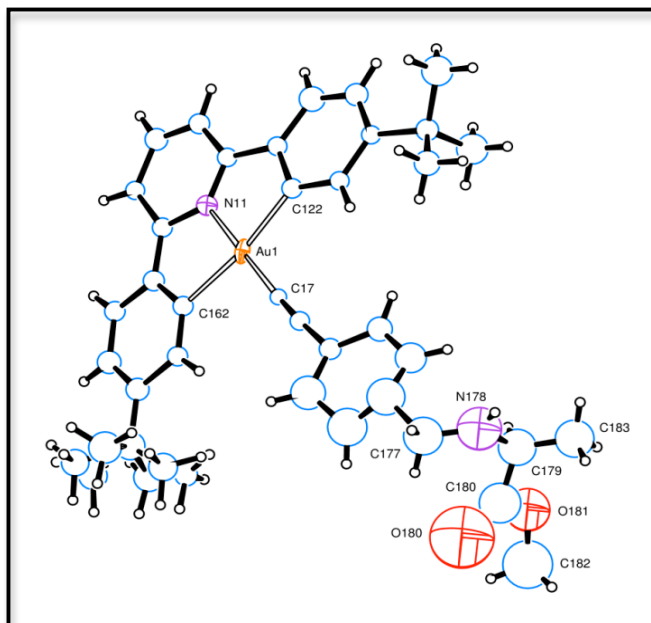
1-Ethynyl-4-benzyl-L-alanine methyl ester (105 mg, 0.05 mmol) was added to a solution of (C<sup>^N^C</sup>)AuOH (140 mg, 0.02 mmol) in toluene (20 ml). The mixture was refluxed for 24 hours. The crude product, which was obtained upon removal the solvent under vacuum, was washed with petrol ether 40/60 (10 ml) and ethanol (10 ml) and vacuum dried, to yield an off yellow solid (61 mg, 0.016 mmol, 32%). <sup>1</sup>H-NMR (300 MHz, CD<sub>2</sub>Cl<sub>2</sub>) δ 8.18 (H<sup>f</sup>, d, J = 2.0 Hz, 2H), 7.85 (H<sup>a</sup>, t, J = 8.0 Hz, 1H), 7.55 (H<sup>b</sup>, H<sup>c</sup>, H<sup>g</sup> or H<sup>h</sup> (overlapped), d, J = 8.0 Hz, 4H), 7.46 (H<sup>b</sup>, H<sup>c</sup>, H<sup>g</sup> or H<sup>h</sup> (overlapped), d, J = 8.0 Hz, 2H), 7.32 (H<sup>b</sup>, H<sup>c</sup>, H<sup>g</sup> or H<sup>h</sup> (overlapped), d, J = 8.1 Hz, 2H), 7.32 (H<sup>d</sup>, d, J = 7.0 Hz, 2H), 3.72 (s, 3H), 3.68 (H<sup>i</sup>, d, J = 13.2 Hz, 1H), 3.81 (H<sup>i</sup>, d, J = 13.2 Hz, 1H), 3.40 (H<sup>j</sup>, q, J = 7.0 Hz, 1H), 1.39 (H<sup>e</sup>, s, 18H), 1.32 (H<sup>k</sup>, d, J = 7.0 Hz, 3H). <sup>13</sup>C{<sup>1</sup>H}-NMR (75 MHz, CD<sub>2</sub>Cl<sub>2</sub>) δ 175.9 (C<sup>l</sup>), 166.9 (C<sup>a</sup>), 164.8 (C<sup>h</sup>), 155.2 (C<sup>c</sup>), 146.6 (C<sup>j</sup>), 142.2 (C<sup>g</sup>), 139.1 (C<sub>ipso</sub>, C<sup>m</sup> or C<sup>p</sup>), 133.3 (C<sup>n</sup> or C<sup>o</sup>), 131.7 (C<sup>b</sup>), 128.0 (C<sup>n</sup> or C<sup>o</sup>), 125.3 (C<sub>ipso</sub>, C<sup>m</sup> or C<sup>p</sup>), 124.9 (C<sup>f</sup>), 123.8 (C<sup>e</sup>), 116.2 (C<sup>i</sup>), 100.9 (C<sup>k</sup> or C<sup>l</sup>), 91.9 (C<sup>k</sup> or C<sup>l</sup>), 56.2 (C<sup>f</sup>), 51.6 (C<sup>u</sup> or C<sup>q</sup>), 51.5 (C<sup>u</sup> or C<sup>q</sup>), 35.2 (C<sup>d</sup>), 30.9 (C<sup>v</sup>), 18.9 (C<sup>s</sup>). ν(C≡C): 2151 cm<sup>-1</sup>, ν(C=O): 1736 cm<sup>-1</sup> Anal. Calcd. C<sub>38</sub>H<sub>41</sub>AuN<sub>2</sub>O<sub>2</sub> · 3 H<sub>2</sub>O (found): C, 56.43 (56.19); H, 5.86 (4.65); N, 3.46 (3.70).

*Method 2:*

1-ethynyl-4-benzyl-L-alanine methyl ester (0.03 mg, 0.12 mmol), triethylamine (16.7 μL, 0.12 mmol) and CuI (0.27 mg, 1.42 mmol) were added to a solution of (C<sup>^N^C</sup>)AuCl (35.0 mg, 0.06 mmol) in dichloromethane (10 ml). The mixture was allowed to stir for 1 hour at room temperature. The solution was washed with water, and the organic layer was isolated. The solvent was removed under vacuum and the residue

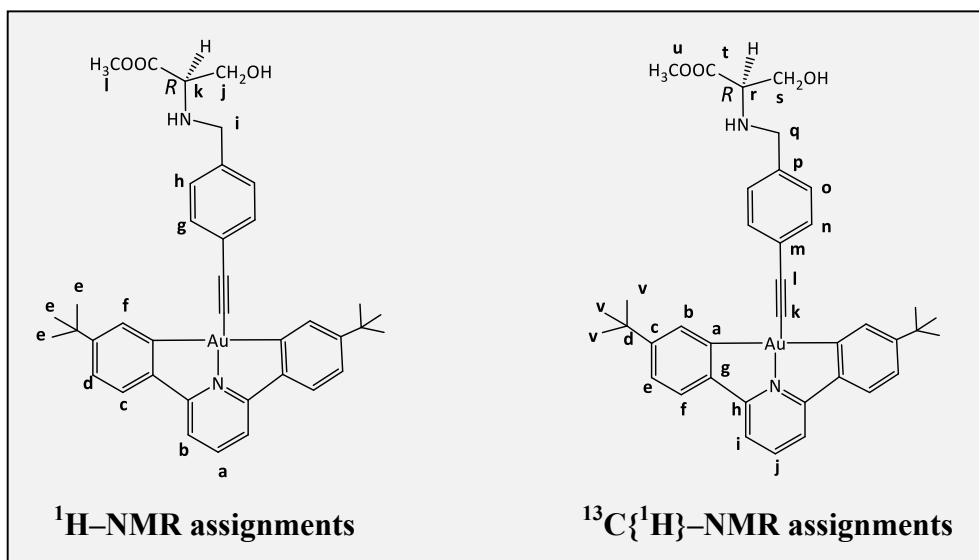
was washed off with petrol ether 40/60 (10 ml) and vacuum dried, to yield a yellow solid (16.7 mg, 0.044 mmol, 37%).

**Table 30.** X-ray crystallography data of complex **5**.



Compound	<b>5</b>
Reference	angelbs4
Formula weight	754.69
Crystal system	orthorhombic
Space group	P 2 <sub>1</sub> 2 <sub>1</sub> 2 <sub>1</sub>
Unit cell dimensions. a (Å)	13.3617(2)
b	34.0972(13)
c	14.7600(2)
α (°)	90
β	90
γ	90
Volume (Å <sup>3</sup> )	6724.6(3)
Z	8
Calculated density (mg/m <sup>3</sup> )	1.491
F(000)	3024
Absorption coefficient μ(mm <sup>-1</sup> )	4.410
Crystal colour, shape	colourless plate
Crystal size (mm <sup>3</sup> )	0.31 x 0.28 x 0.05
θ Range (°)	3.008 to 19.994
No. of unique reflections, R <sub>int</sub>	6253 [R(int) for equivalents = 0.069]
Data/Restraints/Parameters	6253 / 0 / 388
Final R indices (observed data)	R <sub>1</sub> = 0.066, wR <sub>2</sub> = 0.140
Final R indices (all data)	R <sub>1</sub> = 0.074, wR <sub>2</sub> = 0.143
Largest diff. peak and hole (e Å <sup>3</sup> )	1.81 and -1.63

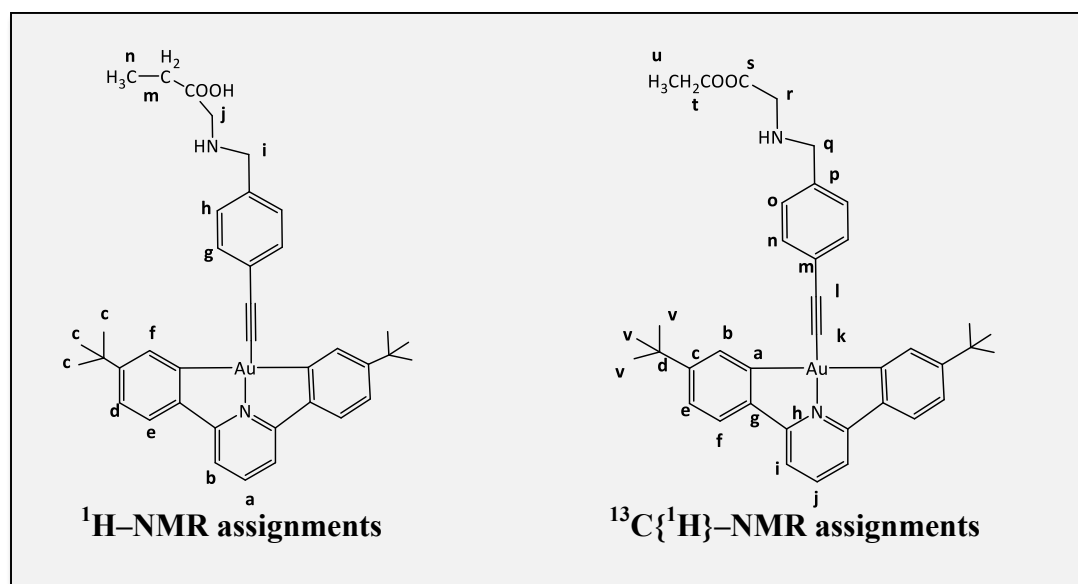
1.5.6.  $(C^{13}N^{15}C)Au-C\equiv C-C_6H_4-CH_2-NH-CH(CH_2OH)-COOCH_3$  (complex 6).



1-Ethynyl-4-benzyl-L-serine methyl ester (64 mg, 0.27 mmol) was added to a solution of  $(C^{13}N^{15}C)AuOH$  (79 mg, 0.14 mmol) in toluene (20 ml). The mixture was refluxed for 24 hours. The crude product, which was obtained upon removal of the solvent under vacuum, was washed with petrol ether 40/60 (10 ml) and vacuum dried, to yield an off yellow solid (110 mg, 0.12 mmol, 45%).  $^1H$ -NMR (300 MHz,  $CD_2Cl_2$ )  $\delta$  8.21 (d,  $J=2.0$  Hz, 2H), 7.89 (t,  $J=9.4$  Hz, 1H), 7.60 (Hc or Hb, d,  $J=8.2$  Hz, 2H), 7.60 (Hc or Hb, d,  $J=8.1$  Hz, 2H), 7.50 (Hg or Hh, d,  $J=8.1$  Hz, 2H), 7.37 (Hg or Hh, d,  $J=8.1$  Hz, 2H), 7.36 (Hd, d,  $J=8.1$  Hz, 2H), 3.89 - 3.72 (Hi and Hj (overlapped), m, 4H), 3.81 (Hl, s, 3H), 3.47 (Hk, q,  $J=4.6$  Hz, 1H), 1.43 (He, s, 18H).  $^{13}C\{^1H\}$ -NMR (75 MHz,  $CD_2Cl_2$ )  $\delta$  166.9 ( $C^a$ ), 164.8 ( $C^h$ ), 155.2 ( $C^c$ ), 146.6 ( $C^g$ ), 142.3 ( $C^j$ ), 138.5 ( $C_{ipso}$ ,  $C^m$  or  $C^p$ ), 133.3 ( $C^b$ ), 131.8 ( $C^n$  or  $C^o$ ), 128.1 ( $C^n$  or  $C^o$ ), 124.9 ( $C^f$ ), 124.3 ( $C_{ipso}$ ,  $C^m$  or  $C^p$ ), 123.8 ( $C^e$ ), 116.4 ( $C^i$ ), 100.8 ( $C^k$  or  $C^l$ ), 92.3 ( $C^k$  or  $C^l$ ), 62.4 ( $C^q$ ,  $C^r$ ,  $C^s$  or  $C^u$ ),

52.0 (C<sup>q</sup>, C<sup>r</sup>, C<sup>s</sup> or C<sup>u</sup>), 51.8 (C<sup>q</sup>, C<sup>r</sup>, C<sup>s</sup> or C<sup>u</sup>), 35.2 (C<sup>d</sup>), 30.9 (C<sup>v</sup>).  $\nu(\text{C}\equiv\text{C})$ : 2153 cm<sup>-1</sup>,  $\nu(\text{C}=\text{O})$ : 1737 cm<sup>-1</sup>. Anal. Calcd. C<sub>38</sub>H<sub>41</sub>AuN<sub>2</sub>O<sub>3</sub> (found): C, 59.22 (59.19); H, 5.36 (5.28); N, 3.63 (3.68).

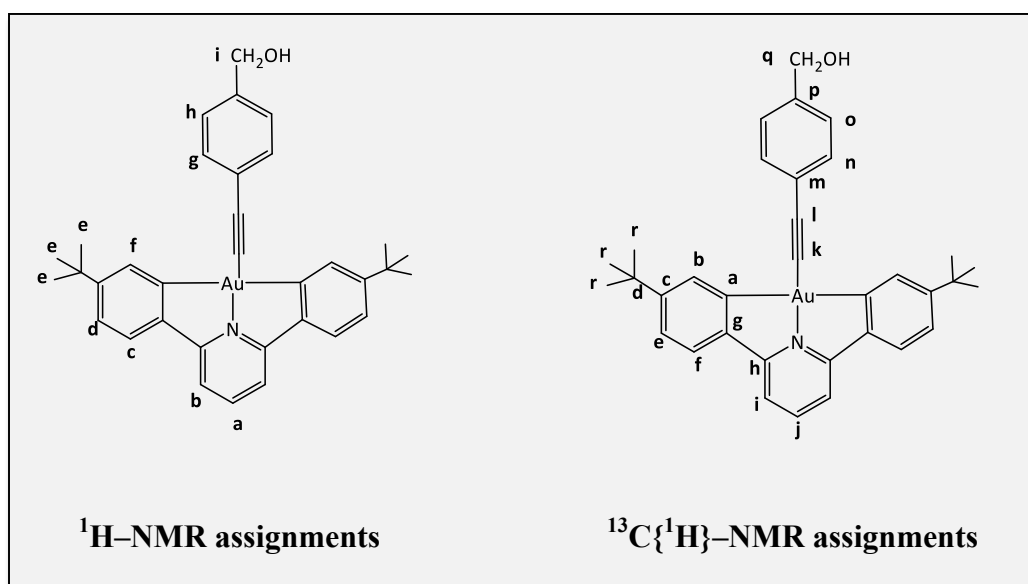
**1.5.7. (C<sup>^</sup>N<sup>^</sup>C)Au-C≡C-C<sub>6</sub>H<sub>4</sub>-CH<sub>2</sub>-NH-CH<sub>2</sub>-COOCH<sub>2</sub>CH<sub>3</sub> (complex 7).**



1-Ethynyl-4-benzyl-Glycine ethyl ester methyl ester (50 mg, 0.35 mmol) was added to a solution of (C<sup>^</sup>N<sup>^</sup>C)AuOH (100 mg, 0.17 mmol) in toluene (20 ml). The mixture was refluxed for 24 hours. The crude product, which was obtained upon removal of the solvent under vacuum, was washed with petrol ether 40/60 (10 ml) and vacuum dried, to yield an off yellow solid (40 mg, 0.12 mmol, 33%). <sup>1</sup>H-NMR (300 MHz, CD<sub>2</sub>Cl<sub>2</sub>) δ 8.22 (H<sup>f</sup>, d, J = 2.0 Hz, 2H), 7.90 (H<sup>a</sup>, t, J = 8.0 Hz, 1H), 7.60 (H<sup>b</sup>, H<sup>e</sup>, H<sup>g</sup>, H<sup>h</sup> (overlapped), d, J = 8.2 Hz, 4H), 7.50 (H<sup>b</sup>, H<sup>e</sup>, H<sup>g</sup>, H<sup>h</sup> (overlapped), d, J = 8.1 Hz, 2H), 7.37 (H<sup>b</sup>, H<sup>e</sup>, H<sup>g</sup>, H<sup>h</sup> (overlapped), d, J = 8.1 Hz, 2H), 7.32 (H<sup>d</sup>, d, J = 7.0 Hz, 2H), 4.21 (H<sup>m</sup>, q, J = 7.2 Hz, 2H), 3.87 (H<sup>i</sup> or H<sup>j</sup>, s, br, 2H), 3.45 (H<sup>i</sup> or H<sup>j</sup>, s, br, 2H), 1.43 (H<sup>c</sup>, s, 18H), 1.31 (H<sup>n</sup>, t, J = 7.2 Hz, 3H). <sup>13</sup>C{<sup>1</sup>H}-NMR (75 MHz, CD<sub>2</sub>Cl<sub>2</sub>) δ 166.9 (C<sup>a</sup>), 164.8 (C<sup>h</sup>), 155.2 (C<sup>c</sup>), 146.6 (C<sup>j</sup>), 142.3 (C<sup>g</sup>), 133.3 (C<sup>n</sup> or C<sup>o</sup>), 131.8 (C<sup>b</sup>), 128.2 (C<sup>n</sup> or

$C^o$ ), 125.5 ( $C_{\text{ipso}}$ ,  $C^m$  or  $C^p$ . One of these carbons is not shown in the spectrum), 124.9 ( $C^f$ ), 123.8 ( $C^e$ ), 116.3 ( $C^i$ ), 100.9 ( $C^k$  or  $C^l$ ), 92.0 ( $C^k$  or  $C^l$ ), 60.7 ( $C^q$  or  $C^r$ ), 35.2 ( $C^d$ ), 31.0 ( $C^v$ ), 14.0 ( $C^u$ ).  $\nu(\text{C}\equiv\text{C})$ : 2149  $\text{cm}^{-1}$ ,  $\nu(\text{C}=\text{O})$ : 1737  $\text{cm}^{-1}$ . Anal. Calcd.  $\text{C}_{38}\text{H}_{41}\text{AuN}_2\text{O}_2$  (found): C, 60.47 (59.93); H, 5.48 (5.22); N, 3.71 (3.82).

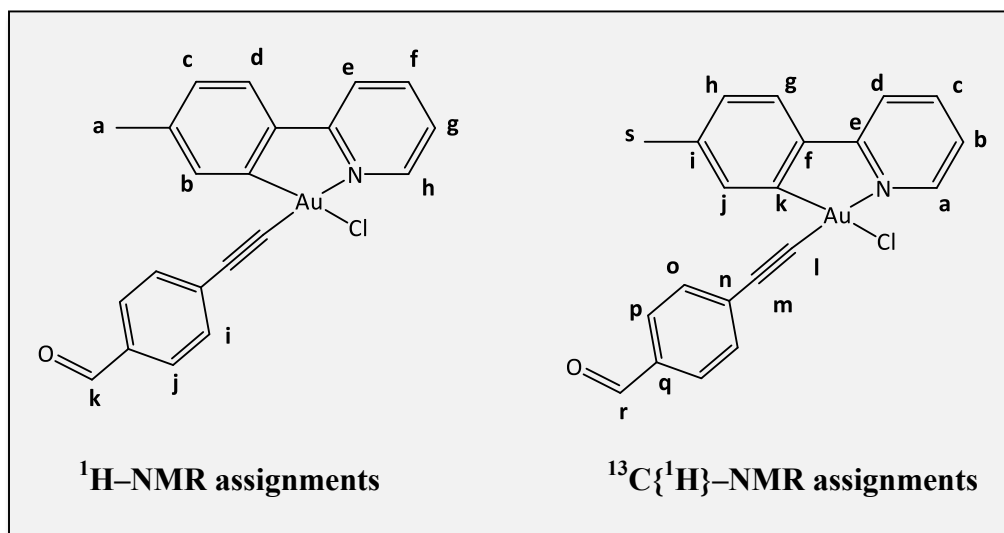
### 1.5.8. $(\text{C}^{\wedge}\text{N}^{\wedge}\text{C})\text{Au}-\text{C}\equiv\text{C}-\text{C}_6\text{H}_4-\text{CH}_2\text{OH}$ (complex 8).



$\text{NaBH}_4$  (120.0 mg, 0.29 mmol) was added to a mixture of **4** (19.8 mg, 0.03 mmol) in methanol (10 ml). The mixture was allowed to stir for 1 hour at room temperature. The solvent was removed under vacuum and the residue was dissolved in dichloromethane (10 ml) and quenched with water. The organic layer was dried with  $\text{MgSO}_4$  and the solvent was removed. The residue was washed with petrol ether 40/60, to yield a yellow solid. (12.6 mg, 0.18 mmol, 64 %).  $^1\text{H}$ -NMR (300 MHz,  $\text{CDCl}_3$ )  $\delta$  8.21 ( $\text{H}^f$ , d,  $J=2.0$  Hz, 2H), 7.79 ( $\text{H}^a$ , t,  $J=8.0$  Hz, 1H), 7.62 ( $\text{H}^d$  or  $\text{H}^c$ , d,  $J=8.0$ , 2H), 7.38 ( $\text{H}^g$  or  $\text{H}^h$ , d,  $J=8.1$ , 2H), 7.37 ( $\text{H}^g$  or  $\text{H}^h$ , d,  $J=8.1$ , 2H), 7.36 ( $\text{H}^d$  or  $\text{H}^c$ , d,  $J=8.0$ , 2H), 7.32 ( $\text{H}^b$ , m, 2H), 4.72 ( $\text{H}^i$  or  $\text{H}^j$ , d,  $J=6.0$  Hz, 2H), 1.39 ( $\text{H}^e$ , s, 18H).  $^{13}\text{C}\{^1\text{H}\}$ -NMR (75 MHz,  $\text{CDCl}_3$ )  $\delta$  167.1 ( $\text{C}^a$ ), 155.2 ( $\text{C}^c$ ), 146.9 ( $\text{C}^h$ ), 146.4 ( $\text{C}^g$ ), 142.1 ( $\text{C}^j$ ), 133.6 ( $C_{\text{ipso}}$ ,  $C^m$  or

$C^p$ ), 132.1 ( $C^b$ ), 126.9 ( $C^n$  or  $C^o$ ), 126.2 ( $C_{ipso}$ ,  $C^m$  or  $C^p$ ), 124.9, 123.8 ( $C^e$ ), 116.0 ( $C^l$ ), 100.9 ( $C^k$  or  $C^l$ ), 92.3 ( $C^k$  or  $C^l$ ), 65.3 ( $C^q$ ), 35.4 ( $C^d$ ), 31.2 ( $C^r$ ). IR spectroscopy to be made.

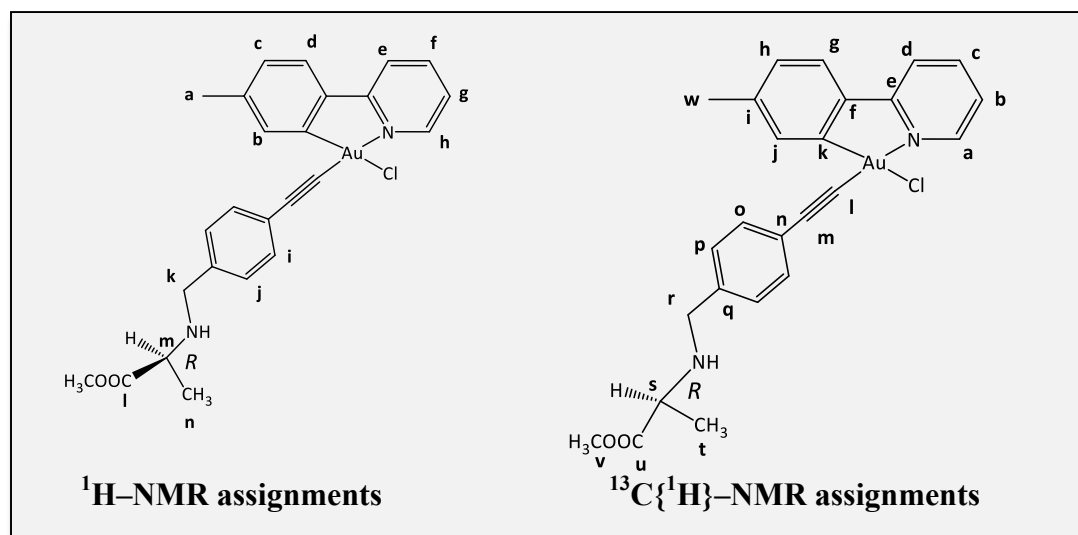
### 1.5.9. (2-*para*-tolylpyridyl)Au-(Cl)C≡C-C<sub>6</sub>H<sub>4</sub>-CHO (complex 11).



4-Ethynylbenzaldehyde (9.7 mg, 0.07 mmol), CuI (0.22 mg, 1.15 mmol) and NEt<sub>3</sub> (21.0 μL, 0.15 mmol) were added to a mixture of (2-*para*-tolylpyridyl)AuCl<sub>2</sub> (32.6 mg, 0.07 mmol) in dichloromethane (10 ml). The mixture was allowed to stir for 1 hour at room temperature. The resulting solution was washed with water (10 ml), and the organic layer was isolated. The solvent was removed under vacuum and the residue was washed with petrol ether 40/60 (10 ml) and vacuum dried, to yield a yellow solid (13 mg, 0.02 mmol, 33 %). <sup>1</sup>H-NMR (300 MHz, CD<sub>2</sub>Cl<sub>2</sub>) δ 10.01 (H<sup>k</sup>, s, 1H), 9.50 (H<sup>h</sup>, d, J = 5.8 Hz, 1H), 8.10 (H<sup>f</sup>, td, J = 8.0, 1.5 Hz, 1H), 7.98 (H<sup>b</sup>, s, 1H), 7.90 (H<sup>e</sup>, d, J = 7.5 Hz, 1H), 7.86 (H<sup>i</sup> or H<sup>j</sup>, d, J = 8.2 Hz, 2H), 7.70 (H<sup>i</sup> or H<sup>j</sup>, d, J = 8.2 Hz, 2H), 7.59 (H<sup>d</sup>, d, J = 7.9 Hz, 1H), 7.46-7.54 (H<sup>g</sup>, m, 1H), 7.24 (H<sup>c</sup>, d, J = 7.8 Hz, 1H), 2.42 (H<sup>a</sup>, s, 3H). <sup>13</sup>C{<sup>1</sup>H}-NMR (75 MHz, CD<sub>2</sub>Cl<sub>2</sub>) δ 191.5 (C<sup>r</sup>), 164.1 (C<sub>ipso</sub>, C<sup>e</sup>), 147.6 (C<sub>ipso</sub>, C<sup>a</sup>, C<sup>i</sup> or C<sup>k</sup>), 147.0 (C<sub>ipso</sub>, C<sup>a</sup>, C<sup>i</sup> or C<sup>k</sup>), 143.4 (C<sub>ipso</sub>, C<sup>a</sup>, C<sup>i</sup> or C<sup>k</sup>), 142.3 (C<sup>c</sup> or C<sup>f</sup>), 139.6 (C<sup>c</sup> or C<sup>f</sup>), 135.3 (C<sub>ipso</sub>, C<sup>n</sup> or C<sup>q</sup>), 135.1 (C<sup>j</sup>), 132.3 (C<sup>o</sup> or C<sup>p</sup>), 131.5 (C<sup>h</sup>), 129.4 (C<sup>o</sup> or

$C^p$ ), 129.3 ( $C^b$  or  $C^g$ ), 125.4 ( $C_{\text{ipso}}$ ,  $C^n$  or  $C^q$ ), 123.8 ( $C^b$  or  $C^g$ ), 120.1 ( $C^d$ ), 96.9 ( $C^l$  or  $C^m$ ), 90.2 ( $C^l$  or  $C^m$ ), 21.8 ( $C^s$ ).  $\nu(C\equiv C)$ : 2164  $\text{cm}^{-1}$ ,  $\nu(C=O)$ : 1691  $\text{cm}^{-1}$ . Anal. Calcd.  $C_{21}H_{15}AuClNO$  (found): C, 47.61 (47.45); H, 2.85 (2.75); N, 2.64 (2.80).

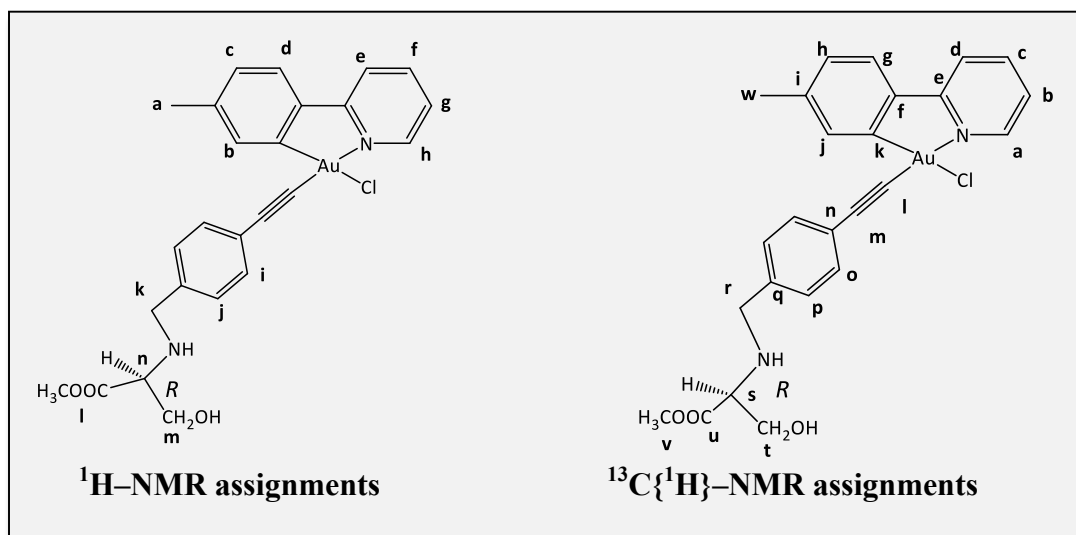
**1.5.10. (2-*para*-tolylpyridyl)Au-(Cl)C $\equiv$ C-C $_6$ H $_4$ -CH $_2$ -NH-CH(CH $_3$ )-COOCH $_3$  (complex 12).**



1-Ethynyl-4-benzyl-L-Alanine methyl ester (85.7 mg, 0.39 mmol), CuI (0.43 mg, 2.25 mmol) and  $\text{NEt}_3$  (41.7  $\mu\text{L}$ , 0.30 mmol) were added to a mixture of (2-*para*-tolylpyridyl)AuCl $_2$  (66.0 mg, 0.15 mmol) in dichloromethane (10 ml). The mixture was allowed to stir for 1 hour at room temperature. The resulting solution was washed with water (10 ml), and the organic layer was isolated. The solvent was removed under vacuum and the residue was extracted with ethanol and washed with petrol ether 40/60 (10 ml) and vacuum dried, to yield a yellow solid (94.5 mg, 0.16 mmol, 41 %).  $^1\text{H-NMR}$  (300 MHz,  $\text{CD}_2\text{Cl}_2$ )  $\delta$  9.48 ( $\text{H}^h$ , dd,  $J = 5.8, 1$  Hz, 1H), 8.08 – 8.05 ( $\text{H}^f$ , m, 1H), 8.02 ( $\text{H}^b$ , d,  $J = 0.8$  Hz, 1H), 7.89 ( $\text{H}^e$ , d,  $J = 8.1$  Hz, 1H), 7.58 ( $\text{H}^d$ , d,  $J = 7.9$  Hz, 1H), 7.40 – 7.31 ( $\text{H}^g$ , m, 1H), 7.32 ( $\text{H}^i$  or  $\text{H}^j$ , d,  $J = 8.0$  Hz, 1H), 7.50 ( $\text{H}^i$  or  $\text{H}^j$ , d,  $J = 8.1$  Hz, 1H), 7.22 ( $\text{H}^c$ , dd,  $J = 7.9, 0.8$  Hz, 1H), 3.71 (H $l$ , s, 3H), 3.82 ( $\text{H}^k$ , d,  $J = 13.4$  Hz, 1H),

3.67 (H<sup>k</sup>, d, J = 13.4 Hz, 1H), 3.38 (H<sup>m</sup>, q, J = 7.0 Hz, 1H), 2.42 (H<sup>a</sup>, s, 3H), 1.30 (H<sup>n</sup>, d, J = 7.0 Hz, 3H). <sup>13</sup>C{<sup>1</sup>H}-NMR (75 MHz, CD<sub>2</sub>Cl<sub>2</sub>) δ 176.0 (Cu), 164.0 (C<sub>ipso</sub>, C<sup>e</sup>), 147.6 (C<sub>ipso</sub>, C<sup>a</sup>, C<sup>i</sup> or C<sup>k</sup>), 146.9 (C<sub>ipso</sub>, C<sup>i</sup> or C<sup>k</sup>), 143.2 (C<sub>ipso</sub>, C<sup>i</sup> or C<sup>k</sup>), 142.1 (C<sup>c</sup> or C<sup>f</sup>), 139.9 (C<sup>c</sup> or C<sup>f</sup>), 139.6 (C<sup>j</sup>), 135.4 (C<sub>ipso</sub>, C<sup>n</sup> or C<sup>q</sup>), 131.7 (C<sup>o</sup> or C<sup>p</sup>), 129.1 (C<sup>h</sup>), 128.0 (C<sup>o</sup> or C<sup>p</sup>), 125.3 (C<sub>ipso</sub>, C<sup>n</sup> or C<sup>q</sup>), 123.8 (C<sup>b</sup> or C<sup>g</sup>), 123.7 (C<sup>b</sup> or C<sup>g</sup>), 120.1 (C<sup>d</sup>), 97.0 (C<sup>l</sup> or C<sup>m</sup>), 84.3 (C<sup>l</sup> or C<sup>m</sup>), 54.2 (C<sup>r</sup> or C<sup>v</sup>), 51.6 (C<sup>r</sup> or C<sup>v</sup>), 21.8 (C<sup>t</sup> or C<sup>w</sup>), 21.2 (C<sup>s</sup>), 18.9 (C<sup>t</sup> or C<sup>w</sup>). ν(C≡C): 2164 cm<sup>-1</sup>, ν(C=O): 1733 cm<sup>-1</sup>. Anal. Calcd. C<sub>25</sub>H<sub>24</sub>AuClN<sub>2</sub>O<sub>2</sub> (found): C, 48.68 (48.57); H, 3.92 (3.86); N, 4.54 (4.48).

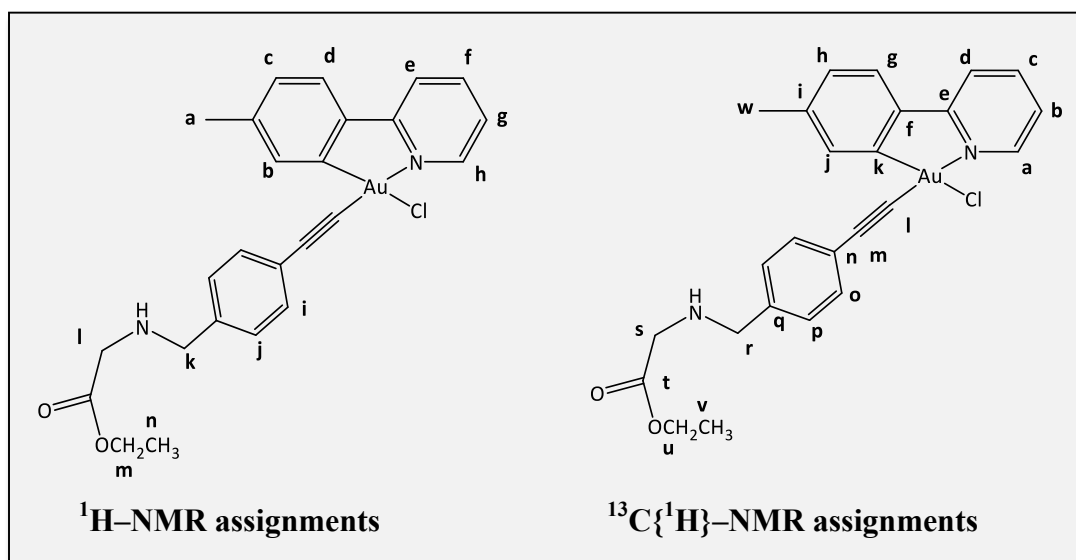
**1.5.11. (2-*para*-tolylpyridyl)Au-(Cl)C≡C-C<sub>6</sub>H<sub>4</sub>-CH<sub>2</sub>-NH-CH(CH<sub>2</sub>OH)-COOCH<sub>3</sub> (complex 13).**



1-Ethynyl-4-benzyl-L-Serine methyl ester (66.1 mg, 0.28 mmol), CuI (0.63 mg, 3.31 mmol) and NEt<sub>3</sub> (80.0 μL, 0.56 mmol) were added to a mixture of (2-*para*-tolylpyridyl)AuCl<sub>2</sub> (125.0 mg, 0.28 mmol) in dichloromethane (10 ml). The mixture was allowed to stir for 1 hour at room temperature. The resulting solution was washed with water (10 ml), and the organic layer was isolated. The solvent was removed under vacuum and the residue was extracted with ethanol and washed with ethanol and petrol

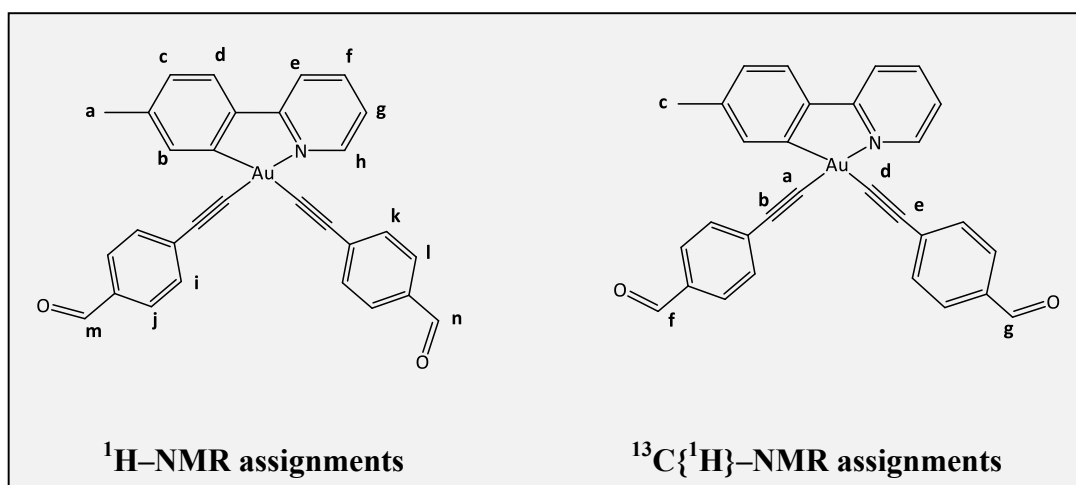
ether 40/60 (10 ml) and vacuum dried, to yield a yellow solid (68.0 mg, 0.11 mmol, 38 %).  $^1\text{H-NMR}$  (300 MHz,  $\text{CD}_2\text{Cl}_2$ )  $\delta$  9.51 ( $\text{H}^{\text{h}}$ , d,  $J = 5.0$  Hz, 1H), 8.13 – 8.06 ( $\text{H}^{\text{f}}$ , td,  $J = 8.0, 1.5$  Hz, 1H), 8.05 ( $\text{H}^{\text{b}}$ , d,  $J = 0.7$  Hz, 1H), 7.90 ( $\text{H}^{\text{e}}$ , d,  $J = 7.9$  Hz, 1H), 7.59 ( $\text{H}^{\text{d}}$ , d,  $J = 7.9$  Hz, 1H), 7.53 – 7.47 ( $\text{H}^{\text{g}}$ , m, 1H), 7.52 ( $\text{H}^{\text{i}}$  or  $\text{H}^{\text{j}}$ , d,  $J = 8.1$  Hz, 2H), 7.33 ( $\text{H}^{\text{i}}$  or  $\text{H}^{\text{j}}$ , d,  $J = 8.0$  Hz, 2H), 7.24 ( $\text{H}^{\text{c}}$ , d,  $J = 7.1$  Hz, 1H), 3.94 – 3.57 ( $\text{H}^{\text{m}}$  and  $\text{H}^{\text{k}}$  (overlapped), m, 4H), 3.74 ( $\text{H}^{\text{l}}$ , s, 3H), 3.43 ( $\text{H}^{\text{n}}$ , dd,  $J = 5.8, 4.7$  Hz, 1H), 2.40 ( $\text{H}^{\text{a}}$ , s, 3H).  $^{13}\text{C}\{^1\text{H}\}\text{-NMR}$  (75 MHz,  $\text{CD}_2\text{Cl}_2$ )  $\delta$  173.2 ( $\text{C}^{\text{u}}$ ), 164.1 ( $\text{C}_{\text{ipso}}, \text{C}^{\text{e}}$ ), 147.6 ( $\text{C}_{\text{ipso}}, \text{C}^{\text{a}}$ ,  $\text{C}^{\text{i}}$  or  $\text{C}^{\text{k}}$ ), 146.9 ( $\text{C}_{\text{ipso}}, \text{C}^{\text{a}}$ ,  $\text{C}^{\text{i}}$  or  $\text{C}^{\text{k}}$ ), 143.2 ( $\text{C}_{\text{ipso}}, \text{C}^{\text{a}}$ ,  $\text{C}^{\text{i}}$  or  $\text{C}^{\text{k}}$ ), 142.2 ( $\text{C}^{\text{c}}$  or  $\text{C}^{\text{f}}$ ), 139.7 ( $\text{C}^{\text{c}}$  or  $\text{C}^{\text{f}}$ ), 139.3 ( $\text{C}^{\text{j}}$ ), 135.5 ( $\text{C}_{\text{ipso}}, \text{C}^{\text{n}}$  or  $\text{C}^{\text{q}}$ ), 131.8 ( $\text{C}^{\text{o}}$  or  $\text{C}^{\text{p}}$ ), 129.1 ( $\text{C}^{\text{h}}$ ), 128.1 ( $\text{C}^{\text{o}}$  or  $\text{C}^{\text{p}}$ ), 125.3 ( $\text{C}_{\text{ipso}}, \text{C}^{\text{n}}$  or  $\text{C}^{\text{q}}$ ), 123.7 ( $\text{C}^{\text{b}}$  or  $\text{C}^{\text{g}}$ ), 120.0 ( $\text{C}^{\text{d}}$ ), 96.9 ( $\text{C}^{\text{l}}$  or  $\text{C}^{\text{m}}$ ), 84.0 ( $\text{C}^{\text{l}}$  or  $\text{C}^{\text{m}}$ ), 62.4 ( $\text{C}^{\text{r}}$  or  $\text{C}^{\text{t}}$ ), 61.0 ( $\text{C}^{\text{r}}$  or  $\text{C}^{\text{t}}$ ), 31.2 ( $\text{C}^{\text{v}}$ ), 21.8 ( $\text{C}^{\text{w}}$ ).  $\nu(\text{C}\equiv\text{C})$ : 2154  $\text{cm}^{-1}$ ,  $\nu(\text{C}=\text{O})$ : 1731  $\text{cm}^{-1}$ . Anal. Calcd.  $\text{C}_{25}\text{H}_{24}\text{AuClN}_2\text{O}_3$  (found): C, 47.44 (47.29); H, 3.82 (3.81); N, 4.43 (4.54).

**1.5.12. (2-*para*-tolylpyridyl)Au-(Cl)C $\equiv$ C-C $_6$ H $_4$ -CH $_2$ -NH-CH $_2$ -COOCH $_2$ CH $_3$  (complex 14).**



1-Ethynyl-4-benzyl-L-Glycine ethyl ester (81.6 mg, 0.37 mmol), CuI (0.41 mg, 2.15 mmol) and NEt<sub>3</sub> (104.0 μL, 0.74 mmol) were added to a mixture of (2-*para*-tolylpyridyl)AuCl<sub>2</sub> (164.0 mg, 0.37 mmol) in dichloromethane (10 ml). The mixture was allowed to stir for 1 hour at room temperature. The resulting solution was washed with water (10 ml), and the organic layer was isolated. The solvent was removed under vacuum and the residue was extracted with ethanol and washed with ethanol and petrol ether 40/60 (10 ml) and vacuum dried, to yield a yellow solid (94.5 mg, 0.15 mmol, 41 %). <sup>1</sup>H-NMR (300 MHz, CD<sub>2</sub>Cl<sub>2</sub>) δ 9.50 (H<sup>h</sup>, d, J = 4.8 Hz, 1H), 8.13 – 8.05 (H<sup>f</sup>, td, J = 8.0, 1.5 Hz, 1H), 8.05 (H<sup>b</sup>, d, J = 0.8 Hz, 1H), 7.90 (H<sup>c</sup>, d, J = 7.9 Hz, 1H), 7.59 (H<sup>d</sup>, d, J = 7.9 Hz, 1H), 7.51 – 7.48 (H<sup>g</sup>, m, 1H), 7.51 (H<sup>i</sup> or H<sup>j</sup>, d, J = 8.0 Hz, 2H), 7.32 (H<sup>i</sup> or H<sup>j</sup>, d, J = 8.0 Hz, 2H), 7.23 (H<sup>c</sup>, d, J = 7.8 Hz, 1H), 4.17 (H<sup>n</sup>, q, J = 7.1 Hz, 3H), 3.81 (H<sup>k</sup> or H<sup>l</sup>, s, b, 2H), 3.39 (H<sup>k</sup> or H<sup>l</sup>, s, b, 2H), 2.42 (H<sup>a</sup>, s, 3H), 1.26 (H<sup>m</sup>, t, J = 7.1 Hz, 2H). <sup>13</sup>C{<sup>1</sup>H}-NMR (75 MHz, CD<sub>2</sub>Cl<sub>2</sub>) δ 176.2 (weak signal), 164.1 (C<sup>t</sup>), 147.6 (C<sub>ipso</sub>, C<sup>a</sup>, C<sup>i</sup> or C<sup>k</sup>), 146.9 (C<sub>ipso</sub>, C<sup>a</sup>, C<sup>i</sup> or C<sup>k</sup>), 143.2 (C<sub>ipso</sub>, C<sup>a</sup>, C<sup>i</sup> or C<sup>k</sup>), 142.1 (C<sup>f</sup> or C<sup>c</sup>), 139.6 (C<sup>j</sup>), 135.5 (C<sub>ipso</sub>, C<sup>n</sup> or C<sup>q</sup>), 131.7 (C<sup>o</sup> or C<sup>p</sup>), 129.1 (C<sup>h</sup>), 128.1 (C<sup>o</sup> or C<sup>p</sup>), 125.3 (C<sub>ipso</sub>, C<sup>n</sup> or C<sup>q</sup>), 123.9 (C<sup>b</sup> or C<sup>g</sup>), 123.7 (C<sup>b</sup> or C<sup>g</sup>), 120.0 (C<sup>d</sup>), 97.1 (C<sup>l</sup> or C<sup>m</sup>), 84.3 (C<sup>l</sup> or C<sup>m</sup>), 60.6 (C<sup>s</sup> or C<sup>r</sup>), 50.1 (C<sup>s</sup> or C<sup>r</sup>), 29.0 (C<sup>u</sup>), 21.8 (C<sup>w</sup>), 14.0 (C<sup>v</sup>). ν(C≡C): 2161 cm<sup>-1</sup>. ν(C=O): 1736 cm<sup>-1</sup>. Anal. Calcd. C<sub>25</sub>H<sub>24</sub>AuN<sub>2</sub>O<sub>2</sub> · H<sub>2</sub>O(found): C, 47.29 (47.69); H, 4.13 (3.57); N, 4.41 (4.53).

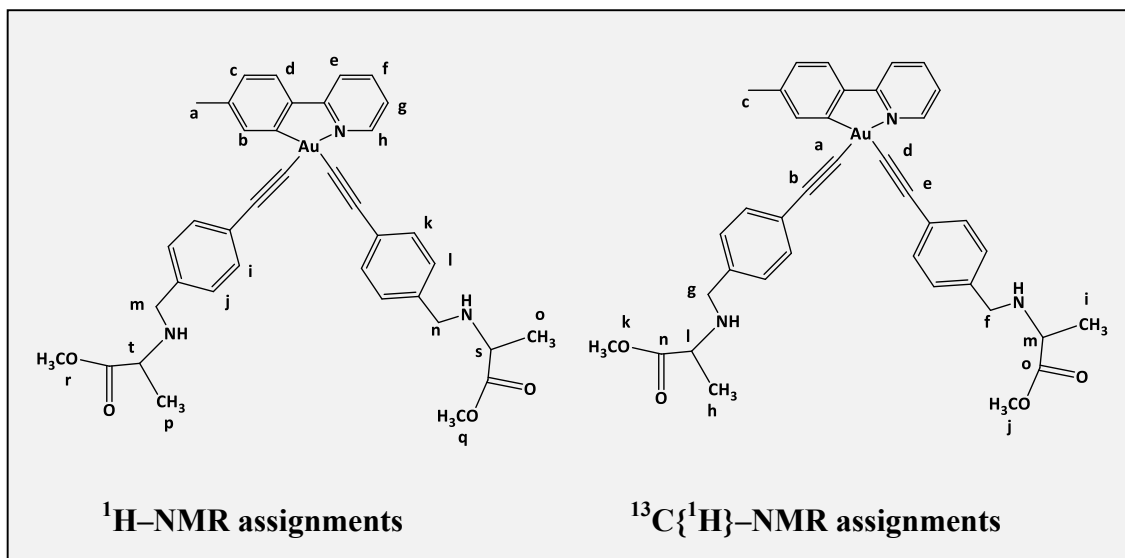
**1.5.13. (2-*para*-tolylpyridyl)Au(-C≡C-C<sub>6</sub>H<sub>4</sub>-CHO)<sub>2</sub> (complex 15).**



4-ethynylbenzaldehyde (46 mg, 0.35 mmol), CuI (0.46 mg, 2.41 mmol) and NEt<sub>3</sub> (67 μL, 1.05 mmol) were added to a mixture of (2-*para*-tolylpyridyl)AuCl<sub>2</sub> (70 mg, 0.16 mmol) in dichloromethane (10 ml). The mixture was allowed to stir for 3 hours at room temperature. The resulting solution was washed with water, and the organic layer was isolated. The solvent was removed under vacuum and the residue was washed with petrol ether 40/60 (10 ml) and vacuum dried, to yield a yellow solid (61.3 mg, 0.10 mmol, 62 %). <sup>1</sup>H-NMR (300 MHz, CD<sub>2</sub>Cl<sub>2</sub>) δ 9.99 (H<sup>m</sup> or H<sup>n</sup>, s, 1H), 10.01 (H<sup>m</sup> or H<sup>n</sup>, s, 1H), 9.57 (H<sup>h</sup>, d, J = 5.1 Hz, 1H), 8.09 (H<sup>f</sup>, d, J = 8.2, 1.3 Hz, 1H), 8.02 (H<sup>b</sup>, s, 1H), 7.92 (H<sup>e</sup>, d, J = 8.0 Hz, 1H), 7.61 – 7.89 (H<sup>i-j</sup>, H<sup>k-l</sup> (overlapped), m, 8H), 7.64 (H<sup>d</sup>, d, J = 8.1 Hz, 1H), 7.44 (H<sup>g</sup>, m, 1H), 7.23 (H<sup>c</sup>, d, J = 7.6 Hz, 1H), 2.42 (H<sup>a</sup>, s, 3H). <sup>13</sup>C{<sup>1</sup>H}-NMR (75 MHz, CD<sub>2</sub>Cl<sub>2</sub>) δ 191.4 (C<sup>f</sup> or C<sup>g</sup>), 167.0 (C<sup>Ar</sup>), 155.2 (C<sup>Ar</sup>), 150.7 (C<sup>Ar</sup>), 142.7 (C<sup>Ar</sup>), 142.6 (C<sup>Ar</sup>), 141.8 (C<sup>Ar</sup>), 136.3 (C<sup>Ar</sup>), 135.0 (C<sup>Ar</sup>), 134.7 (C<sup>Ar</sup>), 132.2 (C<sup>Ar</sup>), 132.0 (C<sup>Ar</sup>), 129.4 (C<sup>Ar</sup>), 128.5 (C<sup>Ar</sup>), 124.9 (C<sup>Ar</sup>), 123.8 (C<sup>Ar</sup>), 123.7 (C<sup>Ar</sup>), 120.3 (C<sup>Ar</sup>), 103.6 (C<sup>a</sup>, C<sup>b</sup>, C<sup>d</sup> or C<sup>e</sup>), 86.1 (C<sup>a</sup>, C<sup>b</sup>, C<sup>d</sup> or C<sup>e</sup>), 90.7 (C<sup>a</sup>, C<sup>b</sup>, C<sup>d</sup> or C<sup>e</sup>), 21.8 (C<sup>c</sup>). ν(C≡C): 2131 cm<sup>-1</sup>, 2162 cm<sup>-1</sup>. Anal. Calcd. C<sub>30</sub>H<sub>20</sub>AuNO<sub>2</sub> (found): C, 57.80 (57.67); H, 3.23 (3.14); N, 2.25 (2.36).

1.5.14. (2-*para*-tolylpyridyl)Au(-C≡C-C<sub>6</sub>H<sub>4</sub>-CH<sub>2</sub>-NH-CH(CH<sub>3</sub>)-COOCH<sub>3</sub>)<sub>2</sub>

(complex 16).



1-Ethynyl-4-benzyl-L-Alanine methyl ester (80.0 mg, 0.37 mmol), CuI (0.53 mg, 2.78 mmol) and NEt<sub>3</sub> (71.0 μL, 0.37 mmol) were added to a mixture of (2-*para*-tolylpyridyl)AuCl<sub>2</sub> (74.0 mg, 0.17 mmol) in dichloromethane (10 ml). The mixture was allowed to stir for 16 h at room temperature. The resulting solution was washed with water (10 ml), and the organic layer was isolated. The solvent was removed under vacuum and the residue was washed off with petrol ether 40/60 (10 ml) and vacuum dried, to yield a yellow solid (43.0 mg, 0.05 mmol, 32 %). <sup>1</sup>H-NMR (300 MHz, CD<sub>2</sub>Cl<sub>2</sub>) δ 9.64 (H<sup>h</sup>, d, J = 5.1 Hz, 1H), 8.03 – 8.09 (H<sup>f</sup> and H<sup>b</sup> (overlapped), m, 2H), 7.90 (H<sup>e</sup>, d, J = 8.1 Hz, 1H), 7.63 (H<sup>d</sup>, d, J = 8.0 Hz, 1H), 7.42 (H<sup>g</sup>, m, 1H), 7.20 (H<sup>c</sup>, d, J = 8.0 Hz, 1H), 3.64 (H<sup>f</sup> or H<sup>q</sup>, s, 3H), 3.66 (H<sup>f</sup> or H<sup>q</sup>, s, 3H), 3.62 – 3.84 (H<sup>m</sup> and H<sup>n</sup> (overlapped), m, 4H), 3.33 – 3.42 (H<sup>s</sup> and H<sup>t</sup>, m, 2H), 2.42 (H<sup>a</sup>, s, 3H), 1.30 (H<sup>o</sup> or H<sup>p</sup>, d, J = 6.8 Hz, 3H), 1.30 (H<sup>o</sup> or H<sup>p</sup>, d, J = 6.9 Hz, 1H). <sup>13</sup>C{<sup>1</sup>H}-NMR (75 MHz, CD<sub>2</sub>Cl<sub>2</sub>) δ, 176.0 (C<sup>n</sup> or C<sup>o</sup>) 166.9 (C<sup>Ar</sup>), 155.8 (C<sup>Ar</sup>), 150.7 (C<sup>Ar</sup>), 142.7 (C<sup>Ar</sup>), 142.5 (C<sup>Ar</sup>), 141.6 (C<sup>Ar</sup>), 139.6 (C<sup>Ar</sup>), 136.3 (C<sup>Ar</sup>), 131.7 (C<sup>Ar</sup>), 131.6 (C<sup>Ar</sup>), 128.2 (C<sup>Ar</sup>), 128.0 (C<sup>Ar</sup>), 124.7 (C<sup>Ar</sup>), 124.5 (C<sup>Ar</sup>), 124.3 (C<sup>Ar</sup>), 123.7 (C<sup>Ar</sup>), 120.1 (C<sup>Ar</sup>), 117.7 (C<sup>Ar</sup>), 103.7 (C<sup>a</sup>, C<sup>b</sup>, C<sup>c</sup> or C<sup>d</sup>), 98.8 (C<sup>a</sup>, C<sup>b</sup>, C<sup>c</sup> or C<sup>d</sup>), 80.2 (C<sup>a</sup>, C<sup>b</sup>, C<sup>c</sup> or C<sup>d</sup>), 78.1 (C<sup>a</sup>, C<sup>b</sup>, C<sup>c</sup> or C<sup>d</sup>),

55.9 ( $C^k$ ,  $C^j$ ,  $C^g$  or  $C^f$ ), 55.4 ( $C^k$ ,  $C^j$ ,  $C^g$  or  $C^f$ ), 51.6 ( $C^k$ ,  $C^j$ ,  $C^g$  or  $C^f$ ), 51.5 ( $C^k$ ,  $C^j$ ,  $C^g$  or  $C^f$ ), 21.8 ( $C^c$ ), 18.9 ( $C^h$  or  $C^i$ ).  $\nu(C\equiv C)$ :  $2153\text{ cm}^{-1}$ ,  $\nu(C=O)$ :  $1732\text{ cm}^{-1}$

## **CHAPTER 2**

# **INTERACTION OF BI- AND TRI-DENTATE CYCLOMETALATED GOLD(III) COMPLEXES WITH DNA SECONDARY STRUCTURES.**

## 2.1. INTRODUCTION

### 2.1.1. Metal complexes in cancer therapy.

Therapeutic applications of metal-based compounds have been largely studied. Although some of these compounds have presented novel medical applications,<sup>36</sup> both their limited selectivity and toxicity have progressively reduced their interest in favour of the more reliable organic compounds.

In 1965 Rosenberg et al.<sup>37</sup> discovered the antiproliferative activity of a platinum complex called cisdiamminedichloroplatinum (**cisplatin**) (Figure 51), which was successfully employed in testicular cancer therapy in 1978. This discovery increased the interest in metal-based drugs, particularly of the cytotoxicity of other metal-based compounds.

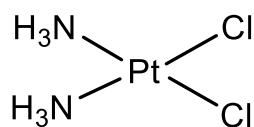


**Figure 51.** *Cisdiamminedichloroplatinum (cisplatin).*

**Cisplatin** has shown to be highly effective in the treatment of testicular and ovarian cancers, and is also employed for treating bladder, cervical, head and neck, oesophageal, and small cell lung cancer.<sup>38</sup>

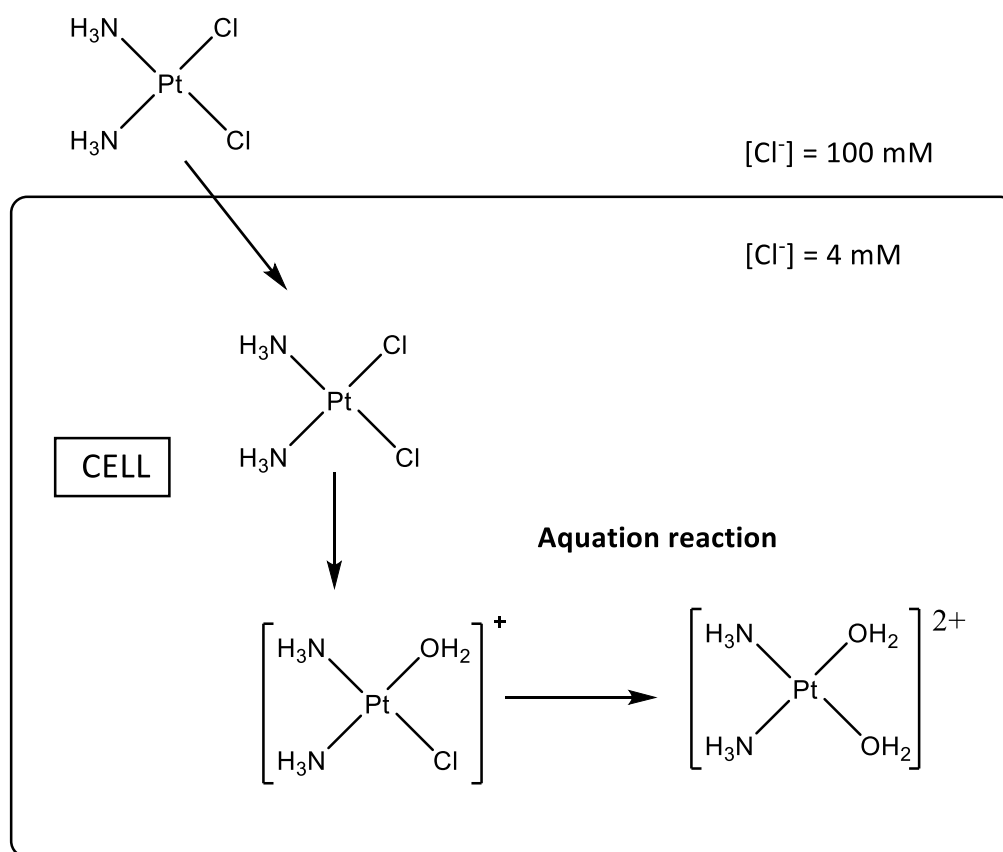


**Figure 52.** Aquation of *cisplatin* in cells (adapted from reference<sup>39</sup>).

It is generally accepted that its antitumor properties are due to the binding of **cisplatin** to genomic DNA (gDNA) in the cell nucleus.<sup>39</sup> The high concentration of chloride ion (100 mM) allows cisplatin to maintain a neutral stable conformation until it enters into the cell.<sup>40</sup> Once **cisplatin** reaches the cell, the low chloride ion concentration (4-12 mM) facilitates **cisplatin** aquation reaction, exchanging the two chloride ions by water or hydroxy ligands, to form the cationic aqua complexes (Figure 52).<sup>39</sup> Cationic molecules with no hydrocarbon components exhibit difficulties to diffuse through the biological membrane. Accordingly, the obtained aqua derivatives from cisplatin may not be able to go out from the cell before binding to DNA, being trapped inside the cell. Both this fact and that no modification of the chemical structure during passive diffusion, may be potential reasons of the high cytotoxicity of cisplatin.<sup>39</sup>

In contrast to the effectiveness of **cisplatin**, both drug resistance (some tumours have developed an intrinsic resistance to **cisplatin**) and significant side effects (loss of fertility, loss of appetite or numbness) have represented limiting factors in its use. These limitations encouraged the development of less toxic **cisplatin** derivatives, such as **carboplatin** and **oxaliplatin** (Figure 53), which were approved for clinical use in 1983 and 2003, respectively.

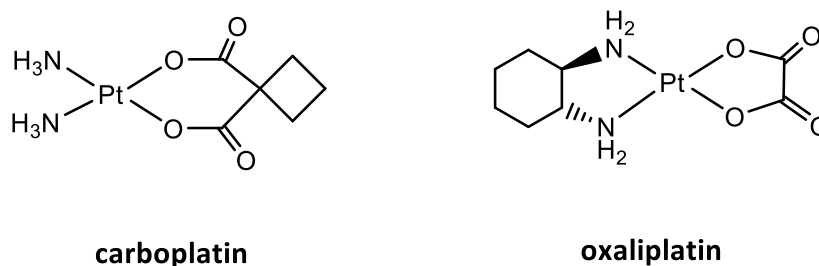


**Figure 53.** *Carboplatin and oxiplatin as less toxic alternatives to cisplatin.*

The successful results obtained with these drugs derived from **cisplatin** encouraged the investigation of the cytotoxicity of other different inorganic compounds.

### 2.1.2. Anti-cancer gold inorganic complexes.

In recent years, gold compounds have drawn attention as a new generation of anticancer agents, showing anti-tumour properties both *in vitro* and *in vivo*.<sup>41</sup> One of the most important reasons to justify the investigations for the potential anti-tumour activity of gold complexes is related to the coordination geometry of gold(III) species. Au(III) is isoelectronic with Pt(II). Au(III) compounds feature a square-planar coordination geometry, corresponding to the 5d<sup>8</sup> outer shell electronic configuration for the gold(III) atom.<sup>42</sup>

### 2.1.2.1. Gold(I) complexes with anti-tumour activity.

In the last decades, gold(I) complexes have shown to be potent cytotoxic agents, with several applications in chrysotherapy (application of gold compounds in medicine). In 2000, Mitchell et al.<sup>43</sup> reported a study of mortality in rheumatoid arthritis patients being treated by chrysotherapy, showing that cancer levels remained steady compared to not treated patients and, in some cases, lower levels were observed. The gold(I) complexes used in chrysotherapy are generally divided into two classes: gold thiolates (**aurothiomalate**, Figure 54a) and triethylphosphinegold(I) tetraacetylated thioglucose species, commonly called **Auranofin**® (Figure 54b).

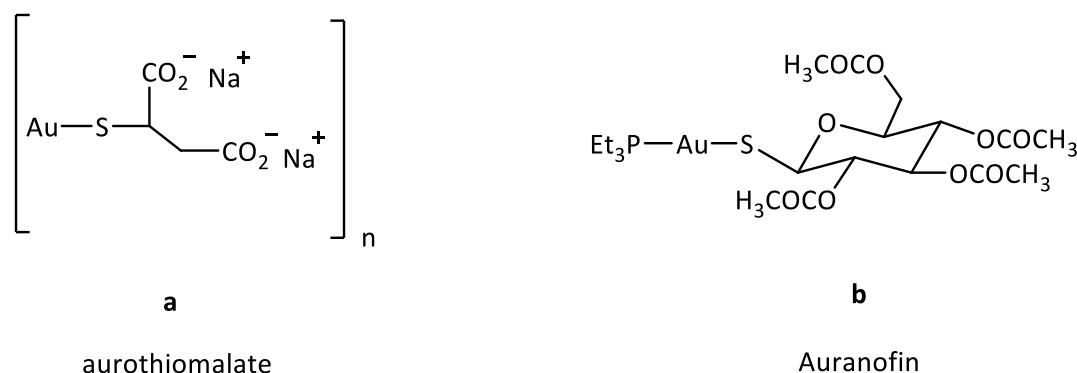


**Figure 54.** Examples of gold complexes used in chrysotherapy.

**Auranofin** is a sulfur-coordinated gold(I) compound, which has been used for the treatment of rheumatoid arthritis, based on its anti-inflammatory and immunosuppressive properties.<sup>44,45,46</sup> In recent years, **Auranofin** has been investigated as an anti-cancer agent, showing remarkable results as anti-tumor agent and exhibiting considerable *in vitro* inhibitory effects. In 1979, Lorber et al.<sup>47</sup> studied the effects of **Auranofin** in cells proliferation. These studies included assessing DNA, RNA, and protein synthesis as measured by incorporation of <sup>3</sup>H-thymidine, <sup>3</sup>H-uridine, and <sup>3</sup>H-leucine into HeLa cells. **Auranofin** was shown to inhibit <sup>3</sup>H-thymidine uptake more rapidly than <sup>3</sup>H-uridine or <sup>3</sup>H-leucine uptake at a gold concentration of 75- 100 µg/dl. These three parameters were inhibited with a 24-hour exposure to 100 µg/dl. The inhibition of <sup>3</sup>H-thymidine uptake

in HeLa for 6 hours with 50 or 100  $\mu\text{g}/\text{dl}$  of gold was found to be irreversible. In addition, HeLa cells demonstrated a remarkable decrease in oxygen uptake after exposure to **Auranofin**. These results confirmed the significant inhibitory effect on essential biological processes and functions exerted by **Auranofin**.

The anti-tumour effects of Auranofin is considerably influenced by the P – Au – S arrangement, which has shown to be one the most relevant reasons to explain its cytotoxicity. The presence of phosphine and thiolate ligands has been demonstrated to increase the cytotoxicity of the complex but, the combination of both in the same compound have revealed a considerable enhancement of cytotoxicity. The promising results shown by **Auranofin** encouraged an expansion of the field of study towards other comparable gold(I) compounds.

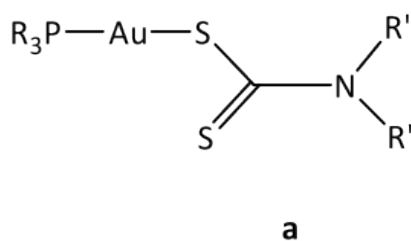


**Figure 55.** *Chemical structure of gold(I) dithiocarbamate derivatives.*

The anti-tumour activity of Auranofin derivatives is influenced by the nature of both thiolate and phosphine groups. Barrios et al.<sup>48</sup> demonstrated that the variations in phosphine ligand can introduce a considerable effect in the inhibition of some enzymes, such as cathepsin B. In addition, the larger size and more lipophilic character of phosphine groups, compared to thiolate groups, play an important role in the enhancement of the diffusion of the gold compounds through the biological membrane, increasing the gold uptake inside the cell. This effect was also investigated by Tiekink et al.,<sup>49</sup> reporting a family of gold(I) dithiocarbamate derivatives where is important to highlight complex **a** (Figure 55), with a linear P-Au-S arrangement characteristic from

**Auranofin**, which was found to be more active than cisplatin in various human cancer cell lines, exhibiting the maximum effect against the ovarian cell line IGROV and the estrogen receptors MCF-7 and EVSA-T.

#### 2.1.2.2. Gold alkynyl complexes.

The study of the anti-tumour properties of gold complexes have been expanded in different directions, for instance towards gold alkynyl complexes. Although luminescence properties have been the most studied area for these complexes, the biological studies of these complexes have not been developed in depth, and there are only few examples in the literature,<sup>50,51,52</sup> most of them of gold(I) complexes. A recent study showed that alkynyl(triphenylphosphine)gold(I) derivatives (Figure 56) exhibit a significant inhibitor activity over the seleno-enzyme thioredoxin reductase (**TrxR**), showing high selectivity over the enzyme glutathione reductase.<sup>52</sup>

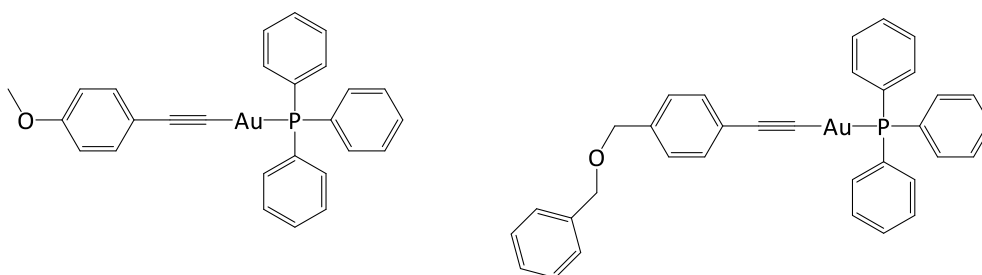


**Figure 56.** *Examples of alkynyl(triphenylphosphine)gold(I) complexes.*

#### 2.1.2.3. Gold complexes bearing amino acid moieties.

In recent years, functionalization of gold(I) complexes with amino acid has been studied. From a biological point of view, the amino acids can deliver the gold atom to

the biological target and, because of the amino acid receptors are overexpressed in tumour cells, these complexes could increase its selectivity towards tumour cells.<sup>53</sup>

Examples of gold(I) complexes functionalized by amino acid ligands are quite scarce in the literature. Gimeno et al.<sup>54</sup> reported the synthesis of gold(I) thiolate complexes, functionalized by amino acids esters. They employed [Au(SpyCOOH)(PPh<sub>3</sub>)] (Figure 57) as precursor, which was previously synthesized by Nomiya et al.<sup>55</sup>

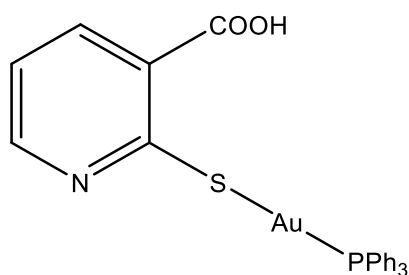
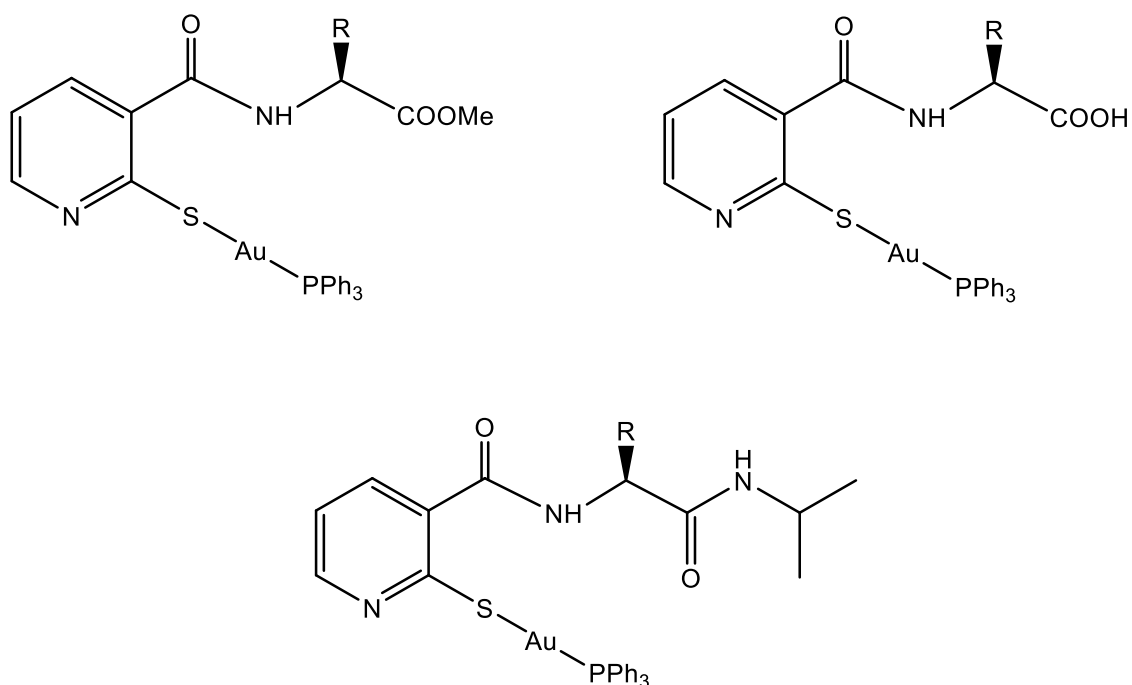


**Figure 57.** Chemical structure of [Au(SpyCOOH)(PPh<sub>3</sub>)].<sup>55</sup>

They considered that the use of **Auranofin** analogues, containing Au-S bond, and the functionalization with amino acids may provide to these complexes with anti-tumour activity against different cell lines. Following this theory, they recently reported the synthesis of NSHC gold (I) compounds functionalized by peptides (NSHC = N-allylbenzothiazolin-2-ylidene).<sup>56</sup> They studied the cytotoxic activity of three families of gold compounds (Figure 58) against three human tumour cell lines A549 (lung carcinoma), Jurkat (T-cell leukaemia), and MiaPaca2 (pancreatic carcinoma). These complexes exhibited good anti-cancer activity, with IC<sub>50</sub> values from 7.4 to 30.5  $\mu$ M in A549 cells, 2.4 to 7.7  $\mu$ M in Jurkat cells, and 8.2 to 27.2  $\mu$ M in MiaPaca2, with the Jurkat cell line the most active.



R = H, Me, iPr, Bn, (CH<sub>2</sub>)<sub>2</sub>SCH<sub>3</sub>, -N(CH<sub>2</sub>CH<sub>3</sub>)CH-

**Figure 58.** Chemical structures of NSHC gold (I) compounds functionalized by amino acid and amino ester derivatives.

#### 2.1.2.4. Cyclometalated gold(III) complexes with anti-tumour activity.

Gold(III) complexes represent a new class of metallodrugs, that have shown remarkable anti-tumour applications in recent years. Since Au(III) and Pt(II) are isoelectronic<sup>36</sup> and isostructural,<sup>36</sup> the biological applications of several Au(III) complexes have been studied. However, the poor stability of Au(III) complexes in physiological media has been the main issue, observing reductive elimination to Au(I) or Au(0) in most of cases.<sup>57</sup>

Pincer ligands provide an alternative to generate cyclometalated gold(III) complexes which are characterized by redox and thermodynamic stability. In addition, the

modification of the steric and electronic properties of the ligands can enhance the lipophilic character of the synthesized gold(III) complexes. Several examples of cyclometalated gold(III) complexes functionalized by pincer ligands have been reported. Complexes functionalized by bi-dentate ( $C^{\wedge}N$ )<sup>58</sup>, tri-dentate ( $C^{\wedge}N^{\wedge}C$ )<sup>59</sup>, ( $N^{\wedge}N^{\wedge}N$ )<sup>60</sup> and ( $N^{\wedge}N^{\wedge}C$ ),<sup>61</sup> and poly-dentate ligands, such as porphyrin derivatives,<sup>62</sup> have shown a remarkable enhancement in terms of stability for biological studies. Pincer ligands stabilize the Au(III) centre, providing a considerable stability in physiological media.

### **2.1.3. Stabilization of secondary DNA structures by gold- based complexes.**

Deoxyribonucleic acid (DNA) represents the major target of antitumor metal complexes. The cytotoxic effects of gold compounds may be a consequence of a direct interaction of them with nuclear DNA. From the few data available and by comparison with platinum(II) complexes, it may be hypothesized that the biological action of gold(III) complexes and, specifically, their antitumor activity is possibly mediated by direct interaction with DNA.<sup>63</sup> A number of studies based on different physicochemical techniques suggest that the probable binding sites for gold(III) are N(1)/N(7) atoms of adenosine, N(7) or C(6)O of guanosine, N(3) of cytidine, and N(3) of thymidine, which are analogous to the possible binding sites for the isoelectronic platinum(II) ion.<sup>64</sup>

#### **2.1.3.1. Double stranded DNA structures stabilized by gold complexes.**

Most DNA molecules are two polymer strands, bound together in a helical fashion by H-bonding and  $\pi$ - $\pi$  stacking, forming a double stranded structure (**dsDNA**). The stability of the dsDNA form depends on three factors:

- GC-content: dsDNA is maintained by strongest for G, C stacks, exhibiting higher stability with high GC content.
- Depending on the sequence: The stacking is sequence specific.
- The length of the sequence. Long DNA helices, with a high GC-content (stronger-interacting strands), will be more stable than short helices, with high AT content (weaker-interacting strands).

There are only a few examples of gold complexes stabilizing dsDNA conformations. In 2000, Oriol et al.<sup>65</sup> reported the synthesis of **chloro glycyhistidinate gold(III)** complex and its DNA binding studies. The binding studies of this complex with calf thymus DNA were carried out by in vitro through circular dichroism (CD) spectroscopy and analysis of the temperature dependence of the DNA helix-to-coil transition.

CD spectra of calf thymus DNA were measured upon addition of increasing amounts of **chloro glycyhistidinate gold(III)** complex. The addition of this complex represented only minor changes of the CD spectrum of calf thymus DNA, suggesting that only small DNA conformational distortions take place. In order to monitor possible alterations of the gold(III) chromophore due to the DNA addition, an excess of calf thymus DNA was added to a solution containing **chloro glycyhistidinate gold(III)** complex in the reference buffer while recording the visible CD spectrum of this complex. The CD spectrum of the gold(III) chromophore did not show remarkable changes after DNA addition, suggesting that gold remains in the +III state and that the global conformation of the complex does not undergo significant modifications.

Following these investigations, Messori et al.<sup>66a</sup> reported a study about the interactions of bipyridyl gold(III) complexes with calf thymus DNA (Figure 59). Although only small effects on DNA conformation and stability were observed, the gold(III)

chromophore was not significantly modified, showing a very weak binding to calf thymus DNA.

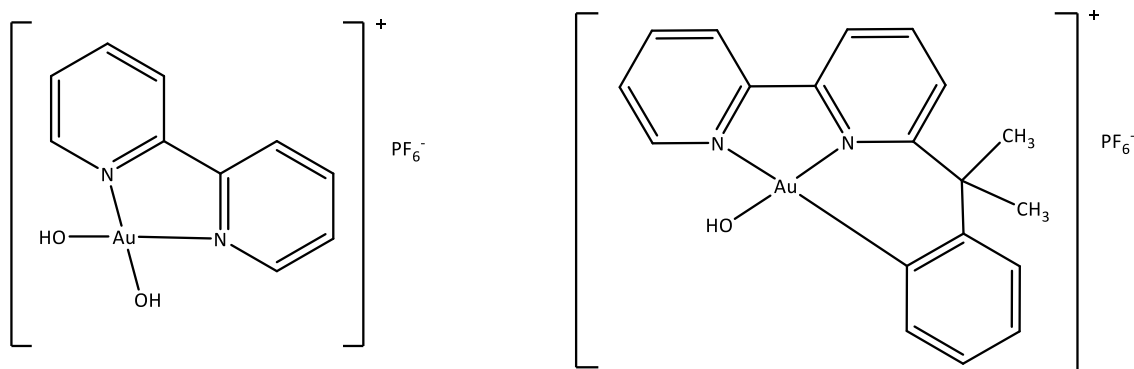


**Figure 59.** Bipyridyl gold(III) complexes, in which binding with calf thymus DNA has been studied.<sup>66a</sup>

In 2006, the same research group<sup>66b</sup> reported the synthesis of dinuclear gold(III) compounds derived from the condensation of two square-planar gold(III) moieties. The interactions of bipyridyl gold(III) complexes with calf thymus DNA was studied. One of the studied complexes called **AuOxo6**<sup>66b</sup> (Figure 60) exhibited a remarkable binding to the DNA double helix. CD spectrum revealed that calf thymus DNA adopts its native B-type conformation, characterized by a positive band at 275 nm and a negative one at about 242 nm. In presence of **AuOxo6**, a decrease of the negative band at 242 nm was observed, which was attributed to a partial loss of the DNA helicity, due to electrostatic interactions between the phosphate groups at the positively charged metal complex. In addition, a remarkable change in the positive peak at 275 nm was observed, associated with a modification of the overall base stacking of the double helix. Moreover, the presence of **Auoxo6** also induced a weak CD band at 345 nm, indicative of the formation an Auoxo6/DNA adduct.

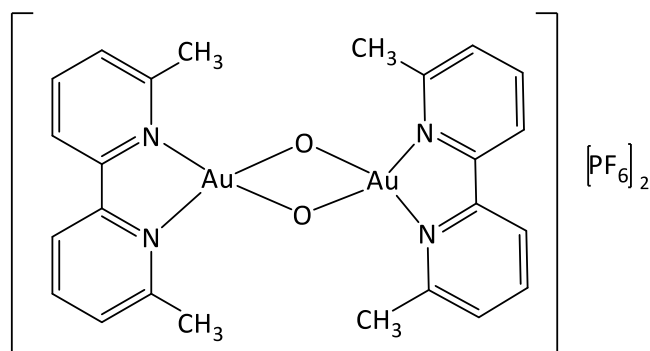


**Figure 60.** *AuOxo6 complex.*<sup>66b</sup>

### 2.1.3.2. G-quadruplex DNA structures. Interaction with Gold(III) complexes.

G-quadruplexes are higher-order DNA and RNA structures formed from G-rich sequences that are built around tetrads of hydrogen-bonded guanine bases.<sup>67</sup> These are four-stranded helical DNA (or RNA) structures, comprising stacks of G-tetrads, which consist of four guanine bases aligned in a co-planar arrangement stabilized by Hoogsteen hydrogen-bonding and monovalent cations, such as  $K^+$  or  $Na^+$  (Figure 61).<sup>68a</sup>

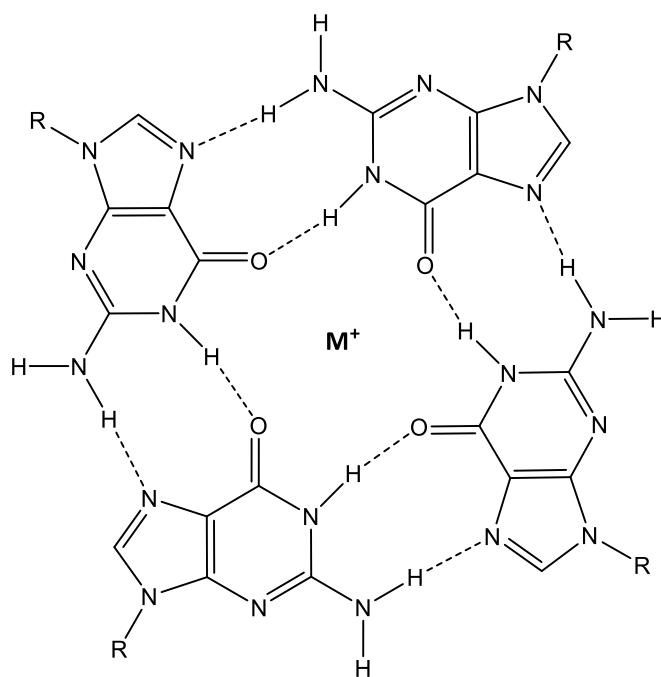


**Figure 61.** *G-quadruplex structure.*

The structure is stabilized through the presence of stacking interactions between the stacked strands. In addition, the presence of monovalent cations increases the stability of the structure because of the strong electrostatic interactions produced between guanidine O6 and cations.<sup>68b</sup>

In 1989, Williamson et al.<sup>69</sup> reported that these sequences form quartets *in vitro*. In 1992, Kang et al.<sup>70</sup> reported the crystal structure of four-stranded *Oxytricha* telomeric DNA, the first example of a G-quadruplex structure. This structure demonstrates that two *Oxytricha* DNA strands can associate to form a G-quadruplex structure. (Figure 62).

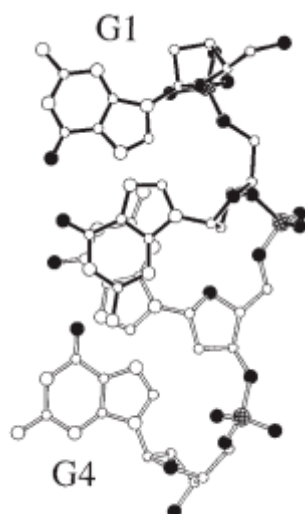


**Figure 62.** Diagram of the four residues G1-G4 viewed perpendicular to base planes.<sup>70</sup>

In 1998, the structures of quadruplexes formed by two different DNA oligonucleotides were reported, as well as the localization and effect of cations on these structures. The presence of these cations played an important role in the stabilization and folding of quadruplexes<sup>71,72</sup> through the electrostatic interactions established with the guanidine carbonyl groups.

Hundreds of ligands based on different structures have been tested for their affinity toward the telomeric G-quadruplex. Recently, great interest has been focused on the

development of novel metal-based agents directed towards this target.<sup>73</sup> Some metal complexes have shown high effectiveness in the stabilization of G-quadruplex structures.<sup>74-76</sup> Some of the metal complexes that have exhibited an interaction with DNA area are generally supported by a planar aromatic ring, where the metal centre responsible for neutralization of the central electron-dense is generated by the carbonyl oxygen of the paired guanines.<sup>73</sup>

Despite the strong interest in targeting DNA G-quadruplexes with metal complexes, only very few examples concern gold complexes have been reported. In 2010, Vilar et al.<sup>77a</sup> reported a pyridine pyrazolate complex  $[Au-(pzpy)_2]Cl$  (Figure 63) as the first G-quadruplex DNA inhibitor. This complex was tested against Human telomer (HTelo) and c-myc, a proto-oncogene, (group of genes that cause normal cells to become cancerous when they are mutated<sup>78a</sup>) that plays an important role in growth control, differentiation and apoptosis (programmed cell death, carried out by the cell itself once it is not longer needed<sup>78b</sup>), being considered one of the most affected genes in human cancers.<sup>77b</sup> This complex showed a strong interaction with quadruplex DNA, giving  $DC_{50}$  values of 0.34  $\mu M$  for c-myc, and 1.03  $\mu M$  for Htelo, which were similar to the values found for a range of good quadruplex DNA binders.<sup>77b</sup>

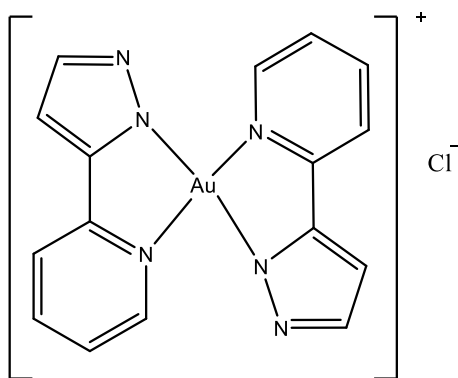


**Figure 63.** Chemical structure of  $[Au-(pzpy)_2]Cl$ .

In 2015, Bazzicaluppi et al.<sup>79</sup> analyzed the interactions of three gold(III) complexes called **Aubipyc**, **Au<sub>2</sub>bipyc** and **Auoxo6**<sup>79</sup> (Figure 64) with human telomeric DNA G-quadruplexes, making use of a variety of physico-chemical methods, such as DNA melting or circular dichroism.

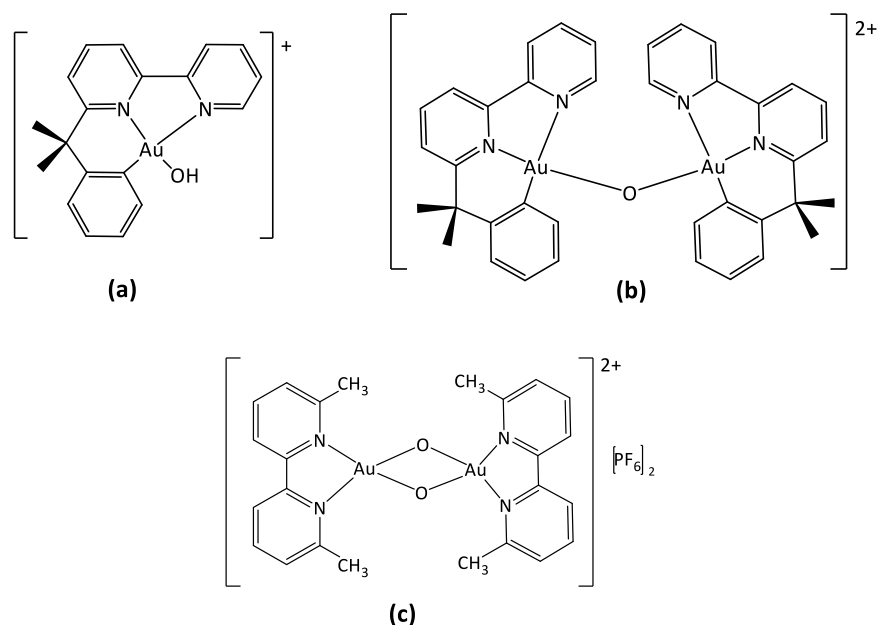


**Figure 64.** Chemical structure of of **Aubipyc** (a), **Au<sub>2</sub>bipyc** (b) and **Auoxo6** (c).<sup>79</sup>

Although these three complexes bind to the G-quadruplex form of human telomeric DNA, their DNA binding modes show differences. Circular dichroism (CD) spectroscopy revealed that both **Aubipyc** (a) and **Au<sub>2</sub>bipyc** (b) bind to telomeric G-quadruplex Tel22 (d[AG<sub>3</sub>(T<sub>2</sub>AG<sub>3</sub>)<sub>3</sub>]) in similar efficiency at room temperature. In contrast, **Auoxo6** (c) showed the most remarkable binding affinity for human telomeric G-quadruplex (Figure 65).

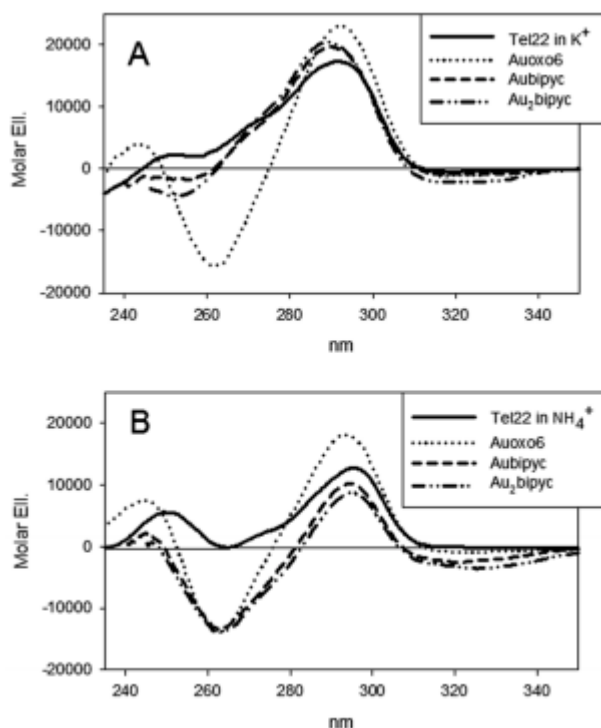


**Figure 65.** CD spectra of 4  $\mu\text{M}$  Tel22 in the presence of Aubipyc,  $\text{Au}_2\text{bipyc}$  and Auoxo6. Spectra were acquired in 10 mM Tris, 50 mM KCl (panel A) or 50 mM  $\text{NH}_4\text{Cl}$  (panel B), pH 7.5, 25  $^\circ\text{C}$ .<sup>79</sup>

As it is shown in Figure 65, both **Aubipyc** and  **$\text{Au}_2\text{bipyc}$**  have presented an increase of the positive peak at 290 nm, indicative of interaction between these Au(III) complexes and Tel22 DNA structure. Regarding **Auoxo6**, the positive peak at 290 nm was more pronounced, and also a negative peak about 260 nm was also observed, indicating that this complex is presenting the most significant binder to Tel22 DNA.

### 2.1.3.3. i-motif DNA structures. Interaction with Gold(III) complexes.

In 1993, Gehring and co-workers<sup>80</sup> found that the DNA sequence d(C<sub>5</sub>T) can form a special four stranded intermolecular nucleic acid secondary structures, maintained by formation of hairpins stabilized by intercalated cytosine-cytosine<sup>+</sup> base pairs at N3, bonded by three hydrogen bonds, intercalated to each other in an antiparallel

orientation. This structure was called the “i-motif” (Figure 66). The name i-motif refers that is probably the only nucleic acid structure with intercalated base pairs.

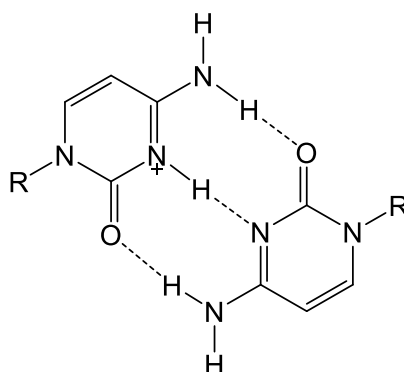


**Figure 66.** *A hemiprotonated cytosine–cytosine<sup>+</sup> base pair that intercalate to the form i-motif structure.*

The arrangement of C·CH<sup>+</sup> pairs may involve four C tracts of cytosine separated by stretches of other bases, folding into an intramolecular i-motif. These sequences have been found in the promoter regions of several oncogenes.<sup>81a</sup>

In general terms, the stability of the genomic intramolecular i-motif sequences depends directly on the length of their loops. i-Motif with long loops have demonstrated to be more stable due to the extra stabilizing interactions of the longer loops.<sup>82a</sup> However, in 2015, Brazier et al.<sup>82b</sup> demonstrated that short loops stabilize more stable structures than long loops. With longer loops, the structure reaches more flexibility, but the interactions become weaker. They reported that forming intramolecular interactions would be the way to stabilize long loop regions, because it would limit the flexibility.

However, the C tracts may be presented in two or four independent nucleic acid strands, producing intermolecular i-motif structures. These C tracts are then arranged as a tetramer composed of two parallel-stranded duplexes that are intercalated in an anti-parallel way. The hemiprotonated configuration C-C<sup>+</sup> plays an important role in

increasing the stability of the structure by increasing the strength of the stacking interactions, which is achieved by formation of C-H...O<sup>83a,83b</sup> C-rich telomeric repeats fold into a stable i-motif at slightly acidic pH.<sup>83,84</sup> However, Rajendran et al.<sup>85</sup> reported that the i-motif structure can be formed even at neutral and slightly basic pH. Recently, Brazier et al.<sup>82b</sup> reported that i-motif structure can be formed in a range of pH from 5.5 to 7, and this stabilization will depend on the composition and length of the loops.

Stabilization of i-motif structures by gold-based complexes is still unknown. Gold nanoparticle-DNA conjugates have shown a wide use for nanoscience and nanotechnology. The combination of both the size-dependent properties of gold nanoparticles and the molecular recognition and biological function of DNA can provide important applications in the sensitive detection of DNA,<sup>85</sup> proteins,<sup>86</sup> and metal ions.<sup>87</sup>

In this chapter, we report the interaction of secondary DNA structures with bi- and tridentate gold (III) complexes functionalized by alkynyl ligands. In our investigations, we have studied the activity of gold(III) complexes stabilized by ligands of the type C<sup>N</sup> and C<sup>N</sup>C. The use of this type of ligand can provide redox and thermodynamic stability to the cyclometallated gold(III) complexes. In addition, these ligands can modify the steric properties of the complexes, increasing the lipophilic character and stability in physiological media of the synthesized complexes, the primary condition required for biological testing.

In this project, the interaction of gold(III) complexes functionalized by amino ester derivatives with DNA secondary structures has been studied. The proposal of this has been focused on the well-known idea that the amino acids are overexpressed in tumour cells and may be able to deliver gold atoms to biological targets.<sup>53</sup>

Our research has focused on the interaction of gold complexes with different DNA secondary structures. DNA interaction is the most recognized anti-tumour target for metallic complexes. Accordingly, the interaction of these complexes with different human secondary DNA structures was investigated, as a preliminary study of cytotoxicity.

## 2.2. RESULTS AND DISCUSSION.

In our investigations, the complexes **4**, **5**, **6**, **7**, **11**, **12**, **13**, **14** and **15** previously reported in chapter 1, were studied (Figure 67).

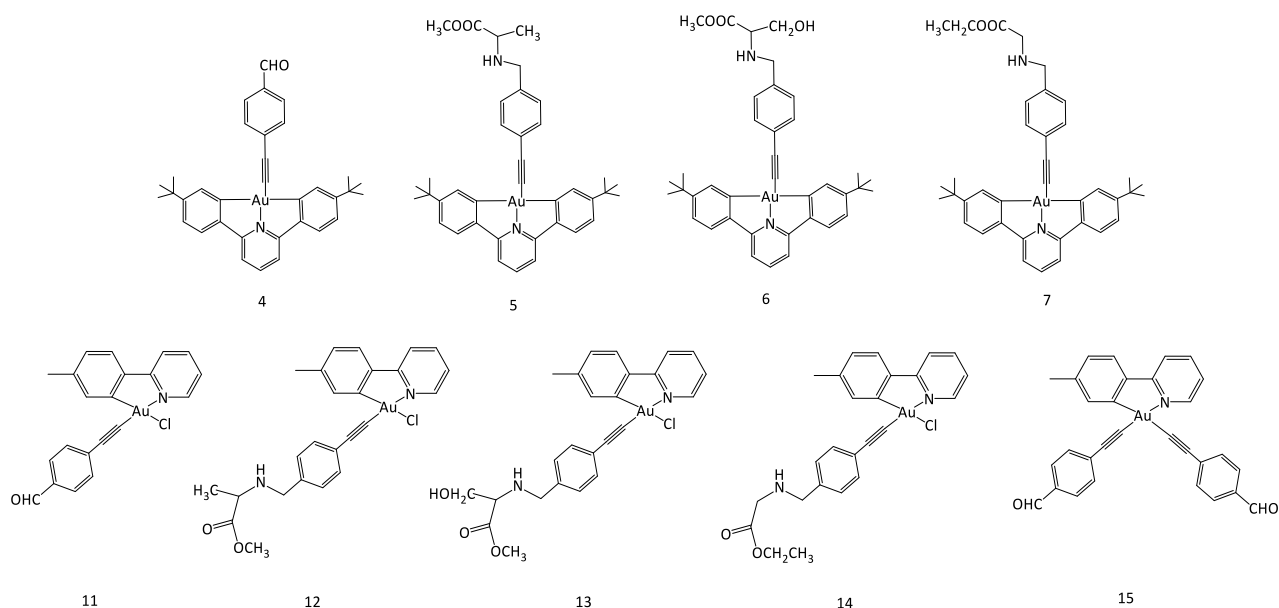


**Figure 67.** Chemical structure of complexes **4**, **5**, **6**, **7**, **11**, **12**, **13**, **14** and **15**.

In this chapter, we report the interaction of secondary DNA structures with bi- and tri-dentate gold (III) complexes functionalized by alkynyl amino ester ligands. These complexes are stabilized by ligands type C<sup>N</sup> and C<sup>N</sup>C. The use of this type of ligand can provide redox and thermodynamic stability to the cyclometallated gold(III) complexes, as well as increasing its lipophilic character and its stability in physiological media, the primary condition required for biological testing.

The interaction of these complexes with DNA secondary structures has been studied making use of different instrumental techniques, such as Fluorescence Resonance Energy Transfer (FRET) melting, circular dichroism, FRET-based titration experiment and UV difference spectroscopy.

- Förster Resonance Energy Transfer (FRET) melting: This method provides a semi-quantification of the interaction between a gold complex and a quadruplex structure by measuring the increase in the melting temperature (temperature in degrees Celsius in which 50% of all molecules of a given DNA sequence are hybridized into a double strand, and 50% are present as single strands) of a quadruplex induced by the presence of the studied gold complex.

- Circular dichroism (CD) spectroscopy: This method allows us to study the effect caused by the gold complexes over the folding and the structural conformation of the employed secondary DNA structures.

- FRET titration experiment: This technique provides an easy and quick method to observe and quantify the folding of the DNA sequence in real time, studying the distance between the donor and acceptor fluorophores labeled in the DNA sequence.

- UV difference spectrum: This technique provides a rapid method of structural characterization of DNA through the observed difference in terms of UV absorbance spectroscopy between the unfolded and folded states.

### **2.2.1. Förster Resonance Energy Transfer (FRET) melting.**

The theoretical analysis of this technique was developed by Theodor Förster. A photon will induce the excitation of one donor molecule and its consequent relaxation to the ground state. This process implies the emission of energy. If the acceptor molecule is not far from the donor, it can take this energy causing its excitation, followed by its

relaxation to the lowest energy state, causing a photon emission. This phenomenon is the main background of the FRET melting technique. Accordingly, this technique let us to measure the distance between the donor and acceptor groups in a biological molecule, for example a DNA sequence. Focused on our field, this technique will allow us to measure if the presence of gold complexes causes a variation of the donor-acceptor distance, which may indicate that the interaction between our complexes and DNA sequences is produced.

Regarding the way to present the results, this technique measures the change of temperature with the fluorescence intensity. As we will see in the graphs, the end of the experiment is reached when we observe the formation of plateau status, which means that all the molecules of the DNA sequence are unfolded. In contrast, at the beginning of the graph all the molecules of the DNA sequence remains folded. The intermediate point in our graph marks the melting temperature  $T_m$ , which it will be explained later in the section.

The most relevant parameters of study in FRET melting experiments are both the FRET efficiency ( $E_{\text{FRET}}$ ) and the melting temperature ( $T_m$ ). FRET efficiency is defined as the fraction of energy transferred for each donor excitation:

$$E_{\text{FRET}} = 1 - (F_{\text{ID}} / F_{\text{ID}}^{\circ}), \text{ where:}$$

$F_{\text{ID}}$ : Fluorescence in presence of complex.

$F_{\text{ID}}^{\circ}$ : Fluorescence in absence of complex.

FRET efficiency ( $E_{\text{FRET}}$ ) depends on different factors:<sup>88</sup>

- The intensity of the donor in absence and presence of the acceptor.
- Fluorescence lifetime of the donor molecule in presence and absence of acceptor ( $\tau_{\text{DA}}$  and  $\tau_{\text{D}}$ , respectively).

- Förster distance ( $R_0$ ) and distance between the energy donor molecule and the energy acceptor ( $r_0$ ).
- Fluorescence intensity of the energy donor molecule in presence and absence of acceptor.

In second place, the melting point is defined as the temperature in degrees celsius where 50% of all the molecules of a DNA sequence are hybridized as a double strand and 50% are present as single strands. Variations of the melting temperature before and after addition of complexes may indicate that the distance between fluorophore has changed.

In our investigations, the aim of this experiment is to study if the presence of gold complex can induce a conformational change of the DNA sequence, producing a variation of the distance between fluorophores, causing folding or unfolding of the DNA sequence compared to the melting profiles of the control sample (in absence of gold complex).

#### **2.2.1.1. FRET melting experiments employing 50, 10 and 1 $\mu$ M solutions of complexes 4 – 7 and 11 – 14.**

In principle, complexes 4 – 7 were tested against HTeloG, Hif-1- $\alpha$ , c-mycC and HTeloC DNA sequences at 50  $\mu$ M. FRET melting profiles were recorded in presence and absence on complex. As we can observe in Figure 68, the presence of complexes 4 – 7 did not induce remarkable changes in terms of melting temperature compare to the melting profile in absence of complexes. In addition, variations of fluorescence were not observed, indicating that the presence of these complexes did not cause any significant variation of the distance between fluorophores, meaning that their presence did not induce conformational modifications of the studied DNA sequences.

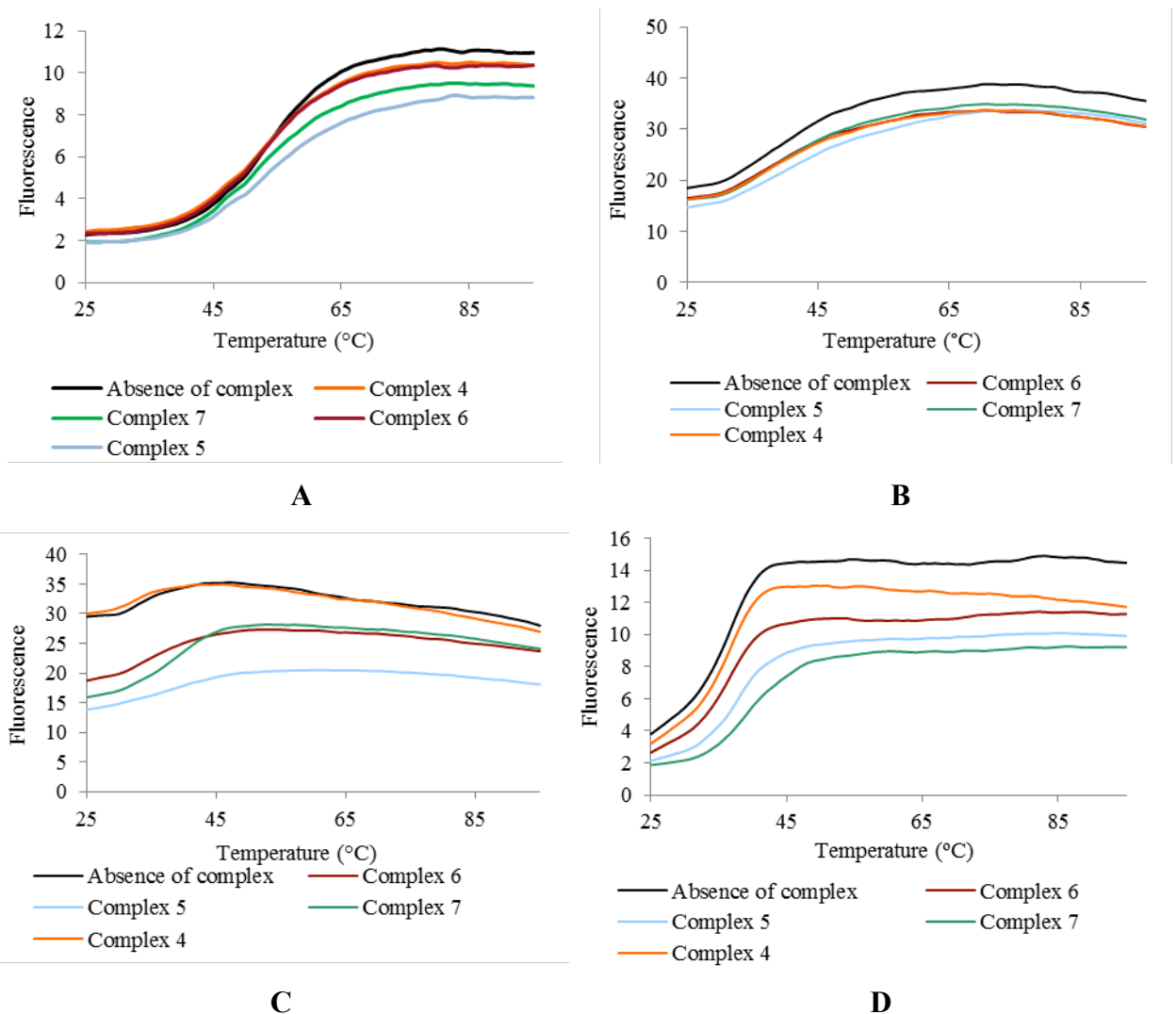


**Figure 68.** FRET melting graphs of HTeloG (A), Hif-1- $\alpha$  (B), c-mycC (C) and HTeloC (D) DNA sequence in absence and presence of complexes 4 – 7 at 50  $\mu$ M concentration in a 50 mM sodium cacodylate buffer at pH 7.4, 7.2, 6.6 and 6, respectively.

In presence of complexes 11 – 14, fluorescence intensity of c-mycC (B), HTeloC (C) and Hif-1- $\alpha$  (D) DNA sequences (Figure 69) remained apparently folded during the whole experiment, i.e, all the molecules of the DNA remained hybridized as double strands. This result may indicate two options: The first one, 50  $\mu$ M concentration of complexes 11 – 14 stabilize these DNA sequences, remaining them folded during the whole experiment. The second one is that precipitation of the complex may have occurred under the employed experimental conditions.

In case of HTeloG DNA sequence, fluorescence intensity remained folded up to 80 °C. At this temperature, fluorescence intensity started to increase, reaching melting temperatures higher than the measurable in the experimental conditions. This result indicates that, in presence of complexes **11 – 14**, HTeloG DNA sequence reaches a melting temperature higher than the measurable 95 °C (higher temperature reported on the employed experimental conditions), becoming needed to change the experimental conditions in order to be able to identify the melting temperature.

HTeloC (**C**), HTeloG (**A**) and Hif-1- $\alpha$  (**D**) DNA sequences in presence of complex **15** did not show noticeable variations of fluorescence at 25 °C compared to the melting profile in absence of complex, indicating that the presence of complex **15** did not cause an additional folding of these sequences. In addition, the melting point remained unchanged in presence of complex **15**, supporting the theory that no interaction between sequences **A**, **C** and **D** and complex **15** has been produced.

In contrast, c-mycC (**B**) sequence in presence of complex **15** underwent a decrease in fluorescence intensity at 25 °C, which may indicate that the presence of this complex causes that fluorophores in c-mycC (**B**) sequence are closer each other, due to the additional folding of the structure. However, fluorescence intensity remained then folded during the whole experiment, which may also indicate precipitation of complex under the employed experimental conditions.

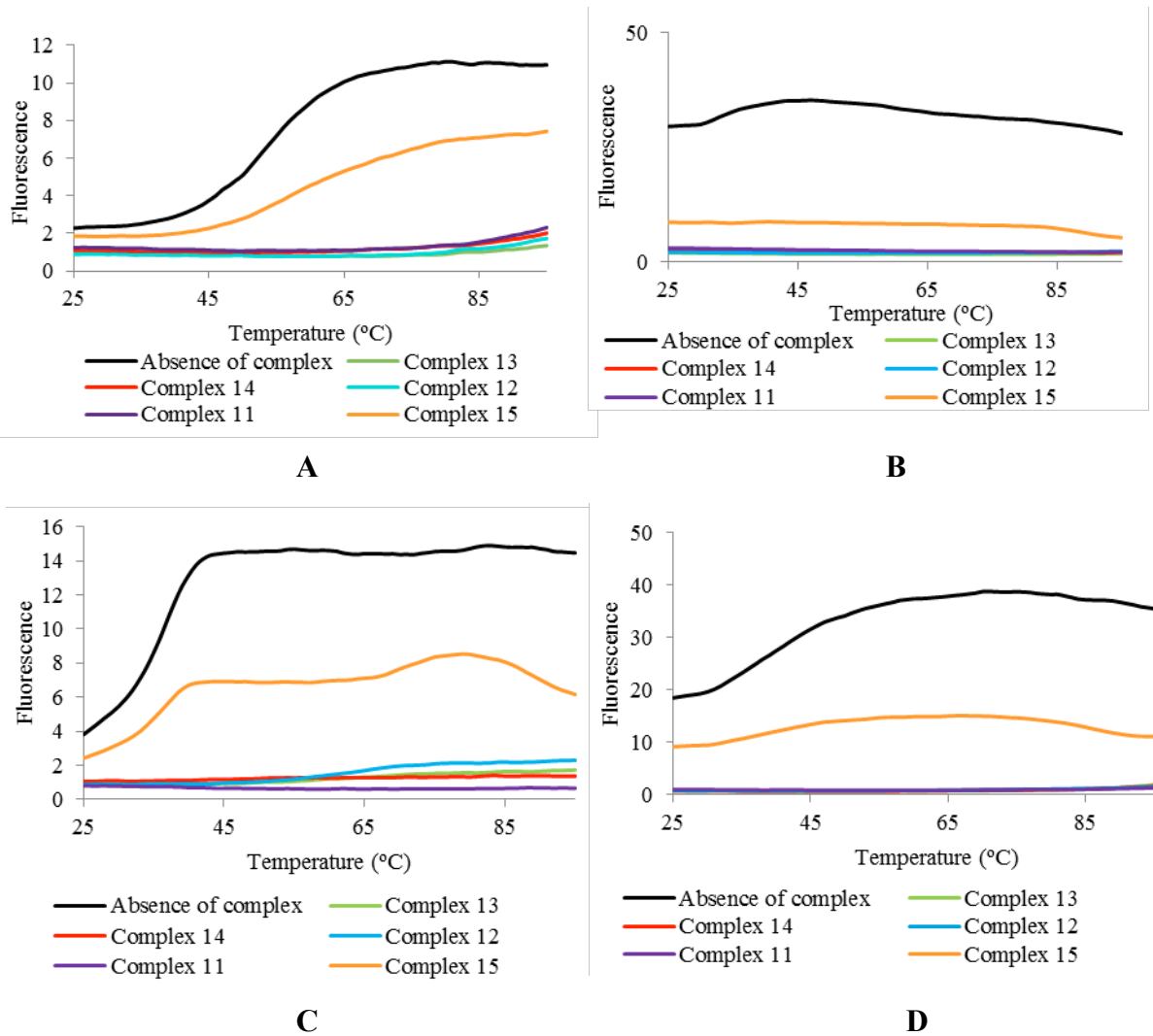


**Figure 69.** FRET melting graphs of HTeloG (A), c-mycC (B), HTeloC (C) and Hif-1- $\alpha$  (D) DNA sequence in absence and presence of complexes 11 – 15 at 50  $\mu$ M concentration in a 50 mM sodium cacodylate buffer at pH 7.4, 6.6, 6 and 7.2, respectively.

The experiment was repeated at lower concentration of complex, in order to obtain more conclusive results. The labelled oligonucleotides HTeloG, Hif-1- $\alpha$ , c-mycC and HTeloC previously prepared as a 400 nM solutions in a 50 mM sodium cacodylate buffer (pH 7.4, 7.2, 6.6 and 6, respectively) were employed. However, concentration of complexes 11 – 14 was modified, preparing 10  $\mu$ M solutions (instead of the 50  $\mu$ M

solutions of the previously used) in a 50 mM sodium cacodylate buffer at pH 7.4, 7.2, 6.6 and 6, and a 50 mM sodium cacodylate buffer and 100 mM of NaCl at pH 7.4.

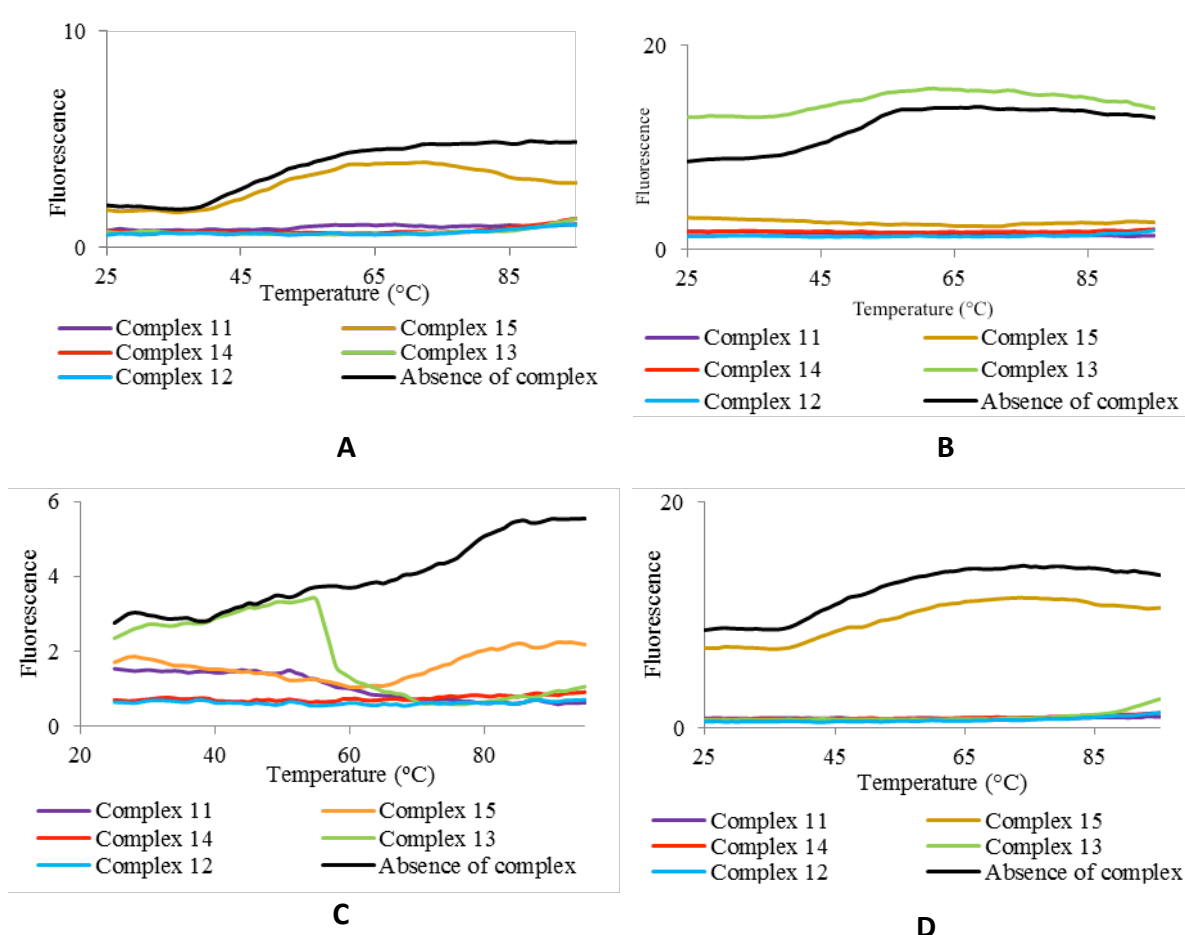


**Figure 70.** FRET melting graphs of *HTeloG* (A), *c-mycC* (B), *HTeloC* (C) and *Hif-1-α* (D) DNA sequence in absence and presence of complexes 11 – 15 at 10  $\mu$ M concentration in a 50 mM sodium cacodylate buffer at pH 7.4, 6.6, 6 and 7.2, respectively.

The use of lower concentration (10  $\mu$ M) of complex 15 showed that the presence of this complex did not induce remarkable variations in the melting profile of *HTeloG*, *HteloC* and *Hif-1-α* DNA sequences. As is shown in Figure 70 A, C and D, melting profiles in presence of complex 15 remained fluorescence intensity unchanged compared to the control sample (in absence of complex), indicating that the presence of this complex

does not cause an additional approachment of the fluorophores, which means that its presence does not induce a different folding than the one shown by the control sample (in absence of complex). These observations were supported by the melting point, which became unchanged compared to the control sample, confirming that complex **15** does not interact with HTeloG, HteloC and Hif-1- $\alpha$  DNA sequences.

FRET melting profiles of HTeloG (**A**), C-mycC (**B**), HTeloC (**C**) and Hif-1- $\alpha$  (**D**) DNA sequences in the presence of complexes **11** – **14** underwent a decrease in fluorescence intensity at 25 °C. This result may indicate that complexes **11** – **14** are able to interact with these DNA sequences, causing that fluorophores are closer each other and folding more the DNA sequence compared to the one in absence of complex (control sample). The melting profiles of remained apparently quenched up to 85 °C, when fluorescence intensity started to increase, indicating that melting temperatures are reached over 95 °C (the maximum temperature employed in our experiments) becoming needed to change the used concentration of gold complex. However, there are other possibilities to explain these results, such as precipitation of complex has taken place under these conditions or an experimental error has been produced. Accordingly, we need more experiments in order to confirm these results.

A particular result was observed for HTeloC DNA sequence in presence of complex **13**. At temperatures over 60 °C, the melting profile underwent a drastic decrease, which may be due to, at temperatures higher than 60 °C, the energy starts to transfer efficiently from the fluorophore to the metal; producing fluorescence quenching.<sup>88d</sup> This effect may be a result of precipitation of the complex.

The experiments to study the interaction of complex **11** – **14** were carried out making use of 1  $\mu$ M concentration of these complexes instead of the 10  $\mu$ M concentration previously used (Figure 71).

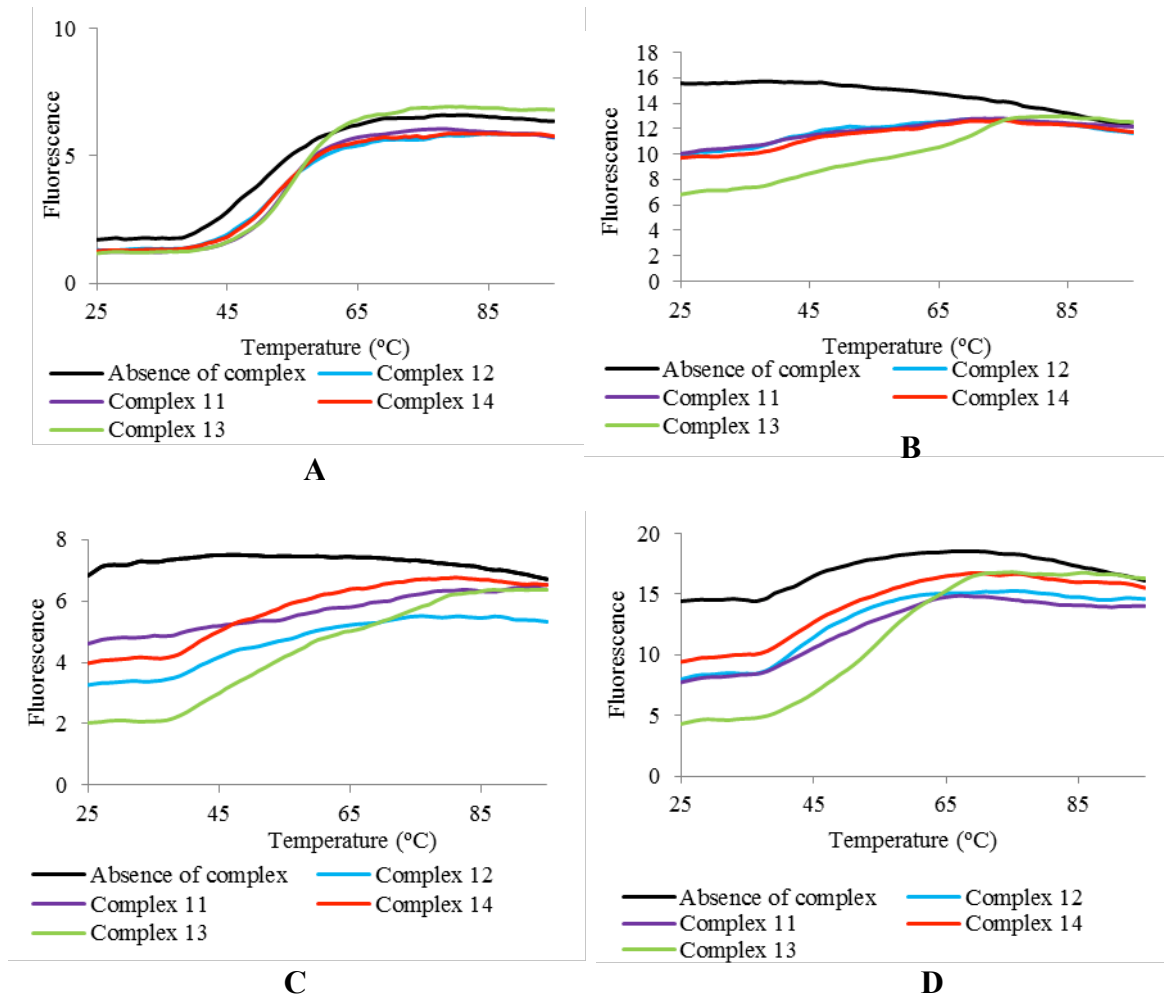


**Figure 71.** FRET melting graphs of *HTeloG* (A), *c-mycC* (B), *HTeloC* (C) and *Hif-1-α* (D) DNA sequence in absence and presence of complexes 11 – 15 at 1  $\mu$ M concentration in a 50 mM sodium cacodylate buffer at pH 7.4, 6.6, 6 and 7.2, respectively.

The introduced change in the experimental conditions (1  $\mu$ M instead of 1  $\mu$ M concentration of complexes 11 – 14) allowed us to obtain clearer results. As it is shown in Figure 71 A, the addition of complexes 11 – 14 did not represent significant a variation of fluorescence intensity, indicating that the presence of them does not cause that the fluorophores are closer each other than the status on absence of complexes, which means that they do not induce additional folding of the sequence. The observed results for fluorescence intensity were supported by the unchanged melting temperature,

indicating that there is not interaction between the studied complexes and HTeloG DNA sequence.

FRET melting profiles of c-mycC and HTeloC DNA sequences (Figure 71 **B** and **C**, respectively) in presence of complexes **11** – **14** showed a slight increase of fluorescence intensity, which indicates that these complexes promote slightly the folding of the DNA structures, causing that chromophores are closer each other. However, this weak effect observed may be explained because of an error within the experiment. This effect was slightly more pronounced for HTeloC DNA (**C**) in presence of complex **13**.

FRET melting profiles of Hif-1- $\alpha$  DNA sequence exhibited the most promising results (Figure 71 **D**). In presence of complexes **11** – **14**, fluorescence intensity decreased noticeably at room temperature, being more pronounced in presence of complex **13**. This decrease indicates that, complexes **11** – **14** are able to interact with Hif-1- $\alpha$  DNA sequence, causing an rapprochement of the fluorophores, increasing the folding of the sequence. In addition, these results were supported by the considerable change of melting temperature in presence of complex **13** ( $\Delta T_m = 10$  °C, Table 31), indicating that, the presence of complex **13**, causes a considerable change of the temperature in which 50% of all molecules of the DNA sequence are hybridized into a double strand, and 50% are presented as single strands, indicative that complex **13** is interacting with Hif-1- $\alpha$  DNA sequence. In contrast, melting temperature did not undergo striking changes in presence of complexes **11**, **12** and **14**.

In order to check if the observed effect of complex **13** in the stabilization of Hif-1- $\alpha$  DNA sequence (observed in the previous experiment through the change of melting temperature) was due to an experimental error, we repeated the experiment only for complex **13**, making use of the same experimental conditions.

**Table 31.** Data of  $\Delta T_m$  of Hif-1- $\alpha$  in absence and presence of 1  $\mu$ M concentration of complexes **11** – **14**.

	$T_m$ (°C)	$\Delta T_m$ (°C)
<b>Hif-1-<math>\alpha</math> (Control) (first measure)</b>	43.5	n/a
<b>Hif-1-<math>\alpha</math> (Control) (second measure)</b>	33.8	n/a
<b>Complex 13 (first measure)</b>	55.8	12.3
<b>Complex 13 (second measure)</b>	44.8	11
<b><math>\Delta T_m</math> (°C) Average</b>		<b>11.65</b>

As it is showed in table 31, the average of  $\Delta T_m$  (°C) values for the two taken measurements is 11.65. In order to determinate the error of the experiment, we calculated the standard deviation of this values according to the average. Accordingly, the obtained value will be 11.65+/-0.65, where the standard deviation ( $\sigma$ ) is 0.65. As we have observed in Table 31, the difference between each measurement and the average is lower than  $2\sigma$ , which may be a proof of the reliability of the measurements. However, because of the samples were high diluted, it would be necessary to carry out the repetition of the experiment in order to verify the results.

Following the FRET melting profiles, our investigations have focused on the study of the interaction of complex **13** with Hif-1- $\alpha$  DNA sequence. However, the interaction of complex **13** with c-mycC and HTeloC DNA sequences, as well as complex **11**, **12** and **14** with Hif-1- $\alpha$ , c-mycC and HTeloC may have also shown interesting results in terms of stabilization of folding DNA structure. For this reason, it may be worthwhile targeting for future investigations, as well as repeating the conducted experiments to check if the reproducibility of the obtained results.

### 2.2.2. Circular dichroism (CD) experiments.

Circular dichroism is based on the difference of absorption of right- and left-handed circularly polarized light exerted by chiral molecules. Circular dichroism (CD) measurements have been used for over 20 years to study the conformations of nucleic acids in solution.<sup>89</sup> The quantity used to describe circular dichroism is called ellipticity. CD spectroscopy is a powerful method for studying DNA-conformational properties, providing many advantages over other methods of conformational analysis:<sup>90</sup>

- Extremely sensitive, letting work with very low concentrations of DNA (20  $\mu\text{g/ml}$ ).
- This technique allows working with both short and long molecules.
- The samples can easily be titrated with various agents, such as salts, alcohols or acids, which induce conformational isomerization in DNA.
- CD spectroscopy distinguishes two-state conformational isomerization between distinct conformers from gradual changes within arrangements characterized by a single energetic minimum.<sup>91</sup>
- Circular dichroism can be also employed to make correlations between infrared spectroscopy and X-ray diffraction, because of its ability to analyze DNA sequences.<sup>92</sup>
- Circular dichroism can provide fast and inexpensive measurements.

The promising results obtained in FRET melting experiments of Hif-1- $\alpha$  in presence of complex **13** encouraged us to employ circular dichroism spectroscopy (CD), in order to study the effect of complex **13** on the folding and conformational changes of DNA.

As it is shown in Figure 72, the CD spectrum of annealed Hif-1- $\alpha$  DNA at pH 7.2 shows a negative signal at 256 nm and a positive signal at 288 nm, which may indicate the formation of cytosine–cytosine<sup>+</sup> base pairs, corresponding to an i-motif structure. DNA

strands rich in cytosine generate quadruplexes, which consist of two parallel homoduplexes connected through hemiprotonated C-C<sup>+</sup> pairs. These duplexes are mutually intercalated in an anti-parallel orientation.<sup>93</sup> Cytosine quadruplexes generate a characteristic CD spectrum with a dominant positive band over 290 nm, and the presence of antiparallel orientation is indicated by a negative peak over 260 nm.<sup>94a</sup>

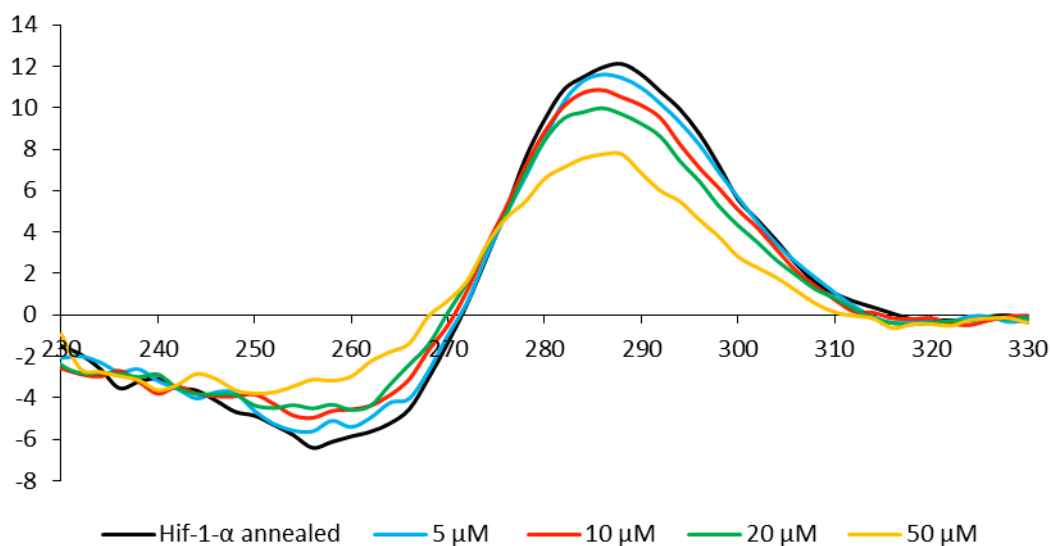


**Figure 72:** CD spectrum of 10  $\mu\text{M}$  concentration of annealed Hif-1- $\alpha$  in 50 mM sodium cacodylate buffer at pH 7.2 (black) with 5  $\mu\text{M}$  (green), 10  $\mu\text{M}$  (red), 20  $\mu\text{M}$  (yellow) and 50  $\mu\text{M}$  (blue) of complex 13.

As it is shown in Figure 73, the presence of complex 13 caused a decrease of amplitude of the bands. This result may indicate that the presence of complex 13 has a little effect in the stabilization of i-motif conformation, causing unfolding of the DNA sequence, or even giving rise a slight formation of an unstructured poly d-(C<sub>n</sub>) single strand.<sup>94b</sup>

However, DNA sequences consisting of GC-rich trinucleotides repetitions, such as the studied one, can adopt B-form duplex and hairpin, being able to transform between them. Hairpin is a variant of B-duplex form, which also contains a single stranded loop. CD spectra of B-forms are characterized by a positive wavelength between 260 – 280 nm, and a negative peak over 245 nm. The position of these bands depends of the sequence. The transition from B-duplex to hairpin is observed in the CD spectrum by a decrease of amplitude of these bands, mainly due to the single-stranded loop. According to this, there is a possibility that Hif-1- $\alpha$  DNA sequence fold a B-duplex conformation and, in presence of complex **13**, this DNA sequence undergoes a conversion to Hairpin conformation, which is reflected in the CD spectrum by a decrease in amplitude of the bands. This conversion has been more pronounced with the increase of concentration of complex **13**, indicating that the conversion may be an effect of dilution. In order to check if the observed conversion is an effect of dilution, an alternative experiment making use of higher concentrations of complex **13** should be conducted. In this point, FRET titration is a high selectivity method that would offer us the possibility to work in a high range of concentrations, providing more accurate results than circular dichroism.

### **2.2.3. FRET titration experiment.**

FRET methods provide a powerful tool to observe the dynamic structural changes of biomolecules, as well as of subpopulations in a heterogeneous mixture.<sup>95</sup> In a FRET experiment, a secondary DNA sequence is labelled with donor and acceptor fluorophores at different positions. FRET titration experiment provides an easy and quick method to observe if the two fluorophores are closer (characteristic of the folding of the sequence) or further apart (characteristic of unfolding).

In our research, we have decided to use FRET titration experiment because of its high sensitivity and selectivity, allowing us to work over a large concentration range. This method can provide us more information and conclusive results than the ones observed from the CD experiment, letting us to check the possibility if the observed results in previously mentioned experiment were effect of dilution. In addition, the most intense fluorescence is observed in compounds containing aromatic functional groups with low-energy  $\pi \rightarrow \pi^*$  transition levels, which may make this experiment a useful tool to identify if complex **13** induces folding of DNA, due to this complex being stabilized by an aromatic ligand type C<sup>N</sup>.

FRET-based titration experiments using the labeled oligonucleotide Hif-1- $\alpha$  at pH 7.2 were carried out. The FRET efficiency ( $E_{\text{FRET}}$ ) was calculated by  $1 - (F_{\text{I}_d}/F_{\text{I}_d}^0)$ , where  $F_{\text{I}_d}^0$  is the fluorescence intensity of the donor in the absence of the acceptor. The experiment was carried out by addition of 0 – 6  $\mu\text{M}$  concentration of complex **13**. As is shown on the Figure 74, in presence of 0 – 2  $\mu\text{M}$  of complex **13**, we observed that FRET efficiency exhibited negative values, which may be an indicative of precipitation of complex. At  $> 2.0 \mu\text{M}$  concentrations of complex **13**,  $E_{\text{FRET}}$  increased steadily, indicative that the fluorophores are closer each other, consistent with the folding of DNA. However,  $E_{\text{FRET}}$  only reaches a maximum value of 0.3, when it would be expected to reach values closer than 1 for folded structures. As is observed in Figure 73, FRET efficiency has not reached a plateau status. This status is reached when, after addition of a certain concentration of complex, FRET efficiency remains steady, indicating that DNA is completely folded. In our case, the FRET efficiency has not reached a plateau, because its values are still increasing. This fact made not possible to confirm if the presence of complex **13** induce the folding of DNA sequence or the presence of complex **13** causes destabilization of DNA sequence. Accordingly, it would

be needed to repeat the experiment employing higher concentrations of complex **13** until plateau is reached, in order to obtain conclusive results.

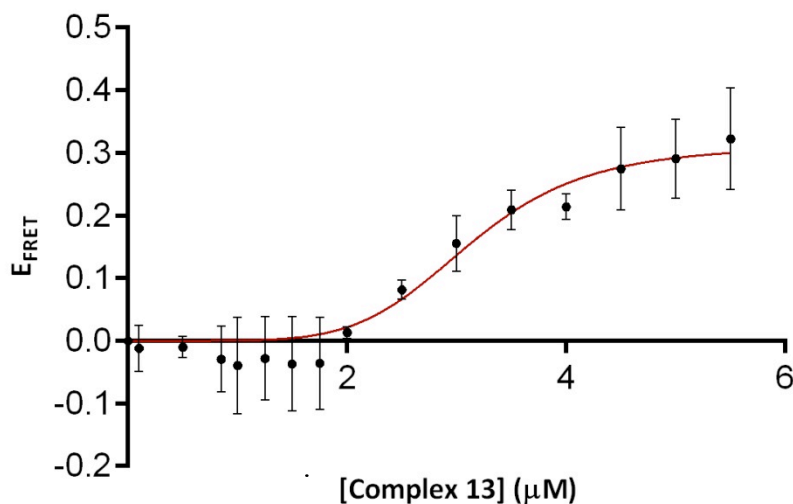


**Figure 73:** *FRET efficiency of 0.1 μM Hif-1-α DNA in 50 mM sodium cacodylate buffer at pH 7.2 with 0–6 μM of complex 13 titrated in. The error bars represent the standard deviation from the mean of two experiments.*

#### 2.2.4. UV difference spectrum.

The stability of the different conformational forms that DNA sequences are able to adopt can be measured by a thermal denaturation experiment. Heating a structured nucleic acid leads to variations in its ultraviolet absorbance, causing a conformational change of the molecule in solution, in particular, because of a disruption of base-stacking interactions.<sup>96</sup> Recording the ultraviolet absorbance spectrum of the unfolded and folded states at different temperatures provides a rapid and inexpensive method of structural characterization of DNA. The difference between these two spectra is called thermal difference spectrum (TDS). In our experiments, the recorded differential spectrum has been isothermal, recording the absorbance of the folded and the unfolded states at the same temperature.

We used UV difference spectroscopy in order to complement the CD experiments as a useful tool for the characterization of nucleic acids in solution and, in our case, determine the type of structure that Hif-1- $\alpha$  sequence can fold after addition of complex **13**. The UV absorbance measurements were only considered in the range from 200 to 300 nm, which are exclusively due to transitions of the planar purine and pyrimidine bases.<sup>96</sup>

As it observed in Figure 74, the UV difference spectrum of the folded and unfolded states at room temperature exhibit a negative differential absorbance peak at 297 nm, which may be due to  $n \rightarrow \pi^*$  transition moments, parallels to the helix axis. This result is linked to an increase of the base stacking, indicative of formation of a folded structure. As it was reported by Mergny et al.,<sup>96</sup> this negative peak may be the result of the partial cytosine deprotonation upon unfolding, corresponding to the formation of i-motif DNA structure. However, if the DNA sequence is folding as an i-motif structure, this peak should exhibit a negative absorbance over -0.6 for this band. In addition, a positive peak over 240 nm, consistent with i-motif DNA structure, should be also observed. As it is represented in Figure 75, although the spectrum presents the highest UV positive absorbance peak in that region, it is not possible to identify precisely the wavelength corresponding to the maximum peak in that region. According to these results, three possible outcome have been presented:

- a) One possibility is that the presence of complex **13** induces unfolding of Hif-1- $\alpha$  DNA sequence. However, the presence of a negative absorbance peak at 297 nm justify that complex **13** is inducing folding of the Hif-1- $\alpha$  sequence. This negative peak is the result of base stacking, which is associated with the formation of a folded structure.

- b) Secondly, it is possible that Hif-1- $\alpha$  DNA sequence may fold in an i-motif structure. The negative peak at 297 nm, which may indicate a partial cytosine deprotonation, corresponding to the i-motif structure. However, the absorbance nearer to 0, compared to the expected one over -0.6 for this band, and the no identification of the positive peak over 240 nm (this area is shown distorted in Figure 75, exhibiting several absorbance peaks, which may be due to an error in the experiment) made not possible to confirm that Hif-1- $\alpha$  DNA sequence folds an i-motif structure.
- c) Another possibility is that the presence of complex **13** induces the folding of a hairpin conformation, instead of an i-motif like structure. This result may be represented by the decrease of the absorbance amplitude, observing an absorbance near to 0 for the band at 297 nm (corresponding to the partial cytosine deprotonation), compared to the expected one for i-motif conformations, over -0.6. This change in absorbance may be an effect of the single stranded loop of the hairpin conformation.

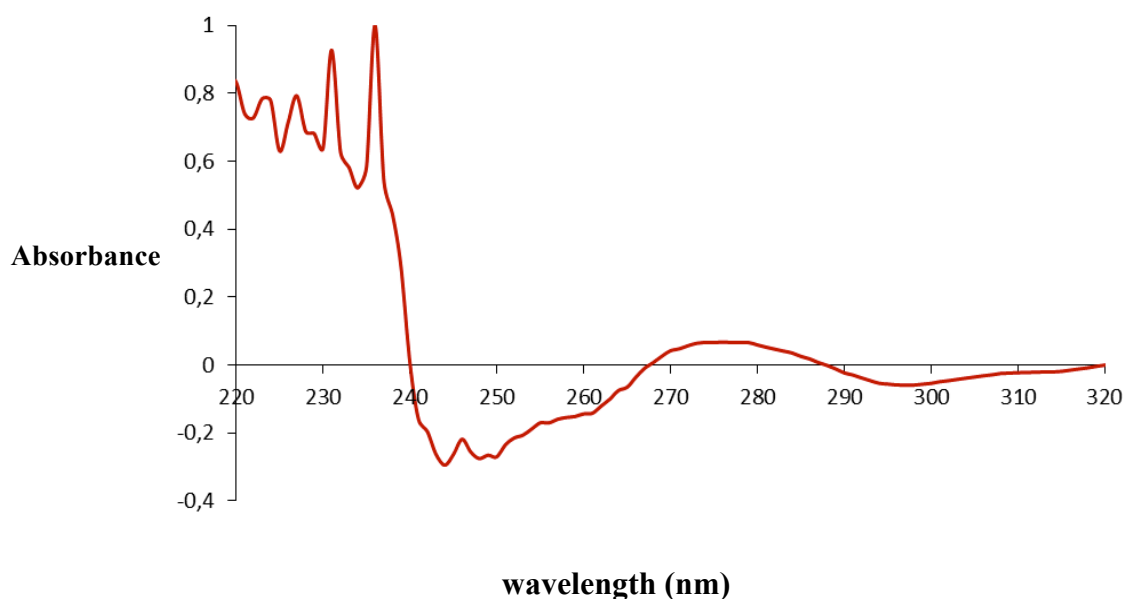


**Figure 74.** *UV difference spectrum of Hif-1- $\alpha$  DNA in presence of 100  $\mu$ M concentration of complex **13**.*

According to the observed spectrum, an electrophoretic mobility experiment may be a suitable technique in order to determine the conformation that the Hif-1- $\alpha$  DNA sequence is folding in the presence of complex **13**. Based on mobility, which depends on both molecular weight and size of the molecules, this technique would allow us to determine if folding is occurring in an i-motif<sup>97</sup> conformation or even if it is unfolded.<sup>97</sup> This experiment would be conducted in a polyacrylamide gel, which has been employed previously to determine i-motif conformations<sup>97</sup>. The comparison of the migration distance between Hif-1- $\alpha$  in absence of complex **13** (which have been proven to fold an i-motif structure) and Hif-1- $\alpha$  in presence of complex **13**, would show to us if the studied DNA sequence is folding in an i-motif conformation in presence of complex **13**. If the migration distances exhibit differences, Hif-1- $\alpha$  DNA sequence in presence of complex **13** would be folding a different conformation. This technique would also help us to determine if Hif-1- $\alpha$  DNA sequence in presence of complex **13** is folding in a hairpin structure, carrying out a comparative electrophoretic mobility experiment against a structure capable to form a hairpin conformation, for instance the DNA sequence 5'-d[CTC-TCT-TCT-CTT-CAT-TTT-TCA-ACACAA-CAC-AC]-3'.<sup>98</sup>

### **2.3. CONCLUDING REMARKS AND PERSPECTIVES.**

In this chapter, the interaction of guanidine and cytosine rich DNA structures with bi- and tri-dentate gold (III) complexes functionalized by alkynyl ligands has been reported using complexes **4**, **5**, **6**, **7**, **11**, **12**, **13** and **14**.

The interaction of these complexes with the DNA structures was studied making use of different instrumental techniques, such as Fluorescence Resonance Energy Transfer (FRET) melting experiments, circular dichroism (CD), FRET-based titration experiment

and UV difference spectroscopy. FRET melting experiments revealed that the most remarkable interaction was produced between complex **13** and Hif-1- $\alpha$  DNA sequence. However, the interaction of complex **13** with c-mycC and HTeloC DNA sequences, as well as with complexes **11**, **12** and **14** with Hif-1- $\alpha$ , c-mycC and HTeloC may have also shown interesting results in terms of stabilization of folding DNA structure, which may be a worthwhile target for future investigations. In contrast, complexes **4** – **7** did not show any remarkable DNA stabilization, which may be due to the rigidity of the ligand framework (diphenylpyridine derivative).

In the absence of metal complexes, the Hif-1- $\alpha$  DNA sequence can fold in an i-motif structure, which was indicated in the circular dichroism profiles by a negative peak at 256 nm and a positive peak at 290 nm, which are characteristics of an i-motif structure. In presence of complex **13**, a decrease of the positive peak was observed, which indicated that this complex interacts with Hif-1- $\alpha$  DNA, promoting the formation of poly-d(C<sub>n</sub>) single-stranded structure or even causing unfolding of the DNA.

FRET titration experiments showed that, in presence of complex **13**, an increase of  $E_{\text{FRET}}$  was observed, indicating that the fluorophores are closer to each other, which is consistent with the folding of the DNA structure. However, FRET efficiency has not reached a plateau status. Accordingly, it has not been possible to confirm whether the DNA structure reaches a complete folding and, if it happens, at what concentration this is achieved. It will therefore be necessary to repeat this experiment using higher concentrations of complex **13** in order to reach plateau status.

Finally, isothermal UV difference spectroscopy exhibited negative peaks at 244 nm and 295 nm, and a positive peak at 270 nm. Despite the fact that the negative peak at 295 nm may indicate partial cytosine deprotonation upon unfolding, corresponding to the formation of i-motif DNA structure, it was not possible to confirm the stabilization of

this structure because there was no positive absorbance at 240 nm, which is taken to be characteristic of folding in an i-motif structure. In addition, the absorbance near to 0, observed for the 270 nm band, may indicate the folding in a hairpin structure, a possibility that was already suggested by the results in the CD spectrum.

Future work of this project will focus on carrying out additional experiments, such as electrophoretic mobility, in order to determine the conformation in which Hif-1- $\alpha$  DNA is folding in presence of complex **13**. In addition, this work should be extended to the study of the interaction of complex **13** with other secondary structures, such as c-mycC, which has shown a slight modification of the melting temperature in presence of complex **13**.

The effects induced by complex **13** may be explained by an aquation mechanism, similar than the one showed for cisplatin in Figure 52. The presence of chloride atom in complex **13** may cause its aquation, forming an aqua derivative, which may lead the interaction with DNA.

A future work may be focused on the design and synthesis of other gold complexes functionalized with specific groups that allow us to increase the affinity and specificity of the molecule for a type of DNA secondary structure.

## **2.4. EXPERIMENTAL**

The labelled oligonucleotides hTeloG (FAM-5'-GGGTTAGGGTTAGGGTTAGGG-3'-TAMRA), Hif-1- $\alpha$  (FAM-5'-CGC-GCT-CCC-GCC-CCC-TCT-CCC-CTC-CCC-GCG-C-3'-TAMRA), hTeloC (5'-FAM-d[TAACCCTAACCCTAACCCTAACCC]-TAMRA-3') and c-mycC were the object of our studies. They were purchased from Eurogentec and HPLC purified. The solid DNA samples were initially prepared as a stock solution in MilliQ water (10  $\mu$ M for HTeloG, HTeloC, Hif-1- $\alpha$  and c-mycC) and

dilutions were carried out in the appropriate buffer, according to the pH in which these DNA structures are stable. In our investigations, sodium cacodylate was chosen as buffer. This buffer has been chosen for DNA interaction studies previously reported,<sup>99,100</sup> mostly due to its ability to remain the pH constant under isothermal conditions. Accordingly, 50 mM sodium cacodylate buffers at pH= 7.4, pH= 7.2, pH= 6.6 and pH= 6 were prepared.

#### **2.4.1. FRET melting experiment.**

The labelled oligonucleotides hTeloG, Hif-1- $\alpha$ , hTeloC and c-mycC were prepared as a 400 nM solution in a 50 mM sodium cacodylate buffer (pH 7.4, 7.2, 6.6 and 6, respectively). The samples were then thermally annealed by heating in a heat block at 95°C for 5 minutes and then allowed to reach room temperature overnight.

Complexes **4 – 7** and **11 – 15** were prepared as 50  $\mu$ M solution in a 50 mM sodium cacodylate buffer at pH 7.4, 7.2, 6.6 and 6. The fluorescence from 25 °C to 95 °C, as well as the temperature at which half of the DNA base pairs dissociate (melting temperature,  $T_m$ ) were monitored. Fluorescence melting curves were determined in a QIAgen Rotor-Gene Q-series PCR machine, using a total reaction volume of 20  $\mu$ L charged in Strip-tubes (QIAgen). Measurements were carried out with excitation at 483 nm and detection at 533 nm. Final analysis of the obtained data was carried out using QIAgen Rotor-Gene Q-series software.

Complexes **4 – 7** and **11 – 15** were prepared as solutions (50  $\mu$ M, 10  $\mu$ M and 1  $\mu$ M) in a 50 mM sodium cacodylate buffer at pH 7.4, 7.2, 6.6 and 6. The fluorescence from 25 °C to 95 °C, as well as the temperature at which half of the DNA base pairs dissociate (melting temperature,  $T_m$ ) were monitored.

#### **2.4.2. Circular dichroism (CD) spectroscopy.**

CD spectra were recorded on a Jasco J-810 spectropolarimeter, using a 1 mm path length quartz cuvette. Human telomeric DNA sequence (Hif-1- $\alpha$ , FAM-5'-CGC-GCT-CCC-GCC-CCC-TCT-CCC-CTC-CCC-GCG-C-3'-TAMRA) was diluted in a buffer containing sodium cacodylate (50 mM, pH 7.2) to achieve a total volume of 200  $\mu$ L. The scans were performed at 20°C over a wavelength range of 200-480 nm with a scanning speed of 200 nm/min, a response time of 1 s, 0.5 nm pitch and 2 nm bandwidth. A blank sample containing only buffer was treated in the same manner and subtracted from the collected data. Solutions of complex **13** were added in small aliquots from 10 to 50  $\mu$ M concentrations. The CD spectra at the different concentrations represent an average of three scans and are zero corrected at 320 nm.

#### **2.4.3. FRET titration experiment.**

Fluorescence titration experiments were performed on a Perkin-Elmer LS-55 fluorescence spectrometer and recorded using a 1 cm path length quartz cuvette. Hypoxia-inducible factor 1-alpha (Hif-1- $\alpha_{\text{FRET}}$ , FAM-5'-CGC-GCT-CCC-GCC-CCC-TCT-CCC-CTC-CCC-GCG-C-3'-TAMRA) was diluted in a buffer containing sodium cacodylate (50 mM, pH 7.2) to achieve a concentration of 0.1  $\mu$ M and a total volume of 200  $\mu$ L. The DNA was not annealed and used immediately after dilution. Solutions of complex **13** were added in small aliquots to the desired proportions. The overall dilution was less than 10%. Excitation of the donor fluorophore was performed at 490 nm and the emission spectra were recorded over a wavelength between 500 and 650 nm at 20

°C. The experiment was carried out in duplicate, and the error bars represent the standard deviation.

#### **2.4.4. UV difference spectroscopy.**

UV spectroscopy experiments were performed on an Agilent Technologies Cary 60 UV-Vis spectrometer and recorded using a low volume quartz cuvette. Hypoxia-inducible factor 1-alpha i-motif (Hif-1- $\alpha$ , FAM-5'-CGC-GCT-CCC-GCC-CCC-TCT-CCC-CTC-CCC-GCG-C-3'-TAMRA) was diluted in a buffer containing sodium cacodylate (50 mM, pH 7.2), to achieve a concentration of 2.5  $\mu$ M and a total volume of 200  $\mu$ L. The DNA annealed and used immediately after dilution. A solution of **13** was added in small aliquots up to 100  $\mu$ M. Spectra were recorded over a wavelength range of 400 - 200 nm at 20 °C in the absence of any **13** and then in the presence of up to 100  $\mu$ M of **13**.

We recorded the UV spectrum either in absence and presence of complex **13** at room temperature, carrying out the differential spectrum between them. This spectrum was calculated by subtraction of the spectrum in absence of **13** from the spectrum in the presence of **13**, and normalized as it is reported on the literature.<sup>101</sup>

**CHAPTER 3**  
**MISCELLANEOUS RESULTS**



### 3.1. INTRODUCTION

Cyclometallated Au(III) complexes are remarkable for their thermal stability and resistance to reduction.<sup>8a</sup> Cycloauration reactions provide products containing five- or six membered ring systems, containing a gold(III)–aryl bond. The use of these ligands has been proven to provide a considerably stabilization to the gold(III) metallic centre, avoiding the reductive elimination step. The ligand has a strong influence on the conditions under which this reaction takes place. The use of nitrogen and oxygen donor ligands has played an important role in order to reach this stabilization against reductive elimination. In 1939, an example of O-type chelates, such as  $\kappa^2$ -acetylacetonato (acac) ligands, was reported to stabilise  $\text{Me}_2\text{Au}^+$  substituents.<sup>102</sup> In the last years, the use of heterocyclic ligands, such as phenylpyridine, 2-anilinopyridines, 2-benzoxypyridines,<sup>103a</sup> 2-phenoxy pyridines<sup>103b</sup> terminal anilides, acetylides and cis-diarylgold(III) species<sup>6,7</sup> (Figure 75) have been proven to conduct successfully cycloauration reactions by activation of an *ortho* C-H bond, forming products containing five- or six membered ring systems characterized by high stability against reductive elimination. In recent years, our research group has reported the synthesis of a variety of gold(III) complexes supported by 2,6-diphenylpyridine derivatives. The conformation of this ligand is suitable to avoid reductive elimination, and also the presence of two phenyl groups surrounding the gold metallic centre provides a high stability to the complex from a thermodynamic point of view, mainly due to the presence of two thermodynamically stable Au – C bonds.

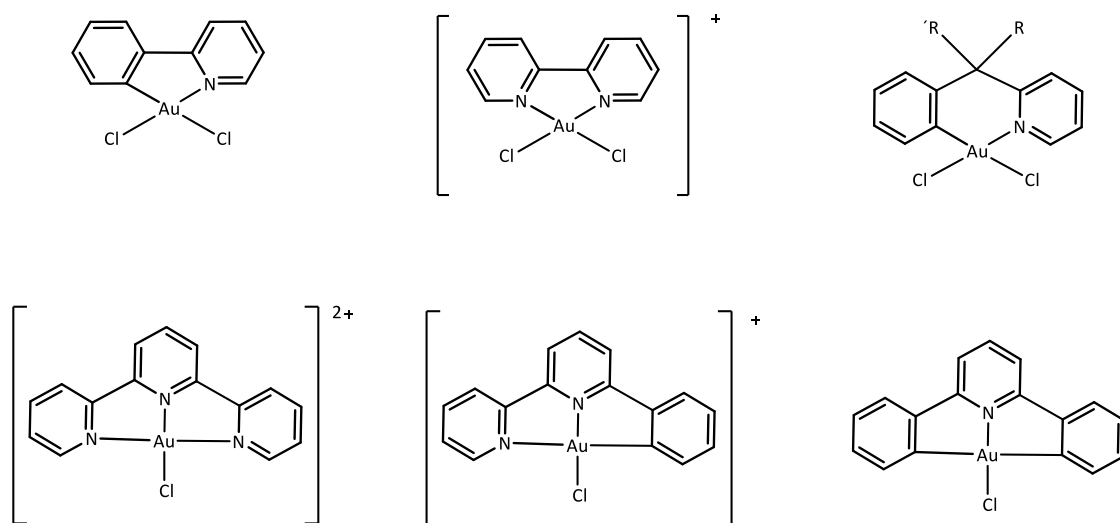


**Figure 75.** Examples of gold(III) centers stabilized by chelating ligands.

In 2012, Bochmann et al.<sup>30</sup> reported the synthesis of the first neutral gold (III) hydroxide complex (Figure 76). This complex exhibited an excellent reactivity as a mild metal base, being able to activate C–H and N–H bonds.

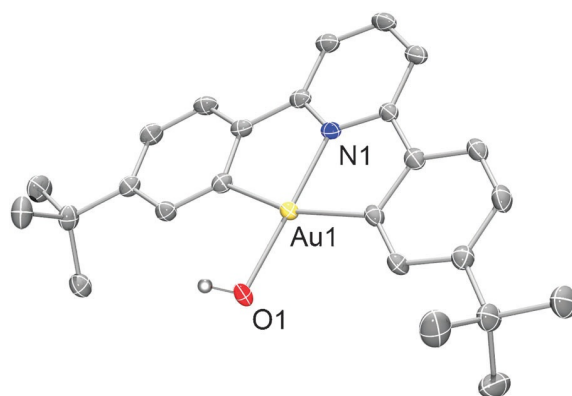


**Figure 76.** ORTEP diagram of  $(C^N^C)Au(III)OH$ .

The excellent reactivity of this complex as mild base resulted in smooth reactions with boronic acids and protic reagents under neutral conditions, to give a variety of gold aryls, alkynyls and heteroaryls, allowing C–H or N–H activation (Scheme 28). These

complexes are thermally very stable. The distribution of the aromatic groups in these complexes played an important role in order to avoid reductive elimination processes. However, the rigid tridentate ligand framework made these complexes reduce considerably the reactivity of these systems. In order to generate more reactive complexes capable of bearing two functionalisable substituents X or L, the synthesis of alternative cyclometallated complexes has been attempted (Figure 77).

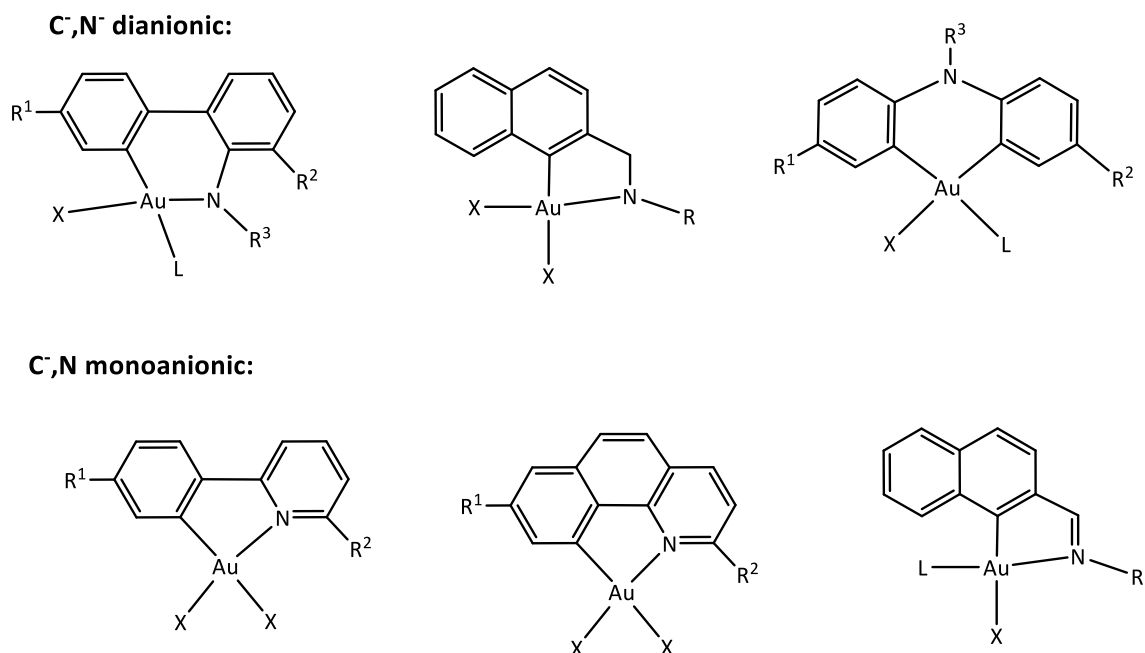


**Figure 77.** Examples of mono- and di- anionic gold(III) complexes stabilized by bidentate type ligands, which has been studied in this project.

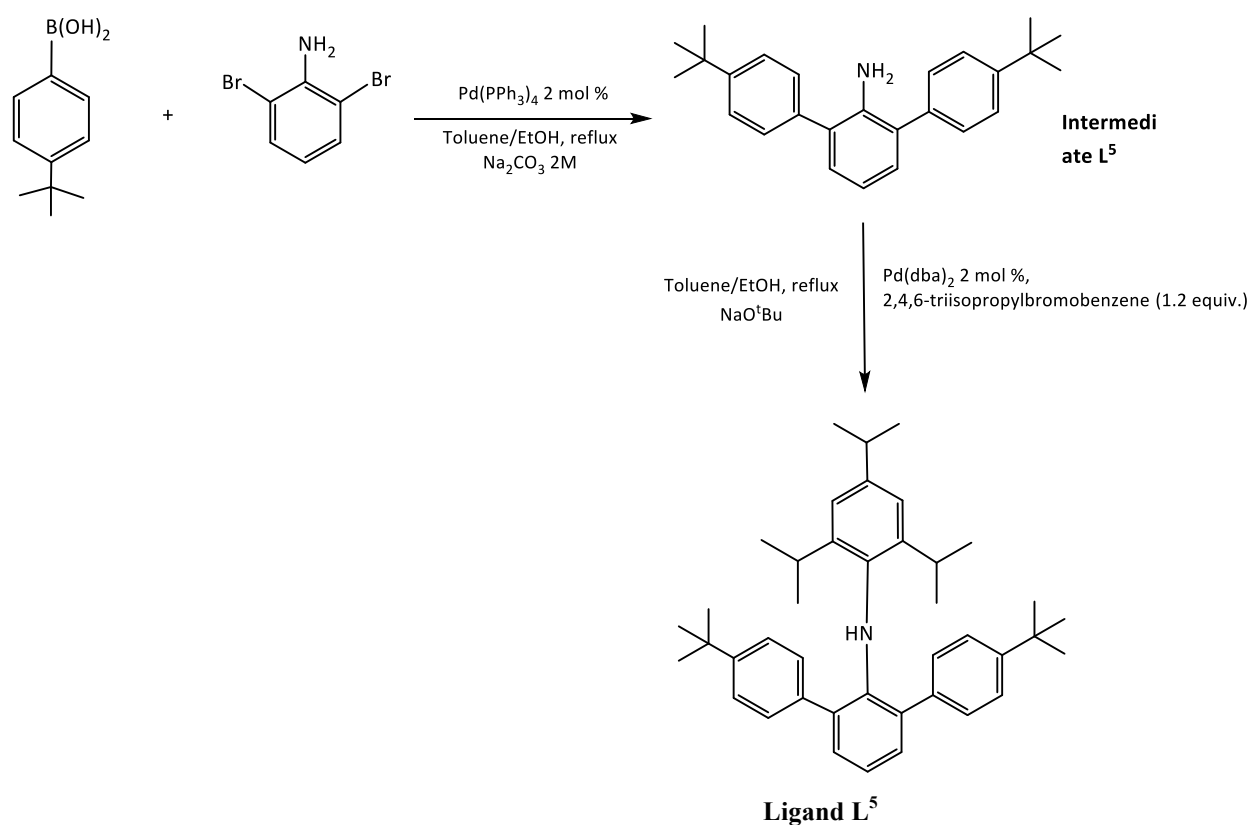
## 3.2. RESULTS AND DISCUSSION

### 3.2.1. Synthesis of ligand L<sup>5</sup>.

Our first attempt was focused on the synthesis of ligand L<sup>5</sup>. This is C,N- dianionic ligand, and its synthesis was planned because, as a more flexible ligand framework, it may be able to be functionalized by two substituents once is coordinated to gold(III) atom, offering more possibilities of functionalization. The coordination of ligand L<sup>5</sup> to

gold(III) centre will allow the synthesis of neutral complexes type  $(C^N)AuX_2$  or  $(C^N)AuX(L)$ .

The planned method of synthesis focused on the synthetic pathway based on Suzuki cross-coupling, followed of C–N coupling based on the Buchwald – Hartwig amination. Accordingly, this route involves two reaction steps. The first one involves the Suzuki cross-coupling of the commercially available 2,6-dibromoaniline and 4-tertbutylboronic acid, and employing  $Pd(PPh_3)_4$  as a catalyst, to yield **intermediate L<sup>5</sup>** (Scheme 28).<sup>104</sup> The second step involves a Buchwald – Hartwig cross coupling reaction, employing  $Pd(dba)_2$  as precursor<sup>104</sup> and diphenylphosphinobinaphthyl (BINAP), a sterically hindered phosphine which has shown high catalytic activity as a ligand in the Buchwald – Hartwig amination.<sup>105</sup>



**Scheme 28:** Synthesis of the ligand **L<sup>5</sup>**.

In 2012, a similar ligand than ligand **L**<sup>5</sup> was synthesized by Ishihara et al.<sup>106</sup> (Figure 78), the only difference being the absence of *tert*-butyl groups in the *para* position on the phenyl rings bonded to the aniline derivative in 1 and 5 positions. In our investigations, we decided to decorate the pro-ligand with *tert*-butyl groups in order to increase the solubility of the ligand and also to facilitate the identification of chemical shifts by <sup>1</sup>H-NMR spectroscopy.

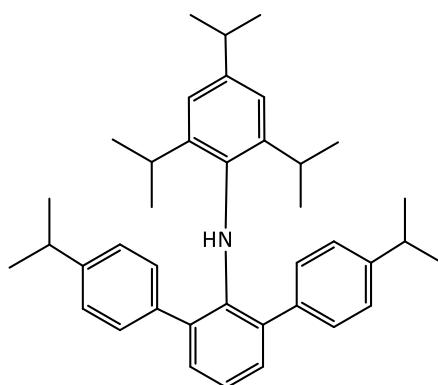


**Figure 78.** Chemical structure of *N*-(2,6-diisopropylphenyl)-2,4,6-triisopropylaniline.<sup>106</sup>

Characterization of ligand **L**<sup>5</sup> was only carried out by <sup>1</sup>H-NMR spectroscopy (Figure 79, Table 38).

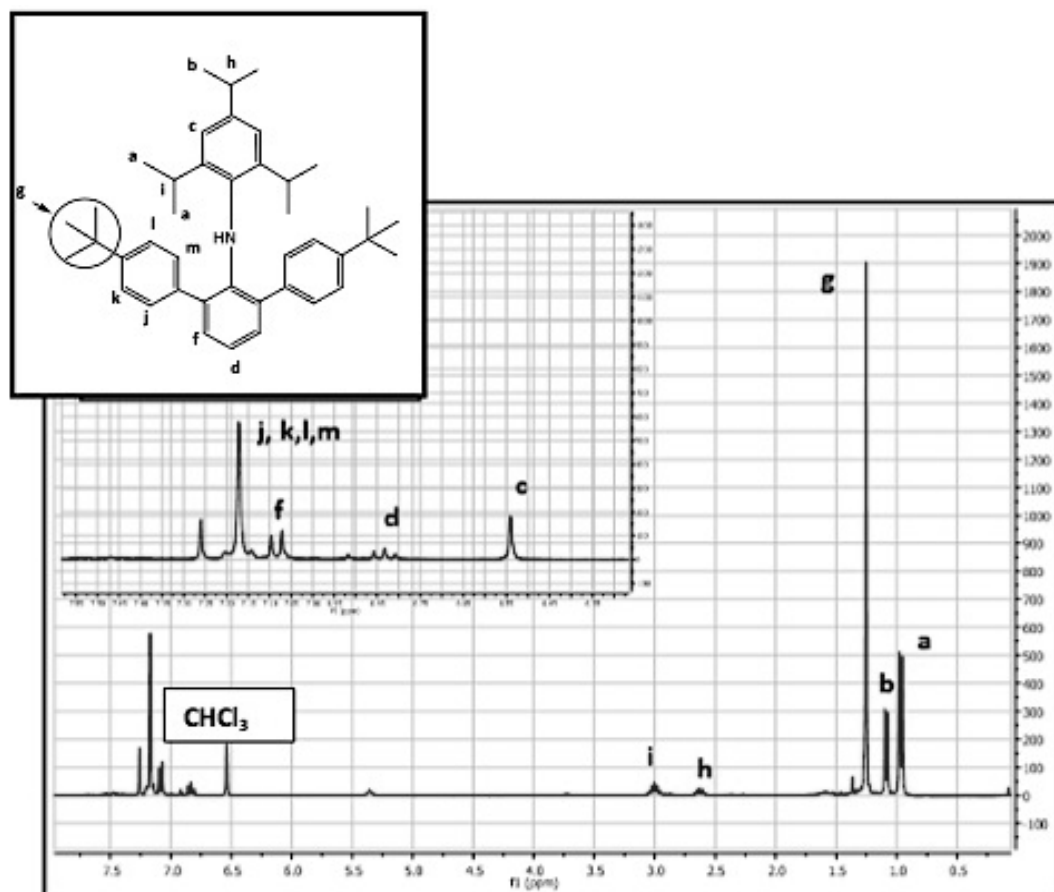


Figure 79.  $^1\text{H-NMR}$  spectrum of ligand  $L^5$  in  $\text{CDCl}_3$ .

Table 38.  $^1\text{H-NMR}$  data of ligand  $L^5$  in  $\text{CDCl}_3$ ,  $\delta(\text{ppm})$  and multiplicity.

Pro – ligand $L^5$	ASSIGNMENT	$^1\text{H}$ (ppm)
	a	0.96 (d, $J = 6.8$ Hz, 12 H)
	b	1.09 (d, $J = 6.9$ Hz, 6 H)
	g	1.25 (s, 18 H)
	h	2.58 – 2.67 (m, 1 H)
	i	2.96 – 3.06 (m, 2 H)
	c	(s, 2H)
	d	(t, 1 H)
	f	7.08 (d, $J = 7.5$ , 2 H)
	j – m (overlapping)	7.17 (m, 8 H)

### 3.2.2. Metalation attempts of ligand L<sup>5</sup>.

#### A. Metalation of ligand L<sup>5</sup> via mercuration pathway.

Ligand L<sup>5</sup> has been subjected to mercuration experiments using both Hg(OAc)<sub>2</sub> and Hg(OAc<sup>F</sup>)<sub>2</sub> as organomercury reagents, following the experimental procedure reported by Parish et al.<sup>13</sup> in 2000. Mercuration of ligand L<sup>5</sup> was monitored by <sup>1</sup>H-NMR spectroscopy over the course of one week, and no changes in the chemical shifts of the aromatic region regarding ligand L<sup>5</sup> were observed. In addition, the characteristic singlet resonance corresponding to the acetate group, once is coordinated, was not showed in the <sup>1</sup>H-NMR spectrum.

This result encouraged us to use Hg(OAc<sup>F</sup>)<sub>2</sub>, a more reactive organomercury reagent than the previously employed Hg(OAc)<sub>2</sub>. <sup>1</sup>H-NMR spectroscopy showed that mercuration of ligand L<sup>5</sup> was produced after three days, when no signals corresponding to ligand L<sup>5</sup> were observed in the <sup>1</sup>H-NMR spectrum (Figure 80).

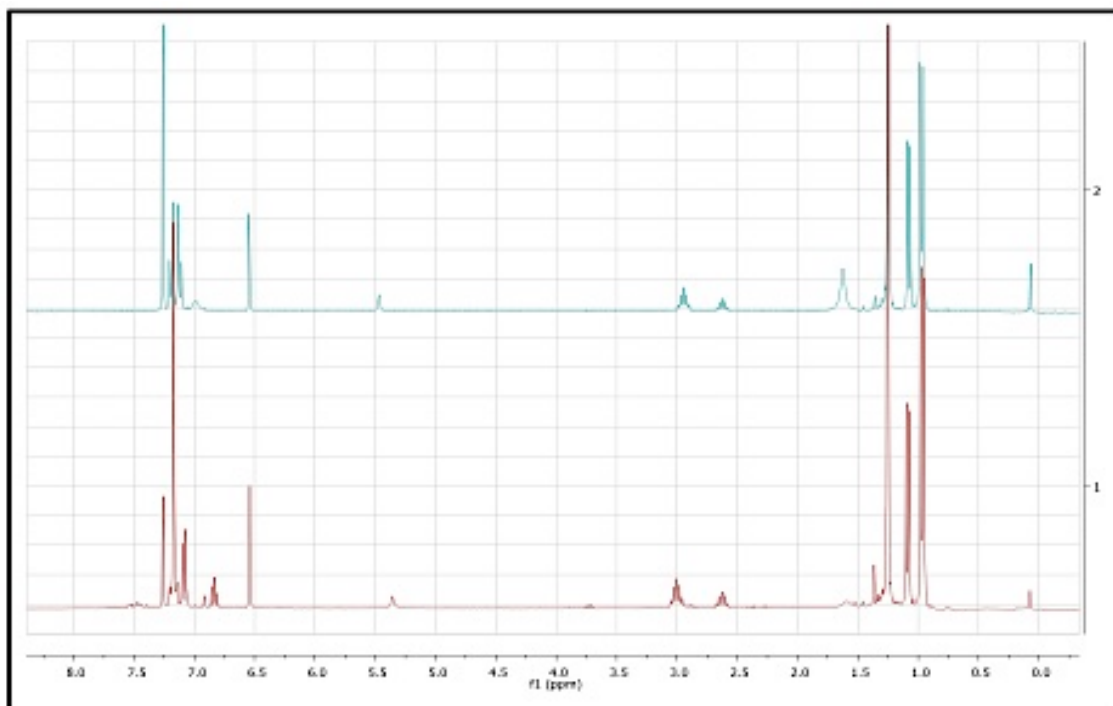


**Figure 80.** <sup>1</sup>H-NMR spectrum of mercuration product (blue spectrum) and ligand L<sup>5</sup> (red spectrum) in CDCl<sub>3</sub>.

Figure 81 showed remarkable changes in the chemical shifts of the mercuration product (blue spectrum) compared to ligand  $L^5$  (red spectrum). However, the absence of a triplet signal corresponding to the aromatic proton located in *para* position to the nitrogen atom may be an indicative that the desired *ortho*-mercuration product was not produced. The synthesized complex was subjected to metathesis by LiCl to yield the corresponding organomercury(II) derivative (**17**), which was recrystallized in the solid state in dichloromethane/methanol by a single crystal X-Ray diffraction (Figure 81).

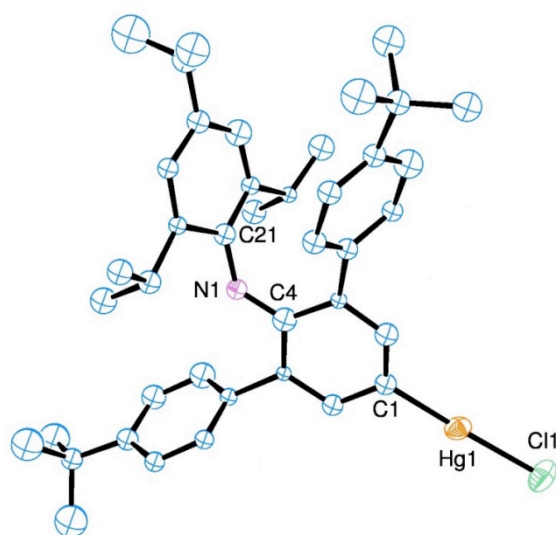
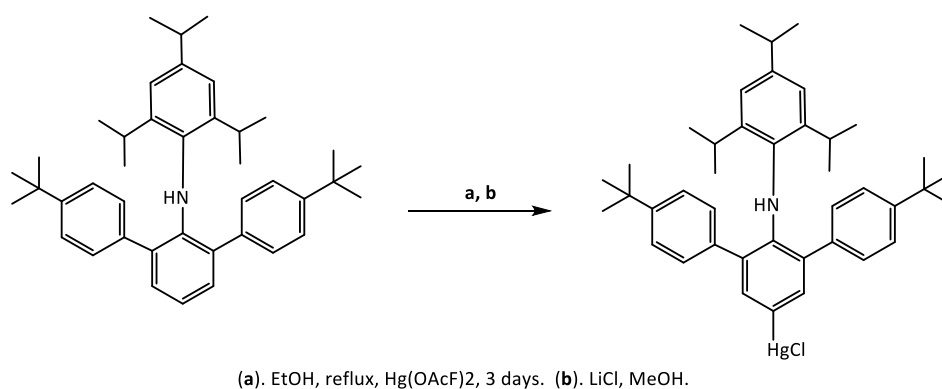


**Figure 81:** Molecular structure of complex organomercury (II) substrate (**17**). (50% probability ellipsoids shown). Hydrogen atoms and the dichloromethane solvent molecule have been omitted for clarity. The heavy atoms Cl and Hg were refined anisotropically and the smaller atoms C and N were refined isotropically (structure defined by Dr. Mark Schormann).

As is shown in ORTEP diagram of organomercury (II) derivative (**17**) (Figure 81), the mercury atom is coordinated in *para* position to the nitrogen atom, and not coordinated to the N atom as it was expected. We discarded to use this complex as starting material because of the position in where mercury was coordinated did not offer us any successful possibility in terms of gold(III) transmetalation.

**Table 32.** Most representative angles (°) and bond distances (Å) of complex 17.

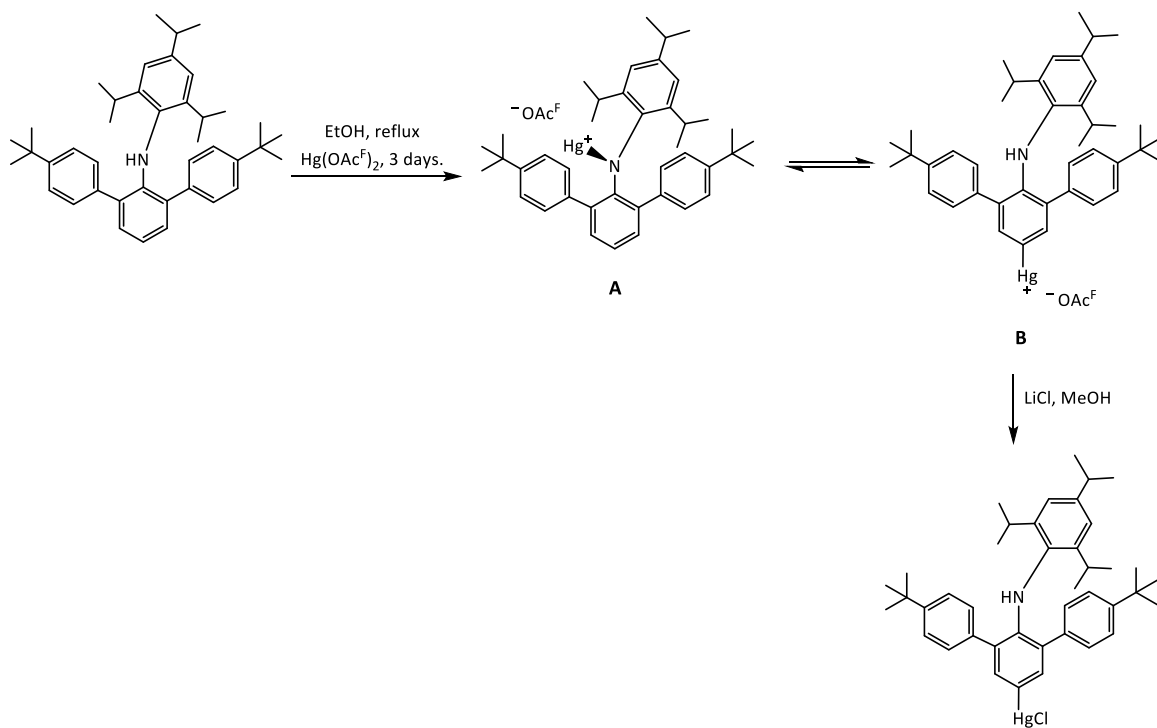
BOND LENGTHS (Å)		ANGLES(°)	
Hg1 – C1	2.05(3)	C4 – N1 – C21	132(2)
Hg1 – Cl1	2.321(8)	C1 – Hg1 – Cl1	175.2(7)
N1 – C4	1.34(3)		
N1 – C21	1.39(3)		



**Scheme 31.** Synthesis of organomercury (II) substrate (17).

One hypothesis to explain this result may be the steric hindrance caused by the isopropyl groups, which could promote the activation of the carbon atom located in *para* position to the nitrogen, forming C – Hg bond. In addition, according to the mesomeric resonance forms, a positive charge on N induces a negative charge on the C located in *para* position, which would be preferentially attacked by Hg<sup>2+</sup>. Another hypothesis is related to the well-known high stability of C – Hg bond compared to N – Hg bond. In the mercuration step, trifluoroacetate tends to attack to the more acidic proton of the –NH- group. Nevertheless, the molecular structure after salt metathesis indicated the formation of a C – Hg bond in *para* position to the nitrogen. Accordingly,

it may be possible that the formation of an equilibrium between **A** and **B** species was produced (Scheme 32), which would tend to be shifted to the more stable **B** species, in which contains the carbon atom located in *para* position to the nitrogen atom is the one activated.



**Scheme 32.** Proposed mechanism of synthesis of organomercury (II) substrate (**17**).

The obtained results encouraged us to study the synthesis of the organomercury substrate of ligand **L**<sup>5</sup> from another different route. In this route, we decided to synthesize a new pro-ligand derived from **L**<sup>5</sup>, including a *tert*-butyl group in *para* position to the nitrogen atom (Figure 82). The aim of this new pathway was to study if mercuration, as well as the activation and formation of C – Hg bond takes place when the carbon atom located in *para* position to the nitrogen atom is substituted by a bulky *tert*-butyl group.

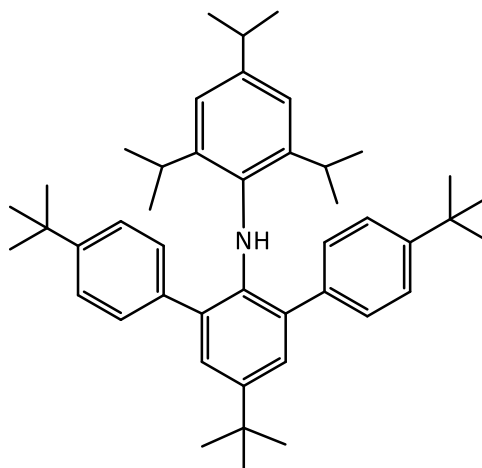
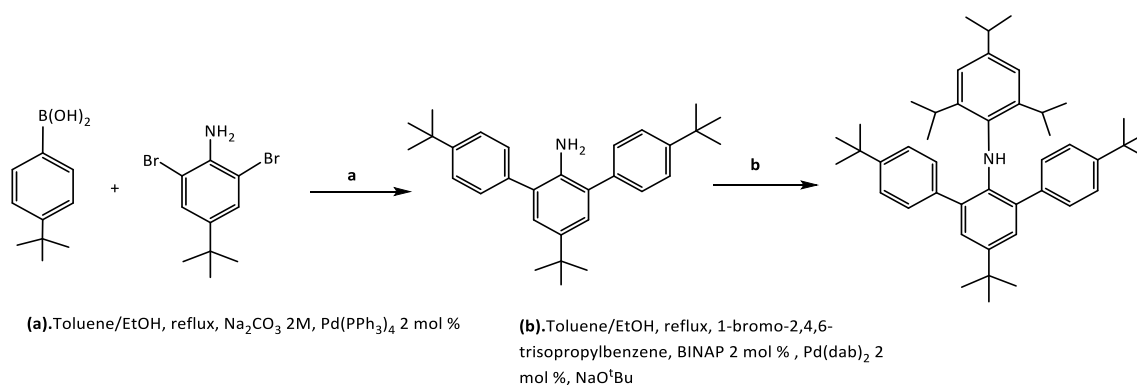


**Figure 82.** *Synthesis of new pro – ligand derived from  $L^5$  ( $L^{5'}$ ), where the carbon atom located in para position to the nitrogen atom is substituted by tert-butyl group.*

The synthesis of this ligand, called  $L^{5'}$ , has been carried out by the usual two steps route. The first step involves a Suzuki cross coupling of the commercially available 4-tert-butyl-2,6-dibromoaniline and 4-tertbutyl-boronic acid, employing  $\text{Pd}(\text{PPh}_3)_4$  as a catalyst. The second step involves a Buchwald – Hartwig cross coupling reaction, employing  $\text{Pd}(\text{dba})_2$  as precursor and diphenylphosphinobinaphthyl (BINAP) as catalyst (Scheme 33).



**Scheme 33:** *Synthesis of ligand  $L^{5'}$ .*

Ligand  $L^{5'}$  was subjected to mercuration using  $\text{Hg}(\text{OAc}^F)_2$  as organomercury reagent.

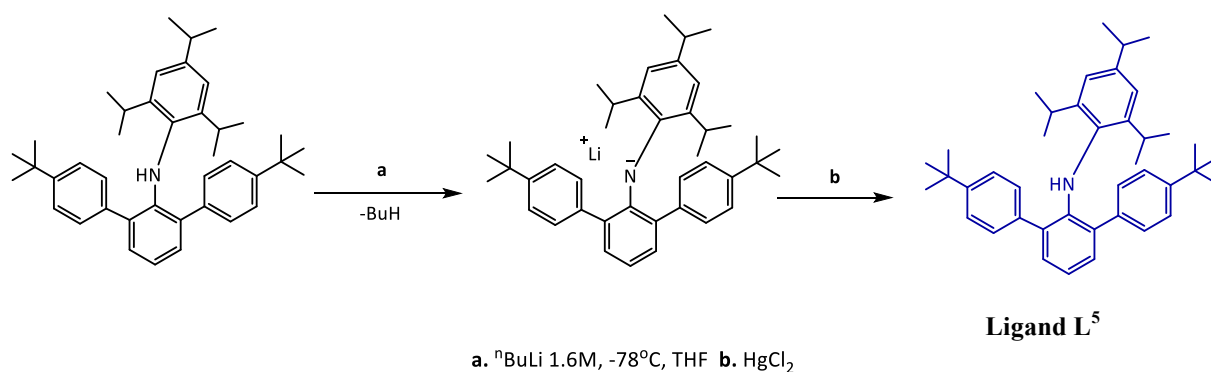
$^1\text{H-NMR}$  spectrum did not show any variation on the aromatic region compared to the

starting starting material. In addition, the  $^{19}\text{F}$ -NMR spectrum only showed the singlet resonance of the trifluoroacetate group corresponding to the non-coordinated organomercury reagent.

### B. Metalation attempts of ligand $\text{L}^5$ via lithiation step.

The failed attempts of metalating ligand  $\text{L}^5$  via the conventional mercuration route brought us to study an alternative pathway to synthesize the expected product. This route involved the inclusion of a lithiation step, previous to mercuration reaction. The aim of this new step was to lithiate the NH group and, in this way, try to orientate the following mercuration in order to active the formation of N – Hg bond via metathesis employing a mercury reagent.

A solution of  $^n\text{BuLi}$  1.6M in hexanes was added dropwise to a solution of ligand  $\text{L}^5$  in THF at  $-78^\circ\text{C}$ . The mixture was allowed to stir for 1 hour at this temperature.  $\text{HgCl}_2$  was added at room temperature. The mixture was allowed to stir at room temperature, monitoring the progress of the experiment by  $^1\text{H}$ -NMR spectroscopy.  $^1\text{H}$ -NMR spectrum showed the initial pro-ligand  $\text{L}^5$  as only product (Scheme 34).

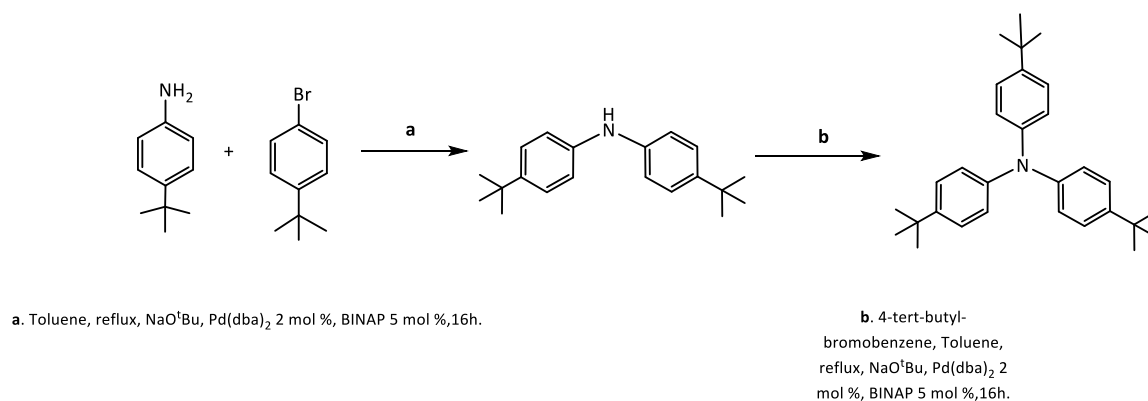


**Scheme 34.** Mercuration experiment of ligand  $\text{L}^5$

The only way to obtain ligand **L**<sup>5</sup> back is through a hydrolysis reaction (Scheme 34). Therefore, the most probable explanation to justify this result may be the presence of water during any of the reaction steps.

### 3.2.3. Synthesis of ligand **L**<sup>6</sup>.

According to the obtained results for pro-ligand **L**<sup>5</sup> and the failure attempts to metalate it, we decided to investigate an alternative C-,N- dianionic ligand framework suitable to be coordinated to the gold(III) centre, allowing the synthesis of complexes type (C<sup>-</sup>N<sup>-</sup>)AuX<sub>2</sub> or (C<sup>-</sup>N<sup>-</sup>)AuX(L). Accordingly, we decided to choose ligand **L**<sup>6</sup>, a known compound, which has been reported in the last years by different research groups, reporting its synthesis by different routes. In our investigations, the synthesis of the known ligand **L**<sup>6</sup> has been carried out via Buchwald – Hartwig cross-coupling, in two reaction steps (Scheme 35), following the experimental procedure reported in the literature.<sup>107</sup>



**Scheme 35:** *Synthesis of ligand **L**<sup>6</sup>.*

Because of ligand **L**<sup>6</sup> has been already reported in the literature, its characterization was only carried out by <sup>1</sup>H-NMR spectroscopy (Figure 83), by comparison with the <sup>1</sup>H-NMR data reported in the literature. In order to check if the experiment had been carried

out successfully, the main difficulty we found was the similarities between  $^1\text{H-NMR}$  spectrum of the intermediate bis(4-tert-butyl-phenylamine) and ligand  $\text{L}^6$ . The signal corresponding to the  $-\text{NH}$  group from bis(4-tert-butyl-phenylamine) was the key point that allowed us to identify that that ligand  $\text{L}^6$  was properly synthesized. Figure 110 shows a comparison between  $^1\text{H-NMR}$  spectrum of the intermediate bis(4-tert-butyl-phenylamine) (red spectrum) and ligand  $\text{L}^6$  (blue spectrum). As it is reported in the literature,<sup>108</sup> the chemical shift corresponding to the proton from  $-\text{NH}$  of bis(4-tert-butyl-phenylamine) is shown at  $\delta$  5.50, which is observed in the red spectrum corresponding to the intermediate ligand. As it is observed in Figure 84, this signal is not observed in the blue spectrum (corresponding to ligand  $\text{L}^6$ ), which indicated that ligand  $\text{L}^6$  had been synthesized.

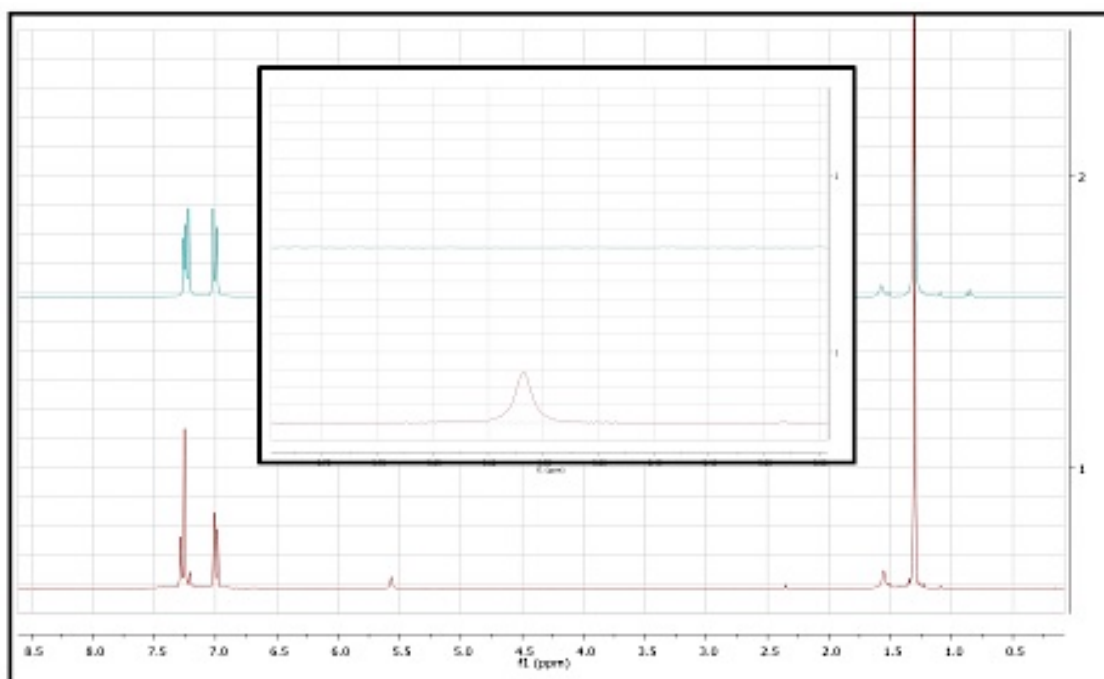


**Figure 83.** Comparison between  $^1\text{H-NMR}$  spectrum of bis(4-tert-butyl-phenylamine) (red spectrum) and ligand  $\text{L}^6$  (blue spectrum) in  $\text{CDCl}_3$ .

### 3.2.4. Metalation of ligand **L**<sup>6</sup>.

#### A. Metalation attempts of pro-ligand **L**<sup>6</sup> via mercuration step.

Ligand **L**<sup>6</sup> has been also subjected to mercuration experiments using both Hg(OAc)<sub>2</sub> and Hg(OAc<sup>F</sup>)<sub>2</sub> as organomercury reagents, following the experimental procedure reported by Parish et al.<sup>13</sup>

The mercuration reaction of ligand **L**<sup>6</sup> was first attempted employing excess Hg(OAc)<sub>2</sub> (1:2 ratio) as organomercury reagent. The reaction was monitored by <sup>1</sup>H-NMR spectroscopy. No changes in the chemical shifts of the aromatic region of the starting material were observed. Moreover, the characteristic singlet resonance corresponding to the coordinated acetate group was not shown, indicating that the mercuration step had not taken place. We therefore employed the more reactive reagent Hg(OAc<sup>F</sup>)<sub>2</sub> which was used in excess (1:4 ratio). However, monitoring of the reaction by <sup>1</sup>H-NMR and <sup>19</sup>F-NMR spectroscopy showed that, once again, no mercuration had taken place, and only the resonances corresponding to the starting material were observed.

#### B. Metalation attempts of ligand **L**<sup>6</sup> via lithiation step.

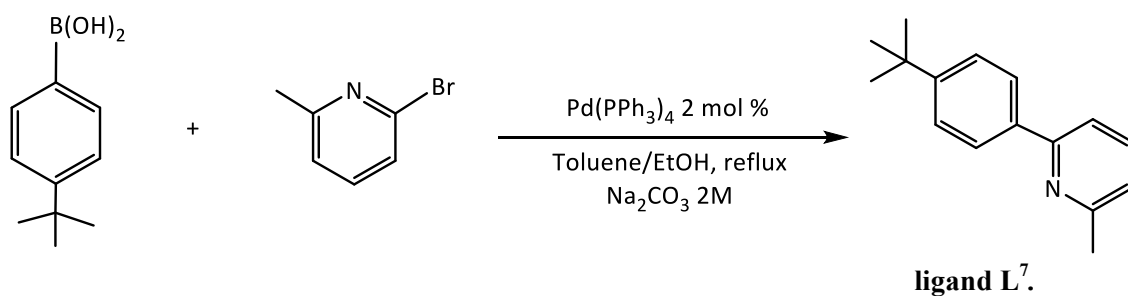
In 1992, Schleyer et al.<sup>108</sup> reported the synthesis of 1,5 – dilithiated arenes, which exhibit a remarkable synthetic utility<sup>109</sup> in different fields, such as the preparation of six membered heterocycles by reaction with bifunctional electrophiles.<sup>110</sup> They report the use of TMEDA (Me<sub>2</sub>N-CH<sub>2</sub>CH<sub>2</sub>-NMe<sub>2</sub>) as an reagent capable to increase the reactivity of <sup>n</sup>BuLi to promote the lithiation step.

Accordingly, we attempted the metalation of ligand **L**<sup>6</sup> via lithiation in presence of TMEDA, as reported in the literature, in order to maximize the effect of <sup>n</sup>BuLi. Our aim was to prepare a gold complex from ligand **L**<sup>6</sup> where Au(III) atom is bonding to two phenyl groups. This chelating ligand would provide two negative charges and the gold

centre would have one functionalization site available. However, our different attempts of metalation of ligand **L**<sup>6</sup> by this route were failed.

### 3.2.5. Phenylpyridine derivative ligands: ligands **L**<sup>7</sup> and **L**<sup>8</sup>.

The failed attempts of metalation of the two C-,N- dianionic ligands previously synthesized (ligand **L**<sup>5</sup> and ligand **L**<sup>6</sup>) encouraged us to change the approach and study the synthesis of C-,N monoanionic ligands, other type of ligands which can also allow us the synthesis of species with two functionalization positions, capable to provide high reactivity to the gold(III) complex. Accordingly, ligand **L**<sup>7</sup> was planned as an alternative C-,N monoanionic ligand. Although the synthesis of ligand **L**<sup>7</sup> has been reported in the literature via Kumada–Corriu Cross-Coupling,<sup>111</sup> we have conducted the synthesis of this ligand via a Suzuki cross-coupling between a boronic acid derivative (4-tert-butylphenylboronic acid) and 2-bromo-6-methylpyridine, employing Pd(PPh<sub>3</sub>)<sub>4</sub> as catalyst (Scheme 36).



<sup>1</sup>H-NMR spectroscopy indicated that pro-ligand **L**<sup>7</sup> have been successfully synthesized by comparison with the <sup>1</sup>H-NMR spectrum data reported in the literature for this ligand.<sup>111</sup>

The commercially available 2-(4-methylphenyl)pyridine (pro-ligand **L**<sup>8</sup>) (figure 84) was also considered in our investigations as an example of a C-,N monoanionic ligand.

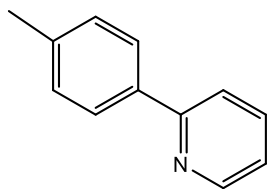


**Figure 84.** Chemical structure of 2-(4-methylphenyl)pyridine (pro-ligand  $L^8$ ).

### 3.2.6. Synthesis of five membered ring cycloaurated complexes **10** and **18**.

The synthesis of the five membered ring cycloaurated complexes **10** and **18** (Figure 85) has been studied through two different pathways. The first one involves the direct auration of ligands  $L^7$  or  $L^8$  with  $H[AuCl_4]$ . The second via involves the mercuriation step, making use of  $Hg(OAc)_2$  as organomercury reagent, and the consequent transmetallation, employing  $K[AuCl_4]$ .

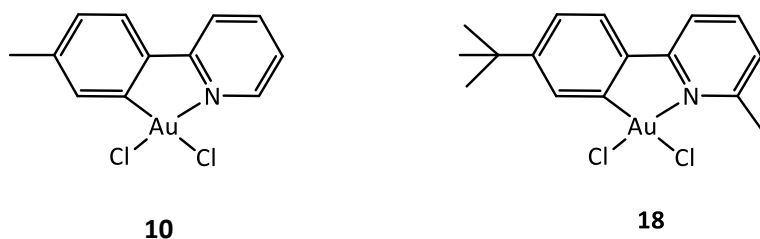
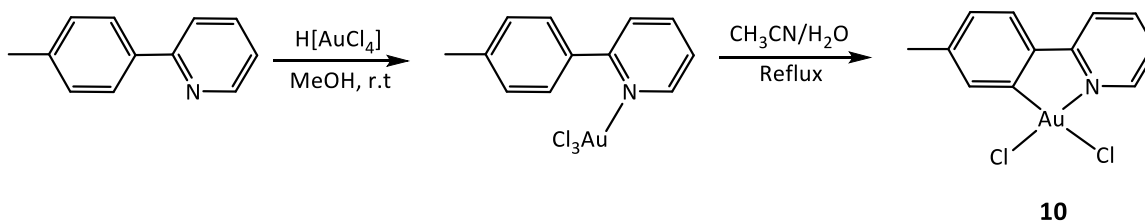


**Figure 85.** Five membered ring cycloaurated complexes **10** and **18**.

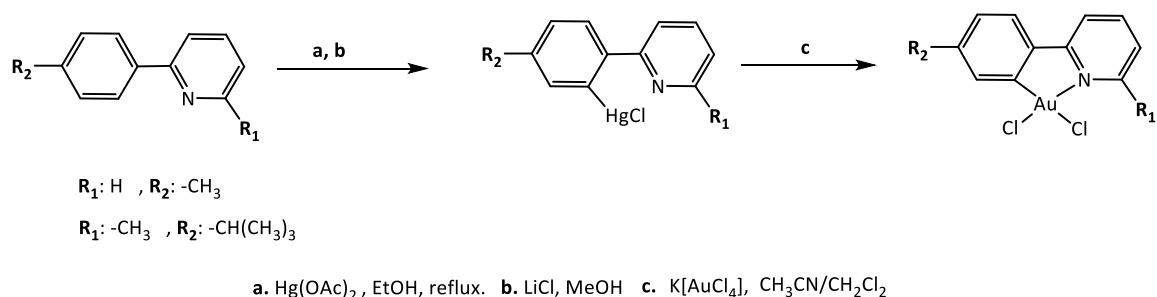
The first route involves the reaction of ligand  $L^8$  with  $H[AuCl_4]$  in MeOH, to give the corresponding N-bonded derivative. When this product was heated in an aqueous acetonitrile solution, the corresponding cyclometallated derivative (N-C)AuCl<sub>2</sub> **10** was obtained in moderate yield (35%, scheme 37).



**Scheme 37.** Synthesis of cyclometallated gold (III) complexes **10** by direct auration.

The second route involves an initial mercuriation reaction of ligands **L**<sup>7</sup> or **L**<sup>8</sup> using Hg(OAc)<sub>2</sub> as organomercury agent, and the consequent transmetallation reaction employing K[AuCl<sub>4</sub>].

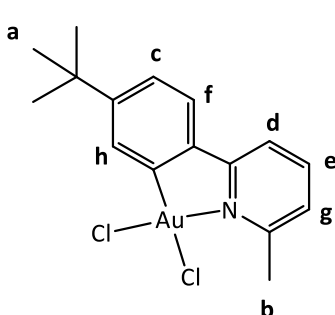
The synthesis of the corresponding organomercury derivative has been carried out according to the experimental procedure reported on the literature.<sup>13</sup> Ligands **L**<sup>7</sup> and **L**<sup>8</sup> have been subjected to mercuriation with Hg(OAc)<sub>2</sub> or Hg(OAc<sup>F</sup>)<sub>2</sub> (Scheme 38) followed by salt metathesis with LiCl to yield the corresponding organomercury(II) derivative (N–C)HgCl. The synthesized mercury derivative undergoes then transmetallation and C – H activation with KAuCl<sub>4</sub> to yield the (N–C)AuCl<sub>2</sub> derivatives. Nevertheless, this pathway involves partial reductive elimination to gold(0).



**Scheme 38.** Synthesis of cyclometallated gold (III) complexes **10** and **19** by transmetallation reaction.

The known complex **10** has been characterized by comparison with the <sup>1</sup>H-NMR data in DMSO-*d*<sup>6</sup> reported in the literature. Complex **19** has been characterized by <sup>1</sup>H-NMR spectroscopy (Figure 86, Table 33) and X-Ray diffraction (Figure 88).

**Table 33.**  $^1\text{H-NMR}$  data of complex **19** in  $\text{CD}_2\text{Cl}_2$ ,  $\delta(\text{ppm})$  and multiplicity.

Complex 19	ASSIGNMENT	$^1\text{H}$ (ppm)
	a	1.35 (s, 9 H)
	b	3.20 (s, 3 H)
	c (overlapped with $\text{CHCl}_3$ )	7.23 (m, 1 H)
	d, g	7.37 (d, $J = 0.8$ Hz, 2 H)
	f	7.67 (d, $J = 7.9$ Hz, 1 H)
	e	7.90 (t, 1 H)
	h	8.00 (s, 1 H)

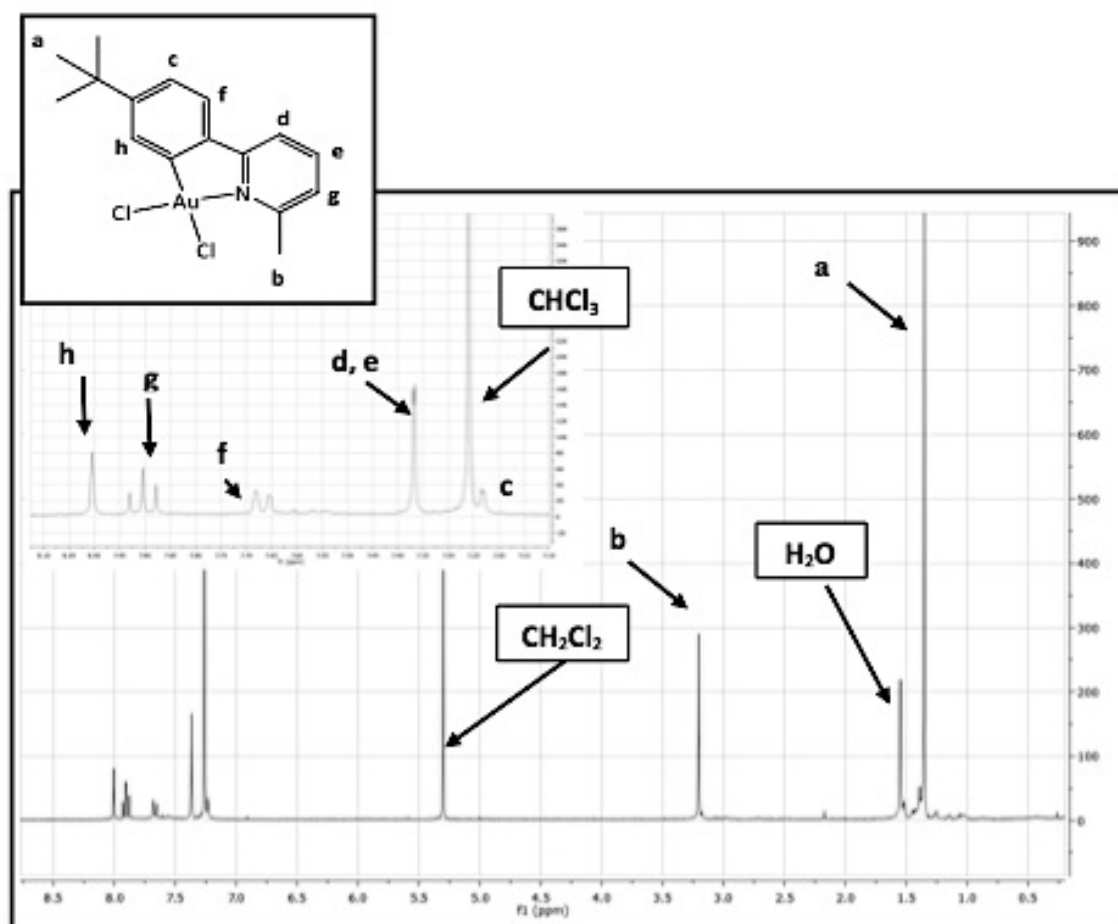


**Figure 86.**  $^1\text{H-NMR}$  spectrum of complex **19** in  $\text{CDCl}_3$ .

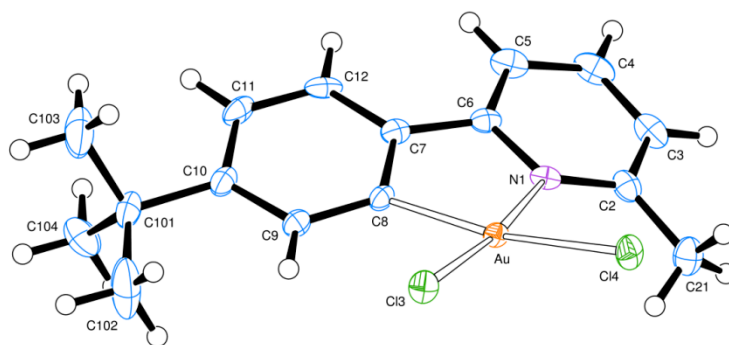


**Figure 87.** Molecular structure of complex **19**. (50% probability ellipsoids shown).

(Structure defined by Dr. David Hughes).

As it shown in Figure 87, the gold atom is four-coordinated in a rather distorted square-planar fashion. The metal atom is displaced 0.14 Å out of the mean-plane of the N1, C8, Cl3, Cl4 atoms. The N – C ligand is tilted 25° from this plane. In the N<sup>^</sup>C ligand, both the pyridyl and phenyl rings are tilted 9° from the central N1, C5, C8, C12 mean-plane.

The observed distortion of the molecular structure of complex **19** (Figure 88) is a phenomenon that has been also observed for another (C<sup>^</sup>N)Au(III) derivatives reported in the literature.<sup>13</sup> Complex **19** gives a distorted square-planar geometry, characteristic of d<sup>8</sup> metal complexes, resulting of coordination of N-AuCl<sub>2</sub> donor set, producing a C-Au-N angle of 81.28° about the gold(III) metal center, found to deviate from the ideal 90° angle of the bidentate C<sup>^</sup>N ligands. Au – N and Au – C bonds lengths of 2.075(3) and 2.008(4) Å, respectively, are found in the observed range for another similar compounds. Au – Cl(3) and Au – Cl(4) bond lengths are found to be 2.2726(9) and 2.3849(9) Å respectively. This difference may be explained because of the *trans* influence to C(8) bonded to gold centre.

**Table 34.** Most representative angles (°) and bond distances (Å) of complex **19**.

BOND LENGTHS (Å)		ANGLES(°)	
Au – Cl(3)	2.2726(9)	C(8) – Au – N(1)	81.28(14)
Au – Cl(4)	2.3849(9)	N(1) – Au – Cl(3)	171.95(9)
Au – N(1)	2.075(3)	N(1) – Au – Cl(4)	99.69(9)
Au – C(8)	2.008(4)	C(8) – Au – Cl(3)	91.06(11)
		C(8) – Au – Cl(4)	168.56(10)
		Cl(3) – Au – Cl(4)	87.32(3)

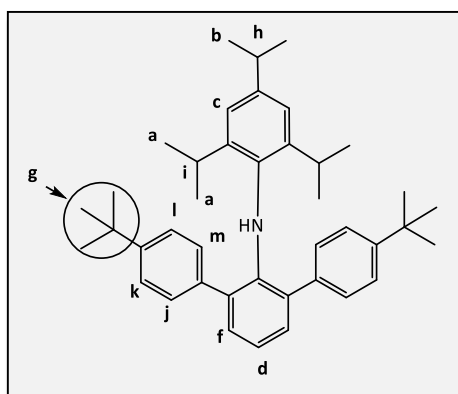
Our first approach focused on C-,N- dianionic ligands, in order to synthesize and study the reactivity of new (C<sup>-</sup>N<sup>-</sup>)AuX<sub>2</sub> and (C<sup>-</sup>N<sup>-</sup>)AuX(L) derivatives. Ligands **L**<sup>5</sup> and **L**<sup>6</sup> were chosen as ligand frameworks. For both of them, the ligand was successfully synthesized, but the different mercuration attempts failed. This result brought us to explore an alternative system, in particular C,N- monoanionic ligands, which have been reported in the literature.<sup>13</sup> Ligands **L**<sup>7</sup> and **L**<sup>8</sup> were chosen as ligand frameworks and, for both of them, either mercuration and transmetallation steps were successfully achieved, to afford the complexes **19** and **10**, respectively. In particular, complex **10** was the starting material employed on this thesis to synthesize C,N- monoanionic ligands functionalized by amino ester derivatives, in order to study the interaction of them with DNA secondary structures, as is reported in chapters 1 and 2.

### 3.3. EXPERIMENTAL

#### 3.3.1. GENERAL CONSIDERATIONS.

Unless otherwise stated, all experiments were performed in air using bench solvents. In such exceptions, manipulations were performed using standard Schlenk techniques under dry nitrogen or a Saffron Scientific glovebox. Nitrogen was purified by passing through columns of supported  $P_2O_5$ , with moisture indicator, and activated 4 Å molecular sieves. Anhydrous solvents were freshly distilled from appropriate drying agents. Ligand **L**<sup>5</sup> was prepared using literature methods.<sup>105,107</sup> 4-tert-butylphenyl-2-methylpyridine (ligand **L**<sup>7</sup>) was prepared using literature methods. Complex **17**, **18** and **19** were also prepared according to literature methods.<sup>13,31</sup> 2-*para*-tolylpyridine (Aldrich),  $Hg(OAc)_2$  (Aldrich) and LiCl were commercially available and used as received.  $^1H$  and  $^{13}C\{^1H\}$  spectrum were recorded using a Bruker DPX300 spectrometer.  $^1H$ -NMR spectrum (300.13 MHz) were referenced to the residual protons of the deuterated solvent used.  $^{13}C\{^1H\}$ -NMR spectrum (75.47 MHz) were referenced internally to the proton-decoupled  $^{13}C$  resonances of the NMR solvent.

#### 3.3.2. N-(2,6-tert-butylphenyl)-2,4,6-triisopropylaniline (Ligand **L**<sup>5</sup>).

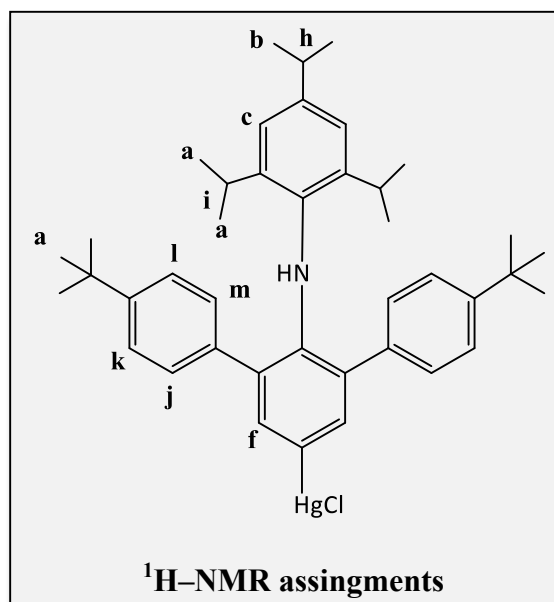


**$^1H$ -NMR assignments**

Ligand **L**<sup>5</sup> was prepared employing literature methods reporting.<sup>105,107</sup>  $^1H$ -NMR (300 MHz,  $CDCl_3$ )  $\delta$  7.17 ( $H^j - H^m$  (overlapping), m, 8 H), 7.08 ( $H^f$ , d,  $J = 7.5$ , 2 H), ( $H^d$ , t, 1

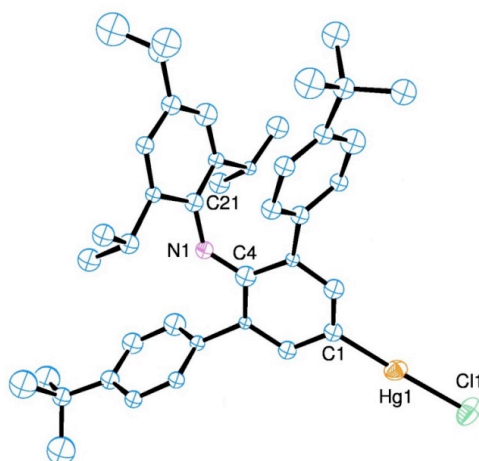
H), ( $H^c$ , s, 2H), 2.96 – 3.06 ( $H^i$ , m, 2 H), 2.58 – 2.67 ( $H^h$ , m, 1 H), 1.25 ( $H^g$ , s, 18 H), 1.09 ( $H^b$ , d,  $J = 6.9$  Hz, 6 H), 0.96 ( $H^a$ , d,  $J = 6.8$  Hz, 12 H).

### 3.3.3. N-(2,6-tert-butyl-4-(HgCl)-phenyl)-2,4,6-triisopropylaniline (Complex 17).



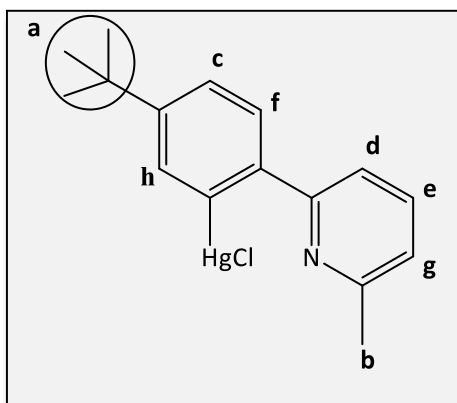
$\text{Hg}(\text{OOC}\text{CF}_3)_2$  (76.0 mg, 0.60 mmol) was added to a solution of pro-ligand **L**<sup>5</sup> (300 mg, 0.54 mmol) in ethanol (10 ml). The mixture was refluxed for 24 hours. The suspension was filtered in hot over a solution of LiCl (46 mg, 1.08 mmol) in degassed metanol. The suspension was refluxed for one hour and chilled overnight. The solvent was filtered off and the white precipitate was dried under vacuum. The precipitate was purified by recrystallization in dichloromethane/metanol, to yield transparent crystals (50 mg, 0.063 mmol, 12%). Very low yield. It is necessary to repeat this reaction in order to carry out a full characterization of the complex by mass spectroscopy and  $^1\text{H-NMR}$  (300 MHz,  $\text{CD}_2\text{Cl}_2$ )  $\delta$  7.16 ( $H^j - H^m$ , dd,  $J = 21.5, 8.3$  Hz, 8H), 6.99 ( $H^f$ , s, br, 2H), 6.55 ( $H^c$ , s, 1H), 2.90 – 2.99 ( $H^i$ , m, 2H), 2.58 – 2.67 ( $H^h$ , m, 1H), 1.25 ( $H^g$ , s, 18 H), 1.08 ( $H^b$ , d,  $J = 6.9$  Hz, 6H), 0.97 ( $H^a$ , d,  $J = 6.8$  Hz, 12H).

**Table 35.** X-ray crystallography data of complex **17**.

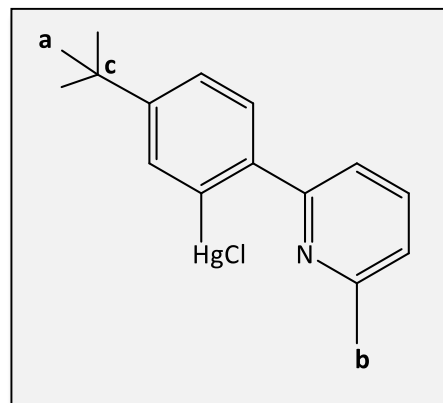


Compound	17
Reference	angell
Formula weight	879.8
Crystal system	triclinic
Space group	P - 1
Unit cell dimensions. a (Å)	9.529(2) Å
b	12.609(4) Å
c	18.005(4) Å
$\alpha$ (°)	101.18(2)°
$\beta$	103.09(2)°
$\gamma$	102.15(2)°
Volume (Å <sup>3</sup> )	1992.5(9)
Z	2
Calculated density (mg/m <sup>3</sup> )	1.466 mg/m <sup>3</sup>
F(000)	888
Absorption coefficient $\mu$ (mm <sup>-1</sup> )	4.092 mm <sup>-1</sup>
Crystal size (mm <sup>3</sup> )	0.15 x 0.06 x 0.06
$\theta$ Range (°)	2.82 to 25.35
No. of unique reflections, R <sub>int</sub>	7280 [R(int) = 0.2848]
Data/Restraints/Parameters	7280 / 0 / 209
Final R indices (observed data)	R1 = 0.1575, wR2 = 0.3129
Final R indices (all data)	R1 = 0.2792, wR2 = 0.3924

### 3.3.4. (6-(4-tert-butylphenyl)-2-methylpyridyl)HgCl (Complex 18).



<sup>1</sup>H-NMR assignments



<sup>13</sup>C{<sup>1</sup>H}-NMR assignments

Hg(OAc)<sub>2</sub> (7.41 g, 23.00 mmol) was added to a solution of pro-ligand L<sup>8</sup> (5.00 g, 23.00 mmol) in ethanol (30 ml). The mixture was refluxed for 48 hours. The suspension was filtered in hot over a solution of LiCl (1.46 g, 34.5 mmol) in methanol (10 ml). The precipitate was filtered off and washed with cold methanol. The residue was dried under vacuum, to yield a white solid (6.64 g, 14.43 mmol, 63%). (170 mg, 0.34 mmol, 64%).  
<sup>1</sup>H-NMR (300 MHz, CDCl<sub>3</sub>) δ 7.94 (H<sup>f</sup>, d, J = 8.3 Hz, 1H), 7.73 – 7.65 (H<sup>d</sup>, H<sup>h</sup> (overlapped), m, 2H), 7.57 (H<sup>e</sup>, d, J = 2.1 Hz, 1 H), 7.42 (H<sup>c</sup>, dd, J = 8.3, 2.1 Hz, 2 H), 7.17 (H<sup>e</sup>, d, J = 6.9, 1.4 Hz, 1 H) 2.73 (H<sup>b</sup>, s, 3 H), 1.36 (H<sup>a</sup>, s, 9 H). <sup>13</sup>C{<sup>1</sup>H}-NMR (75 MHz, CDCl<sub>3</sub>) δ 158.3 (C<sup>Ar</sup>), 155.1 (C<sup>Ar</sup>), 152.8 (C<sup>Ar</sup>), 147.5 (C<sup>Ar</sup>), 139.3 (C<sup>Ar</sup>), 138.1 (C<sup>Ar</sup>), 134.8 (C<sup>Ar</sup>), 126.8 (C<sup>Ar</sup>), 125.9 (C<sup>Ar</sup>), 123.0 (C<sup>Ar</sup>), 117.3 (C<sup>Ar</sup>), 34.9 (C<sup>c</sup>), 31.2 (C<sup>b</sup>), 23.9 (C<sup>a</sup>).

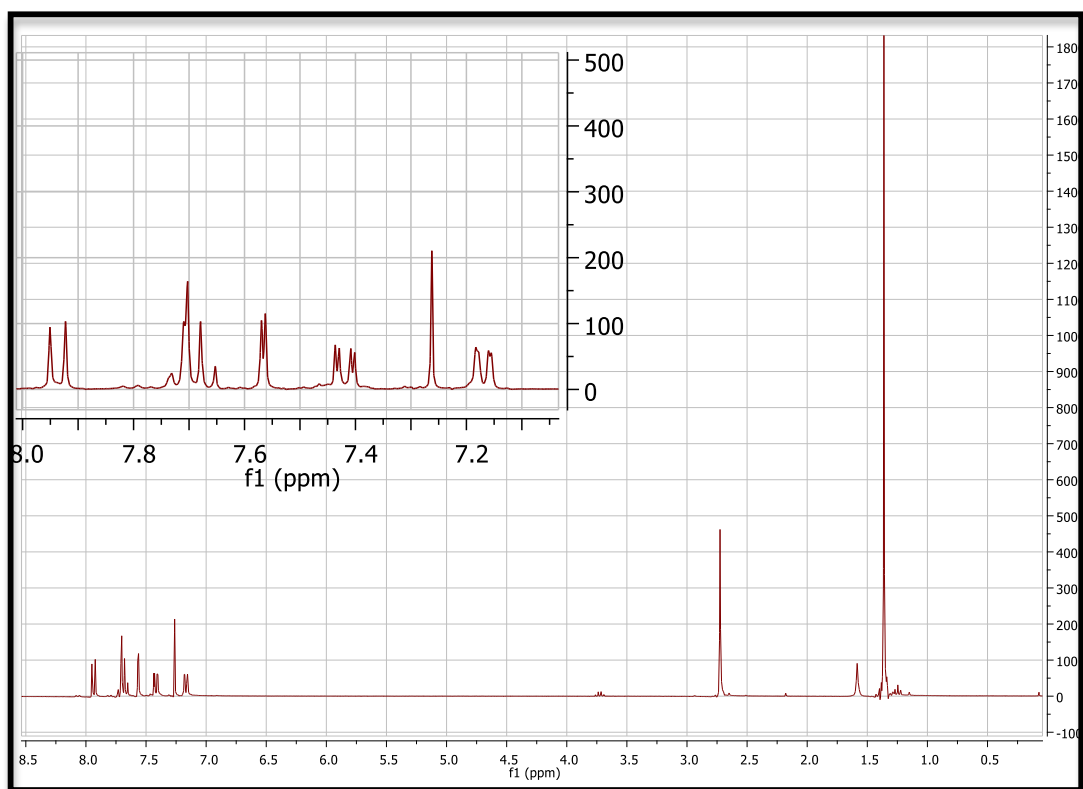


**Figure 88.**  $^1\text{H}$ -NMR spectrum of complex **18** in  $\text{CDCl}_3$ .

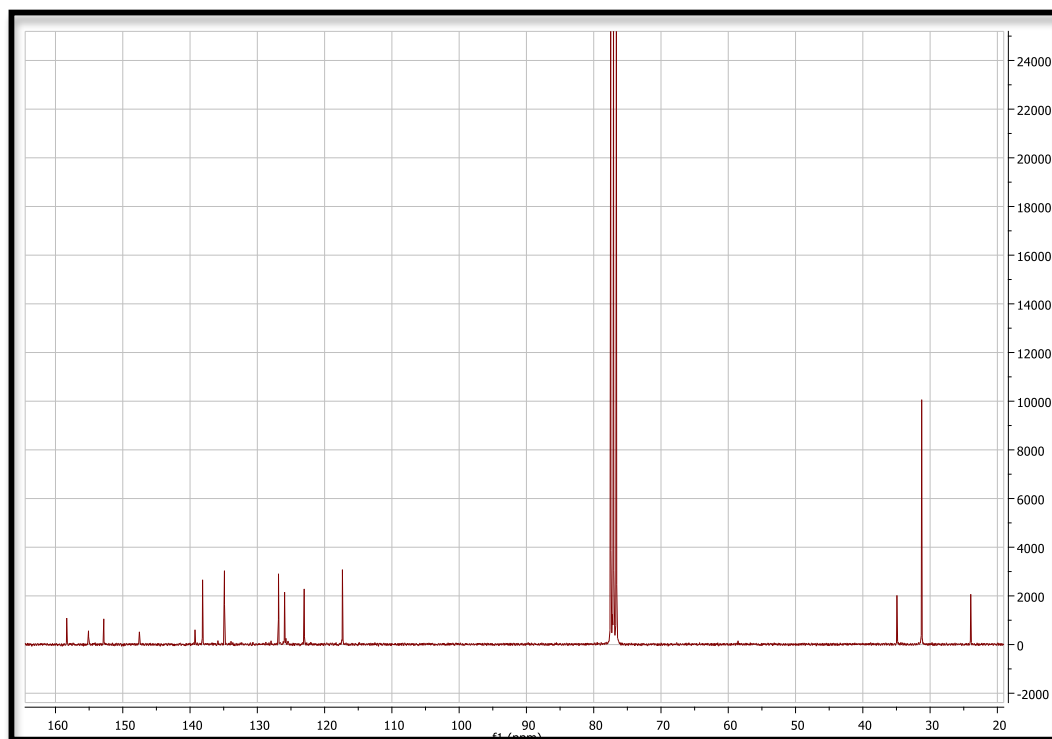
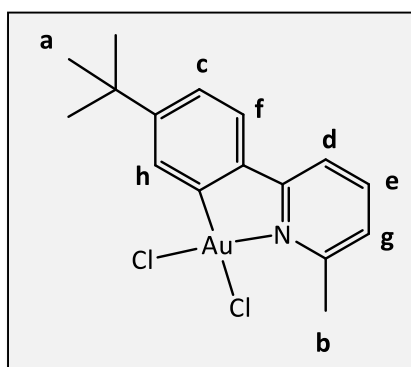


**Figure 89.**  $^{13}\text{C}\{^1\text{H}\}$ -NMR spectrum of complex **18** in  $\text{CDCl}_3$

\*Both the  $^1\text{H}$ -NMR and  $^{13}\text{C}\{^1\text{H}\}$ -NMR (**Figures 88 and 89**) are shown in the experimental section as they are not reported in the results and discussion.

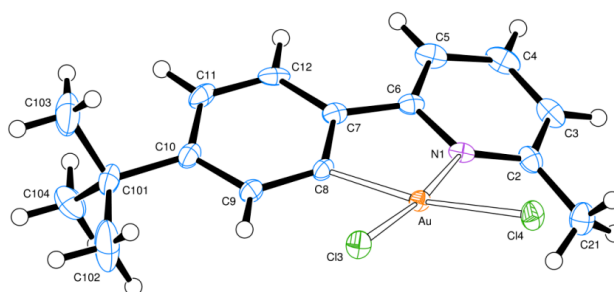
### 3.3.5. (6-(4-tert-butylphenyl)-2-methylpyridyl)AuCl<sub>2</sub> (Complex 19).



#### <sup>1</sup>H-NMR assignments

Pro-ligand **L**<sup>8</sup> (200.0 mg, 0.93 mmol) was added to a solution of KAuCl<sub>4</sub> (350 mg, 0.93 mmol) in acetonitrile/dichloromethane (1:1). The mixture was allowed to stir 16 hours. The solvent was removed under vacuum and the residue was extracted two times with 10 ml of dichloromethane. The solvent was removed to afford a yellow solid (170 mg, 0.34 mmol, 64%). <sup>1</sup>H-NMR (300 MHz, CD<sub>2</sub>Cl<sub>2</sub>) δ 8.00 (H<sup>h</sup>, s, 1 H), 7.90 (H<sup>e</sup>, t, 1 H), 7.67 (H<sup>f</sup>, d, J = 7.9 Hz, 1 H), 7.37 (H<sup>d</sup>, H<sup>g</sup>, d, J = 0.8 Hz, 2 H), 3.20 (H<sup>b</sup>, s, 3 H), 1.35 (H<sup>a</sup>, s, 9 H).

**Table 36.** X-ray crystallography data of complex **19**.



<b>Compound</b>	<b>19</b>
<b>Reference</b>	angelbs5b
<b>Formula weight</b>	492.18
<b>Crystal system</b>	monoclinic
<b>Space group</b>	C2/c
<b>Unit cell dimensions. a (Å)</b>	17.0592(3)
<b>b</b>	8.05458(13)
<b>c</b>	23.8050(5)
<b><math>\alpha</math> (°)</b>	90
<b><math>\beta</math></b>	100.815(2)
<b><math>\gamma</math></b>	90
<b>Volume (Å<sup>3</sup>)</b>	3212.82(11)
<b>Z</b>	8
<b>Calculated density (mg/m<sup>3</sup>)</b>	2.035
<b>F(000)</b>	1872
<b>Absorption coefficient <math>\mu</math>(mm<sup>-1</sup>)</b>	9.480
<b>Crystal colour, shape</b>	yellow-green block
<b>Crystal size (mm<sup>3</sup>)</b>	0.40 x 0.26 x 0.14
<b><math>\theta</math> Range (°)</b>	3.18 to 30.00
<b>No. of unique reflections, <math>R_{int}</math></b>	4689 [R(int) for equivalents = 0.056]
<b>Data/Restraints/Parameters</b>	4689 / 0 / 182
<b>Final R indices (observed data)</b>	$R_1 = 0.028$ , $wR_2 = 0.054$
<b>Final R indices (all data)</b>	$R_1 = 0.029$ , $wR_2 = 0.055$
<b>Largest diff. peak and hole (e Å<sup>3</sup>)</b>	1.73 and -1.02

## ANEXE 1: X-RAY CRYSTALLOGRAPHY INFORMATION OF COMPLEXES

### 5 and 19.

Refinement and solving of compounds **5** and **19** were carried out by Dr. David Hughes at the University of East Anglia. Crystals of each sample were mounted in oil on glass fibres and fixed in the cold nitrogen stream on a diffractometer. Diffraction intensities for compounds **5** and **19** were recorded at 140(2)K on an Oxford Diffraction Xcalibur-3/Sapphire3-CCD diffractometer, equipped with Mo-K $\alpha$  radiation and graphite monochromator. Data were processed using the CrysAlisPro-CCD and -RED programs.<sup>112</sup> The structure was determined by the direct methods routines in the SHELXS program<sup>113</sup> and refined by full-matrix least-squares methods, on F<sup>2</sup>s, in SHELXL.<sup>113</sup> The non-hydrogen atoms were refined with anisotropic thermal parameters. Hydrogen atoms were included in idealised positions and their Uiso values were set to ride on the Ueq values of the parent carbon atoms. Computer programs used in this analysis have been noted above, and were run through WinGX<sup>114</sup> on a Dell Optiplex 755 PC at the University of East Anglia.

## REFERENCES

1. GM. Cooper. *The Cell: Molecular Approach*. Sunderland (MA), 2000, Sinauer associates.
2. B. Rosenberg. *Nature*, 1965, **205**, 698.
3. L. Cattaruzza, D. Fregona, M. Mongiat, L. Ronconi, A. Fassina, A. Colombatti and D. Aldinucci. *Int. J. Cancer*, 2011, **128**, 206–215.
4. K. Thompson and C. Orvig. *Dalton Trans.*, 2006, 761 – 764.
5. M. D. Đurović, Ž. D. Bugarčić, F. W. Heinemann and R. van Eldik. *Dalton Trans.*, 2014, **43**, 3911 – 3921.
6. W. Henderson, *Adv. Organomet. Chem.*, 2006, **54**, 207–265.
7. M. S. Kharasch, H.S. Isbell, *J. Am. Chem. Soc.*, 1931, **53**, 3053 – 3059.
8. a) E. C. Constable, T. A. Leese. *J. Organomet. Chem.*, 1989, **363**, 419–24. b) M. A. Ivanov, M. V. Puzyk. *Russ. J. Gen. Chem.*, 2001, **71**, 1660 – 1661.
9. Y. Fuchita, H. Ieda, Y. Tsunemune, J. Kinoshita-Nagaoka, H. Kawano. *J. Chem. Soc. Dalton Trans.*, 1998, 791 - 796.
10. M. Nonoyama, K. Nakajima, K. Nonoyama. *Polyhedron*, 1997, **16**, 4039 - 4044.
11. V. K.-Y. Lo, K. K.-Y. Kung, M.-K. Wong, C.-M. Che. *J. Organomet. Chem.*, 2009, **694**, 583 – 591.
12. K. K.-Y. Kung, V. K.-Y. Lo, H.-M. Ko, G.-L. Li, P.-Y. Chan, K.-C. Leung, Z. Zhou, M.-Z. Wang, C.-M. Che, M.-K. Wong. *Adv. Synth. Catal.*, 2013, **355**, 2055 – 2070.
13. R. V. Parish, J. P. Wright, R. G. Pritchard, *J. Organomet. Chem.*, **2000**, 596, 165 – 176.
14. D.-A. Rosca, J. A. Wright, D. L. Hughes, M. Bochmann. *Nat. Commun.*, 2013, **4**, 3167/1–3167/7.

15. N. Savjani, D.-A. Roşca, M. Schormann, M.Bochmann. *Angew. Chem.,Int. Ed.*, 2013, **52**, 874–877.
16. K. M.-C. Wong, L.-L. Hung, W. H. Lam, N. Zhu, V. W.-W. Yam. *J. Am. Chem. Soc.*, 2007, **129**, 4350 - 4365.
17. A. Johnson, R. J. Puddephatt, J. L. Quirk. *J. Chem. Soc., Chem. Commun.*, 1972, 938 – 939.
18. A. Johnson, R. J. Puddephatt. *J. Chem. Soc., Dalton Trans.*, 1977, 1384–1388.
19. V. K.-M. Au, K. M.-C. Wong, N. Zhu, and V. W.-W. Yam. *Chem. Eur. J.*, 2011, **17**, 130 – 142.
20. V. W-W. Yam, K. M-C. Wong, L-L. Hung, and N. Zhu. *Angew. Chem. Int. Ed.*, 2005, **44**, 3107 – 3110.
21. J. A. Garg, O. Blacque, and K. Venkatesan. *Inorg. Chem.*, 2011, **50**, 5430 – 5441.
22. O. Schuster, R. Y. Liao, A. Schier, H. Schmidbaur. *Inorg. Chim. Acta*, 2005, **358**, 1429 –1441.
23. O. Schuster, H. Schmidbaur. *Organometallics*, 2005, **24**, 2289 – 2296.
24. a) V.W.W. Yam, S. W. K. Choi, T. F. Lai, W. K. Lee. *J. Chem. Soc., Dalton Trans.*, 1993, 1001 - 1002. b) C. W. Chan, W. T. Wong, C. M. Che. *Inorg. Chem.*, 1994, **33**, 1266 – 1272.
25. J. A. Garg, O. Blacque, T. Fox and K. Venkatesan. *Inorg. Chem.*, 2010, **49**, 11463 - 11472.
26. E. R. Tiekink. *Inflammopharmacology*, 2008, **16**, 138 – 142.
27. L. Ronconi, L. Giovagnini, C. Marzano, F. Bettio, R. Graziani, G. Pilloni and D. Fregona. *Inorg. Chem.*, 2005, **44**, 1867 – 1881.

28. A. Meyer, C. P. Bagowski, M. Kokoschka, M. Stefanopoulou, H. Alborzinia, S. Can, D. H. Vlecken, W. S. Sheldrick, S. Wölfl and I. Ott. *Angew. Chem., Int. Ed.*, 2012, **35**, 8895–8899.
29. B. Bertrand and A. Casini. *Dalton Trans.*, 2014, **43**, 4209.
30. D.-A. Rosca, D. A. Smith and M. Bochmann. *Chem. Commun.*, 2012, **48**, 7247 – 7249.
31. K.-H. Wong, K.-K. Cheung, M. C.-W. Chan, C.-M. Che. *Organometallics*, 1998, **17**, 3505 - 3511.
32. A. Sam; G. Anne-Sophie; L. Paolo; J. Rodolphe; B. Olivier. *Angew. Chem., Int. Ed.*, 2012, **51**, 10808 – 10811.
33. Z. Li, F. W. Fowler and J. W. Lauher. *J. Am. Chem. Soc.*, 2009, **131**, 634 – 643.
34. The University of Hong Kong, V. W. Yam, K. V. Au, M. Chan, M. K. Wong. WO2011/6353 A1, 2011.
35. N. Sewald, H. Jakubke. *Peptides: Chemistry and Biology*; Wiley-VCH: Weinheim, Germany, 2002.
36. B. Rosenberg, et al. *Nature*, 1969, **222**, 385–386.
37. B. Rosenberg. *Nature*, 1965, **205**, 698.
38. V. M. Gonzalez, M. A. Fuertes, C. Alonso, J. M. Perez. *Mol. Pharmacol.*, 2001, **59**, 657.
39. Y. Jung, et al. *Chem. Rev.*, 2007, **107**, 1387–1407.
40. M. E. Howe-Grant, S. J. Lippard. In *Metal Ions in Biological Systems*; H. Sigel, Ed.; Marcel Dekker: New York, 1980; **11**, 63-125.
41. C. F. Shaw. *Chem. Rev.*, 1999, **99**, 2589–2600.
42. G. Jaouen, N. Metzler-Nolte. *Medicinal organometallic chemistry*. Springer, 2010, p. 69.

43. J. F. Fries, D. Bloch, P. Spitz, D. M. Mitchell. *Am. J. Med.*, 1985, **78**, 56–59.
44. R. C. Blodgett. *Am. J. Med.*, 1983, **75**, 86-89.
45. R. M. Snyder, C. K. Mirabelli, S. J. Crooke. *Semin. Arthritis Rheum.*, 1987, **17**, 71-80.
46. K. Hashimoto, C. E. Whitehurst, T. Matsubara, K. Hirohata and P. E. Lipsky. *J Clin. Invest.*, 1992, **89**, 1839–1848.
47. T. M. Simon, D. H. Kunishima, G. J. Vibert, A. Lorber. *Cancer*, 1979, **44**, 1965–1975.
48. S. Gullatineke, A. M. Barrios. *J. Med. Chem.*, **2006**, *49*, 3933–3937.
49. D. de Vos, S. Y. Ho, E. R. T. Tiekink. *Bioinorg. Chem. Appl.*, 2004, **2**, 141-154.
50. E. Schuh, S. M. Valiahdi, M. A. Jakupec, B. K. Keppler, P. Chiba and F. Mohr. *Dalton Trans.*, 2009, 10841–10845.
51. C.-H. Chui, R. S.-M. Wong, R. Gambari, G. Y.-M. Cheng, M. C.-W. Yuen, K.-W. Chan, S.-W. Tong, F.-Y. Lau, P. B.-S. Lai, K.-H. Lam, C.-L. Ho, C.-W. Kan, K. S.-Y. Leung and W.-Y. Wong. *Bioorg. Med. Chem.*, 2009, **17**, 7872–7877.
52. A. Meyer, C. P. Bagowski, M. Kokoschka, M. Stefanopoulou, H. Alborzinia, S. Can, D. H. Vlecken, W. S. Sheldrick, S. Wölfl and I. Ott. *Angew. Chem., Int. Ed.*, 2012, **35**, 8895–8899.
53. N. Sewald, H. Jakubke. *Peptides: Chemistry and Biology*; Wiley-VCH: Weinheim, Germany, 2002.
54. A. Gutiérrez, J. Bernal, M. D. Villacampa, C. Cativiela, A. Laguna and M. C. Gimeno. *Inorg. Chem.*, 2013, **52**, 6473–6480.
55. K. Nomiya, R. Noguchi, T. Shigeta, Y. Kondoh, K. Tsuda, K. Ohsawa, N. Chikaraishi-Kasuga, M. Oda. *Bull. Chem. Soc. Jpn.*, 2000, **73**, 1143.

56. A. Gutiérrez, L. Gracia-Fleta, I. Marzo, C. Cativiela, A. Laguna and M. C. Gimeno. *Dalton Trans.*, 2014, **43**, 17054 – 17066.
57. R. Wai-Yin Sun, D.-L. Ma, E. Lai-Ming Wong and C.-M. Che. *Dalton Trans.*, 2007, 4884–4892
58. a) R. V. Parish, B. P. Howe, J. P. Wright, J. Mack, R. G. Pritchard, R. G. Buckley, A. M. Elsome and S. P. Fricker. *Inorg. Chem.*, 1996, **35**, 1659–1666. b) D. Fan, C.-T.-Yang, J. D. Ranford, P. F. Lee and J. J. Vittal. *Dalton Trans.*, 2003, 2680-2685.
59. K.H. Wong, K.K. Cheung, M.C.W. Chan, and C.M. Che. *Organometallics*, 1998, **17**, 3505 – 3511.
60. a) L. Messori, F. Abbate, G. Marcon, P. Orioli, M. Fontani, E. Mini, T. Mazzei, S. Carotti, T. O’Connell, P. Zanello. *J. Med. Chem.*, 2000, **43**, 3541–3548. b) P. Shi, Q. Jiang, Y. Zhao, Y. Zhang, J. Lin, L. Lin, Z. Guo. *J. Biol. Inorg. Chem.*, 2006, **11**, 745–752.
61. a) G. Marcon, S. Carotti, M. Coronello, L. Messori, E. Mini, P. Orioli, T. Mazzei, M. A. Cinellu and G. Minghetti. *J. Med. Chem.*, 2002, **45**, 1672–1677. b) A. Casini, G. Kelter, C. Gabbiani, M. A. Cinellu, G. Minghetti, D. Fregona, H. H. Fiebig and L. Messori. *J. Biol. Inorg. Chem.*, 2009, **14**, 1139–1149.
62. a) R. W.-Y. Sun, C. K.-L. Li, D.-L. Ma, J. J. Yan, C.-N. Lok, C.-H. Leung, N. Zhu and C.-M. Che. *Chem. Eur. J.*, 2010, **16**, 3097–1113. b) R. D. Teo, H. B. Gray, P. Lim, J. Termini, E. Domeshek and Z. Gross. *Chem. Comm.*, 2014, **50**, 13789–13792.
63. F. Novelli, M. Recine, F. Sparatore, C. Juliano. *Farmaco*, 1999, **54**, 232-236.
64. S.T. Crooke, C. K. Mirabelli. *Am. J. Med.* 1983, **75**, 109-113.
65. S. Carotti, G. Marcon, M. Marussich, T. Mazzei, L. Messori, E. Mini, P. Oriol. *Chemico-Biological Interactions*, 2000, **125**, 29–38.

66. a) G. Marcon, S. Carotti, M. Coronello, L. Messori, E. Mini, P. Orioli, T. Mazzei, M. A. Cinellu and G. Minghetti. *J. Med. Chem.*, 2002, **45**, 1672-1677. b) A. Casini, M. A. Cinellu, G. Minghetti, C. Gabbiani, M. Coronello, E. Mini, and L. Messori. *J. Med. Chem.*, 2006, **49**, 5524 – 5531.
67. S. Masiero, R. Trotta, S. Pieraccini, S. De Tito, R. Perone, A. Randazzo and G. Spada. *Org. Biomol. Chem.*, 2010, **8**, 2683-2692
68. a) J. L. Huppert and S. Balasubramanian. *Nucl. Acids Res.*, 2007, **35**, 406 – 413. b) J. Ren, T. Wang, E. Wang and J. Wang. *Analyst*, 2015, **140**, 2556–2572.
69. A.M. Zahler, J.R. Williamson, T.R. Cech. *Nature*, 1991, **350**, 718-720.
70. C. Kang, X. Zhang, R. Ratliff, R. Moyzis, A. Rich. *Nature*, 1992, **356**, 126-131.
71. A. Kettanl, S. Bouazlz, A. Gorln, H. Zhao. R.A. Jones, D.J. Patel. *J. Mol. Biol.*, 1998, **282**, 619-636.
72. N. Savvas, Dr. Georgiades, N. H. Abd Karim, K. Suntharalingam and Dr. R. Vilar *Angew. Chem. Int. Ed.*, 2010, **49**, 4020 –4034.
73. S. Ghosh, O. Mendoza, L. Cubo, F. Rosu, V. Gabelica, A. J. P. White and R. Vilar, *Chem. Eur. J.*, 2014, **20**, 4772.
74. K. Abd, H. Nurul, O. Mendoza, A. Shivalingam, A. J. Thompson, S. Ghosh, M. K. Kuimova and R. Vilar, *RSC Adv.*, 2014, **4**, 3355.
75. H. Yaku, T. Murashima, D. Miyoshi and N. Sugimoto, *Molecules*, 2012, **17**, 10586.
76. J. Zhang, F. Zhang, H. Li, C. Liu, J. Xia, L. Ma, W. Chu, Z. Zhang, C. Chen, S. Li and S. Wang, *Curr. Med. Chem.*, 2012, **19**, 2957.
77. a) K. Suntharalingam, D. Gupta, P.J. Sanz Miguel, B. Lippert, R. Vilar. *Chem. Eur. J.*, 2010, **16**, 3613- 3616. b) B. Hoffman and D. A. Liebermann. *Oncogene*, 2008, **27**, 6462–c) D. Monchaud, C. Allain, H. Bertrand, N. Smargiasso, F. Rosu, V. Gabelica, A. DeCian, J.L. Mergny, M.P. Teulade- Fichou, *Biochimie*, 2008, **90**, 1207.

78. a) E. D. Adamson. *Development*, 1987, 99, 449–471. b) B. Alberts, A. Johnson, J. Lewis et al. *Molecular Biology of the Cell*. 4th ed. New York: Garland Science; 2002.
79. P. Gratteri, L. Massai, E. Michelucci, R. Rigo, L. Messori, M. A. Cinellu, C. Musetti, C. Sissi and C. Bazzicalupi. *Dalton Trans.*, 2015, **44**, 3633 – 3639.
80. K. Gehring, J. L. Leroy, M. Gueron. *Nature*, 1993, **363**, 561.
81. a) H. A. Day, P. Pavlou, Z. A. E. Waller. *Bioorg. Med. Chem.*, 2014, **22**, 4407–4418. b) A. T. Phan, M. Guéron, J. L. Leroy, *J. Mol. Biol.* 2000, **299**, 123.
82. a) T. A. Brooks, S. Kendrick, L. Hurley. *FEBS J.*, 2010, **277**, 3459. b) S. P. Gurung, C. Schwarz, J. P. Hall, C. J. Cardina and J. A. Brazier. *Chem. Commun.*, 2015, **51**, 5630—5632.
83. J.L. Leroy, M. Gueron, J.L. Mergny, and C. Hélène, *Nucleic Acids Res.*, 1994, **22**, 1600 – 1606.
84. J.L. Mergny, L. Lacroix, X. Han, J.L. Leroy and C. Hélène. *J. Am. Chem. Soc.*, 1995, **117**, 8887 – 8898.
85. A. Rajendran, S. Nakano, N. Sugimoto. *Chem. Commun.*, 2010, **46**, 1299.
86. (a) R. Elgharian, J. J. Storhoff, R. C. Mucic, R. L. Letsinger, C. A. Mirkin. *Science*, 1997, **277**, 1078. (b) H. Li, L. Rothberg. *Proc. Natl. Acad. Sci. U.S.A.* 2004, **101**, 14036. (c) H. Li, L. Rothberg. *J. Am. Chem. Soc.*, 2004, **126**, 10958. (d) J. J. Storhoff, A. D. Lucas, V. Garimella, Bao, Y. B. Müller. *U. R. Nat. Biotechnol.* 2004, **22**, 883.
87. V. Pavlov, Y. Xiao, B. Shlyahovsky, I. Willner. *J. Am. Chem. Soc.* 2004, **126**, 11768.
88. a) J. Liu, Y. Lu. *J. Am. Chem. Soc.* 2003, **125**, 6642. b) S. Y. Lin, S. H. Wu, C. H. Chen., *Angew. Chem., Int. Ed.*, 2006, **45**, 4948. c) J. S. Lee, M. S. Han, C. A. Mirkin. *Angew. Chem., Int. Ed.*, 2007, **46**, 4093. d) T. Pons, I. L. Medintz, K. E. Sapsford, S. Higashiya, A. F. Grimes, D. S. English, H. Mattoussi. *Nanoletters*, 2007, **7**, 3157–3164.

89. X. Li, Y. Peng, J. Ren and X. Qu, *Proc. Natl. Acad. Sci. U. S. A.*, 2006, **103**, 19658 – 19663.
90. D.M. Gray, R.L. Ratliff and M. R. Vaughan, *Methods Enzymol.*, 1992, **211**, 389–406.
91. J. Kypr, I. Kejnovská, D. Renčiuk and M. Vorlíčková. *Nucleic Acids Res.*, 2009, **37**, 1713–1725.
92. J. Kypr and M. Vorlickova. *Gen. Physiol. Biophys.*, 1986, **5**, 415–422.
93. M.F. Maestre. *J. Mol. Biol.*, 1970, **52**, 543–556.
94. J.-L. Mergny, J. Li, L. Lacroix, S. Amrane and J. B. Chaires. *Nucleic Acids Res.*, 2005, **33**, 1 – 6. b) J. M. Dettler, R. Buscaglia, J. Cui, D. Cashman, M. Blynn and E. A. Lewis. *Biophys J.*, 2010, **99**, 561–567.
95. C. Berney and G. Danuser. *Biophys. J.*, 2003, **84**, 3992–4010.
96. J. L. Mergny, L. Lacroix, X. Han, J.L. Leroy, and C. Hélène. *J. Am. Chem. Soc.*, 1995, **117**, 8887–8898.
97. T. Li and M. Famulok. *J. Am. Chem. Soc.* 2013, **135**, 1593–1599.
98. A. Ono, S. Cao, H. Togashi, M. Tashiro, T. Fujimoto, T. Machinami, S. Oda, Y. Miyake, I. Okamoto and Y. Tanaka, *Chem. Commun.*, 2008, 4825–4827.
99. J. L. Mergny. *Biochemistry*, 1999, **38**, 1573 – 1581.
100. H. A. Day, C. Huguin and Z. A. E. Waller. *Chem. Commun.*, 2013, **49**, 7696 – 7698.
101. J. L. Mergny, J. Li, L. Lacroix, S. Amrane, J. B. Chaires. *Nucleic Acids Res.* 2005, **33**, e138.
102. *Modern Supramolecular Gold Chemistry: Gold-Metal Interactions and Applications*. Antonio Laguna (ed.) Wiley-VCH, Weinheim, **2008**, pp. 41-63.

103. a) M. Nonoyama, K. Nakahima and K. Nonoyama. *Polyhedron*, 1997, **16**, 4039. b) Z. Zhu, B. R. Cameron and R. T. Skerlj. *J. Organomet. Chem.*, 2003, **657**, 57.
104. X. Huang, S. L. Buchwald. *Org. Lett.*, 2001, **3**, 3417–3419.
105. A. Rajca, M. Vale and S. Rajca. *J. Am. Chem. Soc.*, 2008, **130**, 9099 – 9105.
106. A. Sakakura, Y. Koshikari, M. Akakura and K. Ishihara. *Org. Lett.*, 2012, **14**, 30–33.
107. T. Michinobu, E. Tsuchida, H. Nishide. *B. Chem. Soc. Jpn.*, 2000, **73**, 1021 – 1027.
108. M. Kranz, H. Dietrich, W. Mahdi, G. Miiller, F. Hampel, T. Clark, R. Hacker, W. Neugebauer, A. J. Kos, and P. von R. Schleyer. *J. Am. Chem. Soc.*, 1993, **115**, 4698 – 4704.
109. N. S. Narasimhan, R. S. Mali, *Synthesis*, 1983, 957.
110. M. Kranz, F. Hampel, T. Clark. *J. Chem. Soc., Chem. Commun.*, 1992, 1247.
111. L. Ackermann, H. K. Potukuchi, A. R. Kapdi, C. Schulzke. *Chem – A. Eur. J.*, 2010, **16**, 3300 – 3303.
112. Programs CrysAlisPro, Oxford Diffraction Ltd., Abingdon, UK (2010).
113. G. M. Sheldrick, SHELX-97 – Programs for crystal structure determination (SHELXS) and refinement (SHELXL), *Acta Cryst.* (2008) **A64**, 112-122.
114. '*International Tables for X-ray Crystallography*', Kluwer Academic Publishers, Dordrecht (1992). Vol. C, pp. 500, 219 and 193.